Title
Subsurface Controls on Carbon Dynamics in a Changing Arctic Ecosystem

Author
Vaughn, Lydia Smith

Publication Date
2017

Peer reviewed|Thesis/dissertation

Subsurface Controls on Carbon Dynamics in a Changing Arctic Ecosystem

By

Lydia Smith Vaughn

A dissertation submitted in partial satisfaction of the

requirements for the degree of

Doctor of Philosophy

in

Energy and Resources

in the

Graduate Division

of the

University of California, Berkeley

Committee in charge:

Dr. Margaret S. Torn, Chair
Professor John Harte
Professor Todd E. Dawson

Summer 2017

Subsurface Controls on Carbon Dynamics in a Changing Arctic Ecosystem

by

Lydia Smith Vaughn

Abstract

Subsurface Controls on Carbon Dynamics in a Changing Arctic Ecosystem

by

Lydia Smith Vaughn

Doctor of Philosophy in Energy and Resources

University of California, Berkeley

Dr. Margaret S. Torn, Chair

With climate change in the Arctic, temperatures are expected to rise at twice the rate as in temperate latitudes. This rapid change has the potential to disrupt local ecosystems and feed back to the global climate as frozen soils thaw and warm. Large stocks of carbon have accumulated in Arctic soils, protected from decomposition by cold, wet, and frozen conditions. With warming and thawing due to climate change, decomposition of this carbon is expected to increase, releasing it to the atmosphere as the greenhouse gases CO_2 and methane. While a number of modeling efforts have attempted to quantify this potential feedback, the future Arctic carbon balance remains unknown due to uncertain mechanisms stabilizing soil carbon and complex interactions between vegetation and soils. In studies based in Barrow, Alaska, I address three sources of this uncertainty: (1) the magnitude of methane emissions following soil thaw, (2) interactions between plants, soil carbon, and microbial decomposers, and (3) the sensitivity of soil carbon cycling changes in microclimate.

First, I ask how methane formation, consumption within the soil, and net emission to the atmosphere may change with soil thaw in the Arctic. Loss of permafrost (perennially frozen ground) can lead to large-scale landscape changes, redistributing water and soil. Such physical changes can strongly influence emissions of methane, a greenhouse gas roughly 25 times as potent as CO_2, whose future emission rates are highly uncertain. Combining field measurements with statistical modeling, I assess soil methane emissions and microbial methane processes (production and consumption) across a gradient of permafrost thaw. In contrast with many previous studies, I find that more degraded sites have lower methane emissions, a different primary methanogenic pathway, and greater methane oxidation than intact permafrost sites. These differences are greater than soil moisture or temperature data can explain. Additional microtopographic controls accounting for these observations may include differences in water flow and vegetation between intact and degraded polygons.

Second, I ask how changes in plant activity due to climate change may influence the rate of soil carbon decomposition (the priming effect), through interactions between plant

roots, microbial decomposers, and soil carbon compounds. In a two-year field experiment, I simulate increased plant root activity and measure its influence on soil carbon decomposition, plant CO_2 uptake, mineral nitrogen availability, and microbial communities. I find no measurable relationship between substrate additions and soil organic matter decomposition, nutrient supply, or microbial population size. Treatment-level differences in primary production, however, indicate possible longer-term interactions between vegetation and decomposition. The absence of a measurable priming effect contrasts with numerous published reports documenting a positive priming effect under tightly controlled conditions. This difference may be due to high background variability in ecosystem respiration, a property of this in situ experiment. This chapter is one of the first studies evaluating this plant-soil interaction in a field experimental context, with a representative degree of environmental variability.

Third, I ask how decomposition rates of fast-cycling and slow-cycling soil carbon may be influenced by microclimatic changes. The rate of soil carbon turnover and its sensitivity to environmental variables such as temperature and oxygen availability are both highly uncertain and highly influential for model predictions of the global carbon cycle. In two laboratory incubations, I use natural abundance radiocarbon measurements of CO_2 and soil organic matter to determine how fast-cycling and slow-cycling carbon pools respond to temperature changes and transitions between anaerobic and aerobic conditions. Using a novel analytical approach, I find that fast- and slow-cycling carbon pools from these Barrow, Alaska soils have comparable temperature sensitivities, with decomposition from both pools increasing by ~40 % for a 5°C temperature increase. Similarly, decomposition rates were highly sensitive to aerobic vs. anaerobic conditions, with no significant difference in sensitivity between pools. Radiocarbon contents of CO_2 and soil organic matter indicate that ancient, slow-cycling carbon is sensitive to decomposition under soil temperature increases and water table changes.

For Miles

TABLE OF CONTENTS

ACKNOWLEDGEMENTS

For twelve weeks in summer, the sun never sets over the Barrow Environmental Observatory. This offers not only hours-long twilights over the Chukchi and Beaufort Seas, but also nearly two thousand uninterrupted daylight hours for sampling in the field. I owe many thanks to people who worked tirelessly through these hours, for without them this dissertation would still be buried in the ground. Above all, I thank Margaret Torn for her guidance and support throughout all stages of this project. Simply put, a graduate student could not hope for a better advisor. As a mentor, Margaret has given hours of her time in meetings and the field. As a scientist, teacher, and coauthor, she combines deep knowledge and persistent scientific inquiry with an ever-sunny outlook and rare generosity. Even at one-thirty in the morning, kneeling over soil chambers in the midnight sun, her enthusiasm never flagged. Margaret's intellect, work ethic, and optimism have been a gift and inspiration.

In the Torn Lab, I found a community of exceptional researchers. Many lab members past and present have helped me collect samples and measurements, interpret my findings, and stay sane throughout. My top field partners-in-crime, Bryan Curtis and Ori Chafe, spent long days measuring gas fluxes and soil temperatures, collecting gas samples, filtering water samples, and coring frozen tundra under winter snows. Their patience and attention to detail were matched only by their boundless energy and love for the tundra. In the lab, Rachel Porras assisted me with all things analytical. With admirable precision, she trained me on the vacuum line, made measurements on the GC, and offered her time for countless other tasks. Thanks as well to Caitlin Hicks Pries and Cristina Castanha for help with laboratory analyses and for discussions about data interpretation. Biao Zhu was central to the planning, fieldwork, and lab analyses for Chapter 3, as were Carolin Bimüller and Rose Abramoff. Melanie Hahn and Julia Siegrist made a number of gas flux and gas well measurements used in Chapter 2.

Members of the NGEE-Arctic team beyond the Torn Lab assisted with this project as well. I owe special thanks to Mark Conrad for his mentorship and hard work in the field and for teaching me all I know about water sampling. Most stable isotope analyses in this dissertation were conducted in his lab, with thanks as well to Markus Bill for manning the instrument with patience, precision, and a salty sense of humor. John Peterson, Neslihan Taş Baas, and Anna-Lena Grauel helped with sample collection or analysis, Craig Ulrich kept me oriented, and Alistair Rogers and Victoria Sloan provided lively conversation in Apartment 4. Leading the NGEE-Arctic project, Stan Wullschleger deserves special thanks for offering mentorship and opportunities to present this research, organizing an unwieldy team of researchers, and laying miles upon miles of trail mat.

On the UC Berkeley Campus, the Harte Lab has been my intellectual home. At the helm, John Harte taught me to balance species-level detail with order-of-magnitude perspective, missing neither the forest nor the trees (or in this case neither the tundra nor the sedges). John has been a warm and thoughtful mentor and committee member, generous with his time while always asking questions I hadn't considered. The Harte Lab members provided feedback on all stages of this project, from sampling strategies and

statistical considerations to broader interpretations. In particular, I thank Danielle Christianson for her friendship and intellectual guidance during many long walks in the hills. Outside the Harte Lab, the broader ERG community kept my research grounded with probing and pragmatic questions. I cannot imagine a more articulate, accomplished, and kind group of students, faculty, staff, and alumni. It is with great pride that I call myself an ERGie and with great gratitude that I look back on the past seven years. Of particular note, I probably wouldn't be graduating without Kay Burns. Like many ERGies past, present, and future, I have Kay to thank for solving all the problems, knowing all the answers, and embodying the spirit of ERG.

Many people have nurtured the love of isotopes upon which this dissertation is built. I offer special thanks to Todd Dawson, whose enthusiasm for stable isotope biogeochemistry left me with a case of isotope fever. As a teacher, mentor, and committee member, Todd has been ever knowledgeable and gracious with his time. In the world of terrestrial radiocarbon, many accomplished scientists taught me the theory and methods I used in Chapter 4. This list begins with Margaret Torn, and also includes Sue Trumbore and Ted Schuur, who taught me foundational theory in the Radiocarbon Short Course; Jen Harden, who took the lead on the Radiocarbon Database and offered her thoughts on turnover time modeling; Karis McFarlane, Francesca Hopkins, and Claudia Czimczik, who shared their field sampling and lab incubation methods; and with special thanks Kate Heckman and Paula Zermeno, who went out of their way to help with radiocarbon analyses.

Finally, my family has supported me from the beginning to the end. To my parents: thank you for instilling in me a sense of wonder and responsibility and a commitment to the pursuit of knowledge. To Mitch: thank you for your patience and perspective and for being there every day. To Miles: thank you for keeping my priorities in line.

Funding for this dissertation was provided by the Biological and Environmental Research program in the U.S. Department of Energy (DOE) Office of Science, through the Next Generation Ecosystem Experiments (NGEE-Arctic); by the University of California Dissertation-Year Fellowship; and by the Philomathia Graduate Student Fellowship in the Environmental Sciences.

CHAPTER 1: INTRODUCTION

On a bench in our lab, an array of glass tubes spills from a beaker like a bouquet of clear flowers. These tubes appear to enclose empty space, sealed on each end with a plug of melted glass. The tubes are not empty, however. Instead, they hold invisible souvenirs from a rapidly changing world: purified samples of CO_2 released from Arctic tundra soils. Before being captured in glass, the carbon in this CO_2 traveled from the atmosphere into plants, from plants into soil, and finally from soil back to CO_2 in a trip that took from minutes to millennia, depending on its route.

Our role as biogeochemists is to trace such routes and measure their timing, to perceive the invisible, to see the unseen. By doing so, we hope to infer past changes, predict future changes, and monitor changes that are currently underway. Some such changes are easily apparent, as when rapidly thawing permafrost erodes into gullies and pits (thermokarst) or when fire passes through a landscape. Others are harder to perceive, either too slow to discern in one or two field seasons, too small to disentangle from background variability, or too integrated with a system to measure independently. In some cases, invisible processes may be rendered visible by natural phenomena, as when bubbles of escaping methane become trapped in the sheen of ice forming on wetland ponds in the fall. Other times we rely on instruments to measure invisible quantities, translating stocks and fluxes of energy or material into numbers on a page or screen. We then craft models with these numbers to identify patterns and relationships among system components or their measurable proxies. In doing so, we aim to draw reliable conclusions about past, present, and future changes: their directions and rates, ecological controls, and ties to broader system feedbacks.

This dissertation was conceived of and written in the context of a wildly uncontrolled experiment. Through fossil fuel burning and other human activities, we have increased the atmospheric concentrations of CO_2, methane, and other greenhouse gases. The concentration of atmospheric CO_2 has grown from 280 ppm in preindustrial times to its current level of >400 ppm, while methane has grown from 700 to 1850 ppb (NOAA). These concentrations continue to increase, altering the atmosphere's ability to store energy with a broad set of ecological consequences such as increased temperatures and altered regimes of precipitation, vegetation, and ocean currents (Ciais *et al.*, 2014). Among this array of changes, numerous feedbacks may magnify or moderate the rate of climate change. Increasing atmospheric CO_2 concentrations, for example, may enhance vegetation productivity, dampening the rise in atmospheric CO_2 (Farrior *et al.*, 2015).

The focus of this dissertation is one such climate change feedback, the soil carbon-climate feedback. As warming temperatures accelerate decomposition of carbon stored in soils, release of this carbon as CO_2 and methane may shrink terrestrial carbon stocks and amplify temperature increases (Knorr *et al.*, 2005). This positive feedback may be particularly important in Arctic ecosystems. There, decomposition progresses slowly in frozen, cold and anaerobic soils, which has led to the accumulation of large soil carbon stores. In regions underlain by permafrost, soils contain an estimated 1,300 Pg of carbon (Hugelius *et al.*, 2014), roughly equal to the total carbon stored in the atmosphere and vegetation biomass combined (Ciais *et al.*, 2014). In recent decades, Arctic ecosystems

have been an atmospheric CO_2 sink and methane source, absorbing an estimated 110 Tg y^{-1} CO_2 and emitting roughly 19 Tg y^{-1} of methane (McGuire *et al.*, 2012). With climate change in the Arctic, temperatures are expected to increase at twice the global rate due to polar amplification (Holland & Bitz, 2003), warming soils, melting permafrost, and changing wetland extents. Such changes are expected to alter the Arctic carbon balance, potentially destabilizing its ancient carbon stores. Models predict that the Arctic will become a source of atmospheric CO_2 before the end of this century, with concurrent increases in methane emissions (Koven *et al.*, 2011, 2015; Schuur *et al.*, 2013; Lawrence *et al.*, 2015). The magnitude of this feedback, i.e., the degree to which Arctic soil warming and associated hydrological changes will increase net CO_2 and methane emissions, is an important source of uncertainty in future climate projections (Schuur *et al.*, 2015).

The following three chapters are organized around three sources of uncertainty in the Arctic soil carbon-climate feedback: the balance of carbon emissions as methane vs. CO_2 (Chapter 2), interactions between plant carbon inputs and soil decomposition rates (Chapter 3), and the sensitivity of soil carbon pools to environmental perturbations (Chapter 4). Each chapter is formatted as a stand-alone journal article that investigates an ecological control on the response of soil carbon turnover to climate change. Study designs employ a range of empirical approaches, including a field survey (Chapter 2), field manipulation (Chapter 3), and lab experiment (Chapter 4). In all cases, I track carbon transformations from soil organic matter to the greenhouse gases CO_2 or methane. Given the complex array of microbial processes, respiration fluxes, and soil carbon pools, such transformations often cannot be measured directly, particularly in situ. Instead, carbon isotopes offer a means to measure these quantities indirectly—a means to see the otherwise unseen. Each of the following chapters employs a unique isotopic approach to distinguish metabolic processes (Chapter 2), trace the fate of a substrate (Chapter 3), or isolate environmental sensitivities (Chapter 4).

The research for this dissertation was conducted through the Next Generation Ecosystem Experiments (NGEE-Arctic), a multi-institution collaboration that unites scientists from a broad range of disciplines. With the overarching goal to improve climate predictions, NGEE-Arctic integrates information from hydrology, plant biology, geophysics, microbial ecology, and biogeochemistry into earth system models. In light of this goal, this dissertation has dual objectives, to describe mechanistic and phenomenological relationships regarding soil carbon cycling while providing information for model evaluation and improvement.

All fieldwork took place on the Barrow Environmental Observatory in Barrow, Alaska (Fig. 1). There, study sites were situated within a natural gradient of permafrost degradation present in polygon tundra, a common tundra type in the Barrow, Alaska region that covers ~250,000 km^2 throughout the Arctic (Donner *et al.*, 2007). In this tundra type, massive wedges of subsurface ice create discrete, polygon-shaped landforms separated by low-lying, saturated or inundated channels (Brown, 1967). These ice wedges grow incrementally from year to year, first generating early-successional polygons with low-lying, inundated centers and dry, elevated rims. When ice wedges thaw due to disturbance or natural succession, the elevated rims degrade and polygon centers drain, generating a drier landscape of smaller polygons with high, dry centers (Drew & Tedrow, 1962; Billings & Peterson, 1980). While this successional process has been ongoing in

Alaska for millennia (Billings & Peterson, 1980), recent decades have seen accelerated transition rates from low-centered to high-centered polygons (Jorgenson *et al.*, 2006).

Along this gradient from low-centered to high-centered polygons, differences in drainage and subsurface ice properties create strong thermal, hydrological, and geochemical gradients (Hubbard *et al.*, 2013; Newman *et al.*, 2015), all of which influence soil carbon dynamics. Accordingly, each study in this dissertation was carefully located to best leverage this variability. Chapter 2 explicitly uses a permafrost degradation gradient to link methane production, oxidation, and emissions to permafrost thaw and associated landscape change (Fig. 2). Chapter 3 targets aerobic processes and shallow rooting depths, and so was sited in high polygon centers with sparse vegetation (Fig, 3). To evaluate soil carbon vulnerability across pools with a broad range of cycling rates, Chapter 4 uses a distributed sampling design across the range of polygon types (Fig. 4).

* * *

Chapter 2 asks how methane formation in anaerobic soils, consumption in aerobic soil layers, and net emission to the atmosphere may change with permafrost degradation. Loss of permafrost (perennially frozen ground) can lead to rapid, large-scale landscape changes and soil water redistribution (Schuur *et al.*, 2007; Lara *et al.*, 2016). In some cases, slumping and subsidence cause inundation, increasing the importance of anaerobic decomposition processes (Wickland *et al.*, 2006; Olefeldt *et al.*, 2013; McCalley *et al.*, 2014). In other instances, drainage pathways form, lowering the water table and oxygenating soils (Fortier *et al.*, 2007; Godin *et al.*, 2014). Such changes strongly influence emissions of methane, a greenhouse gas produced under anaerobic conditions (Cicerone & Oremland, 1988). Due to their complex biogeochemical controls and high spatial and temporal variability, current net methane emissions and gross methane production and consumption have been difficult to quantify, and their predicted responses to climate change remain uncertain (Lawrence *et al.*, 2015). With a global warming potential 25 times that of CO_2 and a relatively short atmospheric lifetime (Ciais *et al.*, 2014), methane has the potential to strongly influence the climate on near-term timescales. To improve the ability of models to represent methane processes and emissions, I ask (1) how do methane production and consumption processes vary across geomorphic and temporal gradients, and (2) how do these subsurface methane processes relate to surface greenhouse gas fluxes?

This chapter synthesizes two years of field measurements from a permafrost degradation gradient of low-centered to high-centered polygons, in which I quantified net fluxes of methane and CO_2 from the soil surface, as well as concentrations and isotopic abundances of dissolved methane and CO_2 from three depths within the soil pore space. Net soil methane emissions are straightforward to measure in the field using soil chambers or eddy covariance methods (Torn & Chapin III, 1993; Baldocchi, 2014; Zona *et al.*, 2016), but rates of production and consumption are more challenging to determine. Methane produced under anaerobic conditions may be rapidly consumed in aerobic soil layers (Cicerone & Oremland, 1988) or may bypass oxidation when transported to the

soil surface in bubbles or plant aerenchyma (hollow tissues common to wetland plants) (Chanton, 2005). Due to this array of competing processes, neither methane production nor methane oxidation can be isolated without manipulating the system to inhibit other processes (Epp & Chanton, 1993). In the absence of direct measurements, stable isotopes provide an indirect means to track these methane processes. Metabolic pathways of methane production or consumption and physical pathways of methane transport fractionate isotopes in characteristic ways (Hornibrook & Aravena, 2010), such that subsurface isotope measurements can be used to differentiate between microbial processes of methane formation and determine the degree of methane oxidation. In combination with ancillary measurements of soil temperature, soil moisture, and vegetation, this chapter uses these flux and isotope measurements to evaluate the influence of environmental factors, permafrost degradation, and polygon microtopography on patterns and mechanisms of net methane efflux.

Chapter 3 investigates how plant-soil interactions may mediate the response of soil carbon decomposition to climate change. Future soil carbon stocks will depend on the balance between plant carbon inputs and organic matter decomposition, which are both expected to change with warming of high-latitude landscapes (McGuire *et al.*, 2009, 2012). Important to this balance, vegetation and decomposition may interact via the quantity, chemistry, and spatial distribution of plant-derived soil carbon inputs. This study addresses the priming effect, one such interaction in which increased root exudation alters the background rate of soil organic matter decomposition through microbial biomass increases, co-metabolism of substrates, induced nitrogen limitation, or other possible mechanisms (Kuzyakov *et al.*, 2000).

This chapter describes a two-year field experiment in which I tested for a priming effect under natural environmental variability, asking how increased carbon substrate inputs (1) affect soil organic matter mineralization rates, (2) influence the temperature sensitivity of decomposition, (3) influence microbial biomass and mineral nitrogen availability, and (4) affect gross primary production. Following pulse additions of glucose to the mineral soil layer, I measured changes in soil organic matter decomposition, microbial biomass, nutrient availability, and vegetation productivity. In order to quantify native soil organic matter decomposition, glucose mineralization, and glucose-carbon incorporation into soils, I traced isotope-labeled carbon from the added glucose into the ecosystem respiration flux, microbial biomass, and soil organic matter. The priming effect has been observed in numerous laboratory and greenhouse experiments (Blagodatskaya & Kuzyakov, 2008), and there is considerable interest in including this process in ecosystem models (Perveen *et al.*, 2014; Sulman *et al.*, 2014; Georgiou *et al.*, 2015; Guenet *et al.*, 2016). Only few studies, however, have evaluated the priming effect with in situ field experiments.

Chapter 4 evaluates the sensitivity of soil carbon decomposition rates to changes in environmental factors such as temperature, moisture, oxygen availability, and depth in the soil profile. As Arctic soils warm and the active layer thickens, soil carbon stores become increasingly available to decomposition. The rate with which this soil carbon will be mineralized to CO_2, however, is not well constrained by field and laboratory measurements. This decomposition rate and its sensitivity to environmental parameters is one of the key uncertainties in high latitude carbon cycle models (Mikan *et al.*, 2002;

Davidson & Janssens, 2006; Koven *et al.*, 2015). In this chapter, I use natural abundance radiocarbon measurements in two soil incubation experiments to ask: (1) how do soil carbon cycling rates vary with depth in the soil and across microtopographic features, (2) how do soil carbon pools with distinct cycling rates respond to temperature changes, and (3) how do anaerobic conditions influence the relative decomposition rates of different carbon pools?

These questions require sorting CO_2 emissions or bulk soil organic matter into separate carbon pools, defined by their decomposition rates (Torn *et al.*, 2009). Whereas many studies infer this pool structure from multiple-pool models and measured CO_2 fluxes (Bridgham *et al.*, 1998; Fierer *et al.*, 2005; Knorr *et al.*, 2005), this chapter uses natural abundance radiocarbon to trace carbon pool dynamics. Radiocarbon (^{14}C), a radioactive carbon isotope with a half-life of 5730 years, resides in atmospheric CO_2 in trace concentrations due to natural production by cosmic rays and anthropogenic inputs from nuclear weapons testing in the 1950s and '60s (Trumbore, 2000)[1]. This radiocarbon becomes incorporated into plants and soil, where it is then lost via decomposition or radioactive decay. Radiocarbon thus functions as a natural tracer of carbon flow through ecological systems. Using the principle of mass balance, we can estimate a soil carbon reservoir's steady-state decomposition rate from its radiocarbon concentration (Torn *et al.*, 2009)[2]. Accordingly, the radiocarbon content of respired CO_2 depends on the decomposition rates of different soil carbon pools.

This chapter presents a novel analytical method based on this general framework of radiocarbon analysis. Using measurements of ^{14}C abundance in bulk soil organic matter and CO_2 respired under different incubation conditions, I evaluate the temperature and oxygen-sensitivities of fast-cycling and slow-cycling carbon pools. Whereas numerous studies have asked how these environmental sensitivities differ among carbon pools by fitting multiple pool models (reviewed in Conant *et al.*, 2011), their conclusions are sensitive to model assumptions (Reichstein *et al.*, 2005). By concurrently measuring changes in the rate and radiocarbon content of CO_2 emissions, I am able to disentangle these effects through empirical measurements.

[1] Nuclear weapons testing in the 1950s and early 1960s roughly doubled the amount of radiocarbon in the atmosphere. Since the nuclear test ban treaty in 1963, this concentration has steadily declined due to exchanges with marine and terrestrial carbon reservoirs.

[2] For samples collected after 1950, this method also requires a time series of atmospheric radiocarbon measurements local to the sampling site.

References

Baldocchi D (2014) Measuring fluxes of trace gases and energy between ecosystems and the atmosphere–the state and future of the eddy covariance method. *Global change biology*, **20**, 3600–3609.

Billings WD, Peterson KM (1980) Vegetational change and ice-wedge polygons through the thaw-lake cycle in Arctic Alaska. *Arctic and Alpine Research*, 413–432.

Blagodatskaya E, Kuzyakov Y (2008) Mechanisms of real and apparent priming effects and their dependence on soil microbial biomass and community structure: critical review. *Biology and Fertility of Soils*, **45**, 115–131.

Bridgham SD, Updegraff K, Pastor J (1998) Carbon, Nitrogen, and Phosphorus Mineralization in Northern Wetlands. *Ecology*, **79**, 1545–1561.

Brown J (1967) Tundra soils formed over ice wedges, northern Alaska. *Soil Science Society of America Journal*, **31**, 686–691.

Chanton JP (2005) The effect of gas transport on the isotope signature of methane in wetlands. *Organic Geochemistry*, **36**, 753–768.

Ciais P, Sabine C, Bala G et al. (2014) Carbon and other biogeochemical cycles. In: *Climate Change 2013: The Physical Science Basis. Contribution of Working Group I to the Fifth Assessment Report of the Intergovernmental Panel on Climate Change*, pp. 465–570. Cambridge University Press.

Cicerone RJ, Oremland RS (1988) Biogeochemical aspects of atmospheric methane. *Global Biogeochemical Cycles*, **2**, 299–327.

Conant RT, Ryan MG, Ågren GI et al. (2011) Temperature and soil organic matter decomposition rates – synthesis of current knowledge and a way forward. *Global Change Biology*, **17**, 3392–3404.

Davidson EA, Janssens IA (2006) Temperature sensitivity of soil carbon decomposition and feedbacks to climate change. *Nature*, **440**, 165–173.

Donner N, Karpov NS, de Klerk P, Joosten H (2007) Distribution, diversity, development and dynamics of polygon mires: examples from Northeast Yakutia (Siberia).

Drew JV, Tedrow JCF (1962) Arctic Soil Classification and Patterned Ground. *Arctic*, **15**, 109–116.

Epp MA, Chanton JP (1993) Rhizospheric methane oxidation determined via the methyl fluoride inhibition technique. *Journal of Geophysical Research: Atmospheres*, **98**, 18413–18422.

Farrior CE, Rodriguez-Iturbe I, Dybzinski R, Levin SA, Pacala SW (2015) Decreased water limitation under elevated CO2 amplifies potential for forest carbon sinks. *Proceedings of the National Academy of Sciences*, **112**, 7213–7218.

Fierer N, Craine JM, McLauchlan K, Schimel JP (2005) Litter quality and the temperature sensitivity of decomposition. *Ecology*, **86**, 320–326.

Fortier D, Allard M, Shur Y (2007) Observation of rapid drainage system development by thermal erosion of ice wedges on Bylot Island, Canadian Arctic Archipelago. *Permafrost and Periglacial Processes*, **18**, 229–243.

Georgiou K, Koven CD, Riley WJ, Torn MS (2015) Toward improved model structures for analyzing priming: potential pitfalls of using bulk turnover time. *Global Change Biology*, **21**, 4298–4302.

Godin E, Fortier D, Coulombe S (2014) Effects of thermo-erosion gullying on hydrologic flow networks, discharge and soil loss. *Environmental Research Letters*, **9**, 105010.
Guenet B, Moyano FE, Peylin P, Ciais P, Janssens IA (2016) Towards a representation of priming on soil carbon decomposition in the global land biosphere model ORCHIDEE (version 1.9.5.2). *Geosci. Model Dev.*, **9**, 841–855.
Holland MM, Bitz CM (2003) Polar amplification of climate change in coupled models. *Climate Dynamics*, **21**, 221–232.
Hornibrook ER, Aravena R (2010) 6 Isotopes and Methane Cycling. *Environmental Isotopes in Biodegradation and Bioremediation*, 167.
Hubbard SS, Gangodagamage C, Dafflon B et al. (2013) Quantifying and relating land-surface and subsurface variability in permafrost environments using LiDAR and surface geophysical datasets. *Hydrogeology Journal*, **21**, 149–169.
Hugelius G, Strauss J, Zubrzycki S et al. (2014) Estimated stocks of circumpolar permafrost carbon with quantified uncertainty ranges and identified data gaps. *Biogeosciences*, **11**, 6573–6593.
Jorgenson MT, Shur YL, Pullman ER (2006) Abrupt increase in permafrost degradation in Arctic Alaska. *Geophysical Research Letters*, **33**.
Knorr W, Prentice IC, House JI, Holland EA (2005) Long-term sensitivity of soil carbon turnover to warming. *Nature*, **433**, 298–301.
Koven CD, Ringeval B, Friedlingstein P et al. (2011) Permafrost carbon-climate feedbacks accelerate global warming. *Proceedings of the National Academy of Sciences*.
Koven CD, Lawrence DM, Riley WJ (2015) Permafrost carbon–climate feedback is sensitive to deep soil carbon decomposability but not deep soil nitrogen dynamics. *Proceedings of the National Academy of Sciences*, 201415123.
Kuzyakov Y, Friedel JK, Stahr K (2000) Review of mechanisms and quantification of priming effects. *Soil Biology and Biochemistry*, **32**, 1485–1498.
Lara MJ, Genet H, McGuire AD et al. (2016) Thermokarst rates intensify due to climate change and forest fragmentation in an Alaskan boreal forest lowland. *Global Change Biology*, **22**, 816–829.
Lawrence DM, Koven CD, Swenson SC, Riley WJ, Slater AG (2015) Permafrost thaw and resulting soil moisture changes regulate projected high-latitude CO_2 and CH_4 emissions. *Environmental Research Letters*, **10**, 094011.
McCalley CK, Woodcroft BJ, Hodgkins SB et al. (2014) Methane dynamics regulated by microbial community response to permafrost thaw. *Nature*, **514**, 478–481.
McGuire AD, Anderson LG, Christensen TR et al. (2009) Sensitivity of the carbon cycle in the Arctic to climate change. *Ecological Monographs*, **79**, 523–555.
McGuire AD, Christensen TR, Hayes D et al. (2012) An assessment of the carbon balance of Arctic tundra: comparisons among observations, process models, and atmospheric inversions. *Biogeosciences*, **9**, 3185–3204.
Mikan CJ, Schimel JP, Doyle AP (2002) Temperature controls of microbial respiration in arctic tundra soils above and below freezing. *Soil Biology and Biochemistry*, **34**, 1785–1795.
Newman BD, Throckmorton HM, Graham DE et al. (2015) Microtopographic and depth controls on active layer chemistry in Arctic polygonal ground. *Geophysical Research Letters*, 2014GL062804.

NOAA ESRL Global Monitoring Division - Global Greenhouse Gas Reference Network.
Olefeldt D, Turetsky MR, Crill PM, McGuire AD (2013) Environmental and physical controls on northern terrestrial methane emissions across permafrost zones. *Global change biology*, **19**, 589–603.
Perveen N, Barot S, Alvarez G et al. (2014) Priming effect and microbial diversity in ecosystem functioning and response to global change: a modeling approach using the SYMPHONY model. *Global Change Biology*, **20**, 1174–1190.
Reichstein M, Kätterer T, Andrén O et al. (2005) Temperature sensitivity of decomposition in relation to soil organic matter pools: critique and outlook. *Biogeosciences*, **2**, 317–321.
Schuur EAG, Crummer KG, Vogel JG, Mack MC (2007) Plant Species Composition and Productivity following Permafrost Thaw and Thermokarst in Alaskan Tundra. *Ecosystems*, **10**, 280–292.
Schuur E a. G, Abbott BW, Bowden WB et al. (2013) Expert assessment of vulnerability of permafrost carbon to climate change. *Climatic Change*, **119**, 359–374.
Schuur E a. G, McGuire AD, Schädel C et al. (2015) Climate change and the permafrost carbon feedback. *Nature*, **520**, 171–179.
Sulman BN, Phillips RP, Oishi AC, Shevliakova E, Pacala SW (2014) Microbe-driven turnover offsets mineral-mediated storage of soil carbon under elevated CO2. *Nature Climate Change*, **4**, 1099–1102.
Torn MS, Chapin III FS (1993) Environmental and biotic controls over methane flux from Arctic tundra. *Chemosphere*, **26**, 357–368.
Torn M, Swanston C, Castanha C, Trumbore S (2009) Storage and turnover of organic matter in soil. *Biophysico-Chemical Processes Involving Natural Nonliving Organic Matter in Environmental Systems*, 219–272.
Trumbore S (2000) Age of soil organic matter and soil respiration: radiocarbon constraints on belowground C dynamics. *Ecological Applications*, **10**, 399–411.
Wickland KP, Striegl RG, Neff JC, Sachs T (2006) Effects of permafrost melting on CO2 and CH4 exchange of a poorly drained black spruce lowland. *Journal of Geophysical Research: Biogeosciences*, **111**, G02011.
Zona D, Gioli B, Commane R et al. (2016) Cold season emissions dominate the Arctic tundra methane budget. *Proceedings of the National Academy of Sciences*, **113**, 40–45.

Figures

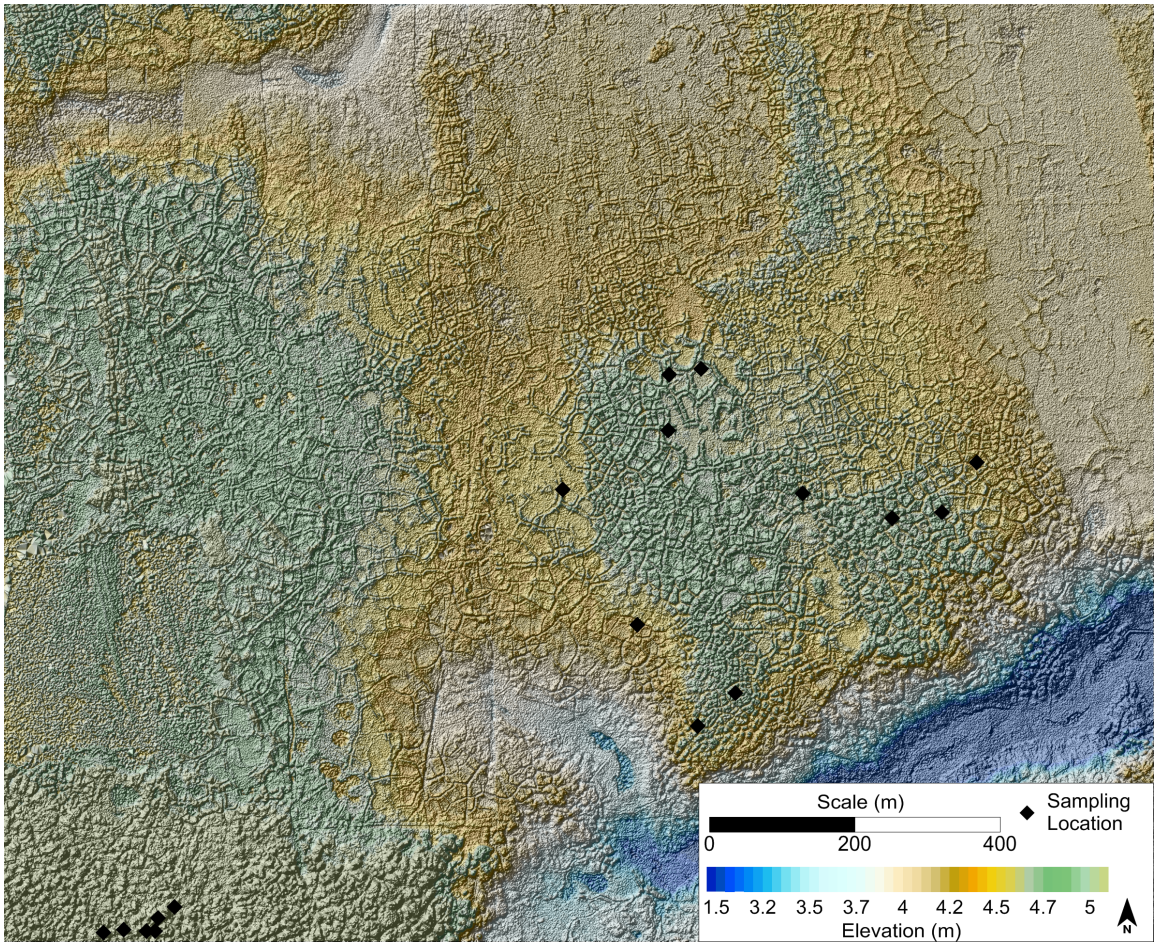

Figure 1. Overview of site locations within the Barrow Environmental Observatory. Polygon sites used in Chapter 3 are clustered in the southwest corner. Other locations were used in Chapter 2 and Chapter 4.

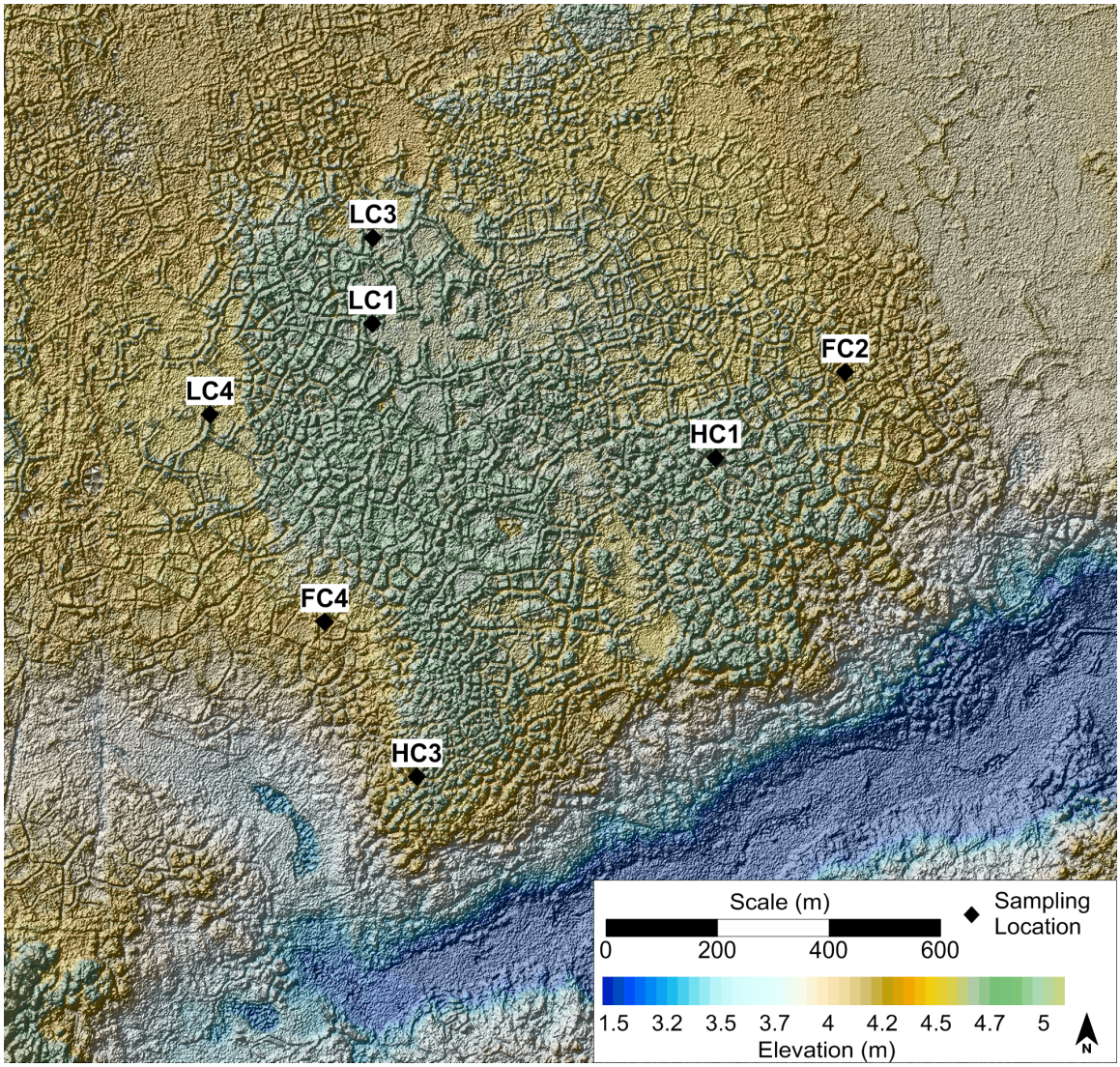

Figure 2. Chapter 2 sampling and measurement locations. Samples were collected from all positions (center, rim, and trough) within individual marked polygons. HC denotes high-centered polygon, FC denotes flat-centered polygon, and LC denotes low-centered polygon.

Figure 3. Chapter 3 experimental blocks. Sampling locations indicate high-centered polygons used as experimental blocks. Each block included high glucose, low glucose, and control mesocosms, as well as duplicate plots for destructive harvests.

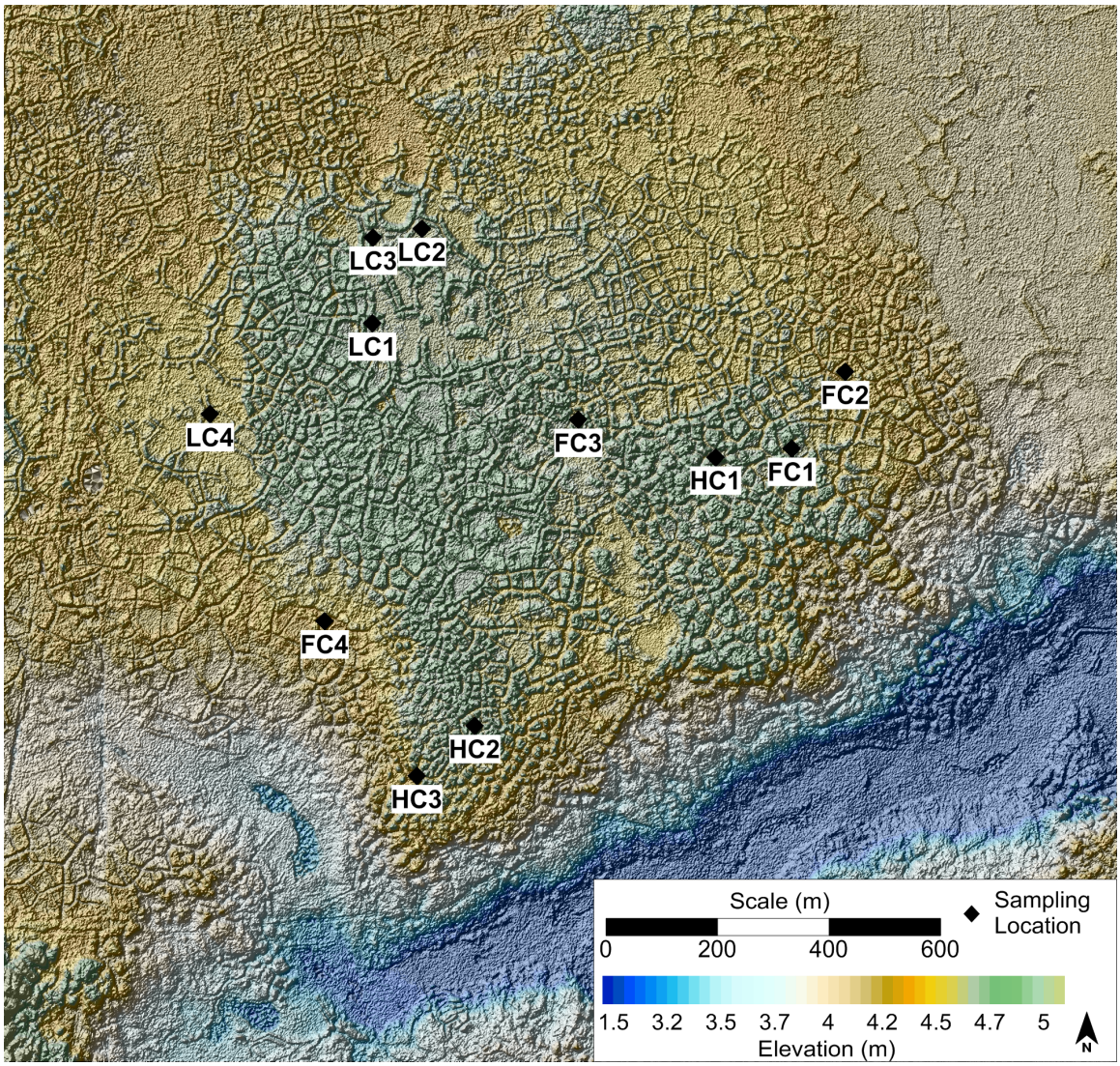

Figure 4. Chapter 4 core sample locations. Soil cores used in incubation studies were collected from the centers of polygons indicated on map. HC denotes high-centered polygon, FC denotes flat-centered polygon, and LC denotes low-centered polygon.

CHAPTER 2: ISOTOPIC INSIGHTS INTO METHANE PRODUCTION, OXIDATION, AND EMISSIONS IN ARCTIC POLYGON TUNDRA

This chapter was previously published as Vaughn LJS, Conrad ME, Bill M, Torn MS (2016) Isotopic insights into methane production, oxidation, and emissions in Arctic polygon tundra. Global Change Biology, *22, 3489-3502. All authors have granted permission for the reproduction of this material. Figure formatting has been modified and text and figures have been moved from the online supporting information into the body of the chapter. In all other ways, this chapter is identical to the original published article.*

Abstract

Arctic wetlands are currently net sources of atmospheric CH_4. Due to their complex biogeochemical controls and high spatial and temporal variability, current net CH_4 emissions and gross CH_4 processes have been difficult to quantify, and their predicted responses to climate change remain uncertain. We investigated CH_4 production, oxidation, and surface emissions in Arctic polygon tundra, across a wet-to-dry permafrost degradation gradient from low-centered (intact) to flat- and high-centered (degraded) polygons. From 3 microtopographic positions (polygon centers, rims, and troughs) along the permafrost degradation gradient, we measured surface CH_4 and CO_2 fluxes, concentrations and stable isotope compositions of CH_4 and DIC at 3 depths in the soil, and soil moisture and temperature. More degraded sites had lower CH_4 emissions, a different primary methanogenic pathway, and greater CH_4 oxidation than intact permafrost sites, to a greater degree than soil moisture or temperature could explain. Surface CH_4 flux decreased from 64 nmol m^{-2} s^{-1} in intact polygons to 7 nmol m^{-2} s^{-1} in degraded polygons, and stable isotope signatures of CH_4 and DIC showed that acetate cleavage dominated CH_4 production in low-centered polygons, while CO_2 reduction was the primary pathway in degraded polygons. We see evidence that differences in water flow and vegetation between intact and degraded polygons contributed to these observations. In contrast with many previous studies, these findings document a mechanism whereby permafrost degradation can lead to local decreases in tundra CH_4 emissions.

Introduction

The high latitude permafrost region plays an important role in the global carbon budget. Historically, this region's soils have been a large net source of atmospheric CH_4, and future CH_4 emissions under climate change remain uncertain. (McGuire *et al.*, 2009, 2012; Mastepanov *et al.*, 2013). Arctic CH_4 emissions are difficult to accurately measure, model, and predict, as complex controls on CH_4 processes generate highly variable CH_4 emissions in both space and time (Whalen & Reeburgh, 1992; Bridgham *et al.*, 2013; Olefeldt *et al.*, 2013). Current estimates of high latitude CH_4 emissions range widely from 9 to 35 Tg CH_4 y^{-} (McGuire *et al.*, 2012), and while most models predict emissions will increase with climate change and associated permafrost degradation (Koven *et al.*, 2011;

Schuur *et al.*, 2013; Lawrence *et al.*, 2015), the magnitude and geographic distribution of this change depend on numerous ecological variables such as soil moisture, water table position, thaw depth, temperature, microbial community, and vegetation composition, stature, and productivity (Wagner *et al.*, 2003; von Fischer *et al.*, 2010; Sturtevant *et al.*, 2012; Tagesson *et al.*, 2012; Mastepanov *et al.*, 2013; Olefeldt *et al.*, 2013). Together, these variables control a suite of processes determining net CH_4 emissions: CH_4 production by methanogenic archaea, CH_4 oxidation by methanotrophic bacteria, and CH_4 transport to the atmosphere (Chanton, 2005; Chanton *et al.*, 2005).

A number of field studies have assessed CH_4 emissions across stages of permafrost degradation, finding that thaw-induced subsidence can increase CH_4 emissions and alter methanogenic pathways (Wickland *et al.*, 2006; Olefeldt *et al.*, 2013; Hodgkins *et al.*, 2014; Johnston *et al.*, 2014; McCalley *et al.*, 2014), with strong correlations between net CH_4 emissions and specific microbial processes (Mondav *et al.*, 2014). These studies underscore the importance of gross metabolic processes as controls on net CH_4 flux and the responsiveness/sensitivity of these processes to thaw-induced changes. Critically, in all of these studies, permafrost thaw increased inundation and active layer thickness due to thermokarst subsidence. In many landscapes, however, permafrost thaw can reduce inundation, as loss of subsurface ice creates drainage channels, redistributing water away from wetlands (Fortier *et al.*, 2007; Godin *et al.*, 2014). Such soil drying and reductions of high latitude wetland area are predicted to be key controls on future Arctic CH_4 emissions (Riordan *et al.*, 2006; Bohn *et al.*, 2007; Avis *et al.*, 2011; Koven *et al.*, 2011), but few field studies have measured CH_4 emissions and their biochemical controls along wet-to-dry gradients of permafrost degradation.

Using a wet-to-dry permafrost degradation gradient, this study evaluates gross CH_4 processes and net CH_4 emissions across stages of drainage and geomorphic succession. In ice wedge polygon tundra in Barrow, Alaska, we combine stable isotope depth profiles with surface flux measurements to investigate process-level controls on surface CH_4 emissions. We ask (1) how do CH_4 production and consumption processes vary across geomorphic and temporal gradients, and (2) how do these subsurface CH_4 processes relate to surface greenhouse gas fluxes? This study makes use of two geomorphic gradients and one temporal gradient: an ice wedge thaw gradient spanning low-centered to flat-centered and high-centered polygons, a finer scale gradient of individual polygon features (centers, rims, and troughs), and a seasonal gradient from July-October.

Covering ~250,000 km^2 throughout the Arctic (Donner *et al.*, 2007), polygon tundra is characterized by ice wedge polygons, microtopographic features ~10-30 m in diameter that are separated by lower-lying, often wet or inundated channels called troughs. These polygons may be classified as low-centered polygons, which have low, wet centers bordered by raised, relatively dry rims; high-centered polygons, with high, well-drained centers and no clear rim delineation; or flat-centered polygons, with intermediate relief between high-centered and low-centered polygons. Polygons form from the growth and thaw of subsurface ice formations known as ice wedges. During earlier polygon successional stages, ice wedges underlie the troughs of low-centered polygons (Brown, 1967), impeding drainage and causing soil uplift through their annual growth and expansion (Drew & Tedrow, 1962). If these primary ice wedges thaw, erosion of polygon

rims can drain the centers of low-centered polygons, leading to the growth of secondary ice wedges and formation of high-centered polygons (Drew & Tedrow, 1962; Billings & Peterson, 1980; MacKay, 2000; Huryn & Hobbie, 2012; Ping *et al.*, 2015). This form of permafrost degradation produces drier equilibrium landscapes, which in the near term are not necessarily accompanied by increased active layer thickness. Between low-centered and high-centered polygons, differences in drainage and subsurface ice properties create strong thermal, hydrological, and geochemical gradients (Liljedahl *et al.*, 2012; Hubbard *et al.*, 2013; Newman *et al.*, 2015; Wainwright *et al.*, 2015).

Succession from low-centered to high-centered polygons has accelerated in Alaska, where thermokarst development over the past three decades has greatly outpaced the historical background landscape succession rate (Jorgenson *et al.*, 2006). Such changes in soil moisture and inundation have large implications for CH_4 emissions. Previous research in polygon-dominated landscapes has found lower CH_4 emissions with decreased soil moisture (Rhew *et al.*, 2007; von Fischer & Hedin, 2007; von Fischer *et al.*, 2010), less inundated area (Sturtevant *et al.*, 2012), and lower water table position (Kutzbach *et al.*, 2004). A more limited set of studies evaluating CH_4 emissions has treated polygon types as distinct geomorphic units, finding higher CH_4 fluxes from low-centered than high-centered polygons (Sachs *et al.*, 2010; Wainwright *et al.*, 2015). No studies to our knowledge, however, have related net CH_4 emissions to gross metabolic CH_4 processes across a range of polygon features.

To investigate CH_4 production, oxidation, and net emissions, this study combines surface trace gas flux measurements with concentrations and stable isotope measurements of CH_4 and co-occurring CO_2. While net CH_4 fluxes are straightforward to measure, the component processes of CH_4 production and oxidation (hereafter referred to as gross processes) cannot be directly observed in situ without an added tracer or inhibitor (Frenzel & Bosse, 1996; von Fischer & Hedin, 2007). The stable isotope compositions of CH_4 provide an indirect approach, as these gross processes fractionate carbon and hydrogen isotopes in characteristic ways. Isotope discrimination during methanogenesis produces CH_4 that is highly depleted in ^{13}C and ^{2}H, whereas CH_4 oxidation enriches the residual CH_4 in the heavier isotopes (Whiticar *et al.*, 1986; Chanton *et al.*, 2005; Hornibrook & Aravena, 2010). Stable isotope analyses have been used to assess CH_4 production pathways (Hornibrook *et al.*, 1997; Conrad, 2005), fractional and absolute CH_4 production and oxidation rates (Liptay *et al.*, 1998; Chanton & Liptay, 2000), CH_4:CO_2 production ratios (Corbett *et al.*, 2013, 2015), and CH_4 transport through hollow plant tissues (Chanton, 2005; Hornibrook, 2009).

Future high latitude CH_4 emissions will depend largely on changes in wetland area (Bohn *et al.*, 2007; Avis *et al.*, 2011; Koven *et al.*, 2011). Field studies are needed to evaluate CH_4 emissions as landscapes become drier or wetter due to thaw, subsidence, and drainage. This study integrates measurements of net CH_4 fluxes and gross CH_4 production and oxidation along a wet-to-dry permafrost degradation gradient in Arctic polygon tundra. Together, this information can be used to identify mechanistic changes underlying net emissions outcomes and identify critical positions in the landscape – particular polygon features that may disproportionately influence the response of landscape-scale CH_4 fluxes to permafrost degradation.

Methods

Site

The Barrow Environmental Observatory (BEO) is located ~6 km east of Barrow, AK (71.3°N, 156.5°W). At the northern tip of Alaska's Arctic coastal plain, Barrow has a maritime climate characterized by long, dry winters and short, moist, cool summers, with a mean annual air temperature of -12°C and mean annual precipitation of 106 mm. Continuous ice-rich permafrost extends to >400 m (Hinkel & Nelson, 2003), overlain by a shallow active layer whose depth varies spatially and interannually from approximately 20 to 60 cm. In and around the BEO, a region of interstitial tundra among thaw lakes and drained thaw lake basins, the land surface has low topographic relief reaching a maximum elevation of ~5 m (Brown *et al.*, 1980; Hubbard *et al.*, 2013), with ~65 % of the ground surface organized into ice wedge polygons (Brown *et al.*, 1980; Lara *et al.*, 2014). Soils in the region are primarily Typic Aquiturbels (53 %), Typic Histoturbels (22 %), and Typic Aquorthels (8.6 %) (Bockheim *et al.*, 1999), formed from late Pleistocene-aged sediments of the Gubik formation (Black, 1964), with low sulfate and nitrate concentrations and abundant iron (Herndon *et al.*, 2015a; Newman *et al.*, 2015). Vegetation cover, height and dominant species vary between polygon types and microtopographic features (Billings & Peterson, 1980; Minke *et al.*, 2009). The most abundant vascular species include the wet tundra graminoids *Carex aquatilis, Eriophorum* species, and *Dupontia fisheri*. Mosses and lichens cover much of the land surface as well, along with limited shrub, forb, and dry tundra graminoid species (Brown *et al.*, 1980; Villarreal *et al.*, 2012).

Field measurements and sample collection

For sample collection and field measurements, we selected seven ice wedge polygons covering a gradient of microtopographic features and subsurface ice properties. We divided these polygons into two categories: (1) low-centered polygons (LC polygons, n=3), with inundated, low-lying centers, large, intact ice wedges and ice-rich permafrost; and (2) flat/high-centered polygons (FHC polygons, n=4), with flat- to high-center relief, smaller, more degraded ice wedges, and lower permafrost ice contents (Hubbard *et al.*, 2013). Within each polygon, we established three 1 × 1 m plots, in the polygon's center, rim, and trough, totaling twenty-one plots. If a FHC polygon lacked a clearly raised rim, we placed the rim plot at the upper limit of the slope between the raised center and the trough. This sampling scheme was thus organized at three levels of spatial resolution: two polygon types (LC polygon and FHC polygon); three polygon positions (center, rim, and trough); and six polygon features, defined as type × position (center, rim, and trough of each polygon type).

From each of these plots, we measured CH_4 flux and ecosystem respiration (R_{eco}), soil moisture, soil temperature, and concentrations and $\delta^{13}C$ of soil pore space CH_4 and CO_2. We measured fluxes of CO_2 and CH_4 on July 10-12, August 7-16, September 4-7, and October 2-4 2013, using opaque static chambers (25 cm diameter, 15-20 cm height). Chambers were tall enough to enclose vegetation and were vented according to Xu *et al.*, (2006) to minimize pressure excursions due to the Venturi effect. In inundated plots, we used a floating chamber whose base extended 4 cm below the water surface. In all other

plots, chambers were seated on PVC bases extending ~15 cm below the soil surface. To minimize disturbance, we installed these bases in June 2013 and left them in place throughout the sampling season. For each flux measurement, we seated the chamber in a 3 cm-deep, water-filled trench in the base's top rim to create an airtight seal. Using a Los Gatos Research, Inc. (LGR) portable Greenhouse Gas Analyzer, we recorded CO_2 and CH_4 concentrations within the chamber over 4-8 minutes, and calculated the flux rate of each gas from the slope of the linear portion of the concentration vs. time curve. As chambers were opaque with no light penetration, measured CO_2 fluxes were equivalent to R_{eco}. Soil moisture and soil temperature were recorded concurrently with each greenhouse gas flux measurement. We measured volumetric water content in the top 10 cm of soil or standing water with a MiniTrase TDR (Soilmoisture Equipment Corp.), and soil temperature at 10cm depth with a thermistor probe. As vegetation and inundation status varied between plots, depths of moisture and temperature measurements were determined from the top of the moss layer, bare soil, or water surface.

On August 7-11 2012, July 12-14 2013, August 10-16 2013, September 3-8 2013, and October 2-5 2013, we collected soil pore water or gas from depths of 10 cm, 20 cm, and the full depth of the thawed layer, approximately 2 cm above the frozen layer. When thaw depth was 20 cm or less, we collected samples from only two depths. Samples were collected using ¼" diameter stainless steel probes inserted in the plots during June 2013, sealed with airtight caps, and left in place throughout the sampling season to reduce disturbance from repeated insertion and removal. At each sampling time, we removed the cap, connected ¼" inner diameter tubing to the probe, and used a peristaltic pump to draw subsurface water or gas through the tubing into a 60 mL syringe. To minimize sample contamination, we assessed tubing and connections for leaks and fully purged the system with soil gas or water before attaching a sampling syringe. If the sampling probe became clogged by thick vegetation or wet soil, we removed the probe, cleaned it, and re-inserted it ~10 cm from the previous insertion point. We filtered water samples in the field through 0.1 mm syringe filters and injected them directly into evacuated glass vials sealed with 14 mm-thick chlorobutyl septa (Bellco Glass, Inc). In cases where syringes contained a mixture of water and gas, we collected and analyzed both sample types. When transferring samples from syringes to vials, precautions were taken to prevent any loss of headspace gas; samples were isolated from the atmosphere using syringe stopcocks and in-line syringe filters, and needles were slowly removed from vials after injection to allow septa to properly to reseal. Samples were stored at 4°C for up to 1 month in Barrow, then transported to Berkeley, CA for analysis. Vials and septa were tested for loss or exchange of headspace gas over this period.

Laboratory analyses and isotope calculations

All isotope and concentration analyses were conducted at the Center for Isotope Geochemistry (CIG) at Lawrence Berkeley National Laboratory, Berkeley, CA. We measured carbon isotope ratios of dissolved inorganic carbon (DIC) in water samples and CO_2 in gas samples using a variation on the technique outlined in Torn *et al.* (2003). We report carbon isotope ratios using the conventional δ-notation relative to Vienna Peedee Belemnite (VPDB), where $\delta^{13}C = (R_{sample}/R_{standard} - 1) \times 1000$ and R is the abundance ratio

of the light to heavy isotope. The carbon isotope ratios of DIC or CO_2 are accurate to ± 0.33 ‰ (1σ) based upon repeated analyses of the laboratory standards.

Carbon isotope ratios of higher concentration CH_4 samples (>300 ppmv) were measured using a Trace Gas Ultra system interfaced to a Delta V Plus mass spectrometer (Thermo Fisher Scientific, Bremen, Germany). CH_4 was chromatographically separated from other gases in the Trace Gas Ultra using an HP-molesieve fused silica capillary column (30 m x 0.320 mm). The CH_4 was then combusted to CO_2 at 1000°C in a capillary ceramic tube loaded with Ni, Cu, and Pt wires, dried and transferred to the IRMS for the carbon isotope measurements. The reproducibility of measured CH_4 $\delta^{13}C$ values using this method is estimated to be ± 0.16 ‰ (1σ) based on repeated analyses of an in-house laboratory standard. The $\delta^{13}C$ values of lower concentration CH_4 samples were analyzed using the Trace Gas pre-concentration system interfaced with a Micromass mass spectrometer as described in Torn *et al.*, (2003). Up to 60 mL of gas was injected into the Trace Gas where CO_2 and water vapor were chemically stripped from the gas before combusting the CH_4 at 1000°C and cryogenically pre-concentrating the resulting CO_2 prior to analysis in the mass spectrometer. The reproducibility of these analyses is ± 0.3 ‰ (1s). $\delta^{13}C$ measurements of CH_4, DIC, and CO_2 were corrected for 3-5 ‰ systematic offsets between the measured $\delta^{13}C$ values of in-house standards and their known isotopic compositions, calibrated with external standards.

Concentrations of CH_4 and CO_2 in gas samples were determined using a 2014 Shimadzu GC. 4.5 mL of gas headspace from sample vials were flushed through a 1 mL stainless steel loop. The two gases were then isolated on a HayeSep-D packed column (4 m x 1/8") and quantified with a flame ionization detector. For water samples, we used Henry's law with measured headspace pressures and water volumes to convert headspace CH_4 concentrations to dissolved CH_4 concentrations. DIC concentrations were calculated from IRMS results, using known sample aliquot volumes and calibrated mass 44 (CO_2) peak areas.

We determined the dominant CH_4 production pathway in each soil profile using two stable isotope abundance metrics. We performed these analyses on the subset of total samples that were collected as water from the full depth of the thawed soil, where CH_4 isotopic compositions were unlikely to have been affected by oxidation, thus representing the values of CH_4 at the time of production. First, acetate cleavage and CO_2 reduction each yield CH_4 whose $\delta^{13}C$ values fall within characteristic ranges (Whiticar *et al.*, 1986; Hornibrook & Aravena, 2010). CH_4 produced by acetate cleavage typically has $\delta^{13}C$ values between -65 and -50 ‰, whereas CH_4 from CO_2 reduction has $\delta^{13}C$ values between -110 and -60 ‰. Second, the apparent fractionation factor ($\alpha_{DIC\text{-}CH4}$) is a measure of the isotope separation between CH_4 and co-occurring DIC (or CO_2) (Hines et al 2008, Whiticar et al 1986, Chanton et al 2006):

$$\alpha_{\text{DIC-CH4}} = \frac{\delta^{13}\text{C} - \text{DIC} + 1000}{\delta^{13}\text{C} - \text{CH}_4 + 1000}$$

$\alpha_{DIC\text{-}CH4}$ is termed *apparent* fractionation, because it is not the fractionation factor for an individual process, but rather a composite metric describing kinetic fractionation during

CO_2 reduction and acetate cleavage (Conrad, 2005) and equilibrium fractionation between carbonate species (Mook *et al.*, 1974). $\alpha_{DIC\text{-}CH4}$ values vary along a continuum between environments where CH_4 is derived entirely from acetate cleavage and those where CH_4 is entirely a product of CO_2 reduction. Measured fractionation factors range from 1.007 to 1.027 for acetate cleavage and from 1.031 to 1.077 for CO_2 reduction (Conrad, 2005), so $\alpha_{DIC\text{-}CH4}$ values increase with increased importance of CO_2 reduction.

Statistical analyses

We analyzed CH_4 flux, R_{eco}, and deep pore water $\delta^{13}C\text{-}CH_4$ individually using linear mixed effects models. We selected models based on Akaike information criterion (AIC) values with backward elimination of random and fixed effects, using significance cutoffs of $p < 0.1$ and $p < 0.05$ for random and fixed effects respectively. p-values for random effects were assessed with likelihood ratio tests, and fixed effect p-values were determined using F tests based on Satterthwaite's approximation for denominator degrees of freedom. We calculated variance inflation factors, using a cutoff of 10 to avoid multicollinearity. Following fixed effect selection, we tested all possible two-way interactions, then performed pairwise comparisons between individual positions, features, or months with Tukey's Honest Significant Difference test, using degrees of freedom from Satterthwaite's approximation. All models included polygon and individual profile as possible random effects. For CH_4 and flux and R_{eco} models, possible fixed effects included polygon type, position, sampling month, top 10 cm soil moisture, and soil temperature at 10 cm depth. For the model of $\delta^{13}C\text{-}CH_4$, possible fixed effects were polygon type, position, and month. We conducted all analyses in R version 3.1.0 "Spring Dance" (2014-04-10), using the packages LME4 (Bates *et al.*, 2014) for linear mixed effects modeling, lmerTest (Kuznetsova *et al.*, 2014) for significance testing and model selection, and multcomp (Hothorn *et al.*, 2008) for pairwise comparisons.

Because CH_4 fluxes, R_{eco} measurements, and soil temperature measurements had skewed distributions, we log-transformed these variables for all statistical analyses. Model estimates and associated p-values reflect these transformed data. In all figures, however, we present non-transformed data to ease visual interpretation.

Results

CH_4 flux and ecosystem respiration

Surface CH_4 flux displayed clear patterns among polygon types and sampling dates (Table 1, Fig. 1a). When observations were averaged across the July-October 2013 season for each polygon type, mean CH_4 fluxes were 6.8 nmol m^{-2} s^{-1} from FHC polygons and 64 nmol m^{-2} s^{-1} from LC polygons. Averaged across all locations, mean CH_4 fluxes peaked in August, increasing from 37 to 45 nmol m^{-2} s^{-1} from July to August, then decreased to 25 nmol m^{-2} s^{-1} in September and 18 nmol m^{-2} s^{-1} in October. LC polygons strongly influenced this temporal trend, their CH_4 flux dropping from 85 nmol m^{-2} s^{-1} in July and August to 39 nmol m^{-2} s^{-1} in October. During this period, FHC polygons' CH_4 flux decreased from only 15 to 3 nmol m^{-2} s^{-1}. To identify important predictors of CH_4 flux, we generated a suite of models including all possible combinations of predictor variables: polygon type, position, soil temperature at 10 cm depth, soil moisture from 0-10 cm depth, and/or sampling month. We then compared these models' AIC values to

select the optimal model. The final model (AIC = 194.4) included polygon type ($p < 0.001$), position ($p < 0.01$), soil temperature ($p < 0.01$), and the interactions between type and position ($p < 0.001$), type and temperature ($p < 0.01$), and temperature and position ($p < 0.01$) as predictor variables, excluding both soil moisture and sampling month (Table 2). With a significance cutoff of $p < 0.05$, CH_4 emissions were significantly different between all but three pairs of polygon features (Table 3). These three exceptions were FHC polygon centers and edges (0.51 and 0.54 nmol m^{-2} s^{-1}), LC polygon centers and troughs (88 and 87 nmol m^{-2} s^{-1}), and LC polygon edges and FHC polygon troughs (17 and 20 nmol m^{-2} s^{-1}). Soil temperature, a significant predictor of CH_4 flux, peaked at the time of peak emissions: July in LC polygons and August in FHC polygons (Fig. 1, Fig. 2).

R_{eco} varied temporally, but did not vary significantly among locations (Table 1, Fig. 1b). The optimal model predicting R_{eco} (AIC = 175) included only sampling month ($p < 0.001$) as a significant fixed effect (Table 2). The highest R_{eco} fluxes were measured in July and August (1.1 and 1.5 μmol m^{-2} s^{-1}, not significantly different), then decreased between August and September to 0.71 μmol m^{-2} s^{-1} ($p < 0.001$), and decreased further from September to October to 0.44 μmol m^{-2} s^{-1} ($p < 0.001$) (Table 3). Notably, FHC polygon troughs had high R_{eco} in July relative to other sampling months and polygon features (Fig. 1b).

Dissolved gas concentrations

For all polygon features, CH_4 concentrations increased with depth in the soil to high concentrations at the frost table (Fig. 3a). These deep CH_4 concentrations were highest in features with saturated or inundated surface soils: LC polygon centers and troughs of both polygon types. Even in FHC polygon centers and rims, however, where net surface CH_4 emissions were near zero, deep CH_4 concentrations were greater than 100 μM. Particularly in polygon rims and troughs, between-type differences in surface CH_4 fluxes were not mirrored by deep CH_4 concentrations. Instead, patterns in surface flux corresponded more closely with concentrations at 10 cm and 20 cm. Of the six polygon features examined, the two with lowest net CH_4 fluxes – centers and rims of FHC polygons – had average 10 cm CH_4 concentrations only slightly greater than zero, at 1.3 and 1.0 μM respectively. Among the remaining four features, the two with highest CH_4 flux – centers and troughs of LC polygons – had high CH_4 concentrations at all depths. Between LC polygon rims and FHC polygon troughs, which had intermediate CH_4 flux rates, LC polygon rims had both higher CH_4 emissions and higher 20 cm CH_4 concentrations. The apparent disconnect between deep dissolved CH_4 and surface emissions suggests that three possible mechanisms underlie differences in net CH_4 fluxes: (1) different CH_4 production rates in shallow soil, (2) different CH_4 transport rates from deep soils to the atmosphere, and/or (3) different oxidation rates in shallow soils.

DIC concentrations varied less than did those of dissolved CH_4 (Fig. 3b). DIC sources may include in situ CO_2 production by root respiration, aerobic or anaerobic respiration, fermentation, or methanogenesis, or transport to the sampling location by diffusion or advection. DIC sinks are primarily diffusion or advection in soil pore water or CH_4 production via CO_2 reduction. Mean DIC concentrations generally increased with depth, but in FHC polygon centers, LC polygon centers, and LC polygon rims, the

highest DIC concentrations were measured at 20 cm, indicating higher CO_2 production at 20 cm than at the frost table.

Methane production pathways

^{13}C abundances in CH_4 and DIC from deep pore water were used to compare CH_4 production pathways among polygon types and positions (Fig. 4), following published approaches (Whiticar *et al.*, 1986; Hornibrook *et al.*, 1997; Conrad, 2005; Hornibrook & Aravena, 2010). Because these samples were collected from deep, saturated soils with limited oxygen availability (Lipson *et al.*, 2012), their $\delta^{13}C$ values reflect CH_4 at the time of production, without isotopic fractionation due to bacterial aerobic CH_4 oxidation. Similarly, we assumed anaerobic CH_4 oxidation had a negligible effect on measured CH_4 isotopes. While anaerobic CH_4 oxidation has been demonstrated in terrestrial soils, concurrent CH_4 production is thought to proceed far more rapidly, particularly in highly methanogenic soils (Blazewicz *et al.*, 2012; Gupta *et al.*, 2013). Additionally, we assumed measured $\delta^{13}C$ values of CH_4 were not affected by kinetic fractionation during transport through the soil profile. Ebullition and advection through plant aerenchyma tissues are non-fractionating processes, but isotopic fractionation may occur during diffusive transport through plants (Popp *et al.*, 1999; Chanton, 2005; Hornibrook, 2009). It is possible that such fractionation may have occurred, isotopically enriching residual soil CH_4. However, studies have shown that this fractionation occurs primarily within the plant tissues themselves, creating a $\delta^{13}C$ gradient between heavier CH_4 within plant aerenchyma and lighter CH_4 emitted from plant tissues to the atmosphere (Chanton *et al.*, 1992a, 1992b; Tyler *et al.*, 1997), with little effect on soil pore space $\delta^{13}C$-CH_4.

Including all sampling dates, deep pore water $\delta^{13}C$-CH_4 values were 17 ‰ enriched from LC polygons relative to FHC polygons ($p << 0.001$), and significant interactions were found between polygon type and position ($p < 0.01$) and between position and sampling month ($p < 0.001$). Between-type differences in $\delta^{13}C$-CH_4 were most pronounced for centers and least pronounced for troughs (Table 2), and $\delta^{13}C$-CH_4 was significantly higher in all 2013 months relative to 8/2012, but did not change significantly over the 2013 season (Table 3). Including all sampling dates, 12 of 12 samples from LC polygon centers (mean $\delta^{13}C$-CH_4 = -52.3 ‰) and 8 of 10 samples from LC polygon troughs (mean $\delta^{13}C$-CH_4 = -59.1 ‰) had $\delta^{13}C$-CH_4 values within the range characteristic of acetate cleavage, -65 to -50 ‰ (Table 1) (Whiticar *et al.*, 1986; Hornibrook & Aravena, 2010). In contrast, 10 of 10 samples from FHC polygon centers (mean $\delta^{13}C$-CH_4 = -79.8 ‰), 8 of 8 samples from FHC polygon rims (mean $\delta^{13}C$-CH_4 = -79.7 ‰), and 6 of 8 samples from FHC troughs (mean $\delta^{13}C$-CH_4 = -68.3 ‰) had $\delta^{13}C$-CH_4 values within the range typical of CO_2 reduction, -110 to -60 ‰ in an ecosystem with C_3 vegetation. $\delta^{13}C$-CH_4 values from LC polygon rims (mean $\delta^{13}C$-CH_4 = -61.3 ‰) were divided among the plausible ranges of both pathways, with 6 samples between -50 and -65 ‰ and 4 samples below -65 ‰, with both methanogenic processes likely operating concurrently (Whiticar, 1999).

The difference in $\delta^{13}C$ between co-occurring CH_4 and DIC, referred to as the apparent fractionation factor, $\alpha_{DIC\text{-}CH4}$, provides an additional line of evidence that the dominant methanogenic pathways differed between polygon types. As shown in crossplots of $\delta^{13}C$-DIC vs. $\delta^{13}C$-CH_4 (Fig. 5), $\alpha_{DIC\text{-}CH4}$ values displayed the same patterns as

$\delta^{13}C$, with acetate cleavage more important in LC than FHC polygons. $\alpha_{DIC\text{-}CH4}$ values from polygon centers and rims showed clear separation between LC and FHC polygons, with values clustering around 1.07 for FHC polygons and around 1.04-1.05 for LC polygons. Troughs displayed some clustering of $\alpha_{DIC\text{-}CH4}$ values for each polygon type, but this separation between $\alpha_{DIC\text{-}CH4}$ ranges of LC and FHC polygons was smaller than in centers and rims.

Apparent fractionation factors between CH_4 and CO_2 below 1.055 are generally thought to indicate acetate cleavage, while values above 1.065 result from CO_2 reduction (Conrad, 2005). In this analysis, $\delta^{13}C$ was measured from bulk DIC rather than CO_2. Because of equilibrium isotopic fractionation between dissolved CO_2 and bicarbonate (Mook *et al.*, 1974), our calculated $\alpha_{DIC\text{-}CH4}$ values may thus be slightly higher than values calculated from $\delta^{13}C\text{-}CO_2$. At the acidic pH range typical of this study site (Zona *et al.*, 2011), H_2CO_3 is the dominant carbonate species, so we would expect only small ^{13}C differences between CO_2 and total DIC. Even so, we conducted an empirical sensitivity analysis to assess the potential for carbonate equilibrium fractionation to influence $\alpha_{DIC\text{-}CH4}$. We measured both $\delta^{13}C$-DIC and vial headspace $\delta^{13}C\text{-}CO_2$ from a subset of deep pore water samples, finding that isotope separation ranged from 0.2 to 5.7 ‰. To account for the maximum possible influence on $\alpha_{DIC\text{-}CH4}$, we applied a 5.7 ‰ correction to $\delta^{13}C$-DIC values to generate a conservative uncertainty band, which decreased calculated $\alpha_{DIC\text{-}CH4}$ values by 0.0065. Including this range of error, $\alpha_{DIC\text{-}CH4}$ values above 1.059 can be interpreted to indicate CO_2 reduction. With these considerations, we still found acetate cleavage dominated all LC polygon features. CO_2 reduction dominated in FHC polygons features, with acetate cleavage more important in FHC polygon troughs than in other FHC polygon features.

$\delta^{13}C$ depth profiles

Depth profiles of $\delta^{13}C\text{-}CH_4$ displayed similar spatial patterns to those of surface fluxes (Fig. 6). $\delta^{13}C$ abundance in pore space CH_4 increased toward the soil surface in four of the six polygon features, a depth trend that would be expected from CH_4 oxidation in shallow soil layers. Among these four features, the difference in mean $\delta^{13}C\text{-}CH_4$ between 10 cm and the frost table was greatest in FHC polygon rims ($\Delta\delta^{13}C$ = 18.4 ‰) and FHC polygon centers ($\Delta\delta^{13}C$ = 13.1 ‰), where surface CH_4 flux rates were lowest. By comparison, LC polygon rims and FHC polygon troughs had both lower surface CH_4 fluxes and lower $\delta^{13}C\text{-}CH_4$ depth gradients ($\Delta\delta^{13}C$ = 7.9 and 5.5 ‰ respectively). The only two features that did not display this $\delta^{13}C\text{-}CH_4$ depth gradient were those with the highest surface CH_4 fluxes: LC polygon centers and LC polygon troughs. There, the highest $\delta^{13}C\text{-}CH_4$ values occurred at 20 cm depth. We note that these two features were inundated at all times, with mean water depths of 8.0 ± 2.1 and 6.7 ± 1.6 cm respectively (data not shown), so their 10 cm samples were collected near the sediment surface or from standing water.

Discussion

High latitude soils are a large source of atmospheric CH_4 (Whalen & Reeburgh, 1992; McGuire *et al.*, 2012; Mastepanov *et al.*, 2013). Current earth system models project that Arctic tundra CH_4 emissions will increase with climate change (Koven *et al.*, 2011;

Lawrence *et al.*, 2015; Schuur *et al.*, 2015). However, landscape-scale processes may influence CH_4 emissions in ways that these models are only beginning to represent. To better understand the relationship between landscape change and CH_4 dynamics, we combined measurements of surface CH_4 flux with subsurface CH_4 concentration and $\delta^{13}C$ profiles to assess (1) how CH_4 production and consumption processes vary with permafrost degradation and microtopography, and (2) how these subsurface processes relate to net CH_4 and CO_2 fluxes. Beyond confirming that CH_4 fluxes from wetter, LC polygons are higher than from drier, FHC polygons, we found that the dominant CH_4 production pathway differed between polygons types, with acetate cleavage more important in high-production locations. In addition, CH_4 emissions decreased with permafrost degradation, beyond the degree that would be expected from moisture changes alone.

CH_4 fluxes were on average ~10 times higher from LC polygons than FHC polygons (Table 1). While soil moisture (Fig. 7) mirrored the positive moisture-CH_4 relationship that has been documented in Arctic polygon tundra (Sachs *et al.*, 2010; Kim, 2015), other tundra types (Torn & Chapin III, 1993; Christensen *et al.*, 1995; McCalley *et al.*, 2014), and thermokarst landscapes (Walter *et al.*, 2007; Desyatkin *et al.*, 2009), the differences in CH_4 flux between polygon types were greater than variations in moisture or temperature alone could explain. Specifically, we found that polygon type, geomorphic position, and soil temperature were the only significant main effects in our optimal model of CH_4 flux (Table 2). Soil moisture did not emerge as a significant predictor variable, but this result does not imply that soil moisture and CH_4 flux were unrelated. Instead, the predictor variables polygon type and position accounted for soil moisture information, along with additional explanatory power that modified the soil moisture-CH_4 flux relationship. Pairwise comparisons between positions within the two polygon types highlight the kind of unexpected feature-level differences that underlie this model result (Table 3). Rims from LC vs. FHC polygons had a 30-fold difference in mean surface CH_4 flux, in spite of comparable temperatures, thaw depths, and moisture contents (Fig. 2, Fig. 7). Similarly, FHC polygon troughs had only ~20 % the CH_4 emissions of LC polygon troughs, with nearly equal soil moisture. In contrast to CH_4 flux, we found that surface CO_2 flux, equivalent to R_{eco}, depended primarily on sampling month, a variable that captures temporal changes in temperature, plant productivity, and microbial community. The R_{eco} model did not find polygon type or position to be significant predictor variables, indicating that carbon availability and turnover did not map strongly to microtopography or permafrost degradation, and thus cannot account for observed CH_4 flux variations.

The dominant CH_4 production pathway differed between high- and low-emission areas. Based on $\delta^{13}C$-CH_4 values, CH_4 production in locations with high surface emissions (e.g., LC polygons and FHC troughs) occurred primarily by acetate cleavage, whereas production in areas with low emissions (FHC polygons) was dominated by CO_2 reduction (Table 2, Fig. 4). The relationship between surface CH_4 flux and deep pore-water $\delta^{13}C$-CH_4 held not only between polygon types but also among positions within each polygon type. We observed the highest and lowest $\delta^{13}C$-CH_4 values in features with the greatest and least CH_4 emissions, respectively (LC polygon centers and troughs vs. FHC polygon centers and rims).

This analysis assumes that measured $\delta^{13}C\text{-}CH_4$ values reflect in situ production, with most sampled CH_4 produced in the soil column, not imported by lateral transport. Supporting evidence includes low flow rates (Liljedahl *et al.*, 2012) relative to in situ cycling rates within LC polygons and low CH_4 concentrations in the runoff of FHC polygon centers.

In addition to our observed relationship between surface CH_4 flux rates and subsurface $\delta^{13}C\text{-}CH_4$ values, several lines of evidence suggest that acetate cleavage is correlated with higher production rates. Acetate cleavage dominates methanogenesis when organic matter is abundant and surface fluxes are high (Galand *et al.*, 2010; Hershey *et al.*, 2014), whereas CO_2 reduction is more important in systems with low organic matter inputs, abundant terminal electron acceptors, and low surface flux rates, such as sulfate-rich marine sediments (Oremland & Taylor, 1978; Crill & Martens, 1983; Whiticar *et al.*, 1986). Similarly, laboratory incubations of high latitude soils have found higher rates of CH_4 production when acetate cleavage rather than CO_2 reduction dominates (Kotsyurbenko *et al.*, 2007; Liebner *et al.*, 2015). Moreover, theoretical reaction stoichiometries also predict acetate cleavage will dominate CH_4 production unless electron flow to methanogens is limited by competition or biochemical inhibition (Conrad, 1999; Ye *et al.*, 2012; Bridgham *et al.*, 2013). Applied to our results, this relationship between CH_4 production rate, CH_4 flux, and $\delta^{13}C\text{-}CH_4$ suggests that CH_4 production rate was an important control on surface CH_4 flux. In locations with high surface CH_4 emissions and less negative $\delta^{13}C\text{-}CH_4$ values such as LC polygon centers and troughs, CH_4 was produced rapidly via acetate cleavage. In FHC polygon centers and rims, acetate oxidation using dissolved oxygen, iron (III), or sulfate may have limited acetate availability to methanogens, leading to low rates of methanogenesis by CO_2 reduction. Thus, we infer that a direct control on net CH_4 emissions, CH_4 production rate, maps predictably to polygonal tundra features.

Previous studies have noted that as much as 90 % of CH_4 production is oxidized in the soil profile (King, 1992; Le Mer & Roger, 2001), so biotic oxidation can be an important determinant of surface CH_4 flux rates. Based on subsurface CH_4 concentrations, flux rates, and $\delta^{13}C\text{-}CH_4$ depth profiles (e.g., Fig. 4, Fig. 6), we find that oxidation plays an important role in some but not all geomorphic positions, with the greatest degree of oxidation in FHC polygon centers and rims and the least influence of oxidation in LC polygon centers and troughs. Deep subsurface CH_4 concentrations indicate that substantial methanogenesis occurred at all locations, even those with minimal net surface emissions. Mediating the relationship between this subsurface production and surface emissions, steep depth profiles of $\delta^{13}C\text{-}CH_4$ show that CH_4 oxidation attenuated this gross production in low-emission sites.

While other studies have used $\delta^{13}C\text{-}CH_4$ depth profiles to derive quantitative estimates of CH_4 oxidation, we chose to use this dataset to infer qualitative differences in CH_4 oxidation (Fig. 6). If the $\delta^{13}C\text{-}CH_4$ of production and the oxidation fractionation factor were known or assumed, $\delta^{13}C\text{-}CH_4$ depth profiles could be used to quantitatively calculate fractional CH_4 oxidation (Liptay *et al.*, 1998; Popp *et al.*, 1999; Corbett *et al.*, 2013). In high latitude wetlands, however, methanogenic pathway and thus its isotopic signature can change with depth, due to shifts in substrate availability, temperature, and pH (Hornibrook *et al.*, 1997; Popp *et al.*, 1999; Hornibrook & Aravena, 2010). Further,

documented fractionation factors for CH_4 oxidation range from 1.003 to 1.031, varying by 0.011 within tundra soils alone (King *et al.*, 1989; Happell *et al.*, 1994; Chanton *et al.*, 2005).

Synthesizing isotope, flux, and moisture data, two clear regimes emerge relating soil moisture, CH_4 production, and CH_4 oxidation to net CH_4 emissions. First, hydrologically isolated features with persistently low soil moisture, FHC polygon centers and rims, were dominated by CO_2 reduction and had steep $\delta^{13}C$-CH_4 depth gradients, indicating that both low production and high oxidation contributed to low surface emissions. Second, persistently inundated features, LC polygon centers and troughs, were dominated by acetate cleavage with small or negative $\delta^{13}C$-CH_4 depth gradients. There, high CH_4 production and low CH_4 oxidation yielded high surface emissions. The two remaining features, FHC polygon troughs and LC polygon rims, do not fit clearly into either of these regimes. With roughly equal surface CH_4 emissions but clear soil moisture differences, these features had notable differences in CH_4 production and CH_4 oxidation. Specifically, LC polygon rims had higher deep $\delta^{13}C$-CH_4 values and steeper $\delta^{13}C$-CH_4 profiles than did FHC polygon troughs, indicating higher rates of both production and oxidation. With comparable, moderate CH_4 fluxes but different soil moisture contents and subsurface processes, these are key locations in the landscape where models based on soil moisture might produce the wrong results, highlighting the importance of other upstream controls on CH_4 production and oxidation.

The two proximate controls on surface CH_4 flux –subsurface CH_4 production and oxidation – are influenced by upstream controls that link landscape processes to microbial activity. Two such upstream controls stand out as particularly important for the relationship between permafrost degradation and CH_4 emissions. First, vegetation influences CH_4 production and oxidation through substrate availability, gas transport, and its influence on subsurface pH, temperature, active layer depth, and other factors (Popp *et al.*, 1999; Chanton, 2005), as seen in a positive relationship between surface CH_4 flux and sedge cover or vegetation stature in wet tundra (Schimel, 1995; Ström *et al.*, 2003; von Fischer *et al.*, 2010; Olefeldt *et al.*, 2013). Based on vegetation surveys near our plots (Appendix A), we find the same qualitative relationship between surface CH_4 emissions and plant community composition or canopy height. In particular, percent cover of *Carex aquatilis*, a sedge with aerenchyma known to transport CH_4 (Popp *et al.*, 1999; Ström *et al.*, 2003; Chanton, 2005), has a spatial pattern matching our stable isotope and surface flux measurements. *Carex* cover and vegetation canopy height are high in LC polygon centers and troughs, intermediate in LC polygon rims and FHC polygon troughs, and low in FHC polygon centers and rims. The observed transition to lower-stature, less *Carex*-dominated vegetation across the permafrost degradation gradient suggests that vegetation changes may play an important role in determining the response of CH_4 emissions to future warming-induced landscape changes.

A second upstream control, soil oxygen status, simultaneously controls substrate availability to methanogens (Chapin III *et al.*, 2011), electron acceptor oxidation state (Cappellen & Wang, 1996), and CH_4 consumption rate (Mancinelli, 1995). In unsaturated soils such as FHC polygon centers and rims, oxygen is readily available, inhibiting CH_4 production and promoting oxidation. In saturated soils, the abundance of dissolved oxygen and other electron accepting species depends on the combined

influence of hydrology and geochemistry (Fiedler *et al.*, 2004; Herndon *et al.*, 2015b). Differences in hydrology and redox-active geochemical species between microtopographic features (Newman *et al.*, 2015) correspond to the CH_4 process differences we observed. Important redox indicators, pore water dissolved oxygen (DO) and sulfate concentrations are higher in high-centered polygon centers and troughs than in any low-centered polygon feature (Newman *et al.*, 2015), and modeled runoff rates from high-centered polygons are nearly twice as high as from low-centered polygons (Liljedahl *et al.*, 2012). These geochemical and hydrologic factors may explain the low CH_4 emissions from FHC troughs relative to other saturated or inundated features. Higher flow into high-centered polygon troughs likely imports DO, which is used to oxidize organic substances, iron, and CH_4 produced at depth where more favorable electron acceptors are depleted. (Iron in particular has been shown to be an important redox control on CH_4 production at this site (Herndon *et al.*, 2015a; Miller *et al.*, 2015), whereas sulfate is less likely to play an important role in anaerobic decomposition at this site because it is present only in low abundance.) Thus, we hypothesize that through its influence on redox, hydrology is an important control on CH_4 production and oxidation, leading to differences in CH_4 emissions among saturated polygon features.

We have shown that CH_4 production, CH_4 oxidation, and net CH_4 emissions depend not only on soil moisture and temperature, but also on microtopographic position along a permafrost degradation gradient. Importantly, redox status and vegetation can vary among sites of similar inundation, influencing substrate availability to methanogens and CH_4 availability to methanotrophs. Indeed, as thermokarst affects hydrology and geochemistry through physical subsidence, it also influences vegetation, with rapid changes in species dominance following drainage and subsidence events (Camill *et al.*, 2001; Christensen *et al.*, 2004; Schuur *et al.*, 2007). In addition, soil carbon chemistry and stocks vary among polygon types and features (Ping *et al.*, 1998; Bockheim *et al.*, 1999; Minke *et al.*, 2009; Zona *et al.*, 2011), as thaw-induced erosion redistributes stocks and alters conditions for organic matter accumulation (Anthony *et al.*, 2014; Godin *et al.*, 2014).

The geomorphic consequences of permafrost degradation depend on the quantity and organization of subsurface ice (Ulrich *et al.*, 2014), overall topography (Czudek & Demek, 1970; Schuur *et al.*, 2007; Godin *et al.*, 2014), and other site-specific properties (Jorgenson *et al.*, 2013). In some instances, permafrost thaw creates lakes or wetlands (Christensen *et al.*, 2004; Wickland *et al.*, 2006; Sannel & Kuhry, 2011; Johnston *et al.*, 2014; Klapstein *et al.*, 2014; Natali *et al.*, 2015), but in other instances it drains these features (Yoshikawa & Hinzman, 2003; Smith, 2005; Schuur *et al.*, 2007). The former of these two outcomes has received more attention with respect to CH_4 emissions, but both have important – and different – implications. Whereas research in other Arctic tundra types has found increased CH_4 emissions with permafrost thaw due to increased inundation following subsidence (Wickland *et al.*, 2006; Johnston *et al.*, 2014; McCalley *et al.*, 2014; Natali *et al.*, 2015), we report opposite trends in both CH_4 flux and water status. Overall, the influence of warming on local CH_4 emissions will depend strongly on the interaction between temperature and hydrology. This interaction may change with time; short-term thaw-driven CH_4 flux increases may be followed by longer-term drainage and drying. Given uncertainties regarding polygon succession processes (Ellis *et al.*, 2008), we

cannot predict the degree to which climate warming and permafrost thaw will shift low-centered polygon terrain to drained, flat-centered and/or high-centered polygons. It is known, however, that such a directional change is possible, shifting polygon landscapes to drier, more high-centered equilibria. This change has recently been observed (Jorgenson *et al.*, 2006; Fortier *et al.*, 2007; Godin *et al.*, 2014), suggesting that continued warming should drive more such landscape transitions. To illustrate the potential magnitude of such changes, if 25 % of our study sites area's low-centered polygons transitioned to flat-centered and high-centered polygons, a change consistent with projected changes in Alaska (Jorgenson *et al.*, 2006), our results imply a 19 % decrease in local CH_4 emissions (Appendix B).

In conclusion, our results demonstrate a local reduction in CH_4 emissions with permafrost degradation, counter to most published studies. We find that CH_4 production and surface flux depend categorically on polygon type, even after accounting for soil moisture differences. These findings show that changes in Arctic CH_4 emissions will be site-specific in sign and magnitude, depending on local geochemistry, topography, and patterns of subsidence. Changes in subsurface ice influence hydrological flows, geochemical redistribution, and physical soil carbon uplift, which in turn affect microbial community and activity as well as vegetation, substrate quantity, accessibility, and chemistry, and electron acceptor availability (Christensen *et al.*, 2004; Fiedler *et al.*, 2004; Fortier *et al.*, 2007; Lantz *et al.*, 2009; Hodgkins *et al.*, 2014; McCalley *et al.*, 2014). These processes control CH_4 emissions directly and indirectly, yet are rarely explicit in conceptual frameworks for sampling and understanding CH_4 fluxes or in numerical models that represent them. Despite common predictions for increased Arctic CH_4 emissions, this study documents a landscape-scale mechanism by which the widespread permafrost thaw predicted throughout the Arctic could result in localized decreases in CH_4 emissions.

References

Anthony KMW, Zimov SA, Grosse G et al. (2014) A shift of thermokarst lakes from carbon sources to sinks during the Holocene epoch. *Nature*, **511**, 452–456.

Avis CA, Weaver AJ, Meissner KJ (2011) Reduction in areal extent of high-latitude wetlands in response to permafrost thaw. *Nature Geoscience*, **4**, 444–448.

Bates D, Maechler M, Bolker BM, Walker S (2014) *lme4: Linear mixed-effects models using Eigen and S4. R package version 1.1-7*.

Billings WD, Peterson KM (1980) Vegetational change and ice-wedge polygons through the thaw-lake cycle in Arctic Alaska. *Arctic and Alpine Research*, 413–432.

Black RF (1964) *Gubik Formation of Quaternary age in northern Alaska*. United States Geological Survey.

Blazewicz SJ, Petersen DG, Waldrop MP, Firestone MK (2012) Anaerobic oxidation of methane in tropical and boreal soils: Ecological significance in terrestrial methane cycling. *Journal of Geophysical Research: Biogeosciences (2005–2012)*, **117**.

Bockheim JG, Everett LR, Hinkel KM, Nelson FE, Brown J (1999) Soil organic carbon storage and distribution in Arctic tundra, Barrow, Alaska. *Soil Science Society of America Journal*, **63**, 934–940.

Bohn TJ, Lettenmaier DP, Sathulur K, Bowling LC, Podest E, McDonald KC, Friborg T (2007) Methane emissions from western Siberian wetlands: heterogeneity and sensitivity to climate change. *Environmental Research Letters*, **2**, 045015.

Bridgham SD, Cadillo-Quiroz H, Keller JK, Zhuang Q (2013) Methane emissions from wetlands: biogeochemical, microbial, and modeling perspectives from local to global scales. *Global Change Biology*, **19**, 1325–1346.

Brown J (1967) Tundra soils formed over ice wedges, northern Alaska. *Soil Science Society of America Journal*, **31**, 686–691.

Brown J, Miller PC, Tieszen LL, Bunnell F (1980) *An Arctic ecosystem : the coastal tundra at Barrow, Alaska*. Dowden, Hutchinson and Ross, Inc., Stroudsburg, Pennsylvania.

Camill P, Lynch JA, Clark JS, Adams JB, Jordan B (2001) Changes in Biomass, Aboveground Net Primary Production, and Peat Accumulation following Permafrost Thaw in the Boreal Peatlands of Manitoba, Canada. *Ecosystems*, **4**, 461–478.

Cappellen PV, Wang Y (1996) Cycling of iron and manganese in surface sediments; a general theory for the coupled transport and reaction of carbon, oxygen, nitrogen, sulfur, iron, and manganese. *American Journal of Science*, **296**, 197–243.

Chanton JP (2005) The effect of gas transport on the isotope signature of methane in wetlands. *Organic Geochemistry*, **36**, 753–768.

Chanton J, Liptay K (2000) Seasonal variation in methane oxidation in a landfill cover soil as determined by an in situ stable isotope technique. *Global Biogeochemical Cycles*, **14**, 51–60.

Chanton JP, Martens CS, Kelley CA, Crill PM, Showers WJ (1992a) Methane transport mechanisms and isotopic fractionation in emergent macrophytes of an Alaskan tundra lake. *Journal of Geophysical Research: Atmospheres*, **97**, 16681–16688.

Chanton JP, Whiting GJ, Showers WJ, Crill PM (1992b) Methane flux from Peltandra virginica: stable isotope tracing and chamber effects. *Global Biogeochemical Cycles*, **6**, 15–31.

Chanton JP, Chasar LC, Glaser P, Siegel D (2005) Carbon and hydrogen isotopic effects in microbial methane from terrestrial environments. *Stable Isotopes and Biosphere-Atmosphere Interactions, Physiological Ecology Series*, 85–105.

Chapin III FS, Matson PA, Vitousek P (2011) *Principles of Terrestrial Ecosystem Ecology*. Springer Science & Business Media, 537 pp.

Christensen TR, Jonasson S, Callaghan TV, Havström M (1995) Spatial variation in high-latitude methane flux along a transect across Siberian and European tundra environments. *Journal of Geophysical Research: Atmospheres*, **100**, 21035–21045.

Christensen TR, Johansson T, Åkerman HJ et al. (2004) Thawing sub-arctic permafrost: Effects on vegetation and methane emissions. *Geophysical Research Letters*, **31**, L04501.

Conrad R (1999) Contribution of hydrogen to methane production and control of hydrogen concentrations in methanogenic soils and sediments. *FEMS Microbiology Ecology*, **28**, 193–202.

Conrad R (2005) Quantification of methanogenic pathways using stable carbon isotopic signatures: a review and a proposal. *Organic Geochemistry*, **36**, 739–752.

Corbett JE, Tfaily MM, Burdige DJ, Cooper WT, Glaser PH, Chanton JP (2013) Partitioning pathways of CO2 production in peatlands with stable carbon isotopes. *Biogeochemistry*, **114**, 327–340.

Corbett JE, Tfaily MM, Burdige DJ, Glaser PH, Chanton JP (2015) The relative importance of methanogenesis in the decomposition of organic matter in northern peatlands. *Journal of Geophysical Research: Biogeosciences*, 2014JG002797.

Crill PM, Martens CS (1983) Spatial and temporal fluctuations of methane production in anoxic coastal marine sediments. *Limnology and Oceanography*, **28**, 1117–1130.

Czudek T, Demek J (1970) Thermokarst in Siberia and its influence on the development of lowland relief. *Quaternary Research*, **1**, 103–120.

Desyatkin AR, Takakai F, Fedorov PP, Nikolaeva MC, Desyatkin RV, Hatano R (2009) CH4 emission from different stages of thermokarst formation in Central Yakutia, East Siberia. *Soil Science and Plant Nutrition*, **55**, 558–570.

Donner N, Karpov NS, de Klerk P, Joosten H (2007) Distribution, diversity, development and dynamics of polygon mires: examples from Northeast Yakutia (Siberia).

Drew JV, Tedrow JCF (1962) Arctic Soil Classification and Patterned Ground. *Arctic*, **15**, 109–116.

Ellis CJ, Rochefort L, Gauthier G, Pienitz R (2008) Paleoecological Evidence for Transitions between Contrasting Landforms in a Polygon-Patterned High Arctic Wetland. *Arctic, Antarctic, and Alpine Research*, **40**, 624–637.

Fiedler S, Wagner D, Kutzbach L, Pfeiffer E-M (2004) Element redistribution along hydraulic and redox gradients of low-centered polygons, Lena Delta, northern Siberia. *Soil Science Society of America Journal*, **68**, 1002–1011.

Von Fischer JC, Hedin LO (2007) Controls on soil methane fluxes: Tests of biophysical mechanisms using stable isotope tracers. *Global Biogeochemical Cycles*, **21**, GB2007.

Von Fischer JC, Rhew RC, Ames GM, Fosdick BK, von Fischer PE (2010) Vegetation height and other controls of spatial variability in methane emissions from the Arctic coastal tundra at Barrow, Alaska. *Journal of Geophysical Research*, **115**.

Fortier D, Allard M, Shur Y (2007) Observation of rapid drainage system development by thermal erosion of ice wedges on Bylot Island, Canadian Arctic Archipelago. *Permafrost and Periglacial Processes*, **18**, 229–243.
Frenzel P, Bosse U (1996) Methyl fluoride, an inhibitor of methane oxidation and methane production. *FEMS Microbiology Ecology*, **21**, 25–36.
Galand PE, Yrjälä K, Conrad R (2010) Stable carbon isotope fractionation during methanogenesis in three boreal peatland ecosystems. *Biogeosciences*, **7**, 3893–3900.
Godin E, Fortier D, Coulombe S (2014) Effects of thermo-erosion gullying on hydrologic flow networks, discharge and soil loss. *Environmental Research Letters*, **9**, 105010.
Gupta V, Smemo KA, Yavitt JB, Fowle D, Branfireun B, Basiliko N (2013) Stable Isotopes Reveal Widespread Anaerobic Methane Oxidation Across Latitude and Peatland Type. *Environmental Science & Technology*, **47**, 8273–8279.
Happell JD, Chanton JP, Showers WS (1994) The influence of methane oxidation on the stable isotopic composition of methane emitted from Florida swamp forests. *Geochimica et Cosmochimica Acta*, **58**, 4377–4388.
Herndon EM, Mann BF, Chowdhury TR et al. (2015a) Pathways of anaerobic organic matter decomposition in tundra soils from Barrow, Alaska: Biogeochemistry of Anoxic Arctic Tundra. *Journal of Geophysical Research: Biogeosciences*, n/a–n/a.
Herndon EM, Yang Z, Bargar J et al. (2015b) Geochemical drivers of organic matter decomposition in arctic tundra soils. *Biogeochemistry*, **126**, 397–414.
Hershey AE, Northington RM, Whalen SC (2014) Substrate limitation of sediment methane flux, methane oxidation and use of stable isotopes for assessing methanogenesis pathways in a small arctic lake. *Biogeochemistry*, **117**, 325–336.
Hinkel KM, Nelson FE (2003) Spatial and temporal patterns of active layer thickness at Circumpolar Active Layer Monitoring (CALM) sites in northern Alaska, 1995–2000. *Journal of Geophysical Research: Atmospheres*, **108**, 8168.
Hodgkins SB, Tfaily MM, McCalley CK et al. (2014) Changes in peat chemistry associated with permafrost thaw increase greenhouse gas production. *Proceedings of the National Academy of Sciences*, **111**, 5819–5824.
Hornibrook ERC (2009) The Stable Carbon Isotope Composition of Methane Produced and Emitted from Northern Peatlands. In: *Carbon Cycling in Northern Peatlands* (eds Baird AJ, Belyea LR, Comas X, Reeve AS, Slater LD), pp. 187–203. American Geophysical Union.
Hornibrook ER, Aravena R (2010) 6 Isotopes and Methane Cycling. *Environmental Isotopes in Biodegradation and Bioremediation*, 167.
Hornibrook ERC, Longstaffe FJ, Fyfe WS (1997) Spatial distribution of microbial methane production pathways in temperate zone wetland soils: Stable carbon and hydrogen isotope evidence. *Geochimica et Cosmochimica Acta*, **61**, 745–753.
Hothorn T, Bretz F, Westfall P (2008) Simultaneous Inference in General Parametric Models. *Biometrical Journal*, **50**, 346–363.
Hubbard SS, Gangodagamage C, Dafflon B et al. (2013) Quantifying and relating land-surface and subsurface variability in permafrost environments using LiDAR and surface geophysical datasets. *Hydrogeology Journal*, **21**, 149–169.
Huryn A, Hobbie J (2012) *Land of Extremes: A Natural History of the Arctic North Slope of Alaska*. University of Alaska Press, 329 pp.

Johnston CE, Ewing SA, Harden JW et al. (2014) Effect of permafrost thaw on CO2 and CH4 exchange in a western Alaska peatland chronosequence. *Environmental Research Letters*, **9**, 085004.

Jorgenson MT, Shur YL, Pullman ER (2006) Abrupt increase in permafrost degradation in Arctic Alaska. *Geophysical Research Letters*, **33**.

Jorgenson MT, Harden J, Kanevskiy M et al. (2013) Reorganization of vegetation, hydrology and soil carbon after permafrost degradation across heterogeneous boreal landscapes. *Environmental Research Letters*, **8**, 035017.

Kim Y (2015) Effect of thaw depth on fluxes of CO2 and CH4 in manipulated Arctic coastal tundra of Barrow, Alaska. *Science of The Total Environment*, **505**, 385–389.

King GM (1992) Ecological aspects of methane oxidation, a key determinant of global methane dynamics. In: *Advances in microbial ecology*, pp. 431–468. Springer.

King SL, Quay PD, Lansdown JM (1989) The 13C/12C kinetic isotope effect for soil oxidation of methane at ambient atmospheric concentrations. *Journal of Geophysical Research: Atmospheres*, **94**, 18273–18277.

Klapstein SJ, Turetsky MR, McGuire AD et al. (2014) Controls on methane released through ebullition in peatlands affected by permafrost degradation. *Journal of Geophysical Research: Biogeosciences*, **119**, 2013JG002441.

Kotsyurbenko OR, Friedrich MW, Simankova MV, Nozhevnikova AN, Golyshin PN, Timmis KN, Conrad R (2007) Shift from Acetoclastic to H2-Dependent Methanogenesis in a West Siberian Peat Bog at Low pH Values and Isolation of an Acidophilic Methanobacterium Strain. *Applied and Environmental Microbiology*, **73**, 2344–2348.

Koven CD, Ringeval B, Friedlingstein P et al. (2011) Permafrost carbon-climate feedbacks accelerate global warming. *Proceedings of the National Academy of Sciences*.

Kutzbach L, Wagner D, Pfeiffer E-M (2004) Effect of microrelief and vegetation on methane emission from wet polygonal tundra, Lena Delta, Northern Siberia. *Biogeochemistry*, **69**, 341–362.

Kuznetsova A, Brockhoff PB, Christensen RHB (2014) *lmerTest: Tests for random and fixed effects for linear mixed effect models (lmer objects of lme4 package).. R package version 2.0-11*.

Lantz TC, Kokelj SV, Gergel SE, Henry GHR (2009) Relative impacts of disturbance and temperature: persistent changes in microenvironment and vegetation in retrogressive thaw slumps. *Global Change Biology*, **15**, 1664–1675.

Lara MJ, McGuire AD, Euskirchen ES et al. (2014) Polygonal tundra geomorphological change in response to warming alters future CO2 and CH4 flux on the Barrow Peninsula. *Global Change Biology*, n/a–n/a.

Lawrence DM, Koven CD, Swenson SC, Riley WJ, Slater AG (2015) Permafrost thaw and resulting soil moisture changes regulate projected high-latitude CO_2 and CH_4 emissions. *Environmental Research Letters*, **10**, 094011.

Liebner S, Ganzert L, Kiss A, Yang S, Wagner D, Svenning MM (2015) Shifts in methanogenic community composition and methane fluxes along the degradation of discontinuous permafrost. *Terrestrial Microbiology*, 356.

Liljedahl AK, Hinzman LD, Schulla J (2012) Ice-wedge polygon type controls low-gradient watershed-scale hydrology. In: *Tenth International Conference on Permafrost, Salekhard, Russia*.

Lipson DA, Zona D, Raab TK, Bozzolo F, Mauritz M, Oechel WC (2012) Water table height and microtopography control Biogeochemical cycling in an Arctic coastal tundra Ecosystem. *Biogeosciences*, **9**, 577–591.

Liptay K, Chanton J, Czepiel P, Mosher B (1998) Use of stable isotopes to determine methane oxidation in landfill cover soils. *Journal of Geophysical Research: Atmospheres*, **103**, 8243–8250.

MacKay JR (2000) Thermally induced movements in ice-wedge polygons, western arctic coast: a long-term study. *Géographie physique et Quaternaire*, **54**, 41.

Mancinelli RL (1995) The regulation of methane oxidation in soil. *Annual Reviews in Microbiology*, **49**, 581–605.

Mastepanov M, Sigsgaard C, Tagesson T, Ström L, Tamstorf MP, Lund M, Christensen TR (2013) Revisiting factors controlling methane emissions from high-Arctic tundra. *Biogeosciences*, **10**, 5139–5158.

McCalley CK, Woodcroft BJ, Hodgkins SB et al. (2014) Methane dynamics regulated by microbial community response to permafrost thaw. *Nature*, **514**, 478–481.

McGuire AD, Anderson LG, Christensen TR et al. (2009) Sensitivity of the carbon cycle in the Arctic to climate change. *Ecological Monographs*, **79**, 523–555.

McGuire AD, Christensen TR, Hayes D et al. (2012) An assessment of the carbon balance of Arctic tundra: comparisons among observations, process models, and atmospheric inversions. *Biogeosciences*, **9**, 3185–3204.

Le Mer J, Roger P (2001) Production, oxidation, emission and consumption of methane by soils: a review. *Eur. J. Soil Biol*, **37**, 25–50.

Miller KE, Lai C-T, Friedman ES, Angenent LT, Lipson DA (2015) Methane suppression by iron and humic acids in soils of the Arctic Coastal Plain. *Soil Biology and Biochemistry*, **83**, 176–183.

Minke M, Donner N, Karpov N, de Klerk P, Joosten H (2009) Patterns in vegetation composition, surface height and thaw depth in polygon mires in the Yakutian Arctic (NE Siberia): a microtopographical characterisation of the active layer. *Permafrost and Periglacial Processes*, **20**, 357–368.

Mondav R, Woodcroft BJ, Kim E-H et al. (2014) Discovery of a novel methanogen prevalent in thawing permafrost. *Nature Communications*, **5**.

Mook WG, Bommerson JC, Staverman WH (1974) Carbon isotope fractionation between dissolved bicarbonate and gaseous carbon dioxide. *Earth and Planetary Science Letters*, **22**, 169–176.

Natali SM, Schuur EAG, Mauritz M et al. (2015) Permafrost thaw and soil moisture driving CO_2 and CH_4 release from upland tundra. *Journal of Geophysical Research: Biogeosciences*, n/a–n/a.

Newman BD, Throckmorton HM, Graham DE et al. (2015) Microtopographic and depth controls on active layer chemistry in Arctic polygonal ground. *Geophysical Research Letters*, 2014GL062804.

Olefeldt D, Turetsky MR, Crill PM, McGuire AD (2013) Environmental and physical controls on northern terrestrial methane emissions across permafrost zones. *Global change biology*, **19**, 589–603.

Oremland RS, Taylor BF (1978) Sulfate reduction and methanogenesis in marine sediments. *Geochimica et Cosmochimica Acta*, **42**, 209–214.

Ping CL, Bockheim JG, Kimble JM, Michaelson GJ, Walker DA (1998) Characteristics of cryogenic soils along a latitudinal transect in Arctic Alaska. *Journal of Geophysical Research: Atmospheres (1984–2012)*, **103**, 28917–28928.
Ping CL, Jastrow JD, Jorgenson MT, Michaelson GJ, Shur YL (2015) Permafrost soils and carbon cycling. *SOIL*, **1**, 147–171.
Popp TJ, Chanton JP, Whiting GJ, Grant N (1999) Methane stable isotope distribution at a Carex dominated fen in north central Alberta. *Global Biogeochemical Cycles*, **13**, 1063–1077.
Rhew RC, Teh YA, Abel T (2007) Methyl halide and methane fluxes in the northern Alaskan coastal tundra. *Journal of Geophysical Research*, **112**.
Riordan B, Verbyla D, McGuire AD (2006) Shrinking ponds in subarctic Alaska based on 1950–2002 remotely sensed images. *Journal of Geophysical Research: Biogeosciences*, **111**, G04002.
Sachs T, Giebels M, Boike J, Kutzbach L (2010) Environmental controls on CH4 emission from polygonal tundra on the microsite scale in the Lena river delta, Siberia: CONTROLS ON TUNDRA CH4 FLUX AND SCALING. *Global Change Biology*, no–no.
Sannel ABK, Kuhry P (2011) Warming-induced destabilization of peat plateau/thermokarst lake complexes. *Journal of Geophysical Research: Biogeosciences*, **116**, G03035.
Schimel JP (1995) Plant transport and methane production as controls on methane flux from arctic wet meadow tundra. *Biogeochemistry*, **28**, 183–200.
Schuur EAG, Crummer KG, Vogel JG, Mack MC (2007) Plant Species Composition and Productivity following Permafrost Thaw and Thermokarst in Alaskan Tundra. *Ecosystems*, **10**, 280–292.
Schuur E a. G, Abbott BW, Bowden WB et al. (2013) Expert assessment of vulnerability of permafrost carbon to climate change. *Climatic Change*, **119**, 359–374.
Schuur E a. G, McGuire AD, Schädel C et al. (2015) Climate change and the permafrost carbon feedback. *Nature*, **520**, 171–179.
Smith LC (2005) Disappearing Arctic Lakes. *Science*, **308**, 1429–1429.
Ström L, Ekberg A, Mastepanov M, Røjle Christensen T (2003) The effect of vascular plants on carbon turnover and methane emissions from a tundra wetland. *Global Change Biology*, **9**, 1185–1192.
Sturtevant CS, Oechel WC, Zona D, Kim Y, Emerson CE (2012) Soil moisture control over autumn season methane flux, Arctic Coastal Plain of Alaska. *Biogeosciences*, **9**, 1423–1440.
Tagesson T, Mölder M, Mastepanov M et al. (2012) Land-atmosphere exchange of methane from soil thawing to soil freezing in a high-Arctic wet tundra ecosystem. *Global Change Biology*, **18**, 1928–1940.
Torn MS, Chapin III FS (1993) Environmental and biotic controls over methane flux from Arctic tundra. *Chemosphere*, **26**, 357–368.
Torn MS, Davis S, Bird JA, Shaw MR, Conrad ME (2003) Automated analysis of 13C/12C ratios in CO2 and dissolved inorganic carbon for ecological and environmental applications. *Rapid Communications in Mass Spectrometry*, **17**, 2675–2682.
Tyler SC, Bilek RS, Sass RL, Fisher FM (1997) Methane oxidation and pathways of production in a Texas paddy field deduced from measurements of flux, δl3C, and δD of CH4. *Global Biogeochemical Cycles*, **11**, 323–348.

Ulrich M, Grosse G, Strauss J, Schirrmeister L (2014) Quantifying Wedge-Ice Volumes in Yedoma and Thermokarst Basin Deposits. *Permafrost and Periglacial Processes*, **25**, 151–161.

Villarreal S, Hollister RD, Johnson DR, Lara MJ, Webber PJ, Tweedie CE (2012) Tundra vegetation change near Barrow, Alaska (1972–2010). *Environmental Research Letters*, **7**, 015508.

Wagner D, Kobabe S, Pfeiffer E-M, Hubberten H-W (2003) Microbial controls on methane fluxes from a polygonal tundra of the Lena Delta, Siberia. *Permafrost and Periglacial Processes*, **14**, 173–185.

Wainwright HM, Dafflon B, Smith LJ et al. (2015) Identifying multiscale zonation and assessing the relative importance of polygon geomorphology on carbon fluxes in an Arctic Tundra Ecosystem. *Journal of Geophysical Research: Biogeosciences*, 2014JG002799.

Walter KM, Edwards ME, Grosse G, Zimov SA, Chapin FS (2007) Thermokarst Lakes as a Source of Atmospheric CH4 During the Last Deglaciation. *Science*, **318**, 633–636.

Whalen SC, Reeburgh WS (1992) Interannual variations in tundra methane emission: A 4-year time series at fixed sites. *Global Biogeochemical Cycles*, **6**, 139–159.

Whiticar MJ (1999) Carbon and hydrogen isotope systematics of bacterial formation and oxidation of methane. *Chemical Geology*, **161**, 291–314.

Whiticar MJ, Faber E, Schoell M (1986) Biogenic methane formation in marine and freshwater environments: CO< sub> 2</sub> reduction< i> vs</i>. acetate fermentation—Isotope evidence. *Geochimica et Cosmochimica Acta*, **50**, 693–709.

Wickland KP, Striegl RG, Neff JC, Sachs T (2006) Effects of permafrost melting on CO2 and CH4 exchange of a poorly drained black spruce lowland. *Journal of Geophysical Research: Biogeosciences*, **111**, G02011.

Xu L, Furtaw MD, Madsen RA, Garcia RL, Anderson DJ, McDermitt DK (2006) On maintaining pressure equilibrium between a soil CO_2 flux chamber and the ambient air. *Journal of Geophysical Research*, **111**.

Ye R, Jin Q, Bohannan B, Keller JK, McAllister SA, Bridgham SD (2012) pH controls over anaerobic carbon mineralization, the efficiency of methane production, and methanogenic pathways in peatlands across an ombrotrophic–minerotrophic gradient. *Soil Biology and Biochemistry*, **54**, 36–47.

Yoshikawa K, Hinzman LD (2003) Shrinking thermokarst ponds and groundwater dynamics in discontinuous permafrost near council, Alaska. *Permafrost and Periglacial Processes*, **14**, 151–160.

Zona D, Lipson DA, Zulueta RC, Oberbauer SF, Oechel WC (2011) Microtopographic controls on ecosystem functioning in the Arctic Coastal Plain. *Journal of Geophysical Research*, **116**.

Tables and Figures

Table 1
Mean surface greenhouse gas fluxes and deep pore water $\delta^{13}CH_4$

Polygon type	Feature	CH_4 flux (nmol m^{-2} s^{-1})			CO_2 flux (μmol m^{-2} s^{-1})			$\delta^{13}CH_4$* (‰)		
		mean	sd	n	mean	sd	n	mean	sd	n
Low-centered	LC Center	88.4	46	12	0.727	0.37	12	-52.3	4.7	12
	LC Rim	17.4	13	12	0.771	0.54	12	-61.3	7.9	10
	LC Trough	87.0	50	12	0.843	0.61	12	-59.1	6.8	10
	All LC positions	64.3	52	36	0.780	0.50	36	-57.2	7.4	32
Flat/high-centered	FHC Center	0.505	1.0	17	0.805	0.59	17	-79.8	4.7	10
	FHC Rim	0.538	0.95	16	0.940	0.81	16	-79.7	5.8	8
	FHC Trough	19.6	20	16	1.39	0.93	16	-68.3	4.5	8
	All FHC positions	6.75	14	49	1.04	0.81	49	-76.2	7.2	26

Note: Values are averages across all sampling dates for each polygon type and feature. $\delta^{13}C$ values were measured from water samples collected at the frost table in August 2012 and July – October 2013.

Table 2
Fixed effects included in linear mixed effects models for CH_4 flux, CO_2 flux, and deep pore water $\delta^{13}CH_4$

Model	Fixed effect	DF	F value	Pr > F
CH_4 flux (AIC = 168.8)	polygon type	56.782	54.819	6.894e-10 ***
	$\log_{10}$(temperature)	56.405	10.729	0.001807 **
	position	51.832	6.052	0.004342 **
	type × position	21.902	15.157	7.377e-05 ***
	type × $\log_{10}$(temperature)	56.180	8.634	0.004778 **
	position × $\log_{10}$(temperature)	56.926	5.763	0.005256 **
CO_2 flux (AIC = 175.0)	month	64.041	28.946	5.997e-12 ***
$\delta^{13}CH_4$ (AIC = 369.0)	polygon type	18.515	71.717	8.694e-08 ***
	position	19.038	2.536	0.1056001
	month	40.126	8.906	3.034e-05 ***
	type × position	18.529	9.856	0.0012151 **
	month × position	39.756	4.216	0.0009954 ***

Significance codes: 0 *** 0.001 ** 0.01 * 0.05 . 1

Table 3
Results of Tukey's Honest Significant Difference test for linear mixed effects models predicting CH_4 flux, CO_2 flux, and $\delta^{13}CH_4$

Model	Predictor variable	Contrasted levels	t value	Pr > |t|
CH_4 flux	Type × position	LC center – FHC center	11.028	<0.001 ***
	Type × position	LC rim – FHC center	7.417	<0.001 ***
	Type × position	LC trough – FHC center	10.992	<0.001 ***
	Type × position	FHC rim – FHC center	-0.020	1.0000
	Type × position	FHC trough – FHC center	7.873	<0.001 ***
	Type × position	LC rim – LC center	-3.474	0.0229 *
	Type × position	LC trough – LC center	-0.045	1.0000
	Type × position	FHC rim – LC center	-11.077	<0.001 ***
	Type × position	FHC trough – LC center	-3.745	0.0126 *
	Type × position	LC rim – FHC rim	7.415	<0.001 ***
	Type × position	LC trough – FHC rim	11.037	<0.001 ***
	Type × position	FHC trough – FHC rim	7.907	<0.001 ***
	Type × position	LC trough – LC rim	3.431	0.0252 *
	Type × position	FHC trough – LC rim	-0.031	1.0000
	Type × position	LC trough – FHC trough	3.698	0.0139 *
CO_2 flux	Sampling month	8/2013 – 7/2013	1.714	0.3251
	Sampling month	9/2013 – 7/2013	-2.482	0.0727 .
	Sampling month	10/2013 – 7/2013	-7.007	<0.001 ***
	Sampling month	9/2013 – 8/2013	-4.196	<0.001 ***
	Sampling month	10/2013 – 8/2013	-8.739	<0.001 ***
	Sampling month	10/2013 – 9/2013	-4.499	<0.001 ***
$\delta^{13}CH_4$	Position	rim – center	0.427	0.90493
	Position	trough – center	3.706	0.00515 **
	Position	trough – rim	3.365	0.01031 *
	Sampling month	7/2013 – 8/2012	4.253	0.00116 **
	Sampling month	8/2013 – 8/2012	3.407	0.01236 *
	Sampling month	9/2013 – 8/2012	2.979	0.03674 *
	Sampling month	10/2013 – 8/2012	2.846	0.05068 .
	Sampling month	8/2013 – 7/2013	-1.389	0.63596

(table continues)

Model	Predictor variable	Contrasted levels	t value	Pr > |t|
	Sampling month	9/2013 – 8/2013	-1.178	0.76153
	Sampling month	10/2013 – 7/2013	-1.431	0.60908
$\delta^{13}CH_4$	Sampling month	9/2013 – 8/2013	-0.012	1.00000
	Sampling month	10/2013 – 8/2013	-0.231	0.99934
	Sampling month	10/2013 – 9/2013	-0.190	0.99969

Significance codes: 0 *** 0.001 ** 0.01 * 0.05 . 1

Note: p-values were calculated using Satterthwaite's approximation for denominator degrees of freedom

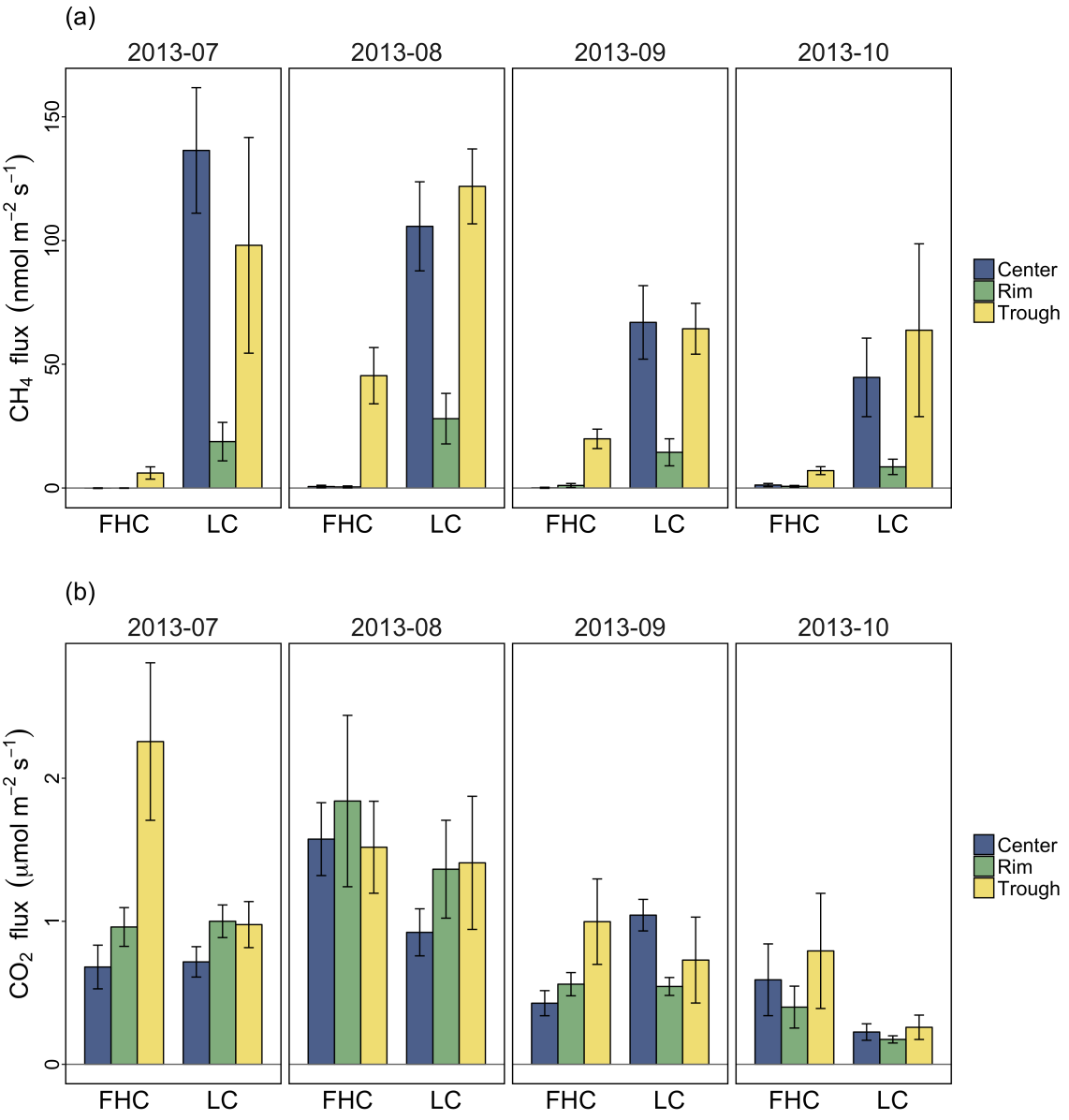

Figure 1. Greenhouse gas emissions, classified by polygon type, position, and measurement month. (a) Net CH_4 flux in nmol CH_4 m^{-2} s^{-1} and (b) ecosystem respiration in μmol CO_2 m^{-2} s^{-1} were measured from each feature of 4 flat/high-centered (FHC) and 3 low-centered (LC) polygons. Standard errors were calculated from field replicates.

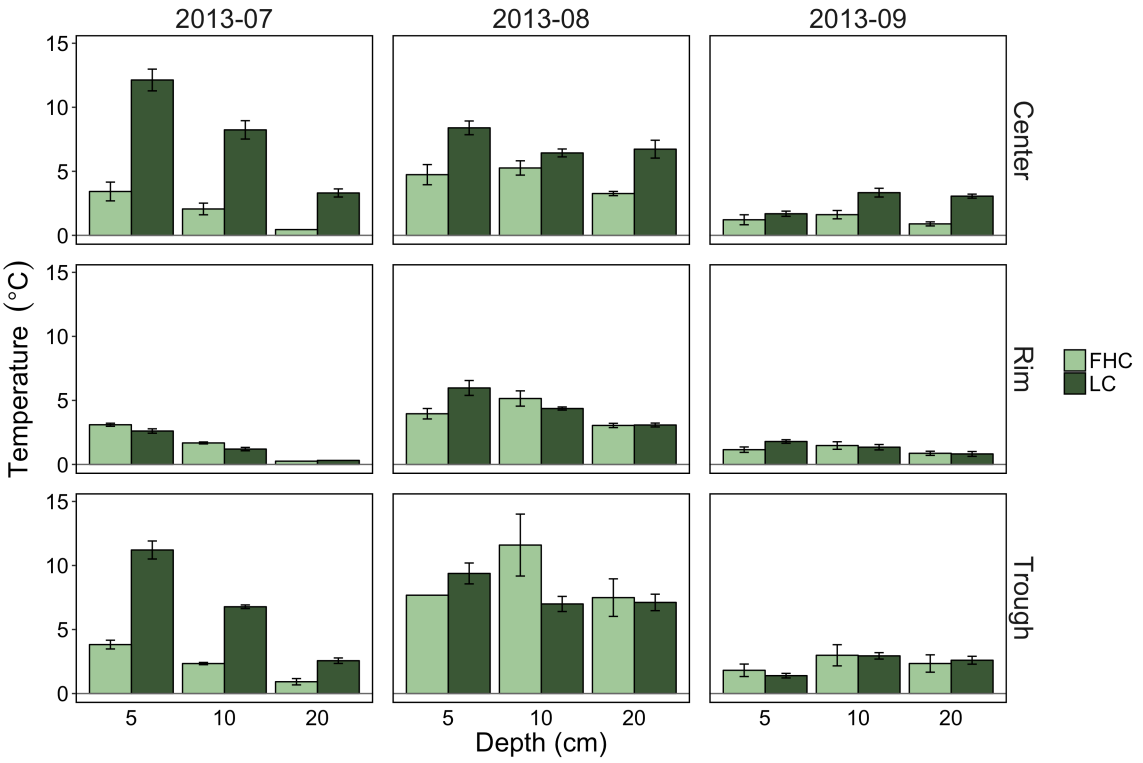

Figure 2. Soil temperature depth profiles, classified by polygon type, position, and month. Light green bars are flat/high-centered (FHC) polygons and dark green bars are low-centered (LC) polygons.

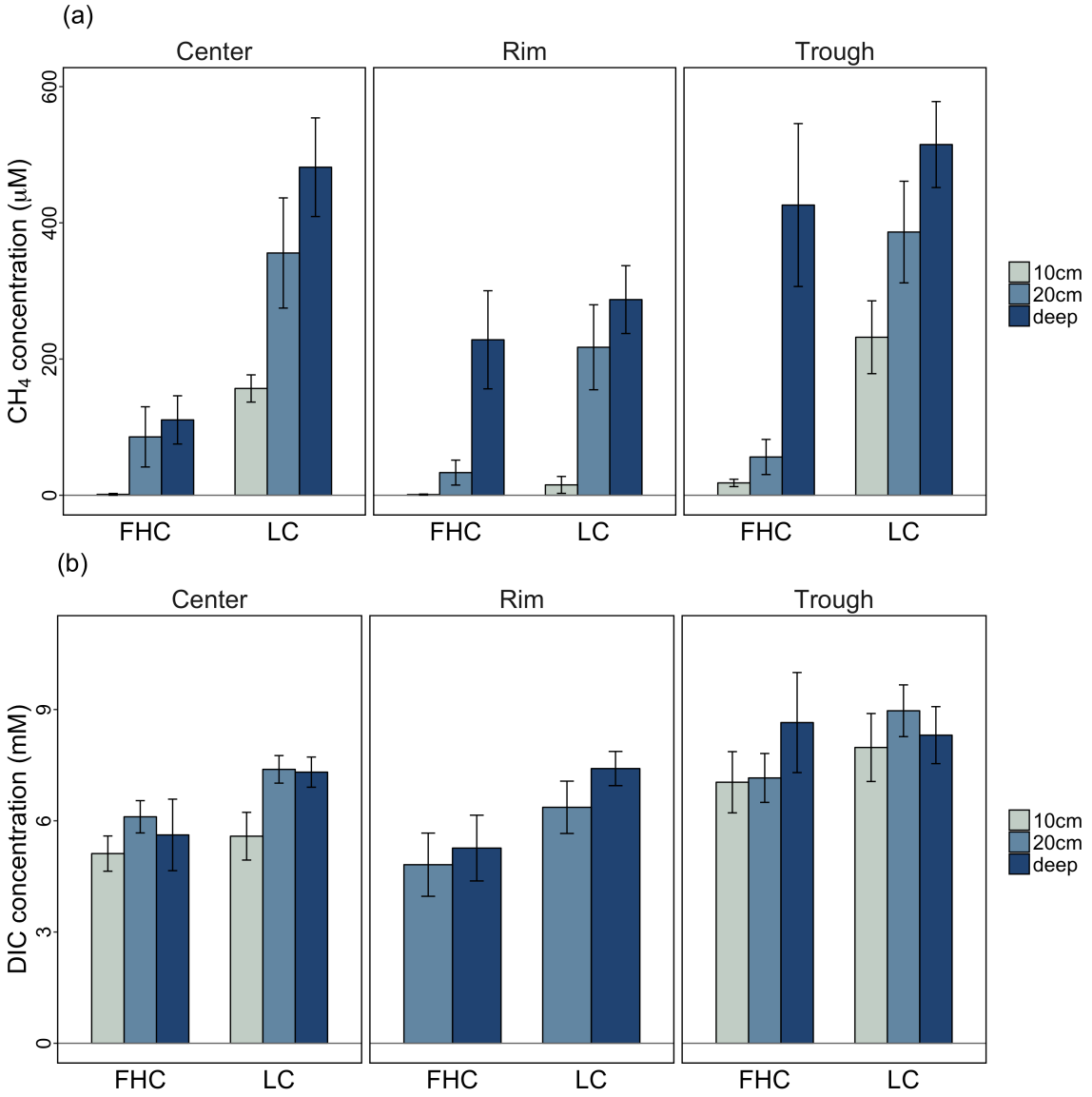

Figure 3. Concentration depth profiles of (a) dissolved CH_4 and (b) DIC in soil pore water. Results are classified by polygon type, position, and depth from the soil surface. Mean concentrations and standard errors include water samples collected in August 2012 and monthly from July – October 2013 from 4 flat/high-centered and 3 low-centered polygons. Data presented here include water samples only, and do not include gas samples.

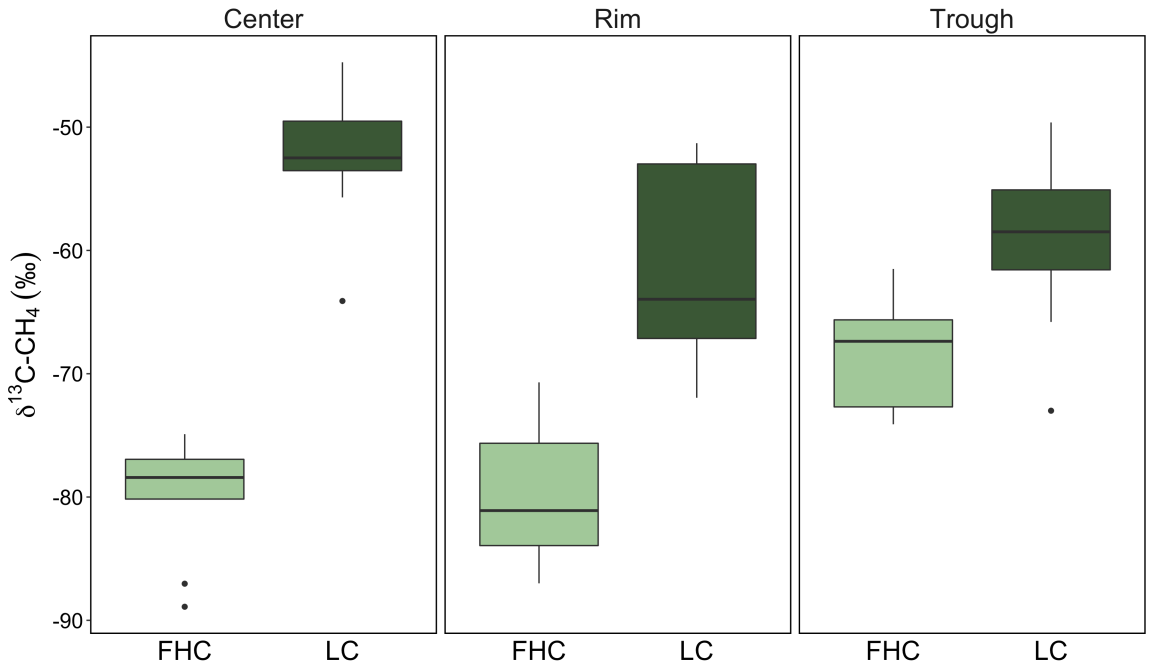

Figure 4. $\delta^{13}C$ of CH_4 in water samples collected from the frost table. Data are classified by polygon type and position, and include all sampling dates from August 2012 and July – October 2013. Box plots indicate median and first and third quartiles, with whiskers extending to the farthest values within 1.5 times the upper and lower quartiles. Outliers beyond this range are shown as points.

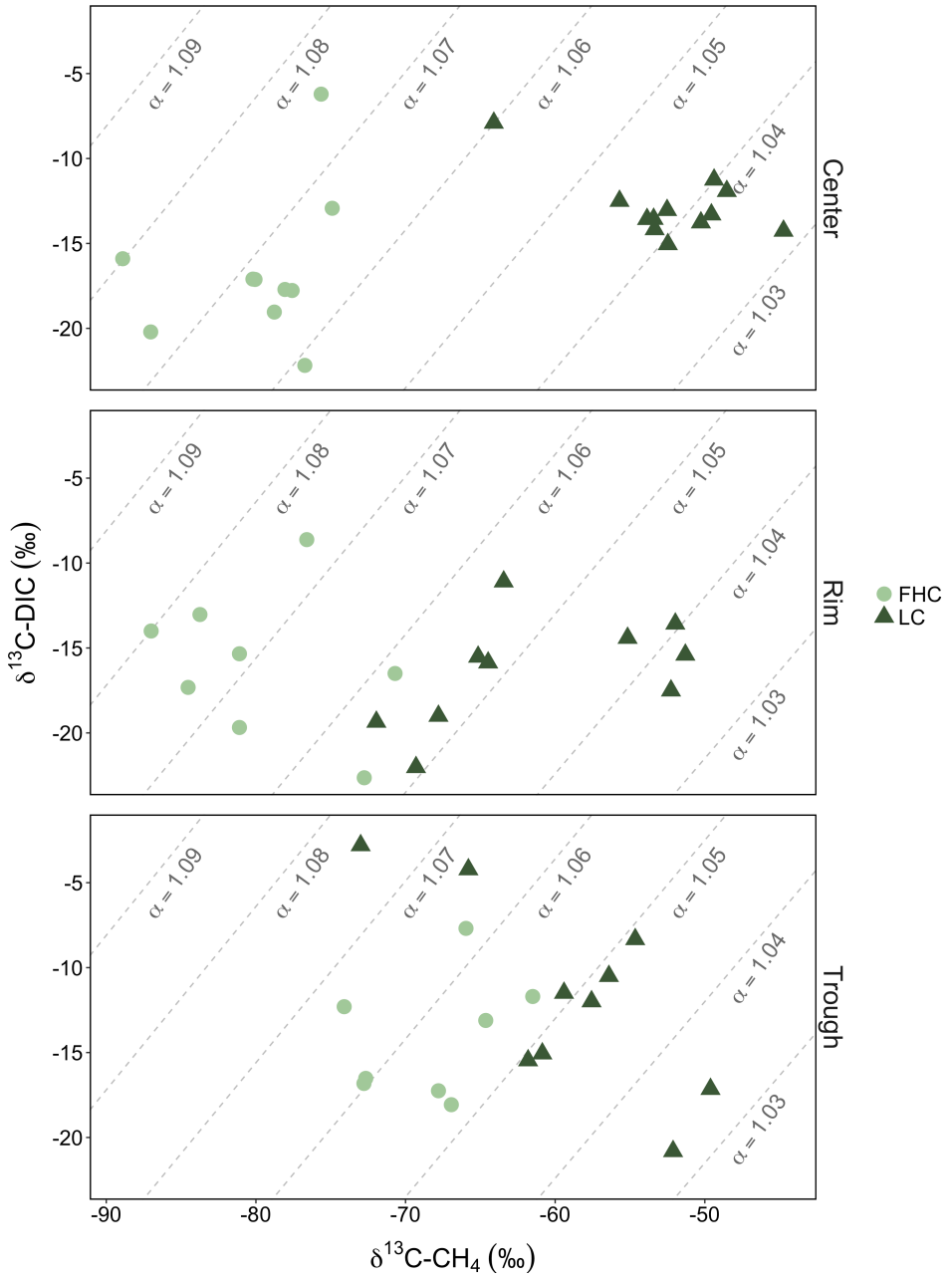

Figure 5. Crossplots showing δ^{13}C-DIC and δ^{13}C-CH_4 of individual soil pore water or gas samples. Dark triangles are flat/high-centered (FHC) polygons, and light circles are low-centered (LC) polygons. Dashed diagonal lines show equal fractionation between CH_4 and co-occurring DIC, with the fractionation factor (α) decreasing from top left to bottom right of each panel.

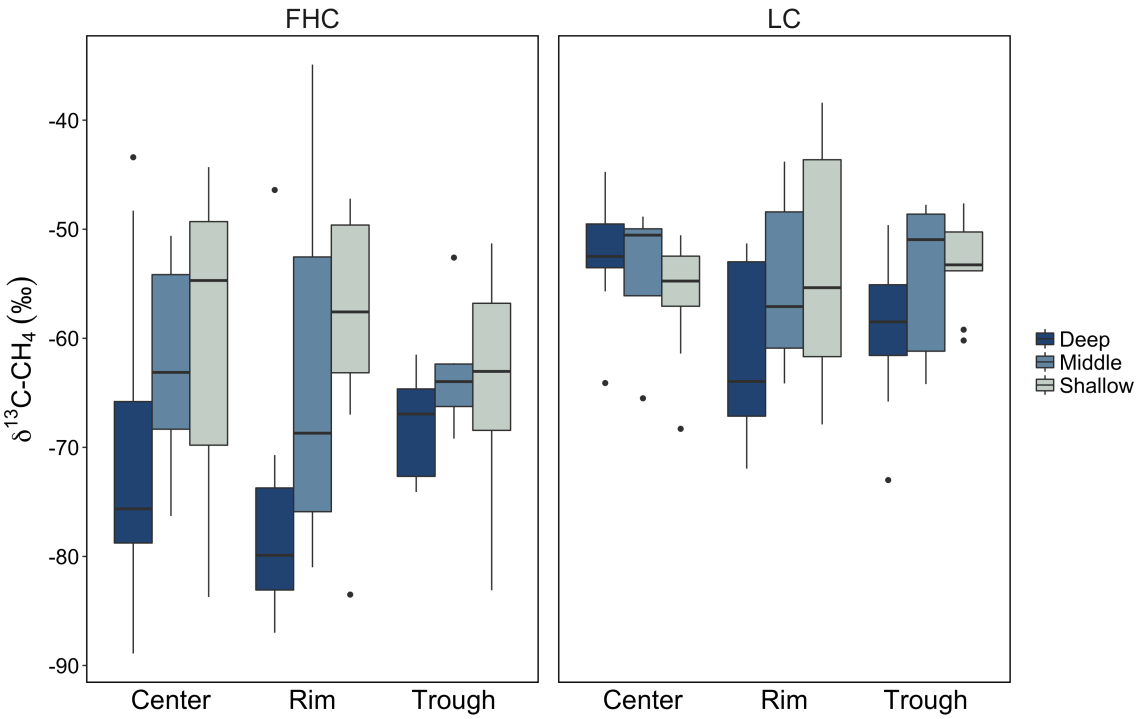

Figure 6. Depth profiles of $\delta^{13}CH_4$ within the soil pore space. Data are classified by polygon type, position, and depth from the soil surface. Shallow samples were collected from 10 cm below the surface and deep samples were collected from the frost table. The middle depth increment includes samples collected from 20 cm below the surface if total thaw depth was greater than 20 cm. If a soil profile's thaw depth was ≤ 20 cm, any sample deeper than 10 cm was classified as deep.

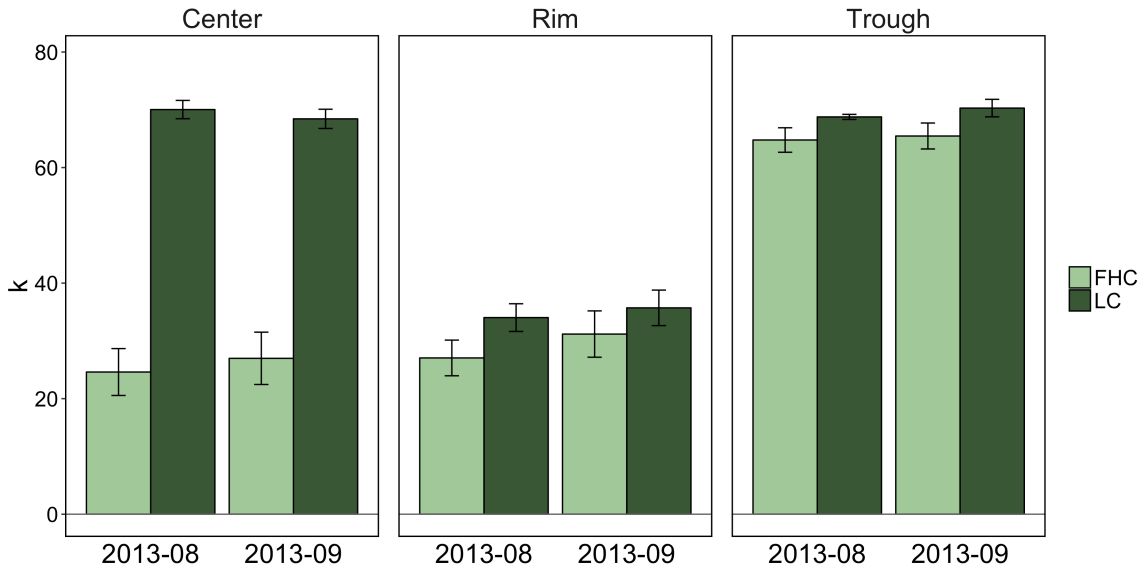

Figure 7. TDR measurements of top 10 cm soil moisture, shown as dielectric constant (k). Measurements are classified by polygon type, position, and month. Light green bars are flat/high-centered (FHC) polygons and dark green bars are low-centered (LC) polygons.

CHAPTER 3: SOIL CARBON INPUTS AND ECOSYSTEM RESPIRATION: A FIELD PRIMING EXPERIMENT IN ARCTIC COASTAL TUNDRA

Abstract

In Arctic ecosystems, climate change is expected to influence soil carbon stocks through changes in both plant carbon inputs and organic matter decomposition rates (McGuire *et al.*, 2009). This study addresses the potential for a priming effect, an interaction between these changes in which increased inputs of root-derived carbon alter SOM decomposition rates via microbial biomass increases, co-metabolism of substrates, or induced nitrogen limitation (Kuzyakov *et al.*, 2000; Blagodatskaya & Kuzyakov, 2008). Despite numerous laboratory and greenhouse priming experiments and increased interest for ecosystem models, few studies have evaluated the priming effect with in situ field manipulations. In a two-year field experiment in Barrow, Alaska, we tested for a priming effect under natural environmental variability. In September 2014 and August 2015, we added 6.1 g of ^{13}C-labeled glucose to 25 cm diameter mesocosms, 15 cm below the soil surface in the mineral soil layer, and quantified effects on the rate and temperature sensitivity of native (non-glucose) ecosystem respiration and GPP. Following the 2014 treatment, soil samples were collected at 1 and 3 weeks for microbial biomass carbon and $^{13}C/^{12}C$ analysis, and ion exchange membranes were buried for 20 days to assess nitrate and ammonium availability. In contrast with many laboratory incubation studies using soils from a broad range of ecosystems, we observed no significant priming effect, detecting no treatment effect on background ecosystem respiration or total microbial biomass carbon. To best inform models representing complex and dynamic ecosystems, this study calls for further research relating theory, laboratory findings, and field experimentation.

Introduction

For the past 10,000 years, high-latitude ecosystems have been a net carbon sink (Harden *et al.*, 1992; Smith *et al.*, 2004), with soils underlain by permafrost accumulating an estimated 1,300 Pg of carbon due to slow decomposition rates in cold, anoxic, or frozen soils (Hugelius *et al.*, 2014). With climate change projected to bring warmer temperatures and longer growing seasons to the Arctic, ecological conditions controlling the ecosystem carbon balance are expected to change (Ciais *et al.*, 2014). Increased vegetation productivity due to longer snow-free seasons (Post *et al.*, 2009), warmer temperatures (Hinzman *et al.*, 2005), accelerated nutrient cycling (Nadelhoffer *et al.*, 1991; Mack *et al.*, 2004), and CO_2 fertilization (Oechel *et al.*, 1994; Norby *et al.*, 2005) are predicted to enhance ecosystem carbon uptake. Concurrently, decomposition rates are expected to increase due to thawing and warming soils (Natali *et al.*, 2011; Schuur *et al.*, 2015; Webb *et al.*, 2016) , wetland drainage (Natali *et al.*, 2015), and thermal erosion (Osterkamp *et al.*, 2009; Lara *et al.*, 2016). The future high-latitude carbon balance depends on these two flows, carbon uptake by vegetation and carbon emission by decomposition. Changes to these flows are challenging to predict, due to a broad set of controls, unknown future conditions, and a suite of interactions between aboveground and belowground systems (McGuire *et al.*, 2009, 2012).

Interactions between vegetation and decomposition are numerous and bidirectional. Plants influence decomposition directly through the quantity and chemistry of litter inputs to soils (Hobbie, 1996; Saleska *et al.*, 2002; Cornwell *et al.*, 2008) and indirectly through their influence on microclimate (Smith & Johnson, 2004; Liancourt *et al.*, 2011). Simultaneously, decomposition affects plants directly through nutrient provision (Attiwill & Adams, 1993) and indirectly through soil formation (Jenny, 1994). In addition to these examples, many other reciprocal interactions link aboveground and belowground plant and soil systems, all of which are sensitive to climate. In high-latitude ecosystems in particular, warming temperatures, longer growing seasons, and altered soil moisture may change vegetation species distributions and productivity patterns (Chapin *et al.*, 1995; Pearson *et al.*, 2013), microbial communities and their activity (Allison *et al.*, 2010), and organic matter turnover rates (Davidson & Janssens, 2006). Through tight linkages between these systems, vegetation-decomposition feedbacks may enhance or dampen these changes, with consequences for high-latitude carbon stocks.

This study investigated one particular vegetation-decomposition interaction: the influence of a change in labile carbon inputs to soils on soil organic matter (SOM) decomposition. With climate change in the Arctic, plant carbon inputs to soils may change in magnitude, seasonality, and spatial distribution. In permafrost landscapes, where rooting depth and species distributions are constrained by seasonal thaw (Dennis *et al.*, 1978; Jorgenson *et al.*, 2001; Minke *et al.*, 2009), changes in vegetation carbon include not only increased productivity but also changes in rooting depth as soils thaw earlier and deeper and dominant plant functional types change (Sturm *et al.*, 2001; Hudson & Henry, 2009; Iversen *et al.*, 2015). With an expanding rhizosphere and increased rhizodeposition as litter or exudation, the release of readily-hydrolyzable carbon compounds can alter rates of SOM mineralization in a phenomenon known as the priming effect (Blagodatskaya & Kuzyakov, 2008; de Graaff *et al.*, 2010; Finzi *et al.*, 2015; Murphy *et al.*, 2015). A positive priming effect increases SOM mineralization through a range of proposed mechanisms including energy provision to microbes for enzyme production, activation of dormant microorganisms, microbial nutrient mining to balance stoichiometric needs, increased decomposer population size, or co-metabolism (production of enzymes that act on multiple substrates) (Kuzyakov *et al.*, 2000; Fontaine *et al.*, 2004; Blagodatskaya & Kuzyakov, 2008). Alternatively, a negative priming effect decreases SOM mineralization if microorganisms preferentially utilize the new substrate rather than mineralize SOM (pool substitution) (Hamer & Marschner, 2005; de Graaff *et al.*, 2010). Numerous studies have demonstrated the priming effect in a broad range of soils and ecosystems, some conducted in the field (e.g., Van Kessel *et al.*, 2000; Hoosbeek *et al.*, 2004; Hartley *et al.*, 2012), many in the greenhouse (e.g., Kuzyakov & Cheng, 2001; Fu & Cheng, 2002; Dijkstra & Cheng, 2007; Bengtson *et al.*, 2012), and even more using laboratory soil incubations (e.g., De Nobili *et al.*, 2001; Fontaine *et al.*, 2004, 2007; de Graaff *et al.*, 2010; Hartley *et al.*, 2010; Wild *et al.*, 2014; Murphy *et al.*, 2015). To date, however, no published field studies have investigated the priming effect in Arctic tundra.

Across the experimental literature, the sign and magnitude of the priming effect vary widely with environmental and experimental conditions (Kuzyakov & Cheng, 2001; de Graaff *et al.*, 2010; Hartley *et al.*, 2010; Drake *et al.*, 2013; Wild *et al.*, 2014). Although

some syntheses have been conducted (Kuzyakov *et al.*, 2000; Blagodatskaya & Kuzyakov, 2008; Finzi *et al.*, 2015; Luo *et al.*, 2016), relationships between the priming effect and individual experimental drivers remain largely uncertain, and even less is known about non-linear, complex, interacting effects among these drivers. By incorporating vegetation-decomposition interactions, computational models may offer a framework to investigate such complex priming interactions. Indeed, a number of recent modeling studies have addressed the priming effect either directly (Perveen *et al.*, 2014; Sulman *et al.*, 2014; Guenet *et al.*, 2016) or indirectly (Foereid *et al.*, 2014; Groenigen *et al.*, 2014; Riley *et al.*, 2014), but wide variation in structural representations and priming metrics make highly variable model findings challenging to evaluate (Wieder *et al.*, 2015; Georgiou *et al.*, 2017). Additionally, some computational models may incorrectly attribute changes in soil carbon cycling to the priming effect (Georgiou *et al.*, 2015; Koven *et al.*, 2015). To evaluate and improve such models requires synthesizing a range of empirical data spanning a broad set of ecosystems and environmental conditions. While controlled laboratory studies of isolated, one-way interactions can improve model parameterizations, model benchmarking requires observational and experimental field evidence of more complex, bidirectional effects.

A challenge central to priming effect experiments is separating changes in native SOM decomposition from mineralization of newly added substrates. One observational approach that field studies have employed is to compare carbon stocks of paired plots with comparable soils but distinct vegetation (Hartley *et al.*, 2012). This method can relate cumulative, long-term soil carbon changes to realistic scenarios of vegetation change, but misses short-term changes in SOM mineralization dynamics. Alternatively, experimental studies often add an isotopically labeled substrate and partition respired CO_2 into two source pools, the added substrate and native SOM (Phillips & Gregg, 2001). This method is regularly used in laboratory and greenhouse studies, either by directly injecting labeled carbon compounds into the soil or by growing plants in a CO_2 atmosphere whose isotopic signature is distinct from the soil (Cheng *et al.*, 2003; Conde *et al.*, 2005; Bader & Cheng, 2007; Fontaine *et al.*, 2007; Wild *et al.*, 2014). While this approach is straightforward under tightly controlled laboratory or greenhouse conditions, it poses technical challenges for field manipulations, as the labeled substrate or evolved CO_2 may be transported away from the measurement location by diffusion or advection. Some FACE experiments have overcome this challenge by applying the isotopic tracer over a large footprint for an extended period of time (Van Kessel *et al.*, 2000; Hoosbeek *et al.*, 2004; Carney *et al.*, 2007), but these experiments require monitoring changes in soil carbon pools rather than fluxes and cannot differentiate between belowground influences on vegetation growth and the CO_2 fertilization effect. Finally, some studies have adopted a hybrid field-laboratory approach, adding substrates in the field and measuring their effect on SOM decomposition with laboratory soil incubations (Langley *et al.*, 2009; Drake *et al.*, 2015). This method preserves some ecological complexity but measures SOM decomposition changes in a controlled, isolated environment not necessarily reflective of field conditions.

Recent soil incubation experiments have observed a positive priming effect in high-latitude soils, finding increased decomposition following carbon substrate amendments (Hartley *et al.*, 2010; Wild *et al.*, 2014, 2016). By isolating decomposition

processes under controlled environmental conditions, such incubation studies complement observational evidence that vegetation changes may alter Arctic soil carbon stocks (Hartley *et al.*, 2012). Missing, however, are experimental field manipulations studying Arctic vegetation-decomposition interactions in the presence of active vegetation, under natural environmental variability. Here we report on the first study to our knowledge that has evaluated the priming effect with in situ manipulations in Arctic tundra.

In a two-year field experiment in Barrow, Alaska, we amended soils with a ^{13}C-labeled simple carbon substrate and quantified its fate in CO_2, soil, and microbial biomass. Making use of a shallow permafrost table, we isolated columns of active layer soil to limit substrate or CO_2 losses via diffusion or advection, measuring carbon exchange changes in situ with surface soil chambers. To evaluate the effects on SOM mineralization and vegetation growth, we asked four primary questions: how does substrate addition (1) affect SOM mineralization rates, (2) influence the temperature sensitivity of decomposition, (3) influence microbial biomass and mineral nitrogen availability, and (4) affect gross primary production? With these four questions, we aimed to investigate not only the presence, sign, and magnitude of a priming effect, but also its relation to background variability in temperature, associated belowground mechanistic changes, and secondary interactions with vegetation. Such secondary decomposition-vegetation interactions, generally overlooked by laboratory soil incubation studies, may generate feedbacks between ecosystem carbon uptake and emission processes.

Methods

Site and experimental setup

At the northern end of the Alaskan Arctic coastal plain, the Barrow Environmental Observatory lies ~6 km east of the village of Barrow, Alaska (71.3N, 156.5W). Barrow has a mean annual temperature of -12°C and mean annual precipitation of 106 mm, with long, dry winters and short, moist, cool summers. The land surface has low topographic relief up to 5 m elevation (Brown *et al.*, 1980; Hubbard *et al.*, 2013) and a shallow active layer ranging from 20 to 60 cm underlain by continuous ice-rich permafrost to depths greater than 400 m (Hinkel & Nelson, 2003). Formed from the late Pleistocene Gubic formation (Black, 1964), soils in the region are dominated by Typic Aquiturbels (53 %), Typic Histoturbels (22 %), and Typic Aquorthels (8.6 %) (Bockheim *et al.*, 1999). Within the Barrow Environmental Observatory, we sited this experiment in a region of high-centered ice-wedge polygons, discrete landscape units formed from freezing and thawing processes (Billings & Peterson, 1980). Individual polygons, roughly 10 m in diameter and separated by low-lying, saturated troughs, had dry, aerobic surface soils and sparse vegetation dominated by *Luzula arctica*, *Vaccinium vitis idaea*, and several moss and lichen species (Sloan *et al.*, 2014a).

Within the study region, we chose 6 polygons of roughly equal thaw depth, some of which showed signs of active thermokarst development such as slumping and bare soil at their margins. On August 24, 2014, we established a block within each polygon consisting of 3 25 cm diameter mesocosms. Mesocosms were isolated from the surrounding soil with 45 cm-long PVC columns, inserted vertically in the soil to span the

full active layer depth (32-44 cm). Thaw depth at this time was near its annual maximum, so frozen soil at the base of the column provided a barrier against diffusion and leaching. To each mesocosm's top rim, we glued a 4 cm high collar fitted with a 3 cm deep trench made to seat a static soil chamber. The trench was filled with water to create an airtight seal between the chamber and base. Mesocosms rested for 2 days following installation to allow soils to recover from disturbance.

To assess surface vegetation abundance and variability, we harvested aboveground vegetation on August 25 from one 25 cm diameter circle per block, adjacent to the installed mesocosms. Vegetation was sorted immediately into vascular and nonvascular (moss + lichen) components, oven dried at 60°C, and weighed.

On August 26, 27, and 28, we measured baseline surface fluxes of CO_2 and CH_4 using opaque static soil chambers, vented according to Xu *et al.*, (2006) to minimize pressure excursions due to the Venturi effect. For each measurement, we monitored CO_2 and CH_4 concentrations within the chamber for 3-7 minutes using a Los Gatos Research, Inc. (LGR) portable Greenhouse Gas Analyzer. Flux of each gas was calculated from the linear region of the concentration vs. time curve.

Field manipulations, measurements and sample collection
2014

On August 29, 2014, we injected one of three treatment solutions into each mesocosm, for a set of three treatment levels per block. The high glucose treatment contained 6.125 g of ^{13}C-labeled glucose in 122.5 mL DDI water, the low glucose treatment contained 1.225 g of ^{13}C labeled glucose in 122.5 mL DDI water, and the control treatment contained 122.5 mL DDI water. We chose glucose quantities to equal 50 % and 10 % of the estimated microbial biomass carbon (MBC) in a 10 cm thick layer of soil, with microbial biomass estimated to be 2 % of the known soil carbon contents of nearby polygons. The glucose had an isotopic enrichment of 6 atom %, made from a mixture of 99 atom % and natural abundance glucose. We injected solutions through hypodermic needles into the mineral soil, 15 cm below the soil surface in a 5 × 5 grid of 2.5 cm cells. This distributed the solution evenly across the soil layer for a total of 25 injections per 0.49 m^2 plot. From each mesocosm, we used opaque static chambers to measure post-treatment surface fluxes of CO_2 and CH_4 on August 29, 30, and 31, and September 2, 4, 7, 10, 13, 16, and 19. Trace gas fluxes were measured with opaque static chambers as described above.

On August 31, we established a set of three duplicate plots within each block for destructive sampling. Replicate plots received the same glucose or control treatments as the primary plots as well as a set of probes containing cation and anion exchange membranes (Plant Root Simulator (PRS™) probes, Western Ag Innovations) for measuring nitrate and ammonium availability (Hangs *et al.*, 2004; Drohan *et al.*, 2005; Johnson *et al.*, 2005). Ion exchange membranes were inserted vertically in each duplicate plot, spanning a layer of soil 10-20 cm in depth. On August 20, ion exchange membranes were excavated, rinsed free of soil with DI water, and sent to Western Ag for analysis. 1" diameter soil cores were collected from replicate plots on August 8 and 20 for analysis of carbon and nitrogen content, MBC, and ^{13}C recovery in bulk soil and microbial biomass.

2015

On August 1, 2015, high glucose and control solutions were injected again into the primary mesocosms, repeating the 2014 treatment protocol. For use in a concurrent experiment, vertical temperature probes had been installed in the control mesocosms on July10 and 11, 2015, along with matching dummy probes in the high glucose mesocosms to maintain consistent conditions across all mesocosms.

Surface fluxes of CO_2 and CH_4 were measured from high glucose and control mesocosms on June 23 and July 9, 12, 29, 30, and 31 (before the second injection) and August 2, 4, 6, 9, 13, 24, 26, and 29, and September 1 (after the second injection). In addition to opaque static chambers, in which CO_2 flux is equivalent to ecosystem respiration (R_{eco}), we measured net ecosystem exchange (NEE) with transparent chambers on June 23, July 29 and 30, August 2, 4, 6, 9, and 29, and September 1. To calculate NEE from the concentration vs. time curve, we used only the first 60 seconds of each measurement, as slopes subsequently decreased, likely due to plant stomatal responses to reduced CO_2 within the chamber. At the time of each flux measurement, air temperature and soil temperature at 5, 10, 15, and 20 cm depths were measured using a hand-held thermocouple probe, and soil moisture in the top 10, 20, and 30 cm of soil was measured concurrently using a MiniTrase TDR (Soilmoisture Equipment Corp). Soil temperature and moisture measurements were made 10 cm outside each mesocosm to avoid the disturbance of repeated probe insertion and removal.

On June 24, July 29 and 30, August 2, 4, 6, 9, 13, and 26, and September 1, immediately following each trace gas measurement, we left chambers in place for 60-80 minutes during which we collected 5 25 mL gas samples at 15-20 minute intervals to evaluate ^{13}C abundance in R_{eco} using the Keeling plot method (described below) (Keeling, 1958). Samples were collected in 60 mL syringes with gastight stopcocks and injected immediately into 22 mL glass vials with 14 mm gas impermeable butyl rubber stoppers (Geo-Microbial Technologies, Inc).

2016

On April 21, 2016, we used a SIPRE coring auger to collect 4.9 cm diameter × 40 cm depth soil cores from the high glucose and control mecosoms in blocks 4-6. With the active layer completely frozen, no soil compression occurred during sampling, and carbon, nitrogen, and ^{13}C measurements reflect the condition of the soil upon winter freeze-up (i.e., fall 2015). Frozen soil cores from the remaining high glucose and control mesocosms (blocks 1-3) were collected on November 9, 2016 to a depth of 50 cm. All cores were shipped frozen to Berkeley, CA, for further analysis.

On July 21 and 22, 2016, R_{eco} and NEE were measured from the six intact mesocosms with opaque and transparent soil chambers. Additionally, to quantify background spatial variability, R_{eco} and NEE were measured from 18 locations within high-centered polygons adjacent to those used in the priming manipulation.

Calculations and laboratory analyses

R_{eco} partitioning

Measured ^{13}C abundance in R_{eco} was used to partition total R_{eco} in high glucose mesocosms into its component sources, glucose mineralization (R_G) and native (non-

glucose) respiration (R_N). To determine the isotopic composition of total R_{eco}, we applied the Keeling plot method (Keeling, 1958) to each set of 5 25 mL samples collected in 2015, which uses CO_2 concentration and isotope data in a two-pool isotopic mixing model to differentiate R_{eco} from the background atmosphere. Briefly, we measured CO_2 concentrations on a 2014 Shimadzu GC, using 4 mL of gas from each sample vial. CO_2 was isolated on a HayeSep-D packed column (4 m × 1/8") and quantified with a flame ionization detector. Following GC measurement, we measured carbon isotope ratios of the CO_2 remaining in vials with a Micromass Trace Gas pre-concentration system interfaced with a Micromass JA series Isoprime isotope ratio mass spectrometer, as described in Torn et al (2003). To avoid measurement errors due to mass dependency, we optimized injection volumes of full-concentration samples to constrain peak sizes within a narrow range. Using measured CO_2 concentrations and carbon isotope ratios, we constructed a separate Keeling plot for each set of 5 samples collected from a given mesocosm, plotting the ^{13}C abundance in CO_2 from each sample against the reciprocal of its CO_2 concentration. With each plot, we estimated linear relationships with geometric mean regressions (Bowling *et al.*, 2002; Knohl *et al.*, 2004) and calculated R_{eco} ^{13}C values as the y-intercept of each regression, using standard least squares regressions to approximate the standard error of the intercept (Pataki *et al.*, 2003). For accurate calculations across a broad range of source ^{13}C abundances, we used atom % notation for all Keeling plots and associated calculations (Hayes, 2004), where atom % $^{13}C = (^{13}C/(^{13}C + ^{12}C))$.

We noted that the first (lowest-concentration) data points were systematically non-linear across all Keeling plots. We determined that this non-linearity was due to methodological error, as initial samples were collected within 5 minutes of the chamber being placed on the mesocosm, a period in which transient adjustments in autotrophic respiration due to light exclusion likely caused anomalous CO_2 concentrations or isotopic fractionations. Accordingly, these points were omitted from regressions, leaving 4-point linear Keeling plots. Keeling plots were omitted from the dataset if CO_2 concentrations or ^{13}C values did not change monotonically throughout (n = 6) or if $R^2 < 0.95$ (n = 18), leaving 52 high glucose and 49 control Keeling plots in the analysis.

To partition each treatment plot R_{eco} measurement into R_N and R_G, we used a two end-member mixing model based on the formulation from Phillips and Gregg (2001):

$$^{13}C\text{-}R_{eco} = f_G \times {}^{13}C\text{-}R_G + f_N \times {}^{13}C\text{-}R_N$$

$$f_G + f_N = 1$$

in which ^{13}C-R_G is the known isotopic composition of added glucose (6 atom %) and ^{13}C-R_N, the isotopic composition of background (non-glucose) respiration, was calculated separately for each sampling date as the average ^{13}C-R_{eco} from the control mesocosms. As with Keeling plots, all mixing model calculations were performed using atom % units. Calculated fractional contributions of R_N and R_G to total R_{eco} (f_N and f_G) were then applied to CO_2 efflux measurements to calculate absolute rates of R_N and R_G:

$$f_N \times R_{eco} = R_N$$

$$f_G \times R_{eco} = R_G$$

To ensure data quality, we evaluated CO_2 flux measurements according to two criteria. First, flux chamber measurements were omitted from the dataset if the CO_2 accumulation curve lacked a clear linear range. Second, we omitted any flux measurements with slope estimate standard error > 0.05 and parameter relative standard error (PRSE) > 5, defined as PRSE = $100 \times (SE_{slope}/estimate_{slope})$ (Sileshi, 2014). This dual set of criteria avoided biasing the dataset toward low fluxes (if SE alone were used) or high fluxes (if PRSE alone or R^2 were used).

Solid sample analysis

Soil cores collected in 2014 were stored at 5°C and processed within 2 days of field sampling. First, we divided each core into 3 depth increments: 0-10 cm, 10-20 cm, and 20-30 cm. To compensate for a limited amount of soil compression during the coring process, depth increments were adjusted to the actual sampling depth according to a power function that assumes the degree of compression increases with soil depth. The 10-20 cm increments were immediately homogenized and subset for analyses of microbial biomass, gravimetric water content, carbon and nitrogen content, and carbon isotopic composition. The 0-10 cm and 20-30 cm increments were frozen and stored at -19°C until further processing.

We measured carbon content and carbon isotopic composition of microbial biomass from 10-20 cm increment subsamples using chloroform fumigation extraction (Vance *et al.*, 1987; Bruulsema & Duxbury, 1996). Briefly, soil subsamples were divided into two further subsamples, one for immediate extraction and one for extraction following fumigation. Unfumigated subsamples were extracted with 50 g 0.05 M K_2SO_4 solution, shaken slowly for 1 hour, filtered through #1 Whatman filter paper, then stored at -19°C until further processing. To fumigate remaining subsamples, we placed soils in a desiccator alongside a beaker containing 30 mL of ethanol-free chloroform, drawing a vacuum on the open desiccator to boil the chloroform for 5 minutes. We then closed the desiccator and released the vacuum, forcing the chloroform into the soil particles. This procedure was repeated a second time and samples were left to fumigate in the dark for 5 days under vacuum. Following fumigation, the desiccator chamber and soil samples were flushed of chloroform and immediately extracted with 0.05 M K_2SO_4, following the same procedure as the unfumigated soils. Fumigated extracts were stored at -19°C until further processing.

We measured carbon concentrations in fumigated and unfumigated extracts with a TOC-VCSH total organic carbon analyzer (Shimadzu Corporation, Kyoto, Japan), and calculated carbon contents per mass of extracted soil. For each 10-20 cm core increment, the MBC content was then calculated as the difference in carbon content between the fumigated and unfumigated soils, using a correction factor of 0.35 to account for extraction efficiency (Sparling *et al.*, 1990):

$$\mathrm{MBC} = \frac{\mathrm{C_{fumigated}} - \mathrm{C_{unfumigated}}}{0.35}$$

For $^{13}C/^{12}C$ analysis of K_2SO_4 extracts, we dried 1.5 mL aliquots in tin capsules in a desiccator at room temperature over a period of 3 days. Capsules were loaded into an ECS 4010 elemental analyzer (Costech Analytical Technologies, Inc.) coupled to a Delta V^{plus} isotope ratio mass spectrometer (Thermo Fischer Scientific), using Montana soil standards ranging from 0.05, 1, 2.5, 5, and 7.5 mg to calibrate optimal peak height. Repeated analyses of in-house standards yielded analytical precision of ± 0.13 ‰ (1σ, n=40) and ± 0.14 ‰ (1σ, n=34).

^{13}C abundance in microbial biomass ($^{13}C_M$) was calculated from ^{13}C and carbon content results using the following mass balance equations:

$$^{13}\mathrm{C_F} = f_S \times {}^{13}\mathrm{C_{UF}} + f_M \times {}^{13}\mathrm{C_M}$$

$$f_S + f_M = 1$$

where $^{13}C_F$ and $^{13}C_{UF}$ are the ^{13}C abundances in the fumigated and unfumigated subsamples in atom % units, and f_S and f_M are the fractional contributions of non-microbial and microbial carbon in the fumigated extract.

Soil cores collected in April and November 2016 were stored at -19°C until further processing. All 2016 cores were divided while frozen into 10 cm depth increments, and November 2016 soils were then further sub-sectioned into horizons, if a distinct horizon boundary was found within a depth increment. A suite of analyses was then performed on all core increments from both 2014 and 2016. First, we measured gravimetric water content by air-drying soils at 55°C to constant mass. Dried soils were then ground, measured into tin capsules, and loaded into an ECS 4010 elemental analyzer (Costech Analytical Technologies, Inc.) coupled to a Delta V^{plus} isotope ratio mass spectrometer (Thermo Fischer Scientific) for carbon, nitrogen, and $^{13}C/^{12}C$ analysis. Optimal peak height was calibrated with atropine standards ranging from 0.2, 0.5, and 1.2 mg, and repeated analysis of an in-house standard yielded analytical precisions of ± 0.40 % for carbon, ± 0.05 % for nitrogen, and ± 0.24 ‰ for $\delta^{13}C$ (1σ, n=14). Samples of air-dried soils were oven dried at 105°C to constant mass to correct calculated C and N values for residual moisture. Additionally, we calculated bulk density of each 2016 increment from its frozen core volume and dry weight. Bulk density was not calculated for 2014 samples because of uncertainty associated with soil compression during sampling.

While all isotopic calculations were performed in atom % units, results are presented in units of parts per thousand (‰) using conventional δ-notation relative to Vienna Peedee Belemnite (VPDB), where $\delta^{13}C = (R_{sample}/R_{standard} - 1) \times 1000$ and R is the abundance ratio of ^{13}C to ^{12}C.

Statistical analyses

We evaluated a priming effect using two statistical tests. First, we used a linear mixed effects model to test for differences in R_N and its temperature sensitivity between

high glucose and control plots. Using post-treatment data from the 2015 glucose addition, this model evaluated potential predictors of log-transformed R_N. After calculating variance inflation factors to rule out multicollinearity, we included the following potential predictor variables: treatment (high glucose or control), 15 cm soil temperature, measurement date, and two two-way interactions, treatment × temperature and treatment × measurement date. To control for repeated measures, we included a random effect for mesocosm nested within polygon. Incremental *F*-tests were used to determine which fixed effects significantly predicted R_N, using Satterthwaite's approximation for denominator degrees of freedom.

Second, we evaluated the priming effect by testing for a change in R_N following the 2015 glucose addition. To compare CO_2 efflux rates among sampling dates, we first removed a confounding temperature effect by normalizing all 2015 R_N measurements to a standard temperature using Q_{10} values. Briefly, Q_{10} was calculated individually for each mesocosm over the full 2015 measurement period, assuming an exponential relationship between R_{eco} and soil temperature at 5 cm depth. This exponential assumption proved to be robust (Fig. 1), providing better overall empirical fits than an Arrhenius relationship. Q_{10} values were then use to adjust each R_N value to its equivalent rate at 7°C, which fell within every mesocosm's observed temperature range. With these normalized R_N values, we then used a linear mixed effects model to test for a step change in R_N following the glucose addition treatment. This model included R_N as the response variable and two predictor variables: measurement date and a categorical variable assigning each measurement into a pre-treatment or post-treatment class (pre/post). We included mesocosm as a random effect to account for repeated measures, and evaluated predictor variables using incremental *F*-tests as above.

To evaluate belowground responses to glucose addition, we applied a simple ANOVA to 2014 ion exchange membrane data to test for differences in NO_3^-, NH_4^+, and total N availability among glucose addition and control treatments. Additionally, differences in MBC among treatments were evaluated separately on each sampling date using a simple ANOVA.

Finally, we calculated GPP from the transparent and opaque chamber measurements (NEE and R_{eco} respectively), according to GPP = R_{eco} - NEE. Using a linear mixed effects model, we evaluated two relationships between GPP and the high glucose treatment: (1) the immediate effect of the 2015 glucose addition on GPP, and (2) the influence of the 2014 glucose addition on 2015 GPP. Potential predictors of GPP included treatment (high glucose or control), measurement date, time of day, air temperature, 5 cm soil temperature, pre/post, and two interaction terms: treatment × date and treatment × pre/post. As above, we included a random effect for chamber nested within block to account for repeated measures and evaluated potential predictors using incremental *F*-tests.

To evaluate the likelihood of detecting a significant treatment effect against the given degree of background variability in R_{eco}, we conducted a power analysis using simulated data across a range of priming levels varying from 0 % (no priming) to 100 % (priming-induced doubling of R_N). For each priming level, 6 R_N values were simulated for each post-treatment measurement date, 8/2, 8/4, 8/6, 8/9, 8/26, and 9/1. Simulated values were drawn from a normal distribution with the mean and standard deviation of

that date's control mesocosm R_{eco} measurements, then multipled by a scaling factor (e.g., 1.2 for a 20 % priming level). A linear mixed effects model was used to test for a difference between control and simulated data. As with the measured data, we evaluated whether treatment was a significant predictor of log-transformed R_N, accounting for repeated measures with a random effect for mesocosm nested within polygon. We repeated this exercise 400 times for each priming level and calculated the power as the percentage of runs in which treatment (simulated vs. control) significantly predicted log-transformed R_N with $\alpha = 0.05$. The minimum detectable priming effect was determined using a power cutoff of 80 %.

All statistical analyses were conducted in R version 3.2.1 "World-Famous Astronaut" (2015-06-18), using the packages LME4 (Bates *et al.*, 2014) for linear mixed effects modeling and lmerTest (Kuznetsova *et al.*, 2014) for significance testing.

Results

Glucose decomposition

We generated a robust set of Keeling plots using 2015 surface emission samples to evaluate the isotopic composition of R_{eco} from treatment and control mesocosms. The CO_2 concentration range in each plot was large enough to minimize error in the intercept estimate (Pataki *et al.*, 2003), yet small enough and with large enough isotopic source differences to limit concerns due to non-linearity within non-steady-state chambers (Nickerson & Risk, 2009; Shibistova *et al.*, 2012). With ^{13}C end-members calculated from Keeling plots, we used a 2-pool mixing model to partition 2015 R_{eco} into glucose-derived and native (non-glucose derived) components. Mixing model results demonstrate that as expected, the glucose addition treatment altered both the absolute rate and source composition of the R_{eco} flux, with glucose decomposition accounting for up to 25 % of total CO_2 efflux from high glucose mesocosms (Fig. 2, Fig. 3). The peak in the fraction of R_{eco} attributed to glucose-carbon mineralization occurred rapidly following treatment, within the first week in most mesocosms (Fig. 3). The peak in absolute rates of glucose-carbon mineralization occurred slightly later, but still within 10 days of the glucose addition treatment (Fig. 2).

Priming of native R_{eco}

Over the month following the 2015 glucose addition treatment, rates of non-glucose derived R_{eco} (R_N) ranged spatially and temporally from 0.30 to 2.4 μmol m^{-2} s^{-1} in high glucose mesocosms and 0.26 to 2.0 μmol m^{-2} s^{-1} in control mesocosms, with mesocosm-averaged mean values ranging from 0.48 to 1.4 μmol m^{-2} s^{-1} (Table 3, Fig.2). This R_N flux did not differ significantly between treatments, indicating that glucose addition did not stimulate a measurable priming effect. Additionally, although R_G contributed up to 25 % of total R_{eco} in high glucose mesocosms (Fig. 2, Fig. 3), we found no significant difference in total R_{eco} between high glucose and control mesocosms over the post-treatment period. Results of a power analysis indicate that the lack of an observed treatment effect may have been due to high background variability in R_{eco} (Table 4). With the observed degree of background variability, achieving a statistical power of 80 % would have required a treatment-induced increase in R_N of > 55 %.

To evaluate whether glucose addition influenced the temperature sensitivity of decomposition, we assessed the interaction between treatment and temperature as a potential model predictors (Fig. 4). This interaction was not significant, indicating that the influence of temperature on R_N did not differ significantly between high glucose and control mesocosms. Instead, the relationship between temperature and $\log_{10}(R_{eco})$, equivalent to Q_{10}, had greater variation among polygons than between treatments within individual polygons (Fig. 1).

In case a priming effect were obscured by chance systematic differences in background R_{eco} rates between high glucose and control mesocosms, we compared R_N measurements before and after the glucose addition, normalized to 7°C (Fig. 5). As with the previous statistical test, we detected no priming effect, finding no significant differences in R_N between pre-treatment and post-treatment measurements in either high glucose or control mesocosms (Table 3).

Microbial biomass carbon and ^{13}C

At 9 and 20 days following the 2014 glucose addition, the stock of microbial biomass carbon (MBC) in the 10-20 cm soil depth increment ranged spatially among blocks and treatments from 0.12 to 3.4 mg C per g soil (Table 1). Elevated MBC $\delta^{13}C$ values between 150 and 820 ‰ indicate microbial uptake of glucose-derived carbon, with the fraction of MBC derived from glucose ranging spatially and among treatments from 1.5 to 30 %. Total MBC did not change significantly from the first sampling date to the second, nor did it differ significantly between high glucose and control mesocosms. Additionally, after subtracting the fraction of MBC derived from added glucose, we detected no significant difference between treatments in non-glucose-derived MBC. The absence of significant treatment effects on either total MBC or non-glucose MBC indicates that neither microbial population growth nor pool substitution were detectable over background variability.

Nitrogen availability

Following the 2014 glucose additions, we used ion exchange membranes in duplicate plots to evaluate cumulative nitrate and ammonium availability in blocks 1-5. Over this 20-day period, we found no significant differences in nutrient supply among glucose addition treatments. With the exception of block 5, nitrate and ammonium availability ranged from 0 to 0.56 and 0 to 0.055 μg N cm^{-2} d^{-1} respectively, with total nitrogen availability ranging from 0 to 0.575 μg N cm^{-2} d^{-1} (Fig. 6). In block 5, we measured unusually high supply rates of both nitrate and ammonium from the high and low glucose mesocosms, 2.4 and 0.49 μg N cm^{-2} d^{-1} in the high glucose mesocosm and 0.96 and 0.58 μg N cm^{-2} d^{-1} in the low glucose mesocosm. The lack of significant treatment effect, even when block 5 was included in the analysis, suggests that glucose addition neither induced nor suppressed microbial release of nitrogen from SOM. Interestingly, polygon 5 had higher 2015 R_{eco} rates than other blocks, particularly from its high glucose mesocosms (Fig. 1, Fig. 2), as well as relatively high soil nitrogen contents (data not shown), possibly indicating a link between nitrogen availability and SOM turnover rates.

Glucose addition and recovery

Recovery of the ^{13}C label in SOM 9 and 20 days following the 2014 glucose addition (Table 1) indicated that the percentage of total added glucose carbon remaining in the top 30 cm of soil varied widely among mesocosms, from as low as 1.7 % to as high as 65 % (Table 2). Soil cores collected in April 2016 indicate that upon freeze-up in 2015, 55 ± 6.2 % of the total (two-year) addition remained in the active layer soil. By November 2016, only 30 ± 8.9 % of the total added carbon remained. Depth profiles of soil carbon isotopic composition indicate that not all glucose remained at the initial injection depth, with significant glucose recovery in soils shallower than 10 cm and deeper than 20 cm.

Soil MBC and ^{13}C recovery data allowed us to estimate the relative magnitude of the carbon addition in comparison to MBC, a metric shown in previous studies to predict the priming effect magnitude (Blagodatskaya & Kuzyakov, 2008). Soil MBC varied widely among mesocosms, ranging from 0.12-3.4 mg per g soil in the 10-20 cm layer (Table 1), consistent with previous measurements from high-latitude subsurface organic or mineral soils (Jones *et al.*, 2000; Gornall *et al.*, 2007; Sistla *et al.*, 2013). Given that MBC tends to decrease dramatically with soil depth (Kaiser *et al.*, 2007), glucose:MBC ratios are sensitive to the vertical transport of glucose within the profile evidenced by ^{13}C recovery data (Table 2). We estimate that if 50 % of the added glucose moved rapidly from the 10-20 cm layer into the surface and deeper horizons, resulting high glucose addition rates would have equaled ~30-160 % of the MBC stock, a range that includes our target addition rate of 50 % MBC.

Vegetation productivity

To evaluate short-term and year-long influences of glucose addition on vegetation productivity, we monitored GPP during the 2015 season, before and after the August 1 glucose addition treatment. Over the 2015 sampling season, GPP was significantly lower in high glucose mesocosms than in controls (Table 5, Fig. 7). Mean GPP from high glucose mesocosms was 1.82 ± 0.20 μmol CO_2 m^{-2} s^{-1} in the pre-treatment period and 1.48 ± 0.11 μmol CO_2 m^{-2} s^{-1} over the full 2015 season, while in controls it was 2.95 ± 0.21 μmol CO_2 m^{-2} s^{-1} in the pre-treatment period and 2.03 ± 0.16 μmol CO_2 m^{-2} s^{-1} over the full 2015 season. GPP also varied significantly by sampling date (Table 5, Fig. 7), decreasing roughly 3-fold from June to late August to low values on the order of 1 μmol CO_2 m^{-2} s^{-1}. No significant change in GPP immediately followed the August 1 glucose addition, nor did we find a significant interaction between treatment and measurement date.

On July 21 and 22, 2016, we measured GPP from the 6 remaining intact mesocosms and 18 additional locations atop adjacent high-centered polygons. GPP within the 6 remaining intact mesocosms was comparable to that measured from high glucose mesocosms in June-August 2015 (2.27 ± 0.39 μmol CO_2 m^{-2} s^{-1} on July 21 and 2.17 ± 0.42 μmol CO_2 m^{-2} s^{-1} on July 22), but notably lower in the adjacent mesocosms (0.944 ± 0.12 μmol CO_2 m^{-2} s^{-1} on July 21 and 1.05 ± 0.17 μmol CO_2 m^{-2} s^{-1} on July 22). This systematic difference between our experimental mesocosms and adjacent locations was likely due to a sheltering effect from the PVC mesocosms, decreasing wind-driven soil desiccation and promoting vegetation growth over the three-year period. The magnitude of this sheltering effect was roughly equal to the difference in 2015 pre-treatment GPP,

suggesting that the glucose addition treatment reduced the sheltering effect on GPP by approximately half.

Discussion

Under a changing climate, future Arctic soil carbon storage depends on the balance of two fluxes, plant-derived soil carbon inputs and losses via SOM decomposition (McGuire *et al.*, 2012). Additionally, interactions between these two fluxes may occur, with the potential to further destabilize soil carbon stocks. In a process known as the priming effect, increased rhizosphere carbon inputs can enhance SOM decomposition (Blagodatskaya & Kuzyakov, 2008; Finzi *et al.*, 2015), as shown in numerous greenhouse and laboratory studies (e.g., Cheng *et al.*, 2003; Dijkstra & Cheng, 2007; Fontaine *et al.*, 2007; de Graaff *et al.*, 2010; Wild *et al.*, 2014; Murphy *et al.*, 2015). Such studies have shown that increased rhizodeposition in the form of simple sugars, other compounds exuded by roots, or cellulose can stimulate strong increases in SOM decomposition, with reported SOM mineralization rates as high as ~10 × their background rates (Bader & Cheng, 2007). By utilizing laboratory soil incubations or controlled greenhouse conditions, however, most priming studies to date have measured this effect in the absence of natural environmental variability and other plant-soil interactions. In this two-year field manipulation combining a carbon substrate addition with field-measured respiration rates, we evaluated priming in the presence of—and relative to—background variability. Following a ^{13}C tracer into respired CO_2 and microbial biomass, we found that while glucose addition directly influenced decomposition, it did not measurably alter the rate or temperature sensitivity of R_N. Further, we conducted a sensitivity analysis, finding that background variability in R_{eco} would likely obscure any priming-induced increase in C mineralization smaller than 55 %.

Measured effects of glucose addition

To assess direct effects of the glucose addition treatment on microbial processes, we measured glucose carbon mineralization to CO_2 and incorporation into microbial biomass. Elevated $\delta^{13}CO_2$ and mixing model results (Table 3) demonstrate that the added glucose was actively decomposed, comprising up to 25 % of the total R_{eco} flux (Fig. 2). Similarly, spatially averaged $\delta^{13}C$ values of MBC ranged from 150 ± 92 to 820 ± 490 ‰ in high glucose mesocosms (Table 1), indicating that on average, between 4 and 18 % of the carbon in microbial biomass was derived from added glucose. Together, these findings indicate that added glucose directly influenced decomposition dynamics, either by increasing the total rate of microbial carbon mineralization and/or uptake, or by shifting microbial substrate preference toward glucose over native SOM.

While glucose addition directly influenced decomposition and microbial carbon uptake, it altered neither the background rate nor the temperature sensitivity of R_{eco} (Fig. 4). The lack of significant relationship in the three statistical tests we performed (testing for differences in the rate of R_N between glucose addition and control mesocosms, the temperature sensitivity of R_N between glucose addition and control mesocosms, and the rate of R_N before vs. after the glucose addition) indicates that no measurable priming effect occurred. In contrast with previous studies documenting strong positive priming in soils from similar ecosystems (Hartley *et al.*, 2010; Wild *et al.*, 2014, 2016) and

priming-induced increases in the temperature sensitivity of decomposition (Zhu & Cheng, 2011), we found no respiration-based evidence for interactions between substrate addition and native SOM decomposition rates.

Subsurface measurements of microbial biomass stock and nitrogen availability lend additional support to our R_N findings, indicating no subsurface evidence of a priming effect. If energy available from glucose hydrolysis had stimulated an increase in microbial activity (Kuzyakov *et al.*, 2000), we would expect to have observed the microbial biomass bloom that commonly accompanies a positive priming effect (de Graaff *et al.*, 2010; Drake *et al.*, 2015; Murphy *et al.*, 2015). Instead, samples from 2014 show that while microorganisms incorporated glucose-derived carbon, the total MBC stock remained unchanged between treatment and control mesocosms (Table 1). To maintain a constant MBC stock while incorporating glucose carbon, one of two changes must have occurred. Either microorganisms shifted from SOM to glucose utilization (a negative priming effect, not supported by our R_N analyses) or microbial biomass turnover increased, compensating for additional glucose carbon incorporation. In any of these cases, measurements of MBC stock provide no evidence for a significant positive priming effect. Similarly, ion exchange membrane measurements of mineral nitrogen availability display no significant differences between treatments (Fig. 6). Had a stoichiometric imbalance from added glucose carbon stimulated priming via the microbial nitrogen mining mechanism (Craine *et al.*, 2007; Blagodatskaya & Kuzyakov, 2008; Murphy *et al.*, 2015), we would expect increased nitrogen supply to ion exchange membranes to reflect this increased gross mineralization (Johnson *et al.*, 2005; Bengtson *et al.*, 2012; Finzi *et al.*, 2015). Increased microbial nitrogen immobilization may have balanced changes in gross nitrogen mineralization (Murphy *et al.*, 2015), producing no net increase in supply to ion exchange membranes. Such a case, however, would have been accompanied by increased carbon mineralization, which we did not observe with R_N measurements (Fig. 4). As with MBC, our nitrogen availability measurements thus offer no independent evidence of altered SOM decomposition dynamics.

Conducting this experiment in intact mesocosms enabled us to evaluate changes in vegetation productivity (GPP). Unlike R_N, MBC, and nitrogen availability, we found a significant treatment effect on 2015 GPP, with higher GPP in control than treatment mesocosms, particularly earlier in the season when vegetation was more active (Table 5, Fig. 7). This finding suggests that subsurface changes following the 2014 glucose addition treatment may have persisted through the following year, limiting GPP relative to the water-only controls. GPP measurements in this study were roughly comparable to previous measurements in similar Arctic ecosystems (Williams *et al.*, 2000), but ~2-3 × higher than measurements made from adjacent polygons (Table 6). This difference was likely due to decreased wind-driven soil drying within PVC mesocosms, which promoted plant growth over the two experimental years. Relative to GPP in the adjacent plots, our observed treatment effect within experimental mesocosms suggests that glucose addition may have reduced this sheltering effect on GPP by approximately 50 %. As we observed no short-term influences of glucose addition on nitrogen availability or microbial biomass, our data offer no mechanistic explanations for this observed effect. Instead, we broadly hypothesize that year-long cumulative changes in soil chemistry or decomposition dynamics created a resource limitation for plants, possibly via enhanced

microbe-vegetation nutrient competition (Jackson *et al.*, 1989; Kaye & Hart, 1997). As a negative feedback to plant growth and rhizodeposition, such an interaction could have meaningful long-term impacts on ecosystem carbon exchange.

The measured size of the glucose-GPP effect was relatively large; the predicted response of GPP to the 2014 glucose addition (-0.54 μmol m^{-2} s^{-1}) (Table 5) was approximately 2 × the broader spatial variance in baseline GPP, as measured from a survey of 18 adjacent high-centered polygon locations on July 21 and 22, 2016 (0.27 μmol m^{-2} s^{-1}). Nevertheless, due to the limited spatial coverage (n=6) and study period, we hesitate to draw strong conclusions from this result. Instead, we suggest that a possible bidirectional interaction between vegetation and decomposition merits further study. For example, we hypothesize that glucose remaining in the soil upon freeze-up may have stimulated microbial immobilization of nutrients released during spring thaw (Grogan *et al.*, 2004; Edwards *et al.*, 2006), limiting nutrient availability to vegetation. By decreasing rhizodeposition, this hypothesized effect could constitute a negative feedback between substrate addition and decomposition rate. Evaluating this type of vegetation-decomposition feedback calls for multi-season studies tracking nutrient availability and decomposition. Importantly, our observed GPP effect highlights a shortcoming of laboratory incubation experiments. While such experimental designs have the advantage of more easily detecting changes in R_N, they may miss interactions or feedbacks present in complex, intact ecosystems.

Statistical considerations

From both surface (R_N) and subsurface (MBC and N availability) results, we observed no detectable priming effect. This finding places an upper bound on the possible magnitude of primed carbon, but it does not preclude the possibility that a priming effect occurred, as temporal and spatial variability limited our detection capabilities. Based on power analysis simulation (Table 4), the priming effect would have had to produce a sustained 55 % increase in R_N over the month following glucose addition to be detectable over background R_{eco} variability. Furthermore, a transient change in R_N could prove even harder to detect, particularly if the timing of a response varied among polygons. Partitioned flux results show no evidence of a transient, temporally variable priming effect (Fig. 2), but even a moderate sustained priming effect would have been obscured by variability in R_{eco} among polygons and mesocosms.

In a fully field-based experiment, variability in autotrophic respiration presents a particular challenge for detecting a priming effect. The priming effect pertains specifically to heterotrophic respiration (R_H), which many previous priming studies have isolated by excluding vegetation in laboratory soil incubations (De Nobili *et al.*, 2001; Fontaine *et al.*, 2004, 2007; Langley *et al.*, 2009; de Graaff *et al.*, 2010; Hartley *et al.*, 2010; Wild *et al.*, 2014; Drake *et al.*, 2015; Murphy *et al.*, 2015). In contrast, this study's field respiration fluxes include the other component of R_{eco}, aboveground and belowground autotrophic respiration (R_A). Because R_A should not be sensitive to short-term changes in SOM or glucose mineralization, it does not risk confounding our R_N measurements. It does, however, present an additional source of background variability, a challenge incubation experiments easily avoid. To minimize the influence of R_A on total R_N, we conducted this experiment late in the growing season, after the peak in vegetation

productivity (Dennis *et al.*, 1978; Zona *et al.*, 2014) but before low soil temperatures limited decomposition rates (Sloan *et al.*, 2014b). Nevertheless, August 2015 GPP data (Fig. 7) indicate that vegetation remained active until late in the measurement period. As such, R_A contributions to R_N background variability may have partially masked priming-induced changes in R_H.

The relative contribution of R_A to the total R_{eco} flux depends on the vegetation's productivity and carbon use efficiency (CUE = NPP/GPP), with higher rates of R_A from more productive and less efficient vegetation. In some Arctic tundra ecosystems, respiration from relatively productive and inefficient vascular plants may account for a large percentage of R_{eco} (Billings *et al.*, 1978; Silvola *et al.*, 1996; Crow & Wieder, 2005), with root respiration alone contributing as much as 15-45 % of total R_{eco} (Iversen *et al.*, 2015) (though few studies have differentiated between root respiration and the microbial breakdown of root-derived products). In such cases, high rates of both root and aboveground respiration may limit detection of a priming effect in an intact soil-plant system, if priming-induced changes in R_H were small relative to R_A variability. In other cases, however, R_A may play a lesser role. Most of the above literature values for R_A pertain to systems dominated by vascular vegetation, whereas our experimental mesocosms had a relatively low abundance of vascular plants, with mosses and lichens comprising the majority of aboveground biomass (Fig. 8). Compared with vascular plants, mosses often have low productivity (Oechel & Sveinbjörnsson, 1978) and high CUE, with measured CUE values as high as 0.81, as compared to vascular vegetation values closer to 0.5 (Street *et al.*, 2013). In particular, deep-rooted and productive *Carex*, *Dupontia*, and *Eriophorum* species, common to many of these previous studies, had minimal coverage at our study site (Sloan *et al.*, 2014a). Given their low cover of vascular vegetation, we believe our experimental mesocosms were less influenced by R_A than are many other high-latitude systems. Overall, however, while features particular to our experimental site reduced the contribution of R_A to background R_N variability, the presence of vegetation in a field manipulation increased the challenge of detecting a change in R_H.

Ecological considerations

Beyond background variability, specific ecological features of our study may explain the lack of priming that we observed. First, low temperatures may have limited a temperature-sensitive priming response (Zhu & Cheng, 2011). Soil temperatures throughout this study, 3.9°C ± 0.82°C at 15 cm depth, were considerably lower than incubation temperatures used in previous priming experiments, which range from 10°C - 25°C (Fontaine *et al.*, 2007; Langley *et al.*, 2009; de Graaff *et al.*, 2010; Hartley *et al.*, 2010; Wild *et al.*, 2014, 2016; Drake *et al.*, 2015; Murphy *et al.*, 2015). If dormant soil microorganisms were more immediately controlled by temperature than by substrate availability, cold conditions may have limited their activation in response to the glucose pulse. Additionally, energy converted from glucose catabolism by the active microbial community may have been insufficient at low temperatures to hydrolyze more chemically complex and temperature-sensitive (Davidson & Janssens, 2006; Feng *et al.*, 2008; Cusack *et al.*, 2010) components of SOM. Second, stoichiometry may have inhibited priming. The C:N ratio of added substrate can strongly influence the decomposition response in

site-specific ways (Kuzyakov *et al.*, 2000; Drake *et al.*, 2013). Whereas a high C:N ratio may stimulate SOM mineralization via nitrogen mining (Murphy *et al.*, 2015), it may alternatively inhibit priming if insufficient nitrogen is available for enzyme synthesis (Drake *et al.*, 2013). In high-latitude soils in particular, mineral nitrogen availability tends to be low due to slow rates of fixation, deposition, and internal cycling (Hobbie *et al.*, 2002), leaving our system particularly sensitive to stoichiometric constraints. With no supplemental nitrogen amendment, microorganisms may have been unable to utilize the energy and carbon from glucose catabolism to increase enzyme production. If we had added not only glucose alone, but additionally a mineral nitrogen supplement or a nitrogen-containing carbon substrate, our soils may have produced a measurable increase in SOM decomposition (Mack *et al.*, 2004; Drake *et al.*, 2013).

In previous studies documenting a positive priming effect, rates of primed CO_2 production have been low relative to those of substrate-derived CO_2 (Falchini *et al.*, 2003; Fontaine *et al.*, 2004, 2007; Hamer & Marschner, 2005; de Graaff *et al.*, 2010; Hartley *et al.*, 2010). In general, CO_2 evolution from mineralization of experimentally added substrates has been equal to or greater than the total background rates of CO_2 mineralization, a direct system perturbation far larger than our experiment utilized. In this study, while R_G likely contributed substantially to total CO_2 evolution from the 10-20 cm soil layer, the total surface R_N flux included CO_2 produced in both shallower and deeper soils. From organic surface soils in particular (Table 1), where the glucose addition was diluted by large stocks of rapidly-cycling carbon (Trumbore, 2000), high CO_2 production rates and high background variability may have masked an effect originating primarily from the 10-20 cm layer.

The quantity of glucose added in this study was far lower than that used in the majority of priming studies but closer to a plausible change in rhizodeposition. Doubling this study's background rate of CO_2 evolution—a perturbation comparable to most previous priming experiments (Falchini *et al.*, 2003; Fontaine *et al.*, 2004, 2007; Hamer & Marschner, 2005; de Graaff *et al.*, 2010; Hartley *et al.*, 2010)—would have required adding glucose at five to ten times our experimental rate, approximately 30 to 60 g glucose per mesocosm. This rate is far higher than feasible root exudation increases, particularly as a pulse addition. With the conservative assumptions that root exudation equals 10 % of total net carbon fixation (Loya *et al.*, 2002; Farrar *et al.*, 2003), the NPP/GPP ratio equals 0.5 (Turner *et al.*, 2006; Zhang *et al.*, 2009), and average GPP over the June-September growing season (June-September) equals 0.8 μmol m^{-2} s^{-1} (Olivas *et al.*, 2010, 2011), a glucose addition this large would be equivalent to ~50-100 years of carbon fixation at current productivity rates (Appendix C). Viewed in this context, a step change this large would offer little predictive insight, even if it were able to stimulate a measurable priming effect. Given that the magnitude of primed carbon release is unlikely to scale linearly with the substrate addition rate (Blagodatskaya & Kuzyakov, 2008), evaluating the priming effect under realistic conditions is crucial for predicting future changes.

Conclusion

In conclusion, our field glucose addition experiment produced no measurable change in R_N, MBC, or nitrogen availability. Following a direct system perturbation, we measured no priming effect above background variability in SOM decomposition and R_A.

While the inclusion of surface vegetation in our study design posed challenges for detecting a priming effect, it allowed us to measure significant treatment-level differences in GPP. As such, this study highlights an important tradeoff inherent to priming studies. Field priming manipulations are challenged by high spatial and temporal variability in decomposition and vegetation process rates, but capture bidirectional vegetation-decomposition interactions. In contrast, tightly controlled incubation studies offer practical methodological advantages and reduce confounding variables, but have a limited capacity to represent real, potentially complex processes in undisturbed ecosystems. In spite of inherent challenges, we emphasize the importance of studying rhizosphere interactions in intact, in situ ecosystems, under realistic scenarios of change. Importantly, our findings suggest that other biogeochemical factors, variable in both space and time, may influence carbon exchange more strongly than a change in subsurface carbon supply. Looking forward, quantifying these influences and incorporating feedbacks between vegetation and decomposition demands an integrated approach that combines laboratory and modeling studies with field experiments capturing the full range of natural variability.

References

Allison SD, Wallenstein MD, Bradford MA (2010) Soil-carbon response to warming dependent on microbial physiology. *Nature Geoscience*, **3**, 336–340.

Attiwill PM, Adams MA (1993) Nutrient cycling in forests. *New Phytologist*, **124**, 561–582.

Bader NE, Cheng W (2007) Rhizosphere priming effect of Populus fremontii obscures the temperature sensitivity of soil organic carbon respiration. *Soil Biology and Biochemistry*, **39**, 600–606.

Bates D, Maechler M, Bolker BM, Walker S (2014) *lme4: Linear mixed-effects models using Eigen and S4. R package version 1.1-7*.

Bengtson P, Barker J, Grayston SJ (2012) Evidence of a strong coupling between root exudation, C and N availability, and stimulated SOM decomposition caused by rhizosphere priming effects. *Ecology and Evolution*, **2**, 1843–1852.

Billings WD, Peterson KM (1980) Vegetational change and ice-wedge polygons through the thaw-lake cycle in Arctic Alaska. *Arctic and Alpine Research*, 413–432.

Billings WD, Peterson KM, Shaver GR (1978) Growth, Turnover, and Respiration Rates of Roots and Tillers in Tundra Graminoids. In: *Vegetation and Production Ecology of an Alaskan Arctic Tundra* (ed Tieszen LL), pp. 415–434. Springer New York.

Black RF (1964) *Gubik Formation of Quaternary age in northern Alaska*. United States Geological Survey.

Blagodatskaya E, Kuzyakov Y (2008) Mechanisms of real and apparent priming effects and their dependence on soil microbial biomass and community structure: critical review. *Biology and Fertility of Soils*, **45**, 115–131.

Bockheim JG, Everett LR, Hinkel KM, Nelson FE, Brown J (1999) Soil organic carbon storage and distribution in Arctic tundra, Barrow, Alaska. *Soil Science Society of America Journal*, **63**, 934–940.

Bowling DR, McDowell NG, Bond BJ, Law BE, Ehleringer JR (2002) 13C content of ecosystem respiration is linked to precipitation and vapor pressure deficit. *Oecologia*, **131**, 113–124.

Brown J, Miller PC, Tieszen LL, Bunnell F (1980) *An Arctic ecosystem : the coastal tundra at Barrow, Alaska*. Dowden, Hutchinson and Ross, Inc., Stroudsburg, Pennsylvania.

Bruulsema TW, Duxbury JM (1996) Simultaneous Measurement of Soil Microbial Nitrogen, Carbon, and Carbon Isotope Ratio. *Soil Science Society of America Journal*, **60**, 1787.

Carney KM, Hungate BA, Drake BG, Megonigal JP (2007) Altered Soil Microbial Community at Elevated CO_2 Leads to Loss of Soil Carbon. *Proceedings of the National Academy of Sciences of the United States of America*, **104**, 4990–4995.

Chapin FS, Shaver GR, Giblin AE, Nadelhoffer KJ, Laundre JA (1995) Responses of Arctic Tundra to Experimental and Observed Changes in Climate. *Ecology*, **76**, 694–711.

Cheng W, Johnson DW, Fu S (2003) Rhizosphere Effects on Decomposition. *Soil Science Society of America Journal*, **67**, 1418.

Ciais P, Sabine C, Bala G et al. (2014) Carbon and other biogeochemical cycles. In: *Climate Change 2013: The Physical Science Basis. Contribution of Working Group I*

to the Fifth Assessment Report of the Intergovernmental Panel on Climate Change, pp. 465–570. Cambridge University Press.
Conde E, Cardenas M, Ponce-Mendoza A, Luna-Guido ML, Cruz-Mondragón C, Dendooven L (2005) The impacts of inorganic nitrogen application on mineralization of 14C-labelled maize and glucose, and on priming effect in saline alkaline soil. *Soil Biology and Biochemistry*, **37**, 681–691.
Cornwell WK, Cornelissen JH, Amatangelo K et al. (2008) Plant species traits are the predominant control on litter decomposition rates within biomes worldwide. *Ecology Letters*, **11**, 1065–1071.
Craine JM, Morrow C, Fierer N (2007) Microbial Nitrogen Limitation Increases Decomposition. *Ecology*, **88**, 2105–2113.
Crow SE, Wieder RK (2005) Sources of co2 emission from a northern peatland: root respiration, exudation, and decomposition. *Ecology*, **86**, 1825–1834.
Cusack DF, Torn MS, McDowell WH, Silver WL (2010) The response of heterotrophic activity and carbon cycling to nitrogen additions and warming in two tropical soils. *Global Change Biology*.
Davidson EA, Janssens IA (2006) Temperature sensitivity of soil carbon decomposition and feedbacks to climate change. *Nature*, **440**, 165–173.
Dennis JG, Tieszen LL, Vetter MA (1978) Seasonal Dynamics of Above- and Belowground Production of Vascular Plants at Barrow, Alaska. In: *Vegetation and Production Ecology of an Alaskan Arctic Tundra* (ed Tieszen LL), pp. 113–140. Springer New York.
Dijkstra FA, Cheng W (2007) Interactions between soil and tree roots accelerate long-term soil carbon decomposition. *Ecology Letters*, **10**, 1046–1053.
Drake JE, Darby BA, Giasson M-A, Kramer MA, Phillips RP, Finzi AC (2013) Stoichiometry constrains microbial response to root exudation- insights from a model and a field experiment in a temperate forest. *Biogeosciences*, **10**, 821–838.
Drake TW, Wickland KP, Spencer RGM, McKnight DM, Striegl RG (2015) Ancient low–molecular-weight organic acids in permafrost fuel rapid carbon dioxide production upon thaw. *Proceedings of the National Academy of Sciences*, 201511705.
Drohan PJ, Merkler DJ, Buck BJ (2005) Suitability of the Plant Root Simulator Probe for Use in the Mojave Desert. *Soil Science Society of America Journal*, **69**, 1482.
Edwards KA, McCulloch J, Peter Kershaw G, Jefferies RL (2006) Soil microbial and nutrient dynamics in a wet Arctic sedge meadow in late winter and early spring. *Soil Biology and Biochemistry*, **38**, 2843–2851.
Falchini L, Naumova N, Kuikman PJ, Bloem J, Nannipieri P (2003) CO2 evolution and denaturing gradient gel electrophoresis profiles of bacterial communities in soil following addition of low molecular weight substrates to simulate root exudation. *Soil Biology and Biochemistry*, **35**, 775–782.
Farrar J, Hawes M, Jones D, Lindow S (2003) How Roots Control the Flux of Carbon to the Rhizosphere. *Ecology*, **84**, 827–837.
Feng X, Simpson AJ, Wilson KP, Dudley Williams D, Simpson MJ (2008) Increased cuticular carbon sequestration and lignin oxidation in response to soil warming. *Nature Geoscience*, **1**, 836–839.

Finzi AC, Abramoff RZ, Spiller KS, Brzostek ER, Darby BA, Kramer MA, Phillips RP (2015) Rhizosphere processes are quantitatively important components of terrestrial carbon and nutrient cycles. *Global Change Biology*, **21**, 2082–2094.

Foereid B, Ward DS, Mahowald N, Paterson E, Lehmann J (2014) The sensitivity of carbon turnover in the Community Land Model to modified assumptions about soil processes. *Earth System Dynamics*, **5**, 211.

Fontaine S, Bardoux G, Abbadie L, Mariotti A (2004) Carbon input to soil may decrease soil carbon content. *Ecology letters*, **7**, 314–320.

Fontaine S, Barot S, Barré P, Bdioui N, Mary B, Rumpel C (2007) Stability of organic carbon in deep soil layers controlled by fresh carbon supply. *Nature*, **450**, 277–280.

Fu S, Cheng W (2002) Rhizosphere priming effects on the decomposition of soil organic matter in C4 and C3 grassland soils. *Plant and Soil*, **238**, 289–294.

Georgiou K, Koven CD, Riley WJ, Torn MS (2015) Toward improved model structures for analyzing priming: potential pitfalls of using bulk turnover time. *Global Change Biology*, **21**, 4298–4302.

Georgiou K, Abramoff RZ, Harte J, Riley WJ, Torn MS (2017) Microbial community-level regulation explains soil carbon responses to long-term litter manipulations. *Nature Communications (submitted)*.

Gornall JL, Jónsdóttir IS, Woodin SJ, Wal RV der (2007) Arctic mosses govern below-ground environment and ecosystem processes. *Oecologia*, **153**, 931–941.

De Graaff M-A, Classen AT, Castro HF, Schadt CW (2010) Labile soil carbon inputs mediate the soil microbial community composition and plant residue decomposition rates. *New Phytologist*, **188**, 1055–1064.

Groenigen KJ van, Qi X, Osenberg CW, Luo Y, Hungate BA (2014) Faster Decomposition Under Increased Atmospheric CO2 Limits Soil Carbon Storage. *Science*, **344**, 508–509.

Grogan P, Michelsen A, Ambus P, Jonasson S (2004) Freeze–thaw regime effects on carbon and nitrogen dynamics in sub-arctic heath tundra mesocosms. *Soil Biology and Biochemistry*, **36**, 641–654.

Guenet B, Moyano FE, Peylin P, Ciais P, Janssens IA (2016) Towards a representation of priming on soil carbon decomposition in the global land biosphere model ORCHIDEE (version 1.9.5.2). *Geosci. Model Dev.*, **9**, 841–855.

Hamer U, Marschner B (2005) Priming effects in different soil types induced by fructose, alanine, oxalic acid and catechol additions. *Soil Biology and Biochemistry*, **37**, 445–454.

Hangs RD, Greer KJ, Sulewski CA (2004) The effect of interspecific competition on conifer seedling growth and nitrogen availability measured using ion-exchange membranes. *Canadian Journal of Forest Research*, **34**, 754–761.

Harden JW, Mark RK, Sundquist ET, Stallard RF (1992) Dynamics of Soil Carbon During Deglaciation of the Laurentide Ice Sheet. *Science*, **258**, 1921–1924.

Hartley IP, Hopkins DW, Sommerkorn M, Wookey PA (2010) The response of organic matter mineralisation to nutrient and substrate additions in sub-arctic soils. *Soil Biology and Biochemistry*, **42**, 92–100.

Hartley IP, Garnett MH, Sommerkorn M et al. (2012) A potential loss of carbon associated with greater plant growth in the European Arctic. *Nature Climate Change*, **2**, 875–879.
Hayes JM (2004) An introduction to isotopic calculations. *Woods Hoel Oceanographic Institute, Woods Hole, MA*.
Hinkel KM, Nelson FE (2003) Spatial and temporal patterns of active layer thickness at Circumpolar Active Layer Monitoring (CALM) sites in northern Alaska, 1995–2000. *Journal of Geophysical Research: Atmospheres*, **108**, 8168.
Hinzman LD, Bettez ND, Bolton WR et al. (2005) Evidence and Implications of Recent Climate Change in Northern Alaska and Other Arctic Regions. *Climatic Change*, **72**, 251–298.
Hobbie SE (1996) Temperature and Plant Species Control Over Litter Decomposition in Alaskan Tundra. *Ecological Monographs*, **66**, 503–522.
Hobbie SE, Nadelhoffer KJ, Högberg P (2002) A synthesis: The role of nutrients as constraints on carbon balances in boreal and arctic regions. *Plant and Soil*, **242**, 163–170.
Hoosbeek MR, Lukac M, van Dam D et al. (2004) More new carbon in the mineral soil of a poplar plantation under Free Air Carbon Enrichment (POPFACE): Cause of increased priming effect? *Global Biogeochemical Cycles*, **18**, GB1040.
Hubbard SS, Gangodagamage C, Dafflon B et al. (2013) Quantifying and relating land-surface and subsurface variability in permafrost environments using LiDAR and surface geophysical datasets. *Hydrogeology Journal*, **21**, 149–169.
Hudson JMG, Henry GHR (2009) Increased plant biomass in a High Arctic heath community from 1981 to 2008. *Ecology*, **90**, 2657–2663.
Hugelius G, Strauss J, Zubrzycki S et al. (2014) Estimated stocks of circumpolar permafrost carbon with quantified uncertainty ranges and identified data gaps. *Biogeosciences*, **11**, 6573–6593.
Iversen CM, Sloan VL, Sullivan PF et al. (2015) The unseen iceberg: plant roots in arctic tundra. *New Phytologist*, **205**, 34–58.
Jackson LE, Schimel JP, Firestone MK (1989) Short-term partitioning of ammonium and nitrate between plants and microbes in an annual grassland. *Soil Biology and Biochemistry*, **21**, 409–415.
Jenny H (1994) *Factors of Soil Formation: A System of Quantitative Pedology*. Courier Corporation, 322 pp.
Johnson DW, Verburg PSJ, Arnone JA (2005) Soil extraction, ion exchange resin, and ion exchange membrane measures of soil mineral nitrogen during incubation of a tallgrass prairie soil. *Soil Science Society of America Journal*, **69**, 260.
Jones MH, Fahnestock JT, Stahl PD, Welker JM (2000) A Note on Summer CO2 Flux, Soil Organic Matter, and Microbial Biomass from Different High Arctic Ecosystem Types in Northwestern Greenland. *Arctic, Antarctic, and Alpine Research*, **32**, 104–106.
Jorgenson MT, Racine CH, Walters JC, Osterkamp TE (2001) Permafrost degradation and ecological changes associated with a warmingclimate in central Alaska. *Climatic change*, **48**, 551–579.

Kaiser C, Meyer H, Biasi C, Rusalimova O, Barsukov P, Richter A (2007) Conservation of soil organic matter through cryoturbation in arctic soils in Siberia. *Journal of Geophysical Research: Biogeosciences*, **112**, G02017.

Kaye JP, Hart SC (1997) Competition for nitrogen between plants and soil microorganisms. *Trends in Ecology & Evolution*, **12**, 139–143.

Keeling CD (1958) The concentration and isotopic abundances of atmospheric carbon dioxide in rural areas. *Geochimica et Cosmochimica Acta*, **13**, 322–334.

Van Kessel C, Horwath WR, Hartwig U, Harris D, LÜscher A (2000) Net soil carbon input under ambient and elevated CO2 concentrations: isotopic evidence after 4 years. *Global Change Biology*, **6**, 435–444.

Knohl A, Werner RA, Brand WA, Buchmann N (2004) Short-term variations in δ13C of ecosystem respiration reveals link between assimilation and respiration in a deciduous forest. *Oecologia*, **142**, 70–82.

Koven CD, Chambers JQ, Georgiou K et al. (2015) Controls on terrestrial carbon feedbacks by productivity versus turnover in the CMIP5 Earth System Models. *Biogeosciences*, **12**, 5211–5228.

Kuznetsova A, Brockhoff PB, Christensen RHB (2014) *lmerTest: Tests for random and fixed effects for linear mixed effect models (lmer objects of lme4 package).. R package version 2.0-11*.

Kuzyakov Y, Cheng W (2001) Photosynthesis controls of rhizosphere respiration and organic matter decomposition. *Soil Biology and Biochemistry*, **33**, 1915–1925.

Kuzyakov Y, Friedel JK, Stahr K (2000) Review of mechanisms and quantification of priming effects. *Soil Biology and Biochemistry*, **32**, 1485–1498.

Langley JA, McKinley DC, Wolf AA, Hungate BA, Drake BG, Megonigal JP (2009) Priming depletes soil carbon and releases nitrogen in a scrub-oak ecosystem exposed to elevated CO2. *Soil Biology and Biochemistry*, **41**, 54–60.

Lara MJ, Genet H, McGuire AD et al. (2016) Thermokarst rates intensify due to climate change and forest fragmentation in an Alaskan boreal forest lowland. *Global Change Biology*, **22**, 816–829.

Liancourt P, Sharkhuu A, Ariuntsetseg L et al. (2011) Temporal and spatial variation in how vegetation alters the soil moisture response to climate manipulation. *Plant and Soil*, **351**, 249–261.

Loya WM, Johnson LC, Kling GW, King JY, Reeburgh WS, Nadelhoffer KJ (2002) Pulse-labeling studies of carbon cycling in arctic tundra ecosystems: Contribution of photosynthates to soil organic matter. *Global Biogeochemical Cycles*, **16**, 1101.

Luo Z, Wang E, Sun OJ (2016) A meta-analysis of the temporal dynamics of priming soil carbon decomposition by fresh carbon inputs across ecosystems. *Soil Biology and Biochemistry*, **101**, 96–103.

Mack MC, Schuur EAG, Bret-Harte MS, Shaver GR, Chapin FS (2004) Ecosystem carbon storage in arctic tundra reduced by long-term nutrient fertilization. *Nature*, **431**, 440–443.

McGuire AD, Anderson LG, Christensen TR et al. (2009) Sensitivity of the carbon cycle in the Arctic to climate change. *Ecological Monographs*, **79**, 523–555.

McGuire AD, Christensen TR, Hayes D et al. (2012) An assessment of the carbon balance of Arctic tundra: comparisons among observations, process models, and atmospheric inversions. *Biogeosciences*, **9**, 3185–3204.

Minke M, Donner N, Karpov N, de Klerk P, Joosten H (2009) Patterns in vegetation composition, surface height and thaw depth in polygon mires in the Yakutian Arctic (NE Siberia): a microtopographical characterisation of the active layer. *Permafrost and Periglacial Processes*, **20**, 357–368.

Murphy CJ, Baggs EM, Morley N, Wall DP, Paterson E (2015) Rhizosphere priming can promote mobilisation of N-rich compounds from soil organic matter. *Soil Biology and Biochemistry*, **81**, 236–243.

Nadelhoffer KJ, Giblin AE, Shaver GR, Laundre JA (1991) Effects of Temperature and Substrate Quality on Element Mineralization in Six Arctic Soils. *Ecology*, **72**, 242–253.

Natali SM, Schuur E a. G, Trucco C, Hicks Pries CE, Crummer KG, Baron Lopez AF (2011) Effects of experimental warming of air, soil and permafrost on carbon balance in Alaskan tundra. *Global Change Biology*, **17**, 1394–1407.

Natali SM, Schuur EAG, Mauritz M et al. (2015) Permafrost thaw and soil moisture driving CO_2 and CH_4 release from upland tundra. *Journal of Geophysical Research: Biogeosciences*, n/a–n/a.

Nickerson N, Risk D (2009) A numerical evaluation of chamber methodologies used in measuring the delta(13)C of soil respiration. *Rapid communications in mass spectrometry: RCM*, **23**, 2802–2810.

De Nobili M, Contin M, Mondini C, Brookes PC (2001) Soil microbial biomass is triggered into activity by trace amounts of substrate. *Soil Biology and Biochemistry*, **33**, 1163–1170.

Norby RJ, DeLucia EH, Gielen B et al. (2005) Forest response to elevated CO2 is conserved across a broad range of productivity. *Proceedings of the National Academy of Sciences of the United States of America*, **102**, 18052–18056.

Oechel WC, Sveinbjörnsson B (1978) Primary production processes in arctic bryophytes at Barrow, Alaska. In: *Vegetation and production ecology of an Alaskan arctic tundra*, pp. 269–298. Springer.

Oechel WC, Cowles S, Grulke N et al. (1994) Transient nature of CO2 fertilization in Arctic tundra. *Nature*, **371**, 500–503.

Olivas PC, Oberbauer SF, Tweedie CE, Oechel WC, Kuchy A (2010) Responses of CO2 flux components of Alaskan Coastal Plain tundra to shifts in water table. *Journal of Geophysical Research: Biogeosciences*, **115**, G00I05.

Olivas PC, Oberbauer SF, Tweedie C, Oechel WC, Lin D, Kuchy A (2011) Effects of Fine-Scale Topography on CO2 Flux Components of Alaskan Coastal Plain Tundra: Response to Contrasting Growing Seasons. *Arctic, Antarctic, and Alpine Research*, **43**, 256–266.

Osterkamp TE, Jorgenson MT, Schuur EAG, Shur YL, Kanevskiy MZ, Vogel JG, Tumskoy VE (2009) Physical and ecological changes associated with warming permafrost and thermokarst in interior Alaska. *Permafrost and Periglacial Processes*, **20**, 235–256.

Pataki DE, Ehleringer JR, Flanagan LB et al. (2003) The application and interpretation of Keeling plots in terrestrial carbon cycle research: APPLICATION OF KEELING PLOTS. *Global Biogeochemical Cycles*, **17**, n/a–n/a.

Pearson RG, Phillips SJ, Loranty MM, Beck PSA, Damoulas T, Knight SJ, Goetz SJ (2013) Shifts in Arctic vegetation and associated feedbacks under climate change. *Nature Climate Change*, **3**, 673–677.

Perveen N, Barot S, Alvarez G et al. (2014) Priming effect and microbial diversity in ecosystem functioning and response to global change: a modeling approach using the SYMPHONY model. *Global Change Biology*, **20**, 1174–1190.

Phillips DL, Gregg JW (2001) Uncertainty in source partitioning using stable isotopes. *Oecologia*, **127**, 171–179.

Post E, Forchhammer MC, Bret-Harte MS et al. (2009) Ecological Dynamics Across the Arctic Associated with Recent Climate Change. *Science*, **325**, 1355–1358.

Riley WJ, Maggi F, Kleber M, Torn MS, Tang JY, Dwivedi D, Guerry N (2014) Long residence times of rapidly decomposable soil organic matter: application of a multi-phase, multi-component, and vertically resolved model (BAMS1) to soil carbon dynamics.

Saleska SR, Shaw MR, Fischer ML, Dunne JA, Still CJ, Holman ML, Harte J (2002) Plant community composition mediates both large transient decline and predicted long-term recovery of soil carbon under climate warming. *Global Biogeochemical Cycles*, **16**, 1055.

Schuur E a. G, McGuire AD, Schädel C et al. (2015) Climate change and the permafrost carbon feedback. *Nature*, **520**, 171–179.

Shibistova O, Yohannes Y, Boy J, Richter A, Wild B, Watzka M, Guggenberger G (2012) Rate of Belowground Carbon Allocation Differs with Successional Habit of Two Afromontane Trees. *PLoS ONE*, **7**, e45540.

Sileshi GW (2014) A critical review of forest biomass estimation models, common mistakes and corrective measures. *Forest Ecology and Management*, **329**, 237–254.

Silvola J, Alm J, Ahlholm U, Nykaenen H, Martikainen PJ (1996) The contribution of plant roots to CO2 fluxes from organic soils. *Biology and fertility of Soils*, **23**, 126–131.

Sistla SA, Moore JC, Simpson RT, Gough L, Shaver GR, Schimel JP (2013) Long-term warming restructures Arctic tundra without changing net soil carbon storage. *Nature*, **497**, 615–618.

Sloan VL, Brooks JD, Wood SJ, Liebig JA, Siegrist J, Iversen CM, Norby RJ (2014a) *Plant community composition and vegetation height, Barrow, Alaska, Ver. 1*. Carbon Dioxide Information Analysis Center, Oak Ridge National Laboratory, Oak Ridge, Tennessee, USA.

Sloan VL, Liebig JA, Hahn MS et al. (2014b) *Soil temperature, soil moisture and thaw depth, Barrow, Alaska, Ver. 1*. Carbon Dioxide Information Analysis Center, Oak Ridge National Laboratory, Oak Ridge, Tennessee, USA.

Smith DL, Johnson L (2004) Vegetation-Mediated Changes in Microclimate Reduce Soil Respiration as Woodlands Expand into Grasslands. *Ecology*, **85**, 3348–3361.

Smith LC, MacDonald GM, Velichko AA et al. (2004) Siberian Peatlands a Net Carbon Sink and Global Methane Source Since the Early Holocene. *Science*, **303**, 353–356.

Sparling GP, Feltham CW, Reynolds J, West AW, Singleton P (1990) Estimation of soil microbial c by a fumigation-extraction method: use on soils of high organic matter content, and a reassessment of the kec-factor. *Soil Biology and Biochemistry*, **22**, 301–307.

Street LE, Subke J-A, Sommerkorn M, Sloan V, Ducrotoy H, Phoenix GK, Williams M (2013) The role of mosses in carbon uptake and partitioning in arctic vegetation. *New Phytologist*, **199**, 163–175.

Sturm M, Racine C, Tape K (2001) Climate change: Increasing shrub abundance in the Arctic. *Nature*, **411**, 546–547.

Sulman BN, Phillips RP, Oishi AC, Shevliakova E, Pacala SW (2014) Microbe-driven turnover offsets mineral-mediated storage of soil carbon under elevated CO2. *Nature Climate Change*, **4**, 1099–1102.

Torn MS, Davis S, Bird JA, Shaw MR, Conrad ME (2003) Automated analysis of 13C/12C ratios in CO2 and dissolved inorganic carbon for ecological and environmental applications. *Rapid Communications in Mass Spectrometry*, **17**, 2675–2682.

Trumbore S (2000) Age of soil organic matter and soil respiration: radiocarbon constraints on belowground c dynamics. *Ecological Applications*, **10**, 399–411.

Turner DP, Ritts WD, Cohen WB et al. (2006) Evaluation of MODIS NPP and GPP products across multiple biomes. *Remote Sensing of Environment*, **102**, 282–292.

Vance ED, Brookes PC, Jenkinson DS (1987) An extraction method for measuring soil microbial biomass C. *Soil Biology and Biochemistry*, **19**, 703–707.

Webb EE, Schuur EAG, Natali SM et al. (2016) Increased wintertime CO2 loss as a result of sustained tundra warming. *Journal of Geophysical Research: Biogeosciences*, **121**, 2014JG002795.

Wieder WR, Allison SD, Davidson EA et al. (2015) Explicitly representing soil microbial processes in Earth system models. *Global Biogeochemical Cycles*, **29**, 2015GB005188.

Wild B, Schnecker J, Eloy Alves RJ et al. (2014) Input of easily available organic C and N stimulates microbial decomposition of soil organic matter in arctic permafrost soil. *Soil Biology and Biochemistry*.

Wild B, Gentsch N, Čapek P et al. (2016) Plant-derived compounds stimulate the decomposition of organic matter in arctic permafrost soils. *Scientific Reports*, **6**, 25607.

Williams M, Eugster W, Rastetter EB, Mcfadden JP, Chapin Iii FS (2000) The controls on net ecosystem productivity along an Arctic transect: a model comparison with flux measurements. *Global Change Biology*, **6**, 116–126.

Xu L, Furtaw MD, Madsen RA, Garcia RL, Anderson DJ, McDermitt DK (2006) On maintaining pressure equilibrium between a soil CO_2 flux chamber and the ambient air. *Journal of Geophysical Research*, **111**.

Zhang Y, Xu M, Chen H, Adams J (2009) Global pattern of NPP to GPP ratio derived from MODIS data: effects of ecosystem type, geographical location and climate. *Global Ecology and Biogeography*, **18**, 280–290.

Zhu B, Cheng W (2011) Rhizosphere priming effect increases the temperature sensitivity of soil organic matter decomposition. *Global Change Biology*, **17**, 2172–2183.

Zona D, Lipson DA, Richards JH et al. (2014) Delayed responses of an Arctic ecosystem to an extreme summer: impacts on net ecosystem exchange and vegetation functioning. *Biogeosciences*, **11**, 5877–5888.

Tables and figures

Table 1
Summary of belowground soil measurements
(a) Cores collected in 2014

Treatment	Date	Depth (cm)	%C	%N	δ^{13}C-SOM (‰)	MBC (mg g^{-1})	δ^{13}C-MBC (‰)	GWC (%)
High glucose	Sept 8	0-10	16.0 ± 10.6	0.647 ± 0.539	-24.2 ± 2.88	--	--	48.5 ± 19.9
		10-20	8.60 ± 4.92	0.425 ± 0.204	-16.6 ± 6.55	0.839 ± 0.326	820 ± 490**	28.9 ± 10.6
		20-30	10.8 ± 5.81	0.573 ± 0.286	-24.3 ± 4.94	--	--	33.5 ± 13.7
	Sept 20	0-10	13.3 ±5.89	0.627 ± 0.252	-20.6 ± 7.87	--	--	44.5 ± 12.5
		10-20	7.78 ± 4.86	0.392 ± 0.252	-19.9 ± 5.67	0.661 ± 0.378	150 ± 91***	29.6 ± 12.0
		20-30	11.5 ± 8.94	0.618 ± 0.543	-22.6 ± 5.26	--	--	32.2 ± 16.0
Low glucose	Sept 8	0-10	12.1 ± 8.39	0.689 ± 0.556	-26.8 ± 0.713	--	--	41.6 ± 16.5
		10-20	8.68 ± 6.05	0.499 ± 0.390	-25.9 ± 1.84	0.940 ± 1.05	290 ± 210	29.7 ± 14.4
		20-30	9.22 ± 8.07	0.527 ± 0.524	-26.1 ± 3.04	--	--	30.3 ± 15.0
	Sept 20	0-10	--	--	--	--	--	37.6 ± 10.8*
		10-20	7.82 ± 4.98	0.415 ± 0.294	-24.5 ± 1.94	0.999 ± 1.19	290 ± 170	29.3 ± 13.19
		20-30	5.66 ± 2.65	0.312 ± 0.175	-26.7 ± 1.91	--	--	24.1 ± 7.91
Control	Sept 8	0-10	16.5 ± 10.8	0.658 ± 0.161	--	--	--	49.2 ± 15.3
		10-20	10.4 ± 4.57	0.564 ± 0.291	-26.9 ± 1.58	0.818 ± 0.537	-21 ±6.2	37.1 ± 11.7
		20-30	11.5 ± 5.79	0.611 ± 0.368	-27.6 ± 1.71	--	--	35.4 ± 11.8
	Sept 20	0-10	14.1 ± 4.39	0.688 ± 0.208	-27.3 ± 0.503	--	--	45.6 ± 9.39
		10-20	8.96 ± 3.43	0.472 ± 0.206	--	0.830 ± 0.662	-20 ± 3.2	27.1 ± 9.73
		20-30	10.0 ± 6.56	0.551 ± 0.404	-28.0 ± 0.714	--	--	30.5 ± 14.4

Note: Values are averaged across polygons with uncertainty ranges indicating standard deviations and n=6 unless otherwise noted.
*n = 5
** One outlier with erroneously negative values was omitted from the calculation.
*** Two outliers with erroneously negative values were omitted from the calculation.

(b) Cores collected in 2016

Treatment	Date	Depth (cm)	n	%C	%N	δ^{13}C-SOM (‰)	Bulk density (g cm^{-3})	GWC (%)
High glucose	April 21	0-10	3	8.06 ± 3.31	0.365 ± 0.135	-23.0 ± 2.67	0.386 ± 0.110	39.0 ± 11.4
		10-20	3	4.97 ± 1.08	0.272 ± 0.0551	-11.6 ±14.0	0.674 ± 0.243	32.5 ± 8.7
		20-30	3	5.46 ± 1.19	0.308 ± 0.0592	2.66 ± 14.5	0.656 ± 0.219	33.0 ± 8.4
		>30	3	6.34 ± 0.217	0.357 ± 0.0388	-11.9 ± 0.188	0.715 ± 0.185	29.8 ± 10.5
	November 9	0-10	3	14.8 ± 9.00	0.787 ± 0.610	-23.4 ± 4.15	0.253 ± 0.136	54.1 ± 21.9
		10-20	3	5.24 ± 3.58	0.297 ± 0.180	-10.2 ± 15.3	0.830 ± 0.221	31.0 ± 8.6
		20-30	3	7.10 ± 2.15	0.393 ± 0.0950	-16.32 ± 8.37	0.938 ± 0.194	26.5 ± 3.7
		>30	3	11.9 ± 4.30	0.637 ± 0.198	-24.7 ± 0.890	0.714 ± 0.090	31.8 ± 9.4
Control	April 21	0-10	3	10.3 ± 7.83	0.403 ± 0.248	-27.6 ± 0.751	0.356 ± 0.225	42.5 ± 9.7
		10-20	3	5.60 ± 1.87	0.277 ± 0.0794	-27.9 ± 0.138	0.764 ± 0.411	35.6 ± 9.7
		20-30	3	7.13 ± 3.22	0.397 ± 0.177	-27.4 ± 0.338	0.785 ± 0.264	33.6 ± 11.2
		>30	3	8.84 ± 3.08	0.503 ± 0.188	-27.6 ± 0.631	0.796 ± 0.152	28.3 ± 5.9
	November 9	0-10	2	25.4 ± 18.7	1.14 ± 0.946	-27.5 ± 0.515	0.250 ± 0.290	79.7 ± 10.1
		10-20	2	11.0 ± 14.0	0.788 ± 1.09	-28.0 ± 0.440	0.931 ± 0.343	37.9 ± 4.5 (n=2)
		20-30	3	6.87 ± 0.569	0.403 ± 0.0208	-27.7 ± 0.873	1.00 ± 0.19	30.1 ± 0.8 (n=2)
		>30	2	22.2 ± 23.5	1.24 ± 1.26	-28.05 ± 0.753	0.676 ± 0.190	27.3 (n=1)

Note: Cores were collected frozen from polygons 1-3 on April 21 and from polygons 4-6 on November 9.

Table 2
Glucose recovery in high glucose and low glucose mesocosms

Treatment	Core sampling date	Glucose added (mg)	Depth (cm)	Glucose recovered (mg)	Recovery rate (%)
High glucose	September 8, 2014	2450	0-10	92.9 ± 15.5	3.79 ± 1.69
			10-20	361 ± 38.4	14.7 ± 1.57
			20-30	140 ± 21.3	5.70 ± 0.870
			Whole profile	593 ± 46.6	24.2 ± 1.90
	September 20, 2014	2450	0-10	252 ± 56.9	10.3 ± 2.32
			10-20	179 ± 19.4	7.29 ± 0.792
			20-30	107 ± 18.6	4.36 ± 0.757
			Whole profile	537 ± 62.9	21.9 ± 2.57
	April 21, 2016	4900	0-10	143 ± 26.7	2.92 ± 0.543
			10-20	609 ± 198	12.4 ± 4.04
			20-30	1160 ± 217	23.6 ± 4.44
			>30	782 ± 73.5	16.0 ± 1.50
			Whole profile	2690 ± 304	54.9 ± 6.21
	November 9, 2016	4900	0-10	167 ± 79.1	3.40 ± 2.61
			10-20	444 ± 49.9	9.06 ± 3.35
			20-30	630 ± 159	12.9 ± 4.65
			>30	207 ± 11.3	4.23 ± 6.30
			Whole profile	1450 ± 185	29.6 ± 8.91
Low glucose	September 8, 2014	491	0-10	14.4 ± 3.37	2.93 ± 0.687
			10-20	44.6 ± 11.1	9.08 ± 2.26
			20-30	55.5 ± 15.8	11.3 ± 3.21
			Whole profile	114.5 ± 19.6	23.3 ± 3.99
	September 20, 2014	491	0-10	--	--
			10-20	61.2 ± 8.31	12.5 ± 1.69
			20-30	3.91 ± 4.36	0.797 ± 0.887
			Whole profile	--	--

Note: Total and percentage glucose recovery was calculated from ^{13}C abundance, carbon content, and total mass of soil cores, scaled to mesocosm area.

Table 3
Summary of 2015 surface trace gas fluxes, partitioned into non-glucose-derived and glucose-derived components

Polygon	Treatment	Post-treatment R_N ($\mu mol\ CO_2\ m^{-2}\ s^{-1}$)	Post-treatment R_G ($\mu mol\ CO_2\ m^{-2}\ s^{-1}$)	Pre-treatment 7°C R_N ($\mu mol\ CO_2\ m^{-2}\ s^{-1}$)	Post-treatment 7°C R_N ($\mu mol\ CO_2\ m^{-2}\ s^{-1}$)
1	High glucose	0.78 ± 0.28 (n = 6)	0.060 ± 0.030 (n = 6)	1.53 ± 0.417 (n = 7)	1.33 ± 0.542 (n = 5)
	Control	0.48 ± 0.19 (n = 7)	--	1.75 ± 0.590 (n = 8)	1.08 ± 0.359 (n = 6)
2	High glucose	0.86 ± 0.28 (n = 5)	0.14 ± 0.076 (n = 5)	1.78 ± 1.69 (n = 7)	0.969 ± 0.278 (n = 4)
	Control	0.75 ± 0.55 (n = 7)	--	0.701 ± 0.0796 (n = 6)	0.931 ± 0.406 (n = 6)
3	High glucose	0.83 ± 0.31 (n = 6)	0.097 ± 0.071 (n = 6)	0.813 ± 0.168 (n = 8)	0.969 ± 0.356 (n = 5)
	Control	0.81 ± 0.22 (n = 7)	--	0.693 ± 0.172 (n = 8)	0.915 ± 0.238 (n = 6)
4	High glucose	0.65 ± 0.21 (n = 6)	0.11 ± 0.043 (n = 6)	0.631 ± 0.0802 (n = 6)	0.797 ± 0.250 (n = 5)
	Control	0.94 ± 0.25 (n = 7)	--	0.819 ± 0.229 (n = 6)	0.937 ± 0.267 (n = 6)
5	High glucose	1.4 ± 0.73 (n = 7)	0.28 ± 0.20 (n = 7)	1.22 ± 0.608 (n = 6)	1.45 ± 0.686 (n = 6)
	Control	1.2 ± 0.48 (n = 7)	--	1.73 ± 0.933 (n = 6)	1.28 ± 0.483 (n = 6)
6	High glucose	0.94 ± 0.27 (n = 7)	0.14 ± 0.063 (n = 7)	1.12 ± 0.105 (n = 6)	1.07 ± 0.229 (n = 6)
	Control	1.2 ± 0.39 (n = 6)	--	1.95 ± 1.64 (n = 6)	1.24 ± 0.324 (n = 6)

Note: Values are temporal averages across pre-treatment sampling dates (June 23 through July 31) and post-treatment sampling dates (August 2 through September 1), with uncertainty ranges indicating standard deviations. Pre-treatment 7°C R_N and post-treatment 7°C R_N reflect R_N values normalized to their equivalent flux at 7°C using mesocosm-specific Q_{10} values.

Table 4
Results of a power analysis using simulated data across a range of priming levels varying from 0 % (no priming) to 100 % (priming-induced doubling of R_N)

Priming level (%)	Power* (%)
0	0.0
10	0.0
20	1.8
30	16
35	28
40	45
45	58
50	71
55	79
60	89
65	90
70	94
75	96
80	96
90	98
100	99

*Calculated as the percentage of simulations with a significant treatment effect (simulated vs. control), using a significance cutoff of $\alpha = 0.05$.

Table 5
Significant predictors of gross primary production between June 23 and September 1, 2016

Fixed effect	Estimate	DF	*F* value	Pr > *F*
Treatment (Control)	0.539	10.108	6.389	0.02976*
Day of year	-0.0288	101.432	47.880	4.17e-10***

Significance codes: 0 *** 0.001 ** 0.01 * 0.05 . 1

Table 6
Gross primary production in experimental mesocosms and adjacent high-centered polygon locations

Mesocosm class	GPP ($\mu mol\ CO_2\ m^{-2}\ s^{-1}$)	
	7/21/16	7/22/16
Control (n=3)	2.37 ± 1.16	2.49 ± 0.91
High glucose (n=2)	2.12 ± 0.54	1.70 ± 1.06
Adjacent polygons (n=18)	0.94 ± 0.45	1.05 ± 0.58

Note: Values are averaged across polygons, with error ranges representing standard deviations.

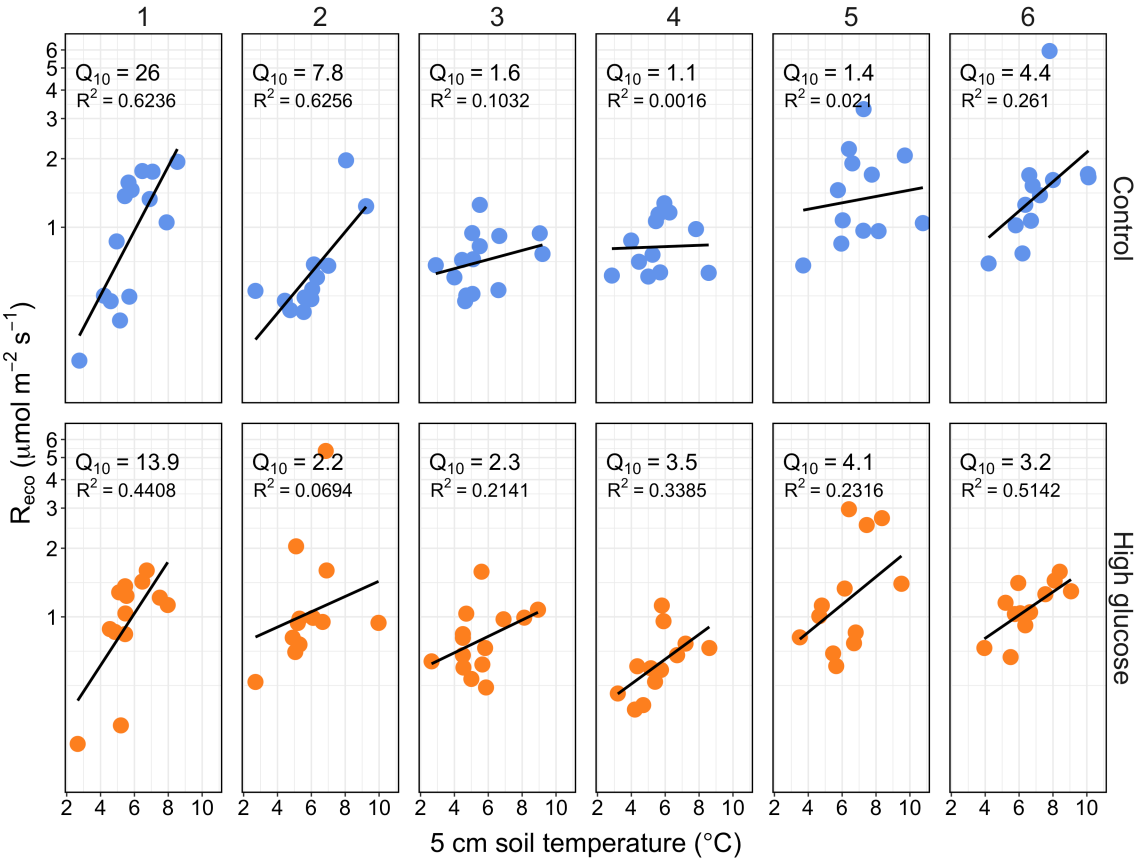

Figure 1. Temperature sensitivity of ecosystem respiration (R_{eco}). Q_{10} was calculated for each mesocosm in polygons 1-6 using all non-partitioned R_{eco} measurements made between June 23 and September 1, 2015.

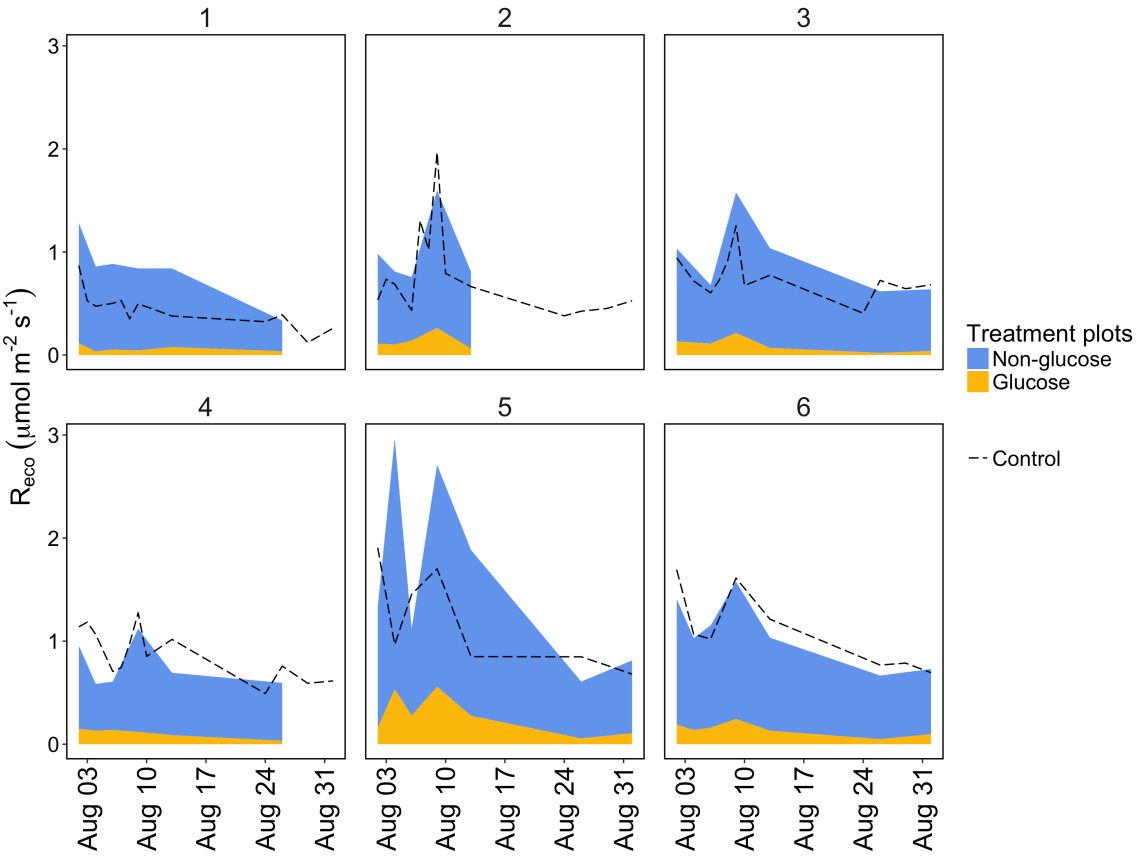

Figure 2. Partitioned ecosystem respiration from individual polygons following 2015 glucose addition. Blue shading is CO_2 efflux in treatment plots derived from native (non-glucose) ecosystem respiration, yellow shading is CO_2 efflux in treatment plots derived from glucose mineralization, and dashed line is total CO_2 efflux in control plots, equivalent to native ecosystem respiration.

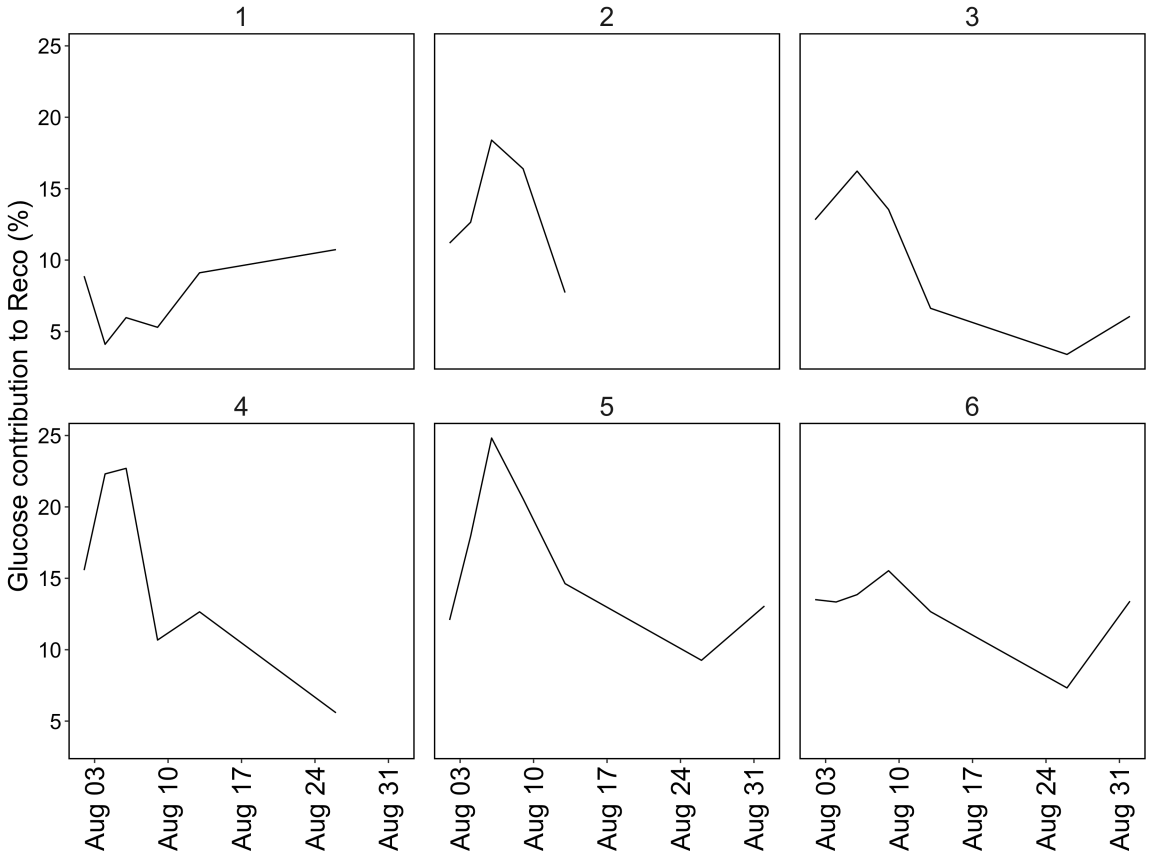

Figure 3. Glucose mineralization following 2015 glucose addition as % of total ecosystem respiration

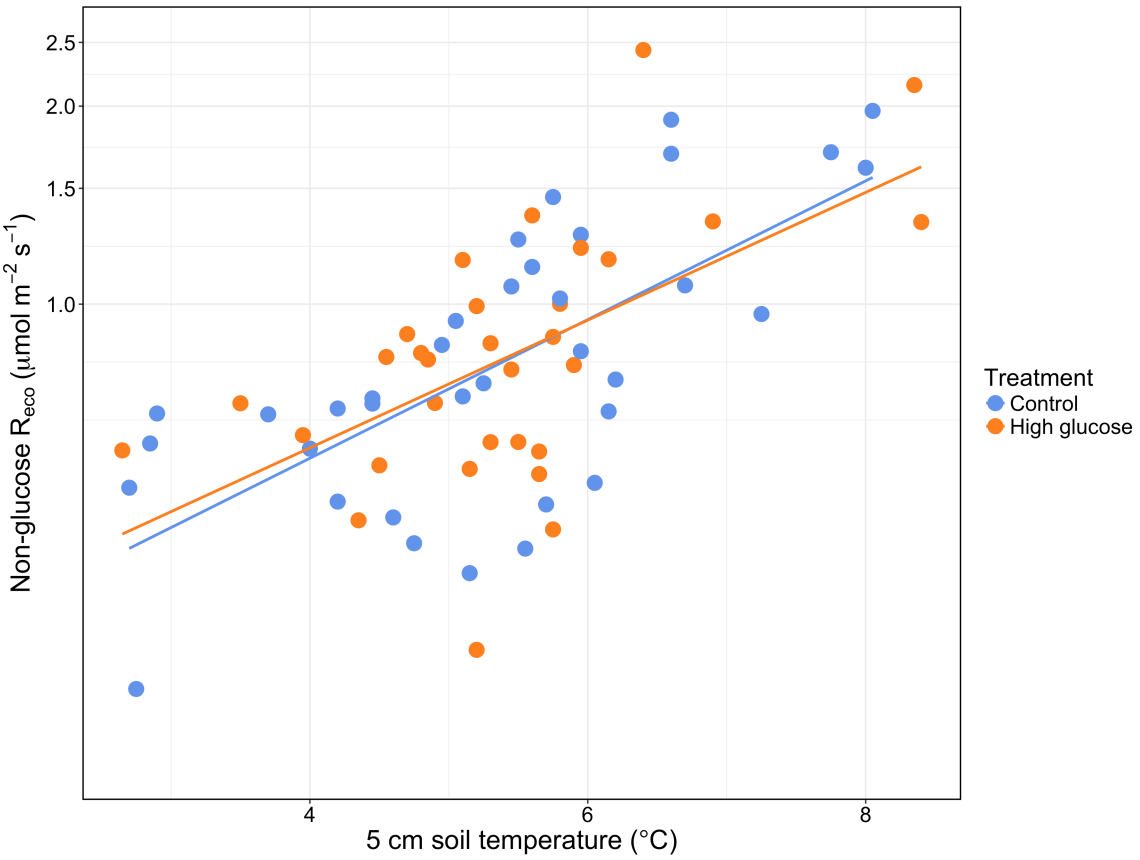

Figure 4. Effect of glucose addition on the rate and temperature sensitivity of native (non-glucose) ecosystem respiration. Data include all measurements made between August 2 and September 1, 2015 in control and high glucose mesocosms.

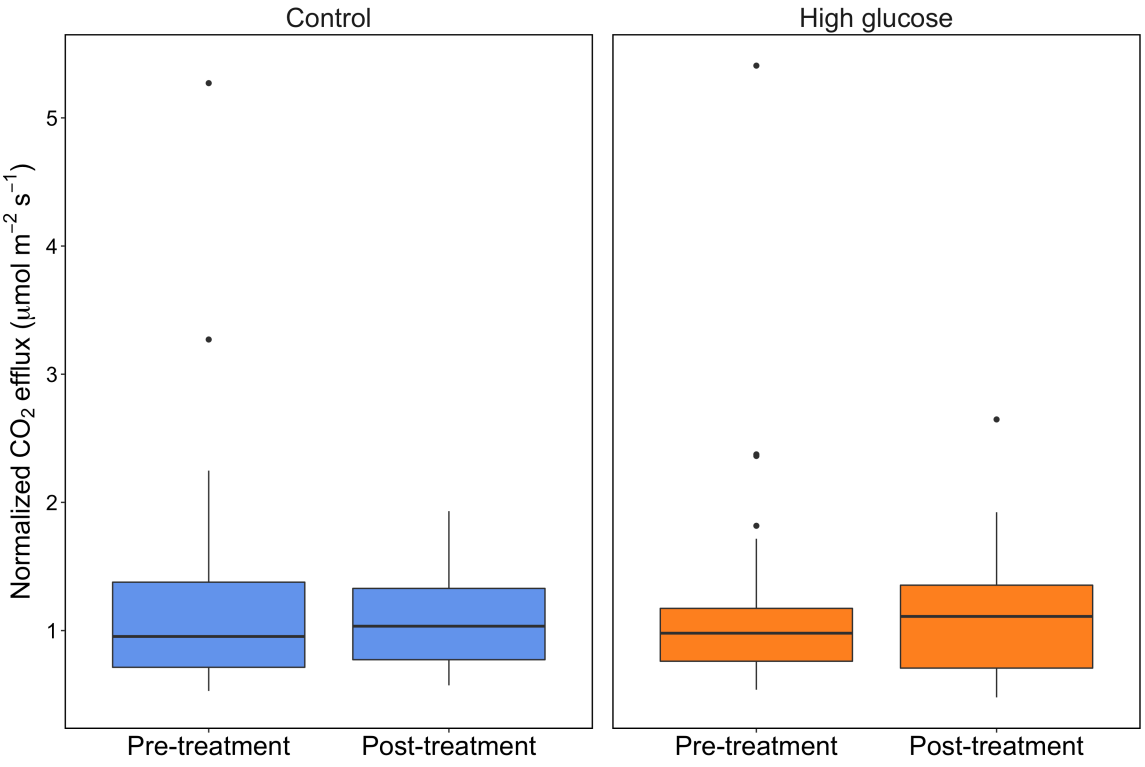

Figure 5. Temperature-normalized ecosystem respiration before and after 2015 glucose addition. Values of CO_2 efflux attributed to native (non-glucose) ecosystem respiration were normalized to 7°C using Q_{10} values calculated individually for each mesocosm. Pre-treatment measurements were made on June 23 and July 9, 12, 29, 30, and 31, and post-treatment measurements were made on August 2, 4, 6, 9, and 26. Boxes indicate median and first and third quartiles, with whiskers extending to the farthest values within 1.5 times the upper and lower quartiles. Outliers beyond this range are shown as points.

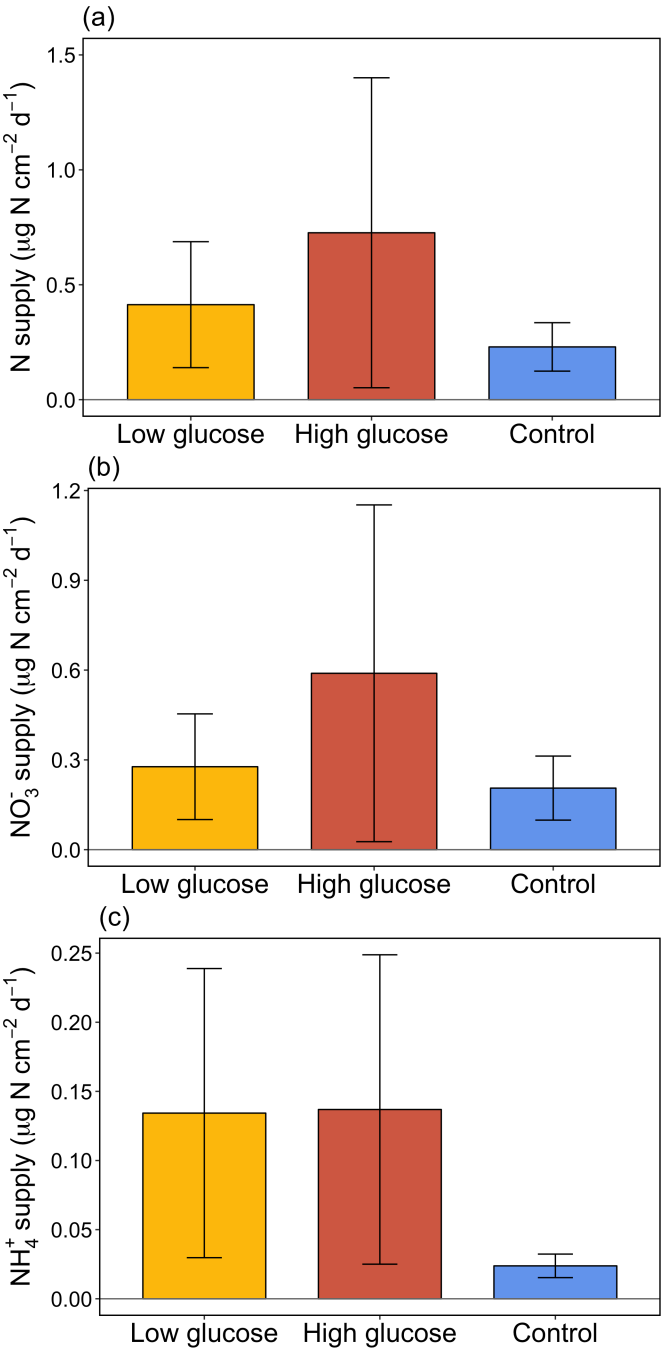

Figure 6. Nitrogen availability in treatment and control mesocosms following 2014 glucose addition treatment. Data represent average availability of (a) total N, (b) NO_3^--N, and (c) NH_4^+-N over a 21-day period, measured with buried ion exchange membranes centered at 15 cm depth. Data for each treatment are averaged across polygons, and error bars represent standard errors.

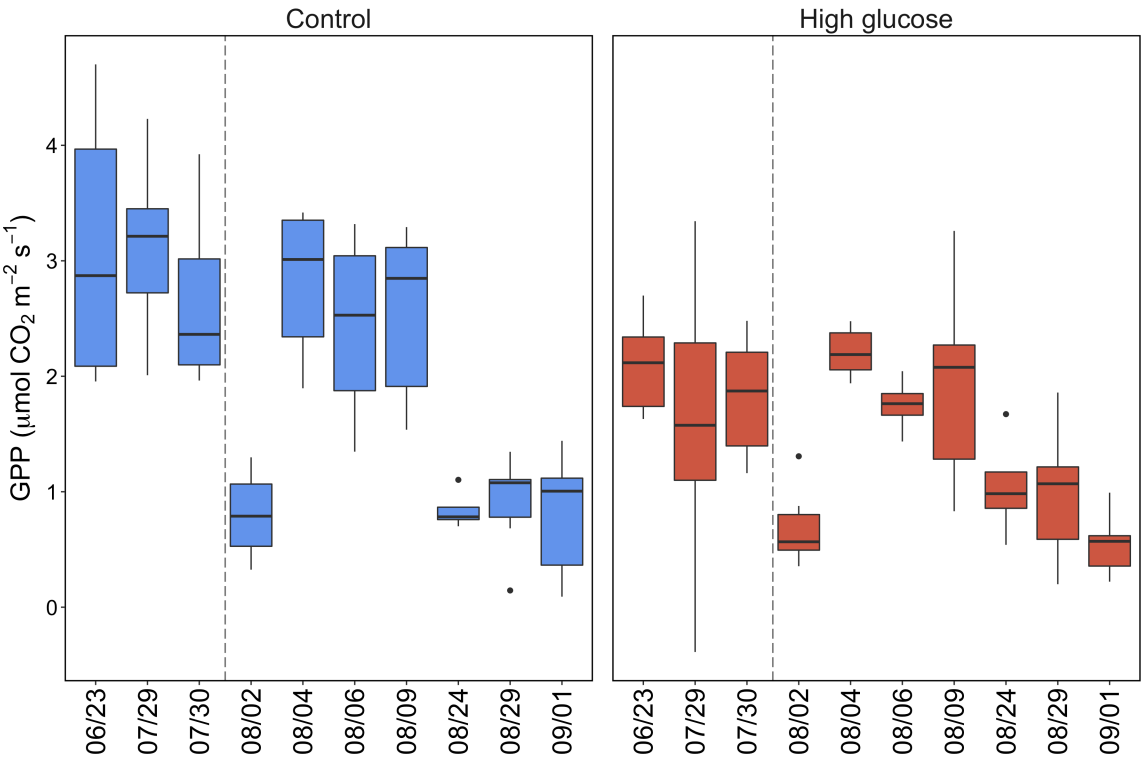

Figure 7. Gross primary production (GPP) in high glucose and control mesocosms in 2015. GPP values were calculated from transparent and opaque soil chamber measurements of NEE and R_{eco}. Data for each date include measurements from polygons 1-6. Boxes indicate median and first and third quartiles, with whiskers extending to the farthest values within 1.5 times the upper and lower quartiles. Outliers beyond this range are shown as points. Dashed vertical line represents glucose addition treatment on 8/1/15.

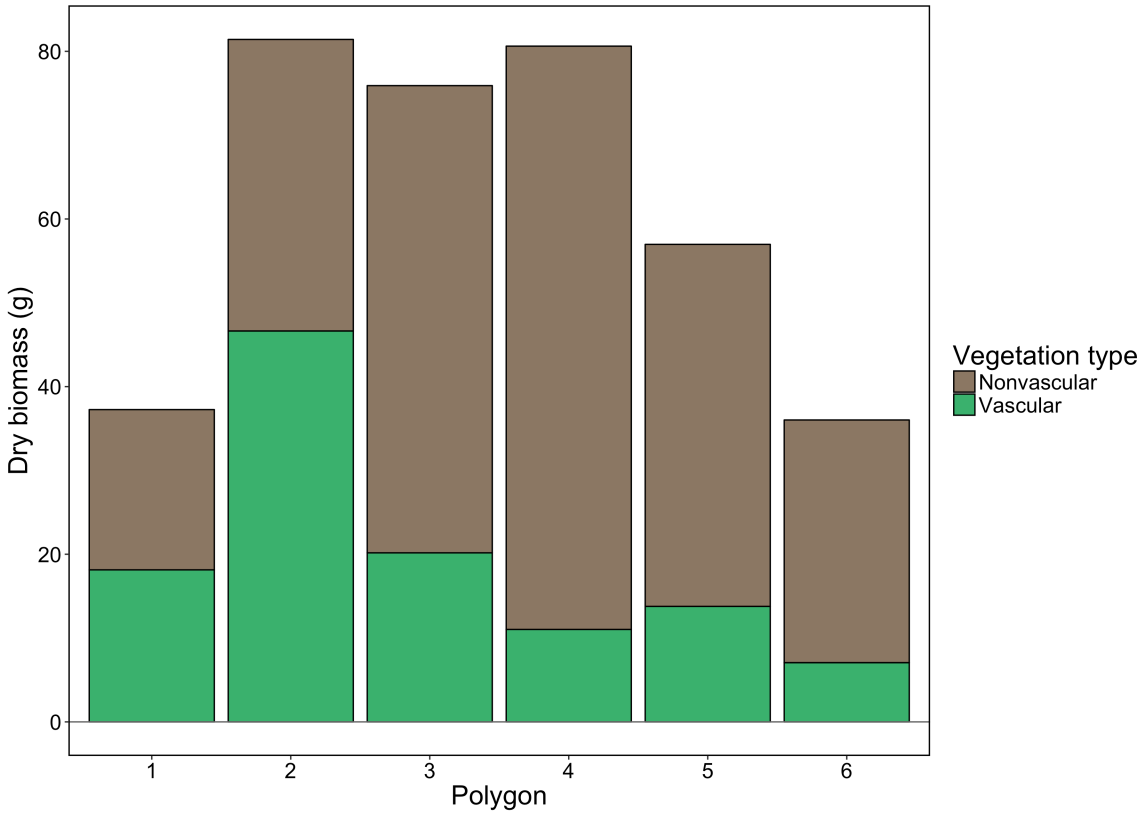

Figure 8. Vegetation biomass in individual polygons. Biomass was sampled destructively from circular patches adjacent to treatment or control mesocosms of equal area. Prior to drying, vegetation was separated into vascular and nonvascular (moss + lichen) components.

CHAPTER 4: RADIOCARBON EVIDENCE THAT MILLENNIAL AND FAST-CYCLING SOIL ORGANIC CARBON ARE EQUALLY RESPONSIVE TO TEMPERATURE OR ANOXIA

Abstract

The response of soil organic carbon storage to changes in temperature and soil drainage depends on the distribution of environmental sensitivities across soil carbon pools. Theoretical predictions that passive soil carbon pools are more sensitive to changes in temperature and shifts from anaerobic to aerobic conditions have strong implications for long-term soil carbon losses. We test this prediction with two incubation experiments with soils from Barrow, Alaska. Using natural abundance radiocarbon, we (1) evaluate the spatial and vertical distribution of fast-cycling and slow-cycling carbon pools in permafrost soils, and (2) test the relative sensitivity of these pools to changes in temperature and oxygen availability. Highly negative $\Delta^{14}C$ values in respired CO_2 and bulk soil organic matter indicate both storage and turnover of old, stabilized carbon, particularly near the base of the active layer. Differences in $\Delta^{14}C$ between the mineralized and non-mineralized carbon fractions suggest that substrate decomposability varies along a turnover time gradient. With a novel method for disentangling the effects of temperature and substrate depletion, we find that slow-cycling carbon is no more sensitive to temperature than is fast-cycling carbon, with a Q_{10} of 2 irrespective of turnover time. Similarly, we found that the age of respired carbon was unaffected by aerobic vs. anaerobic incubation treatments, indicating a similar response between fast- and slow-cycling carbon. We find, therefore, that these ancient soil carbon stores are sensitive to warming or drying, with similar environmental sensitivities across depths and carbon pools. This finding suggests that in these soils, mechanisms other than chemical recalcitrance exert primary control on decomposition rates and/or environmental sensitivities.

Introduction

High latitude soils are an important carbon reservoir. There, cold, frozen, and anaerobic conditions have stabilized soil organic matter, leading to an accumulation of an estimated 1,300 Pg of carbon (Hugelius *et al.*, 2014), roughly equal to that stored in global vegetation and atmospheric CO_2 (Ciais *et al.*, 2014). Over the coming decades, the Arctic is expected to shift from a sink to a source of atmospheric CO_2, as soil warming, permafrost thaw, and water-table changes destabilize this long-stored carbon (Koven *et al.*, 2011; McGuire *et al.*, 2012; Schuur *et al.*, 2015). Such changes have already been seen. Research has documented soil temperature increases (Osterkamp & Romanovsky, 1999; Osterkamp *et al.*, 2009) and permafrost thaw (Jorgenson *et al.*, 2006, 2013), with associated changes in soil hydrology (Hinzman *et al.*, 2005; Andresen & Lougheed, 2015) and increased rates of soil carbon mineralization, particularly from old, previously stable pools (Schuur *et al.*, 2009; Hicks Pries *et al.*, 2013).

Model predictions of high latitude soil carbon losses range widely, from 37 to 174 Pg by 2100 (Schuur *et al.*, 2015). Model sensitivities underlying this range include the parameterized, inherent decomposability of soil carbon stocks (Koven *et al.*, 2015), the temperature sensitivity of carbon mineralization (Mikan *et al.*, 2002; Jones *et al.*, 2003;

Davidson & Janssens, 2006), and soil moisture-driven changes in oxygen availability (Lawrence *et al.*, 2015). Importantly, soil organic matter (SOM) is a heterogeneous reservoir with a range of chemical compositions, cycling rates, and stabilization mechanisms. As such, these model sensitivities depend on the distributions of organic compounds, their physio-chemical states, and their responses to environmental conditions. To describe dynamics of this heterogeneous system, bulk soil carbon can be partitioned into pools, defined operationally by their turnover times or decomposition rates (Torn *et al.*, 2009). These turnover times are functions of substrate chemistry (chemical recalcitrance) (Sollins *et al.*, 1996; Lützow *et al.*, 2006), physical and chemical protection within the soil matrix (Torn *et al.*, 1997), and environmental variables such as temperature and oxygen availability (Davidson & Janssens, 2006). Despite more than a decade of research on soil fractions and turnover times (Christensen, 1992; Gaudinski *et al.*, 2000; Kahle *et al.*, 2003; McFarlane *et al.*, 2013), no consensus has been reached regarding how environmental sensitivities vary across soil carbon pools (Conant *et al.*, 2011), i.e., the degree to which increased temperature or oxygen availability influences carbon pool decomposition rates differently, or shifts material between pools (Hopkins *et al.*, 2012).

Theory and previous research suggest that soil carbon vulnerability to warming and drying may depend on substrate chemistry. Kinetic theory predicts that decomposition of compounds with higher activation energies (i.e., greater chemical stability) should be more sensitive to changes in temperature than more chemically labile substrates (Conant *et al.*, 2011). Similarly, anaerobic conditions may structure carbon pools via thermodynamic limits on decomposition of certain carbon compounds (Keiluweit *et al.*, 2016). If the cycling rate of SOM depends on its chemical composition, theory thus predicts that slow-cycling carbon pools will be particularly sensitive to environmental changes.

A number of observational and modeling studies support this theory, finding that slow-cycling, less decomposable carbon substrate pools are more sensitive to temperature (e.g., Melillo *et al.*, 2002; Fierer *et al.*, 2005; Knorr *et al.*, 2005) and shifts between aerobic and anaerobic conditions (Bridgham *et al.*, 1998; Knoblauch *et al.*, 2013) than rapidly cycling pools. Other studies, however, have found that soil carbon pools have neither different temperature sensitivities (Townsend *et al.*, 1997; Fang *et al.*, 2005) nor distinct chemical compositions (Marschner *et al.*, 2008; Kleber *et al.*, 2011), challenging the relationship between turnover time, substrate chemistry, and temperature- or oxygen-sensitivity. Instead, environmental sensitivities of decomposition may be mediated by complex, whole-ecosystem controls on soil carbon dynamics (Davidson & Janssens, 2006; Schmidt *et al.*, 2011; Dungait *et al.*, 2012). For example, temperature changes may alter mineral associations or other physio-chemical carbon stabilization mechanisms (Torn *et al.*, 1997), influencing decomposition rates irrespective of substrate chemistry.

Numerous studies have used incubation and field experiments to evaluate the temperature and oxygen sensitivities of different carbon pools (Bridgham *et al.*, 1998; Fierer *et al.*, 2005; Knorr *et al.*, 2005; Koch *et al.*, 2007; Hartley & Ineson, 2008; Lefèvre *et al.*, 2014). Without a clear tracer differentiating carbon pools, such studies generally make use of the non-steady state conditions inherent to incubations or field manipulations, estimating the temperature or oxygen sensitivities of different source

pools by fitting multiple pool models with Arrhenius or Arrhenius-type kinetics (Lloyd & Taylor, 1994) to changing CO_2 emissions. A challenge inherent to such studies is that results may be sensitive to predetermined model characteristics (e.g., functional form and number of pools) or other interacting variables. For example, incubation experiments often homogenize soils to generate replicates, which can disturb soil aggregates and physically destabilize carbon (Adu & Oades, 1978; Six *et al.*, 1998). Alternatively, transient responses from pool size changes may be difficult to disentangle from changes in microbial activity (Zogg *et al.*, 1997; Zhang *et al.*, 2005; Bradford *et al.*, 2008).

This study uses natural abundance radiocarbon to evaluate spatial distributions and environmental sensitivities of fast- and slow-cycling soil carbon pools in an Arctic tundra ecosystem. As a naturally occurring tracer of carbon pool dynamics (Trumbore, 2000), radiocarbon in CO_2 reflects the distribution of substrate mineralization rates. This enables us to estimate carbon dynamics metrics from individual measurements without having to fit models to carbon flux data. In two soil incubation experiments, we use radiocarbon measurements of CO_2 and bulk SOM to address three questions:

(1) How do soil carbon cycling rates vary with depth in the soil and across permafrost features? Across distinct microtopographic features, we use radiocarbon measurements of CO_2 and SOM to calculate turnover times of the actively cycling carbon pool, shallow bulk soil carbon, and soil carbon near the permafrost table.

(2) How do soil carbon pools with distinct cycling rates respond to changes in temperature? While radiocarbon has been used to compare the temperature sensitivities of different soil carbon pools (Bol *et al.*, 2003; Hilasvuori *et al.*, 2013), few studies have isolated this effect from substrate depletion and microbial acclimation (Dioumaeva *et al.*, 2002). Through a novel analytical framework incorporating CO_2 production rates and radiocarbon contents, we isolate the temperature sensitivities of fast- and slow-cycling carbon.

(3) How do anaerobic conditions influence the relative decomposition rates of different carbon pools? We use radiocarbon measurements from parallel aerobic/anaerobic incubations to test whether slow-cycling carbon substrates have been selectively preserved due to anaerobic conditions. To our knowledge, no published studies have used radiocarbon to evaluate differences in carbon pool dynamics under aerobic vs. anaerobic conditions.

Methods

Site

Soil samples were collected from the Barrow Environmental Observatory (BEO), which lies ~6 km east of the village of Barrow, Alaska (71.3N, 156.5W), at the northern edge of the Alaskan Arctic coastal plain. Barrow has a mean annual temperature of -12°C and mean annual precipitation of 106 mm, with long, dry winters and short, moist, cool summers. The land surface has low topographic relief up to 5 m elevation and a shallow active layer ranging from 20 to 60 cm underlain by continuous ice-rich permafrost to depths greater than 400 m (Hinkel & Nelson, 2003). Formed from the late Pleistocene Gubic formation (Black, 1964), soils in the region are dominated by Typic Aquiturbels (53 %), Typic Histoturbels (22 %), and Typic Aquorthels (8.6 %) (Bockheim *et al.*, 1999).

Within the BEO, samples were collected from ice wedge polygons, discrete landscape units formed by freezing and thawing processes that cover ~65 % of the ground surface (Billings & Peterson, 1980; Brown *et al.*, 1980; Lara *et al.*, 2014). Low-lying, saturated troughs separate individual polygons, which are 10-20 m in diameter with raised, relatively dry rims at their perimeter. Environmental conditions in polygon centers vary according to polygon type. Low-centered (LC) polygons have standing water and primarily graminoid vegetation; high-centered (HC) polygons have dry surface soils and a greater abundance of mosses and lichens; between HC and LC polygons, flat-centered (FC) polygons have intermediate morphology and subsurface properties. In all polygon types, anaerobic conditions dominate active layer soils near the frost table (Vaughn *et al.*, 2016).

Temperature incubation

On August 14, 2012, we collected 9 1"-diameter soil cores from a range of polygon types (LC, FC, and HC) and positions within polygons (centers, rims, and troughs) representing a broad range of surface vegetation, microtopography, hydrology, and subsurface ice properties. Soil cores were collected with manual soil recovery probes to the base of the thawed soil layer (21-39 cm depth). Cores were refrigerated at 5°C and shipped on ice to Berkeley, CA for incubations and further analyses.

On August 20, we prepared the soil cores for incubation by removing visible live plant material and roots and dividing cores into organic and mineral horizons (2 or 3 increments per core). To minimize disturbance to soil structure, we left core increments intact, without homogenizing or sieving. To account for a limited amount of soil compression during the coring process, depth increments were adjusted to the field sampling depth according to a power function that assumes the degree of compression increases with soil depth. We placed core increments in 8 oz. glass mason jars nested inside 32 oz. glass mason jars fitted with gastight sampling ports. Between the two jars, we added ~2 mL of DI water to limit moisture loss from soil. To avoid artifacts from physical disturbance during core division, we pre-incubated soils for 1 day at 7.5°C and 1 day at 5°C before flushing jars with CO_2-free air to begin the incubation.

The soil incubation proceeded in 3 periods, first for 13 days at 5°C, second for 16 days at 10°C, and third for 21 days at 5°C. At the end of each period, we measured headspace CO_2 concentrations with a LI-820 CO_2 gas analyzer (LI-COR). Using a syringe and stopcock, we collected a 30 mL sample from each incubation jar's sampling port, then passed the sample at ~1 L min^{-1} through a septum at the inflow port of the LI-820. Based on repeated tests, 30 mL of gas was sufficient for a stable, accurate measurement. We then sampled the remaining headspace for radiocarbon analysis using either 500 mL stainless steel sampling canisters or glass serum vials sealed with 14 mm-thick chlorobutyl septa (Bellco Glass, Inc.). Soil was allowed to equilibrate to the new temperature for 4-7 days before jars were flushed with CO_2-free air to begin the next incubation period. At the time of sample collection, headspace CO_2 concentrations ranged from 1,400-30,000 ppm. To assure that jars were properly sealed, we used 4 blanks and 4 1,000 ppm CO_2 standards throughout the incubation.

Anaerobic incubation

On September 8, 2014, we collected 1 1" soil core from each of 3 HC, FC, and LC polygon centers, for a total of 9 cores. Core sampling and storage procedures were the same as in 2012. On September 16, we prepared soil cores for incubation by removing visible live plant materials and roots and dividing each HC or FC core into 2 equal depth increments, which ranged among cores from 8-15.5 cm in length. In the case of LC polygons, from which soil cores included sediment and standing water, we used the surface water as the shallow increment and the sediment as the deep increment. We divided deep core increments lengthwise into two roughly equal subsections and placed all soil samples in incubation jars as described above. Prior to the incubation, soils were pre-incubated for 8 days at 3°C to minimize artifacts from physical disturbance and flush residual O_2 from anaerobic jars. Before and after this pre-incubation period, we flushed incubation jars for 3 minutes with CO_2-free air (aerobic incubations; shallow increment and deep subsection 1) or N_2 (anaerobic incubations; deep subsection 2), then removed 30 mL of gas to seal each jar.

We incubated soils for 379 days at 3°C, testing headspace CO_2 concentrations every 2 weeks by passing a 30 mL sample through a LI-820 CO_2 gas analyzer (LI-COR) and replacing the removed volume with 30 mL of CO_2-free air or N_2. On the final incubation date, we measured CO_2 and CH_4 concentrations using a 2014 Shimadzu GC. CO_2 was isolated on a HayeSep-D packed column (4 m × 1/8") and quantified with a flame ionization detector. To collect sufficient CO_2 for radiocarbon measurements without allowing headspace CO_2 concentrations to rise above 20,000 ppm, we used one of two radiocarbon sampling procedures. From jars with relatively low CO_2 production, we collected headspace gas on the final incubation day. From jars with faster CO_2 accumulation, we collected 1 25 mL headspace subsample every 4 weeks, flushing the jars each time with CO_2-free air or N_2.

Carbon, Nitrogen, and isotope analyses

CO_2 from gas samples was cryogenically purified under vacuum, divided for ^{14}C and ^{13}C analyses, and sealed in 9 mm quartz tubes. 25 mL subsamples from the anaerobic incubation were composited during purification into 1 pair of CO_2 samples per incubation jar. For radiocarbon analysis, we sent samples to Lawrence Livermore National Lab's Center for Accelerator Mass Spectrometry or the Carbon, Water, and Soils Research Lab at the USDA-FS Northern Research Station, where they were prepared and analyzed according to Graven *et al.*, (2007). Briefly, CO_2 was reduced to graphite on iron powder under H_2. ^{14}C abundance was then measured at CAMS using a HVEC FN Tandem Van de Graaff accelerator mass spectrometer or at UC Irvine's Keck Carbon Cycle AMS facility. $^{13}C/^{12}C$ in CO_2 splits was analyzed on the UC Davis Stable Isotope Laboratory GVI Optima Stable Isotope Ratio Mass Spectrometer.

Soils from both incubations were freeze-dried, ground, measured into tin capsules, and loaded into a Costech Analytical Technologies ECS 4010 elemental analyzer coupled to a Thermo Fischer Scientific Delta V^{plus} isotope ratio mass spectrometer for carbon, nitrogen, and $^{13}C/^{12}C$ analysis. Optimal peak height was calibrated with atropine standards ranging from 0.2, 0.5, and 1.2 mg, and analytical precision based on repeated analysis of laboratory standard was ± 0.24 ‰ (1σ, n=14). For radiocarbon analysis,

ground soil samples were sent to the Carbon, Water, and Soils Research Lab, where they were combusted to CO_2 and analyzed as above.

Following the conventions of Stuiver and Polach (1977), radiocarbon results are presented as fractions of the modern NBS Oxalic Acid I (OX1) standard ($F^{14}C$), and deviations in parts per thousand (‰) from the absolute (decay-corrected) OX1 standard ($\Delta^{14}C$). All results have been corrected for mass-dependent isotopic fractionation using ^{13}C measurements.

Turnover time modeling

We used radiocarbon measurements from CO_2 samples and bulk soils to model turnover times using the time-dependent steady state model described in Torn *et al.*, (2009), modified to include residence time of carbon in vegetation:

$$F'_{C,t}C_t = IF'_{\mathrm{atm},t-\mathrm{T_R}} + C_{t-1}F'_{C,t-1}\left(1 - \frac{1}{\tau} - \lambda\right)$$

where:

$F' = \frac{\Delta^{14}C}{1000} - 1$
F'_C = the ratio of ^{14}C in the given carbon pool (CO_2 or bulk soil), normalized to a standard
F'_{atm} = the ratio of ^{14}C in the atmosphere normalized to a standard
I = the input rate of carbon from the atmosphere to the given carbon pool (g C y^{-1})
C = the stock of carbon in the given carbon pool (g)
τ = the turnover time of the given carbon pool (y)
λ = the radioactive decay rate of ^{14}C (1/8267 y)
T_R = the mean residence time of carbon in living plant material (y)
and
$C_t = C_{t-1} = I \times \tau$ at steady state

At steady state, the $\Delta^{14}C$ value of a given carbon pool at time *t* thus depends on its turnover time, its value in the previous year, the mean residence time of carbon in plant material, and the $^{14}C/^{12}C$ ratio in the atmosphere, which has changed continuously since the release of radiocarbon into the atmosphere from nuclear weapons testing between 1950 and the mid 1960s (Trumbore, 2000).

The mean residence time of carbon in plants reflects a mixture of materials with varying transfer rates. Some photosynthates enter the soil within 1 day of fixation (Loya *et al.*, 2002), whereas carbon resides in longer-lived plant organs from ~2 to as long as 15 years before entering the soil organic matter pool (Dennis, 1977; Billings *et al.*, 1978). Accordingly, we assume that across plant organs, plant species, and seasons, the mean value of T_R lies between 0 and 5 years.

Annual atmospheric $\Delta^{14}C$ values were compiled from the IntCal13 dataset (Reimer *et al.*, 2013), measurements from Fruholmen, Norway between 1962-1991 (Nydal & Lövseth, 1996), measurements from Barrow between 1999-2007 (Graven *et al.*,

2012), and measurements from the BEO in 2012, 2013, and 2014 (Appendix D). From roughly the same latitude as Barrow, Fruholmen $\Delta^{14}C$ measurements provide a close approximation for missing Barrow data (Meijer *et al.*, 2008). Because ecosystem CO_2 uptake occurs primarily during the growing season, June-August $\Delta^{14}C$ values were averaged to produce an annualized summer dataset. Data gaps from 1992-1998 and 2008-2011 were filled using an exponential model with measured values from the 10 years surrounding each gap.

Using our measured $\Delta^{14}C$ values and annually resolved atmospheric $\Delta^{14}C$ data, we iteratively solved for each sample's turnover time. We performed this calculation twice, using T_R values of 0 and 5 y to bracket the likely T_R range. Samples containing a large percentage of recently fixed carbon yielded two possible turnover time solutions for each T_R value. In such cases, we chose the appropriate solution either by comparing the two values to other (unique) turnover times within the same profile, or by comparing the measured carbon stock with the carbon stocks calculated from the CO_2 production rate and the candidate turnover times.

Temperature sensitivities of passive and active carbon pools

To evaluate the relationship between temperature sensitivity and carbon cycling rate, we used $\Delta^{14}C_{CO2}$ values from the temperature incubation to partition each measurement of CO_2 evolution into fast-cycling and slow-cycling pools. We then developed an approach that normalized the observed temperature sensitivity of each pool to its temperature sensitivity with no source depletion. First, we defined active and passive pools with assigned turnover times of 50 and 5,000 years. Corresponding to $\Delta^{14}C$ values of +141 and -360 ‰, these theoretical turnover times were chosen to bracket the range of observed $\Delta^{14}C$ values and represent carbon cycling on annual to decadal (active) or millennial (passive) timescales. With these $\Delta^{14}C$ values, we determined fractional contributions of the two carbon pools to total CO_2 production using a two-pool mixing model:

$$\Delta^{14}C_{sample} = f_{passive}(-360\ ‰) + f_{active}(141\ ‰)$$

$$f_{passive} + f_{active} = 1$$

where $f_{passive}$ and f_{active} are the fractional contributions of the passive and active carbon pools and $\Delta^{14}C_{sample}$ is the measured $\Delta^{14}C$ value of a given incubation CO_2 sample. We then used calculated $f_{passive}$ and f_{active} values to calculate the rate of carbon mineralization from each pool ($J_{passive}$ and J_{active}):

$$J_{passive} = f_{passive} \times J_{total}$$

$$J_{active} = f_{active} \times J_{total}$$

where J_{total} is the measured rate of CO_2 production in mg C d^{-1}. We performed this partitioning for each of the three incubation periods from each core increment.

With these partitioned flux data, we tested whether temperature sensitivity differed between active and passive pools. Over the three incubation periods, decomposition rates were influenced not only by temperature, but also by the non-steady-state effects of substrate depletion and microbial community shifts. To isolate the temperature effect, we related the apparent temperature sensitivity (i.e., the difference in CO_2 production between 5°C and 10°C incubation periods) to the temperature-independent change in CO_2 production over time, which we call the *time effect*. First, we calculated two metrics: the change in CO_2 production between periods 1 and 2, at 5°C and 10°C (Δ_2), and the change in CO_2 production from each pool between incubation periods 1 and 3, both at 5°C (Δ_3). Δ_2 quantifies the combined effects of the 5°C temperature increase and the concurrent time effect, and Δ_3 quantifies the change in carbon mineralization due to the time effect alone. Second, we regressed Δ_2 against Δ_3. This regression yielded a close linear relationship whose y-intercept can be interpreted as the temperature effect in the absence of source depletion or microbial acclimation (because that is point where the time effect equals zero). Finally, we tested whether this relationship differed between active pool and passive pool measurements. To test this, we used a linear mixed effects model predicting Δ_2 that included the fixed effect Δ_3, plus random effects for core increment and profile to account for paired active/passive measurements and physical clustering of increments within cores. Using incremental *F*-tests, we evaluated whether this model was changed significantly by the addition of two possible variables: carbon pool (active/passive) or the pool × Δ_3 interaction. Statistical modeling was conducted in R version 3.3.3 "Another Canoe" (2017-03-06), using the packages LME4 (Bates *et al.*, 2014) for model fitting and lmerTest (Kuznetsova *et al.*, 2014) for significance testing.

Sensitivity of soil carbon turnover to aerobic or anaerobic conditions

With data from the anaerobic incubation, we performed a series of one-way ANOVAs to evaluate how soil carbon turnover varied with polygon type and oxygen availability. First, we tested for differences among polygon types in shallow soil $\Delta^{14}C_{CO2}$ and deep soil $\Delta^{14}C_{CO2}$. For the deep soil $\Delta^{14}C_{CO2}$ test, we used $\Delta^{14}C_{CO2}$ from anaerobic incubations. – Due to lower rates of CO_2 production, we assumed these values were less affected by carbon substrate depletion than were $\Delta^{14}C_{CO2}$ values from aerobic replicates. Second, we tested for differences among polygon types in aerobic CO_2 production potential, defined as the whole-core (deep + shallow increments) aerobic CO_2 production rate at 3°C. Because deep core increments were divided into aerobic and anaerobic subsamples, we scaled the CO_2 flux from each anaerobic subsample to the total increment mass prior to division. Third, we tested for differences in $\Delta^{14}C_{CO2}$ between aerobic and anaerobic incubations. When comparing polygon types, we used Tukey's Honest Significant Difference test to evaluate pairwise differences between LC, FC, and HC polygons. Statistical analyses were conducted in R version 3.3.3 "Another Canoe" (2017-03-06).

Results

$\Delta^{14}C$ and turnover times of CO_2 and bulk soil organic matter

This study used radiocarbon measurements of CO_2 and soil organic matter to evaluate how soil carbon turnover varied with soil depth and landscape position. In the temperature incubation, emitted CO_2 became increasingly depleted in radiocarbon with depth (Fig. 1) from as high as +97.2 to as low as -350 ‰. We observed this trend in the anaerobic incubation as well in both emitted CO_2 and bulk soil carbon, but only from FC and HC polygons (Fig. 2). There, $\Delta^{14}C_{CO2}$ values were comparable to those from the temperature incubation, ranging from +90.4 to -347 ‰. $\Delta^{14}C_{SOM}$ values were considerably lower, from -54.6 to -582 ‰. In contrast, $\Delta^{14}C$ values from LC polygons had no consistent depth trend and varied considerably between aerobic and anaerobic replicates, with narrow ranges of +68.5 to -78.0 ‰ for CO_2 and +65.0 to -91.5 ‰ for SOM. Positive $\Delta^{14}C$ values, measured from shallow CO_2 samples of all polygon types and deep CO_2 samples from LC polygons, indicate high percentages of carbon fixed since 1960. Highly negative values, measured at depth from FC and HC polygons, reflect high proportions of old carbon that cycles on the scale of centuries to millennia.

To compare soil carbon cycling rates, we calculated turnover times from $\Delta^{14}C$ values. The turnover times of carbon that was respired, calculated from CO_2 samples (TT_{CO2}), ranged from 100 years in shallow samples to over 4,000 years at depth (Table 1a, Table 2a). While these values varied considerably among profiles and sampling dates, the longest TT_{CO2} values were measured near the permafrost table in high, dry polygon features such as centers of HC polygons and rims of FC and LC polygons. TT_{SOM} values followed the same spatial trend, but were considerably longer than TT_{CO2}, reflecting greater contributions of slowly cycling carbon (Table 2b). TT_{SOM} of shallow samples from FC and HC polygons ranged from 720 to 1,950 y, whereas shallow TT_{SOM} from LC polygons varied between only 150 and 380 years. For deep soil samples, TT_{SOM} ranged from 4,600 to >10,000 y in FC and HC polygons and from 170 to 1,040 y in LC polygons. In one case (LC4-center), TT_{CO2} was longer than TT_{SOM}, suggesting that carbon in the bulk soil cycled more rapidly than that mineralized to CO_2 during the incubation. This counterintuitive result is likely an artifact of the long incubation time, as 15 to 53 % of the carbon in shallow LC samples was mineralized during the anaerobic incubation (across both aerobic and anaerobic treatments), as compared with 0.5 to 4.2 % from other polygon types and depths. With such high mineralization rates in a system with no inputs, these shallow LC samples violated the steady-state assumption of the turnover time model.

Profile soil carbon stocks were higher in 2012 (1.38 to 4.99 g C cm^{-2}) than 2014 (0.258 to 0.615 g C cm^{-2}) due to differences in thaw depth at the time of sampling (and thus length of core) and in the amount of surface moss removed during core division (Table 1b, Table 2b). Comparing cores collected in 2014, carbon contents and decomposability varied among polygon types. Whereas thaw depths were greater in LC polygons (41 to 44 cm) than HC or FC polygons (22 to 23.5 and 16 to 31 cm), LC polygons had lower profile carbon contents (0.28 +/- 0.019 g C cm^{-2}) than HC or FC polygons (0.54 +/- 0.12 and 0.59 +/- 0.030 g C cm^{-2} respectively), due to high water contents in LC polygon samples (Table 2b). Despite these lower carbon contents, however, LC polygon cores produced CO_2 at rates comparable to the other polygon types

(Fig. 3, Fig. 4), suggesting that carbon from these LC polygons was more readily decomposed than from HC or LC polygons.

Temperature sensitivities of soil carbon pools

Using radiocarbon measurements from the temperature incubation, we evaluated how temperature affected the dynamics of soil carbon pools. $\Delta^{14}C_{CO2}$ values decreased monotonically throughout the incubation in nearly all cores (Fig. 1), corresponding to increasingly long carbon turnover times for the carbon in the decomposition flux (Table 1a). This change in substrate utilization was accompanied by a decrease in total CO_2 production between the two 5°C incubation periods (Fig. 3). Together, these observations suggest that readily decomposable carbon substrates became depleted over the course of the experiment, increasing the relative contribution of ^{14}C-depleted, slowly cycling carbon to the total CO_2 flux.

In addition to this source depletion effect, we observed clear temperature sensitivity in the carbon mineralization rate, which peaked during the second (10°C) incubation period (Table 1a, Fig. 3). To compare the temperature sensitivities of different carbon pools, we separated the effect of temperature on each carbon pool from that pool's overall trend in CO_2 production. With active and passive carbon pool CO_2 production rates (turnover times = 50 and 5,000 years) calculated from $\Delta^{14}C_{CO2}$ measurements, we calculated two metrics: Δ_3 = the difference in CO_2 production between periods 1 and 3, i.e., due to source depletion or microbial acclimation (the time effect); and Δ_2 = the difference in CO_2 production between periods 1 and 2, i.e., the temperature response combined with the time effect. We observed a strong positive linear relationship between Δ_2 and Δ_3 (Fig. 5). In all but two cases, CO_2 production decreased between incubation periods 1 and 3, due likely to substrate depletion. The two cases in which CO_2 production increased with time ($\Delta_3 > 0$) may have been due to microbial responses to incubation conditions.

The strong linear relationship between Δ_3 and Δ_2 allowed us to estimate the temperature effect in the absence of source depletion or microbial acclimation. The y-intercept of this relationship (41.2 ± 2.1 from a linear mixed-effects model) estimates the effect of a 5°C temperature increase on CO_2 production with no background change in carbon mineralization, i.e., when $\Delta_3 = 0$ %. We found that neither carbon pool nor the pool × Δ_3 interaction were significant predictors in this model, indicating no significant differences in either the y-intercept or slope between passive and active pools. Rather, both carbon pools displayed the same temperature sensitivity. Thus, after accounting for source depletion, a 5°C temperature increase stimulated a 41.2 % increase in carbon mineralization for both pools, equal to a Q_{10} of ~2.

Carbon turnover under aerobic vs. anaerobic conditions

We used parallel incubations to evaluate the influence of aerobic vs. anaerobic conditions on total decomposition rates and the relative decomposition rates of soil carbon pools. CO_2 evolution rates were higher in aerobic than anaerobic incubations (Table 2a). For individual (divided) samples, we define oxygen sensitivity as the percent difference in carbon mineralization rate between aerobic and anaerobic treatments: $(J_{aerobic} - J_{anaerobic})/J_{anaerobic} \times 100$, where J is the rate of CO_2 production per unit dry soil mass. This

oxygen sensitivity varied widely among soil cores, from 27 % (HC1-center) to 370 % (LC3-center), with no relationship to total CO_2 production rate. Similarly, oxygen sensitivity had no relationship to $\Delta^{14}C_{CO2}$, nor did $\Delta^{14}C_{CO2}$ values differ significantly between aerobic and anaerobic treatments (Table 3, Fig. 2a). These findings indicate that while oxygen sensitivity varied spatially (among cores), it was not significantly different between fast-cycling and slow-cycling carbon pools.

Because of the large difference between treatments in total carbon mineralization, the influence of substrate depletion on $\Delta^{14}C_{CO2}$ was likely greater for aerobic than anaerobic replicates. Fortunately, the direction of this effect—i.e., decreasing aerobic $\Delta^{14}C_{CO2}$ values relative to those in anaerobic incubations—is the same as our tested hypothesis. For this reason, it is unlikely that source depletion masked an influence of oxygen availability on relative carbon pool decomposition rates. Instead, our findings suggest that oxygen availability did not measurably influence either the distribution of carbon among pools or their relative decomposition rate constants.

Discussion

Within the century, high latitude ecosystems are expected to shift from a sink to a source of atmospheric CO_2 due to climate-induced increases in soil carbon mineralization (Koven *et al.*, 2011; McGuire *et al.*, 2012; Schuur *et al.*, 2015). The magnitude of this effect remains uncertain, due in large part to unknown environmental sensitivities of organic matter decomposition (Mikan *et al.*, 2002; Davidson & Janssens, 2006; Koven *et al.*, 2015). With two soil incubation experiments, we evaluated these environmental sensitivities in a set of soils from Arctic Alaska. We asked how soil carbon cycling (1) varies with depth in the soil profile and across permafrost features, (2) responds to changes in temperature, and (3) changes with transitions between aerobic and anaerobic conditions. Using natural abundance radiocarbon measurements of CO_2 and bulk soil organic matter, we distinguished the relative effect of experimental treatments on the fast and slow pools of soil organic carbon.

With CO_2 production rates, $\Delta^{14}C_{CO2}$, and $\Delta^{14}C_{SOM}$ from two soil incubation experiments, we observed clear spatial patterns in soil carbon cycling rates, both vertically in the soil profile and across distinct landscape features. Strong vertical gradients in $\Delta^{14}C_{CO2}$ and $\Delta^{14}C_{SOM}$ (Fig. 1, Fig. 2) reflect a shift from rapidly cycling carbon near the soil surface to more slow-cycling carbon near the permafrost table. This pattern is common to other, less northerly ecosystems and soil types (Paul *et al.*, 1997; Gaudinski *et al.*, 2000; Trumbore, 2000; Torn *et al.*, 2002; Hicks Pries *et al.*, 2013; McFarlane *et al.*, 2013), but our $\Delta^{14}C$ values are comparatively negative at relatively shallow depths. In these high latitude soils, cold, often frozen or anaerobic soils slow carbon cycling at all depths and compress steep vertical $\Delta^{14}C$ profiles into the shallow active layer. Old carbon emissions have been measured from comparable depths in other high latitude sites (Schuur *et al.*, 2009; Hicks Pries *et al.*, 2013, 2015), but the $\Delta^{14}C$ values measured in this study are nearly an order of magnitude lower. As seen in field-based radiocarbon measurements from ecosystem respiration and soil pore space CO_2 (Appendix E) this effect was most pronounced in high, dry microtopographic features such as HC polygon centers and FC polygon rims. There, insulation due to low soil water contents and high moss coverage lead to particularly shallow thaw depths (Dyrness, 1982; Ping *et al.*, 2015) and low $\Delta^{14}C_{CO2}$

and $\Delta^{14}C_{SOM}$ values (Table 2b, Table 3). In contrast, LC polygons had deeper thaw (Table 2b), less negative $\Delta^{14}C$ at depth (Fig. 2), and greater CO_2 production potential (Fig. 4), reflecting the influence of substrate chemistry, physio-chemical state, and environmental variables such as temperature and oxygen availability on carbon cycling rates (Torn *et al.*, 1997; Schmidt *et al.*, 2011).

This study used long-term incubations of different soil depths to fractionate soils into four separate pools: respired CO_2 and residual SOM from near-surface and permafrost table samples. Turnover times calculated from radiocarbon measurements provide a means to compare carbon cycling rates among these pools (Table 1, Table 2). CO_2 samples reflect the pool of carbon being mineralized at each depth. Turnover times of this respired pool ranged broadly, from ~100 to 500 years in shallow samples and from ~200 to >4,000 years at depth. Such long turnover times, particularly from deep samples, demonstrate that carbon that cycles on timescales as long as millennia is available to decomposition under unfrozen conditions. Co-located field-based measurements of radiocarbon in soil surface emissions and soil pore space confirm that these long turnover times reflect *in situ* cycling rates (Appendix E). At only 20 cm depth, soil pore space CO_2 in three locations had calculated turnover times longer than 3000 years (median = 1375 y), and turnover times as long as 1700 years were calculated from surface CO_2 emissions (median = 270 y). In both incubations and in situ soils, we thus see mineralization of very old carbon—so old, in fact, that losses may not be sustainable. In particular, decomposition of these of relic carbon stores is likely to increase with permafrost thaw and active layer warming (Schuur *et al.*, 2013, 2015; Schädel *et al.*, 2014). As seen in other sites undergoing natural or experimental warming (Schuur *et al.*, 2009; Hicks Pries *et al.*, 2013, 2015), such a change may lead to net losses of ancient carbon from these tundra soils.

Following a 379-day incubation at 3°C, carbon in the remaining soil samples reflects more slowly cycling pools. The near-surface SOM pool includes carbon in contact with rhizosphere carbon inputs (Iversen *et al.*, 2015), warmer temperatures, and abundant decomposers (Kaiser *et al.*, 2007; Sistla *et al.*, 2013), whereas near-permafrost SOM is more environmentally isolated, with slower carbon inputs due to shallow rooting depths (Iversen *et al.*, 2015) and slower outputs due to low temperatures and often frozen conditions. Turnover times of these two pools reflect their relative isolation, with near-surface TT_{SOM} values of ~100 to 1,000 years and near-permafrost TT_{SOM} values of ~500 to >10,000 years. Notably, TT_{SOM} values were greater than TT_{CO2} across all samples from both depth increments, indicating gradients of decomposability within each sample.

Turnover times calculated from $\Delta^{14}C$ represent the inverse first-order cycling rates of homogeneous, steady-state pools (Sierra *et al.*, 2017). We note that the carbon pools in this study were not truly homogeneous. Even the most rapidly cycling pools, for instance, had turnover times longer than 100 years. There, much of the carbon likely cycles on annual to decadal timescales, with small inputs from very slow-cycling carbon. Additionally, some samples may not have met the steady-state assumption. In some deep samples in particular, cryoturbation and interannual variations in thaw depth may have isolated soils for years, decades, or centuries (Kaiser *et al.*, 2007; Gittel *et al.*, 2014). From HC1-center, for example, we calculated TT_{SOM} greater than 10,000 years. While it is possible that this indicates the presence of Pleistocene carbon (Jorgenson & Brown,

2005), it more likely reflects non-steady state conditions due to abundant cryoturbation at our site (Bockheim *et al.*, 1999). This study's turnover times, therefore, do not quantify real decomposition rates of homogeneous pools. Rather, they provide a semi-quantitative means of comparison across profiles and depths.

With radiocarbon measurements from the two incubation studies, we tested whether slow-cycling and fast-cycling carbon pools were equally sensitive to differences in temperature or aerobic/anaerobic conditions. We tested the temperature effect with three sequential incubations at 5°C, 10°C, then 5°C, normalizing the change in CO_2 production due to temperature to the overall change in source pool size. We found that the temperature sensitivity of decomposition was invariant across pools, with a constant Q_{10} of ~2 (Fig. 5). By using three sequential incubations of intact cores, we avoided two methodological issues common to incubation studies. First, because treatments were applied to each core in succession, we did not need to homogenize soils to generate replicates. Instead, we minimized disturbance to soil structure and maintained physical soil carbon protection within aggregates (Jastrow *et al.*, 1996). Second, we used the third (5°C) incubation period to account for substrate depletion and/or changes in microbial activity (Bradford *et al.*, 2008; Kirschbaum, 2013). Particularly when using the radiocarbon tracer in non-steady state systems, pool size and temperature effects may otherwise be confounded. With this method, we effectively isolated temperature from other controls on carbon decomposition, finding that passive and active carbon pools were equally temperature-sensitive.

To test the effect of oxygen availability on soil carbon dynamics, we conducted parallel incubations under aerobic and anaerobic conditions, using radiocarbon measurements of respired CO_2 to compare carbon source distributions in the respiration flux. We found no systematic differences in $\Delta^{14}C_{CO2}$ between aerobic and anaerobic replicates (Fig. 2a). If thermodynamic constraints under anaerobic conditions structured carbon pools based on substrate chemistry (Keiluweit *et al.*, 2016), we should have seen increased mineralization of old substrates in aerobic replicates that were previously stabilized by anaerobic conditions. Instead, we found that both fast- and slow-cycling soil pools were highly sensitive to oxygen availability. Total CO_2 production differed clearly between treatments (Table 2a), even though $\Delta^{14}C_{CO2}$ did not. This difference varied widely among soil samples, with notably high oxygen sensitivity in the fast-cycling LC polygon samples. This spatial variability in oxygen sensitivity may be due to differences across cores in substrate chemistry (but not among carbon age classes within cores). Alternatively, oxygen sensitivity may be controlled by other environmental variables such as the availability of alternative electron acceptors for anaerobic respiration (Chowdhury *et al.*, 2014; Herndon *et al.*, 2015), microbial community composition (Mackelprang *et al.*, 2011; Lipson *et al.*, 2013, 2015), or oxygen penetration into soil aggregates (Mangalassery *et al.*, 2013).

If chemical recalcitrance were the primary means of carbon stabilization, substrates with higher activation energy should dominate the slow-cycling carbon pools. Accordingly, kinetic theory predicts that this slow pool should be more sensitive to temperature and oxygen availability than more rapidly cycling, chemically labile carbon (Conant *et al.*, 2011; Keiluweit *et al.*, 2016). We did not observe this relationship. Instead, the lack of correspondence between carbon cycling rates and temperature or

oxygen sensitivities suggests two likely explanations. First, carbon pools, as defined by their cycling rates, may not be chemically distinct (Kleber *et al.*, 2011). This effect may be particularly pronounced in these high-latitude soils where cold, frozen, and/or anoxic conditions inhibit decomposition of all carbon substrates. There, even the most slowly cycling carbon pools may have a broad range of decomposability (Zimov *et al.*, 2006; Paré & Bedard-Haughn, 2013; Strauss *et al.*, 2014). Second, carbon stabilization mechanisms other than chemical recalcitrance may mediate substrate sensitivities to temperature and oxygen availability (Davidson & Janssens, 2006; Gillabel *et al.*, 2010; Schmidt *et al.*, 2011). For example, soil carbon temperature sensitivities may be constrained by low exoenzyme activities and microbial abundances in slow-cycling Arctic soils (Waldrop *et al.*, 2010).

The literature lacks consensus on the relative temperature or oxygen sensitivities of different soil carbon pools. Across a broad range of ecosystems, soils, and substrate types, numerous studies have found negative correlations between carbon decomposability and its sensitivity to temperature (e.g., Melillo *et al.*, 2002; Fierer *et al.*, 2005; Knorr *et al.*, 2005; Koch *et al.*, 2007; Hartley & Ineson, 2008; Hilasvuori *et al.*, 2013) or anoxia (Updegraff *et al.*, 1995; Bridgham *et al.*, 1998; Knoblauch *et al.*, 2013), whereas others align with our findings that fast and slow carbon pools are equally temperature-sensitive (e.g., Townsend *et al.*, 1997; Fang *et al.*, 2005; Reichstein *et al.*, 2005). A review by Conant *et al.*, (2011) suggests the temperature sensitivity-carbon pool relationship depends on incubation methodology. In general, studies that have preserved soil structure have found different temperature sensitivities among pools, whereas the opposite has been found when soils were sieved and homogenized. Accordingly, the relationship between temperature sensitivity and turnover time may be mediated by carbon stabilization mechanisms other than chemical recalcitrance (Davidson & Janssens, 2006). In some cases, as when soils are homogenized, methodological artifacts may thus obscure a temperature response by disturbing aggregate stability. Other times, however, as with our slow-cycling Arctic soils, temperature itself may dominate carbon stabilization, slowing decomposition irrespective of substrate chemistry. In such cases, changes to the substrate age-decomposability relationship are not methodological artifacts, but rather real properties of the experimental treatment.

This study informs not only general models of carbon stabilization and vulnerability, but also quantitative models of soil carbon dynamics. For models representing high latitude carbon dynamics, we find that a Q_{10} of 2 provides a reasonable approximation for soil carbon temperature sensitivity. Notably, we do not find evidence that the Q_{10} parameter should differ among carbon pools. Additionally, our findings support the use of radiocarbon measurements from soil incubations to partition field CO_2 emissions into individual source components (Schuur & Trumbore, 2006; Hicks Pries *et al.*, 2013). This method requires that $\Delta^{14}C$ values of CO_2 emissions be insensitive to incubation conditions, an assumption that has not been well tested (Trumbore, 2006). Our study validates this assumption, finding that radiocarbon contents of CO_2—providing end-member values for mixing model studies—are unaffected by incubation temperature or oxygen availability.

Conclusion

Soil carbon vulnerability to climate change depends on its inherent decomposability and environmental sensitivity. In the high latitudes in particular, carbon stored for centuries or millennia in permafrost or active layer soils may be vulnerable to soil warming and drainage (Schuur *et al.*, 2009; Hicks Pries *et al.*, 2013). Whether or not environmental sensitivities differ among soil carbon pools has strong implications for future carbon stocks (Reichstein *et al.*, 2005). Given the large proportion of soil carbon stored in slow-cycling pools (Schädel *et al.*, 2014), long-term changes in soil carbon stocks are especially sensitive to these pools' dynamics (Davidson & Janssens, 2006). With soils from Arctic Alaska, we found no differences in environmental sensitivity among carbon pools. Slow-cycling and fast-cycling carbon responded comparably to changes in temperature, with decomposition increasing by roughly 40 % under 5°C of warming. Similarly, while soil carbon mineralization depended strongly on oxygen availability, this dependence was no greater for slow-cycling than for fast-cycling carbon. While cold temperatures and anaerobic conditions are key mechanisms for preserving ancient carbon at depth, we thus observed little evidence for selective preservation based substrate chemistry (chemical recalcitrance). Instead, other ecosystem properties such as cold temperatures and often-frozen conditions are likely more important mechanisms for stabilizing carbon in these soils (Schmidt *et al.*, 2011). Importantly, these findings suggest that all carbon in active layer soils will respond to similarly to soil microclimate changes, irrespective of depth or historical cycling rate.

References

Adu JK, Oades JM (1978) Physical factors influencing decomposition of organic materials in soil aggregates. *Soil Biology and Biochemistry*, **10**, 109–115.

Andresen CG, Lougheed VL (2015) Disappearing Arctic tundra ponds: Fine-scale analysis of surface hydrology in drained thaw lake basins over a 65 year period (1948-2013). *Journal of Geophysical Research: Biogeosciences*, 2014JG002778.

Bates D, Maechler M, Bolker BM, Walker S (2014) *lme4: Linear mixed-effects models using Eigen and S4. R package version 1.1-7*.

Billings WD, Peterson KM (1980) Vegetational change and ice-wedge polygons through the thaw-lake cycle in Arctic Alaska. *Arctic and Alpine Research*, 413–432.

Billings WD, Peterson KM, Shaver GR (1978) Growth, Turnover, and Respiration Rates of Roots and Tillers in Tundra Graminoids. In: *Vegetation and Production Ecology of an Alaskan Arctic Tundra* (ed Tieszen LL), pp. 415–434. Springer New York.

Black RF (1964) *Gubik Formation of Quaternary age in northern Alaska*. United States Geological Survey.

Bockheim JG, Everett LR, Hinkel KM, Nelson FE, Brown J (1999) Soil organic carbon storage and distribution in Arctic tundra, Barrow, Alaska. *Soil Science Society of America Journal*, **63**, 934–940.

Bol R, Bolger T, Cully R, Little D (2003) Recalcitrant soil organic materials mineralize more efficiently at higher temperatures. *Journal of Plant Nutrition and Soil Science*, **166**, 300–307.

Bradford MA, Davies CA, Frey SD et al. (2008) Thermal adaptation of soil microbial respiration to elevated temperature. *Ecology Letters*, **11**, 1316–1327.

Bridgham SD, Updegraff K, Pastor J (1998) Carbon, Nitrogen, and Phosphorus Mineralization in Northern Wetlands. *Ecology*, **79**, 1545–1561.

Brown J, Miller PC, Tieszen LL, Bunnell F (1980) *An Arctic ecosystem : the coastal tundra at Barrow, Alaska*. Dowden, Hutchinson and Ross, Inc., Stroudsburg, Pennsylvania.

Chowdhury TR, Herndon EM, Phelps TJ et al. (2014) Stoichiometry and temperature sensitivity of methanogenesis and CO2 production from saturated polygonal tundra in Barrow, Alaska. *Global Change Biology*, n/a–n/a.

Christensen BT (1992) Physical fractionation of soil and organic matter in primary particle size and density separates. In: *Advances in soil science*, pp. 1–90. Springer.

Ciais P, Sabine C, Bala G et al. (2014) Carbon and other biogeochemical cycles. In: *Climate Change 2013: The Physical Science Basis. Contribution of Working Group I to the Fifth Assessment Report of the Intergovernmental Panel on Climate Change*, pp. 465–570. Cambridge University Press.

Conant RT, Ryan MG, Ågren GI et al. (2011) Temperature and soil organic matter decomposition rates – synthesis of current knowledge and a way forward. *Global Change Biology*, **17**, 3392–3404.

Davidson EA, Janssens IA (2006) Temperature sensitivity of soil carbon decomposition and feedbacks to climate change. *Nature*, **440**, 165–173.

Dennis JG (1977) Distribution Patterns of Belowground Standing Crop in Arctic Tundra at Barrow, Alaska. *Arctic and Alpine Research*, **9**, 113.

Dioumaeva I, Trumbore S, Schuur EAG, Goulden ML, Litvak M, Hirsch AI (2002) Decomposition of peat from upland boreal forest: Temperature dependence and sources of respired carbon. *Journal of Geophysical Research: Atmospheres*, **107**, 8222.

Dungait JAJ, Hopkins DW, Gregory AS, Whitmore AP (2012) Soil organic matter turnover is governed by accessibility not recalcitrance. *Global Change Biology*, **18**, 1781–1796.

Dyrness CT (1982) *Control of depth to permafrost and soil temperature by the forest floor in black spruce/feathermoss communities*, Vol. 396. US Dept. of Agriculture, Forest Service, Pacific Northwest Forest and Range Experiment Station.

Fang C, Smith P, Moncrieff JB, Smith JU (2005) Similar response of labile and resistant soil organic matter pools to changes in temperature. *Nature*, **433**, 57–59.

Fierer N, Craine JM, McLauchlan K, Schimel JP (2005) Litter quality and the temperature sensitivity of decomposition. *Ecology*, **86**, 320–326.

Gaudinski JB, Trumbore SE, Davidson EA, Zheng S (2000) Soil carbon cycling in a temperate forest: radiocarbon-based estimates of residence times, sequestration rates and partitioning of fluxes. *Biogeochemistry*, **51**, 33–69.

Gillabel J, Cebrian-Lopez B, Six J, Merckx R (2010) Experimental evidence for the attenuating effect of SOM protection on temperature sensitivity of SOM decomposition. *Global Change Biology*, **16**, 2789–2798.

Gittel A, Bárta J, Kohoutová I et al. (2014) Distinct microbial communities associated with buried soils in the Siberian tundra. *The ISME Journal*, **8**, 841–853.

Graven HD, Guilderson TP, Keeling RF (2007) Methods for High-Precision ^{14}C AMS Measurement of Atmospheric CO_2 at LLNL. *Radiocarbon*, **49**, 349–356.

Graven HD, Guilderson TP, Keeling RF (2012) Observations of radiocarbon in CO2 at seven global sampling sites in the Scripps flask network: Analysis of spatial gradients and seasonal cycles. *Journal of Geophysical Research: Atmospheres*, **117**.

Hartley IP, Ineson P (2008) Substrate quality and the temperature sensitivity of soil organic matter decomposition. *Soil Biology and Biochemistry*, **40**, 1567–1574.

Herndon EM, Mann BF, Chowdhury TR et al. (2015) Pathways of anaerobic organic matter decomposition in tundra soils from Barrow, Alaska: Biogeochemistry of Anoxic Arctic Tundra. *Journal of Geophysical Research: Biogeosciences*, n/a–n/a.

Hicks Pries CE, Schuur EAG, Crummer KG (2013) Thawing permafrost increases old soil and autotrophic respiration in tundra: Partitioning ecosystem respiration using δ13C and Δ14C. *Global Change Biology*, **19**, 649–661.

Hicks Pries CE, Schuur EAG, Natali SM, Crummer KG (2015) Old soil carbon losses increase with ecosystem respiration in experimentally thawed tundra. *Nature Climate Change*, **advance online publication**.

Hilasvuori E, Akujärvi A, Fritze H et al. (2013) Temperature sensitivity of decomposition in a peat profile. *Soil Biology and Biochemistry*, **67**, 47–54.

Hinkel KM, Nelson FE (2003) Spatial and temporal patterns of active layer thickness at Circumpolar Active Layer Monitoring (CALM) sites in northern Alaska, 1995–2000. *Journal of Geophysical Research: Atmospheres*, **108**, 8168.

Hinzman LD, Bettez ND, Bolton WR et al. (2005) Evidence and Implications of Recent Climate Change in Northern Alaska and Other Arctic Regions. *Climatic Change*, **72**, 251–298.
Hopkins FM, Torn MS, Trumbore SE (2012) Warming accelerates decomposition of decades-old carbon in forest soils. *Proceedings of the National Academy of Sciences*, **109**, E1753–E1761.
Hugelius G, Strauss J, Zubrzycki S et al. (2014) Estimated stocks of circumpolar permafrost carbon with quantified uncertainty ranges and identified data gaps. *Biogeosciences*, **11**, 6573–6593.
Iversen CM, Sloan VL, Sullivan PF et al. (2015) The unseen iceberg: plant roots in arctic tundra. *New Phytologist*, **205**, 34–58.
Jastrow JD, Miller RM, Boutton TW (1996) Carbon Dynamics of Aggregate-Associated Organic Matter Estimated by Carbon-13 Natural Abundance. *Soil Science Society of America Journal*, **60**, 801–807.
Jones CD, Cox P, Huntingford C (2003) Uncertainty in climate–carbon-cycle projections associated with the sensitivity of soil respiration to temperature. *Tellus B*, **55**, 642–648.
Jorgenson MT, Brown J (2005) Classification of the Alaskan Beaufort Sea Coast and estimation of carbon and sediment inputs from coastal erosion. *Geo-Marine Letters*, **25**, 69–80.
Jorgenson MT, Shur YL, Pullman ER (2006) Abrupt increase in permafrost degradation in Arctic Alaska. *Geophysical Research Letters*, **33**.
Jorgenson MT, Harden J, Kanevskiy M et al. (2013) Reorganization of vegetation, hydrology and soil carbon after permafrost degradation across heterogeneous boreal landscapes. *Environmental Research Letters*, **8**, 035017.
Kahle MK, Torn M, Jahn MS, others (2003) Carbon storage in coarse and fine clay fractions of illitic soils. *Soil Science Society of America Journal*, **67**, 1732.
Kaiser C, Meyer H, Biasi C, Rusalimova O, Barsukov P, Richter A (2007) Conservation of soil organic matter through cryoturbation in arctic soils in Siberia. *Journal of Geophysical Research: Biogeosciences*, **112**, G02017.
Keiluweit M, Nico PS, Kleber M, Fendorf S (2016) Are oxygen limitations under recognized regulators of organic carbon turnover in upland soils? *Biogeochemistry*, **127**, 157–171.
Kirschbaum MUF (2013) Seasonal variations in the availability of labile substrate confound the temperature dependence of organic matter decomposition. *Soil Biology and Biochemistry*, **57**, 568–576.
Kleber M, Nico PS, Plante A, Filley T, Kramer M, Swanston C, Sollins P (2011) Old and stable soil organic matter is not necessarily chemically recalcitrant: implications for modeling concepts and temperature sensitivity. *Global Change Biology*, **17**, 1097–1107.
Knoblauch C, Beer C, Sosnin A, Wagner D, Pfeiffer E-M (2013) Predicting long-term carbon mineralization and trace gas production from thawing permafrost of Northeast Siberia. *Global change biology*.
Knorr W, Prentice IC, House JI, Holland EA (2005) Long-term sensitivity of soil carbon turnover to warming. *Nature*, **433**, 298–301.

Koch O, Tscherko D, Kandeler E (2007) Temperature sensitivity of microbial respiration, nitrogen mineralization, and potential soil enzyme activities in organic alpine soils. *Global Biogeochemical Cycles*, **21**, GB4017.

Koven CD, Ringeval B, Friedlingstein P et al. (2011) Permafrost carbon-climate feedbacks accelerate global warming. *Proceedings of the National Academy of Sciences*.

Koven CD, Lawrence DM, Riley WJ (2015) Permafrost carbon–climate feedback is sensitive to deep soil carbon decomposability but not deep soil nitrogen dynamics. *Proceedings of the National Academy of Sciences*, 201415123.

Kuznetsova A, Brockhoff PB, Christensen RHB (2014) *lmerTest: Tests for random and fixed effects for linear mixed effect models (lmer objects of lme4 package).. R package version 2.0-11*.

Lara MJ, McGuire AD, Euskirchen ES et al. (2014) Polygonal tundra geomorphological change in response to warming alters future CO2 and CH4 flux on the Barrow Peninsula. *Global Change Biology*, n/a–n/a.

Lawrence DM, Koven CD, Swenson SC, Riley WJ, Slater AG (2015) Permafrost thaw and resulting soil moisture changes regulate projected high-latitude CO_2 and CH_4 emissions. *Environmental Research Letters*, **10**, 094011.

Lefèvre R, Barré P, Moyano FE et al. (2014) Higher temperature sensitivity for stable than for labile soil organic carbon – Evidence from incubations of long-term bare fallow soils. *Global Change Biology*, **20**, 633–640.

Lipson DA, Haggerty JM, Srinivas A, Raab TK, Sathe S, Dinsdale EA (2013) Metagenomic Insights into Anaerobic Metabolism along an Arctic Peat Soil Profile. *PloS one*, **8**, e64659.

Lipson DA, Raab TK, Parker M, Kelley ST, Brislawn CJ, Jansson J (2015) Changes in microbial communities along redox gradients in polygonized Arctic wet tundra soils. *Environmental Microbiology Reports*, **7**, 649–657.

Lloyd J, Taylor JA (1994) On the Temperature Dependence of Soil Respiration. *Functional Ecology*, **8**, 315–323.

Loya WM, Johnson LC, Kling GW, King JY, Reeburgh WS, Nadelhoffer KJ (2002) Pulse-labeling studies of carbon cycling in arctic tundra ecosystems: Contribution of photosynthates to soil organic matter. *Global Biogeochemical Cycles*, **16**, 1101.

Lützow M v., Kögel-Knabner I, Ekschmitt K, Matzner E, Guggenberger G, Marschner B, Flessa H (2006) Stabilization of organic matter in temperate soils: mechanisms and their relevance under different soil conditions – a review. *European Journal of Soil Science*, **57**, 426–445.

Mackelprang R, Waldrop MP, DeAngelis KM et al. (2011) Metagenomic analysis of a permafrost microbial community reveals a rapid response to thaw. *Nature*.

Mangalassery S, Sjögersten S, Sparkes DL, Sturrock CJ, Mooney SJ (2013) The effect of soil aggregate size on pore structure and its consequence on emission of greenhouse gases. *Soil and Tillage Research*, **132**, 39–46.

Marschner B, Brodowski S, Dreves A et al. (2008) How relevant is recalcitrance for the stabilization of organic matter in soils? *Journal of Plant Nutrition and Soil Science*, **171**, 91–110.

McFarlane KJ, Torn MS, Hanson PJ, Porras RC, Swanston CW, Callaham MA, Guilderson TP (2013) Comparison of soil organic matter dynamics at five

temperate deciduous forests with physical fractionation and radiocarbon measurements. *Biogeochemistry*, **112**, 457–476.
McGuire AD, Christensen TR, Hayes D et al. (2012) An assessment of the carbon balance of Arctic tundra: comparisons among observations, process models, and atmospheric inversions. *Biogeosciences*, **9**, 3185–3204.
Meijer HJ, Pertuisot MH, Plicht J van der (2008) High-accuracy 14C measurements for atmospheric CO2 samples by AMS. *Radiocarbon*, **48**, 355–372.
Melillo JM, Steudler PA, Aber JD et al. (2002) Soil warming and carbon-cycle feedbacks to the climate system. *Science*, **298**, 2173–2176.
Mikan CJ, Schimel JP, Doyle AP (2002) Temperature controls of microbial respiration in arctic tundra soils above and below freezing. *Soil Biology and Biochemistry*, **34**, 1785–1795.
Nydal R, Lövseth K (1996) *Carbon-14 measurements in atmospheric CO2 from northern and southern hemisphere sites, 1962-1993*. Oak Ridge National Lab., TN (United States); Oak Ridge Inst. for Science and Education, TN (United States).
Osterkamp TE, Romanovsky VE (1999) Evidence for warming and thawing of discontinuous permafrost in Alaska. *Permafrost and Periglacial Processes*, **10**, 17–37.
Osterkamp TE, Jorgenson MT, Schuur EAG, Shur YL, Kanevskiy MZ, Vogel JG, Tumskoy VE (2009) Physical and ecological changes associated with warming permafrost and thermokarst in interior Alaska. *Permafrost and Periglacial Processes*, **20**, 235–256.
Paré MC, Bedard-Haughn A (2013) Surface soil organic matter qualities of three distinct Canadian Arctic sites. *Arctic, Antarctic, and Alpine Research*, **45**, 88–98.
Paul EA, Follett RF, Leavitt SW, Halvorson A, Peterson GA, Lyon DJ (1997) Radiocarbon dating for determination of soil organic matter pool sizes and dynamics. *Soil Science Society of America Journal*, **61**, 1058–1067.
Ping CL, Jastrow JD, Jorgenson MT, Michaelson GJ, Shur YL (2015) Permafrost soils and carbon cycling. *SOIL*, **1**, 147–171.
Reichstein M, Kätterer T, Andrén O et al. (2005) Temperature sensitivity of decomposition in relation to soil organic matter pools: critique and outlook. *Biogeosciences*, **2**, 317–321.
Reimer PJ, Bard E, Bayliss A et al. (2013) IntCal13 and Marine13 Radiocarbon Age Calibration Curves 0–50,000 Years cal BP. *Radiocarbon*, **55**, 1869–1887.
Schädel C, Schuur EAG, Bracho R et al. (2014) Circumpolar assessment of permafrost C quality and its vulnerability over time using long-term incubation data. *Global Change Biology*, **20**, 641–652.
Schmidt MW, Torn MS, Abiven S et al. (2011) Persistence of soil organic matter as an ecosystem property. *Nature*, **478**, 49–56.
Schuur E a. G, Trumbore SE (2006) Partitioning sources of soil respiration in boreal black spruce forest using radiocarbon. *Global Change Biology*, **12**.
Schuur EA, Vogel JG, Crummer KG, Lee H, Sickman JO, Osterkamp TE (2009) The effect of permafrost thaw on old carbon release and net carbon exchange from tundra. *Nature*, **459**, 556–559.

Schuur E a. G, Abbott BW, Bowden WB et al. (2013) Expert assessment of vulnerability of permafrost carbon to climate change. *Climatic Change*, **119**, 359–374.
Schuur E a. G, McGuire AD, Schädel C et al. (2015) Climate change and the permafrost carbon feedback. *Nature*, **520**, 171–179.
Sierra CA, Müller M, Metzler H, Manzoni S, Trumbore SE (2017) The muddle of ages, turnover, transit, and residence times in the carbon cycle. *Global change biology*, **23**, 1763–1773.
Sistla SA, Moore JC, Simpson RT, Gough L, Shaver GR, Schimel JP (2013) Long-term warming restructures Arctic tundra without changing net soil carbon storage. *Nature*, **497**, 615–618.
Six J, Elliott ET, Paustian K, Doran JW (1998) Aggregation and Soil Organic Matter Accumulation in Cultivated and Native Grassland Soils. *Soil Science Society of America Journal*, **62**, 1367–1377.
Sollins P, Homann P, Caldwell BA (1996) Stabilization and destabilization of soil organic matter: mechanisms and controls. *Geoderma*, **74**, 65–105.
Strauss J, Schirrmeister L, Mangelsdorf K, Eichhorn L, Wetterich S, Herzschuh U (2014) Organic matter quality of deep permafrost carbon – a study from Arctic Siberia. *Biogeosciences Discuss.*, **11**, 15945–15989.
Stuiver M, Polach HA (1977) Discussion reporting of 14 C data. *Radiocarbon*, **19**, 355–363.
Torn MS, Trumbore SE, Chadwick OA, Vitousek PM, Hendricks DM (1997) Mineral control of soil organic carbon storage and turnover. *Nature*, **389**, 170–173.
Torn MS, Lapenis AG, Timofeev A, Fischer ML, Babikov BV, Harden JW (2002) Organic carbon and carbon isotopes in modern and 100-year-old-soil archives of the Russian steppe. *Global Change Biology*, **8**, 941–953.
Torn M, Swanston C, Castanha C, Trumbore S (2009) Storage and turnover of organic matter in soil. *Biophysico-Chemical Processes Involving Natural Nonliving Organic Matter in Environmental Systems*, 219–272.
Townsend AR, Vitousek PM, Desmarais DJ, Tharpe A (1997) Soil Carbon Pool Structure and Temperature Sensitivity Inferred Using CO2 and 13CO2 Incubation Fluxes from Five Hawaiian Soils. *Biogeochemistry*, **38**, 1–17.
Trumbore S (2000) Age of soil organic matter and soil respiration: radiocarbon constraints on belowground C dynamics. *Ecological Applications*, **10**, 399–411.
Trumbore S (2006) Carbon respired by terrestrial ecosystems – recent progress and challenges. *Global Change Biology*, **12**, 141–153.
Updegraff K, Pastor J, Bridgham SD, Johnston CA (1995) Environmental and Substrate Controls over Carbon and Nitrogen Mineralization in Northern Wetlands. *Ecological Applications*, **5**, 151–163.
Vaughn LJS, Conrad ME, Bill M, Torn MS (2016) Isotopic insights into methane production, oxidation, and emissions in Arctic polygon tundra. *Global Change Biology*, n/a–n/a.
Waldrop MP, Wickland KP, White Iii R, Berhe AA, Harden JW, Romanovsky VE (2010) Molecular investigations into a globally important carbon pool: Permafrost-protected carbon in Alaskan soils. *Global Change Biology*, **16**, 2543–2554.

Zhang W, Parker KM, Luo Y, Wan S, Wallace LL, Hu S (2005) Soil microbial responses to experimental warming and clipping in a tallgrass prairie. *Global Change Biology*, **11**, 266–277.

Zimov SA, Davydov SP, Zimova GM, Davydova AI, Schuur E a. G, Dutta K, Chapin FS (2006) Permafrost carbon: Stock and decomposability of a globally significant carbon pool. *Geophysical Research Letters*, **33**, L20502.

Zogg GP, Zak DR, Ringelberg DB, White DC, MacDonald NW, Pregitzer KS (1997) Compositional and Functional Shifts in Microbial Communities Due to Soil Warming. *Soil Science Society of America Journal*, **61**, 475–481.

Tables and Figures

Table 1
Properties of bulk soil and emitted CO_2 in the temperature incubation

(a) Effects of depth, incubation duration, and temperature on the rate, isotopic composition, and turnover time of emitted CO_2

Profile	Depth (cm)	Incubation period	CO_2 flux* (mg C d^{-1})	$\delta^{13}C_{CO2}$ (‰)	Analysis year	$F^{14}C$	$\Delta^{14}C_{CO2}$ (‰)	TT_{CO2} (y)
HC1-rim	0-14	T1 (5°C)	0.211	-29.4	2013	1.033	25.2 ± 3.1	260
		T2 (10°C)	0.135	-27.4	2013	0.9572	-50 ± 2.7	690
		T3 (5°C)	0.0822	-26.9	2017	0.9524	-55.2 ±2.0	730
	14-31	T1 (5°C)	0.208	--	2013	0.7899**	-216.1 ± 3.0**	2440
		T2 (10°C)	0.207	-27.0	2013	0.7109	-294.5 ± 2.3	3610
		T3 (5°C)	0.133	-26.2	2017	0.7037	-301.0 ± 1.3	3730
HC1-trough	0-7	T1 (5°C)	0.495	-27.9	2013	1.0415	33.6 ± 3.5	230
		T2 (10°C)	0.482	-27.7	2013	1.0527	44.7 ± 3.8	200
		T3 (5°C)	0.373	--	--	--	--	--
	7-27	T1 (5°C)	0.0915	-22.7	2013	0.9640	-43.3 ± 3.6	640
		T2 (10°C)	0.107	-27.6	2013	0.9746	-32.8 ± 2.8	560-570
		T3 (5°C)	0.0757	-27.0	2017	0.9806	-27.2 ± 2.0	530
	27-37	T1 (5°C)	0.0646	-25.3	2013	0.9348	-72.3 ± 3.0	870
		T2 (10°C)	0.0822	-27.6	2013	0.9086	-98.3 ± 3.9	1100
		T3 (5°C)	0.0623	-26.4	2017	0.9073	-99.9 ± 1.7	1120
HC3-center	0-13	T1 (5°C)	0.277	-26.4	2013	0.9914	-16.1 ± 2.9	460
		T2 (10°C)	0.287	-26.4	2013	0.9705	-36.8 ± 2.8	590
		T3 (5°C)	0.184	-26.3	2017	0.9712	-36.5 ± 1.7	590
	13-27	T1 (5°C)	0.121	-26.7	2013	0.7976	-208.5 ± 2.5	2340
		T2 (10°C)	0.156	-26.7	2013	0.7729	-232.9 ± 2.2	2670
		T3 (5°C)	0.102	-25.9	2017	0.7632	-242.8 ± 1.4	2810
FC2-center	0-8	T1 (5°C)	0.351	-28.1	2013	1.0317	23.8 ± 3.6	270
		T2 (10°C)	0.353	-28.2	2013	1.0436	35.7 ± 3.0	220-230
		T3 (5°C)	0.215	-27.7	2017	1.0409	32.6 ± 1.9	220-230
	8-26	T1 (5°C)	0.138	-27.2	2013	0.9660	-41.4 ± 2.9	630
		T2 (10°C)	0.135	-28.2	2013	0.9109	-96.0 ± 3.4	1080
		T3 (5°C)	0.0833	--	--	--	--	--
	26-39	T1 (5°C)	0.0833	-22.9	2013	0.7915	-214.6 ± 2.4	2420
		T2 (10°C)	0.113	-27.3	2013	0.7780	-227.9 ± 2.3	2600
		T3 (5°C)	.0757	-27.6	2017	0.7840	-222.3 ± 1.4	2520

(table continues)

Profile	Depth (cm)	Incubation period	CO_2 flux* (mg C d^{-1})	$\delta^{13}C_{CO2}$ (‰)	Analysis year	$F^{14}C$	$\Delta^{14}C_{CO2}$ (‰)	TT_{CO2} (y)
FC2-rim	0-6	T1 (5°C)	0.194	-27.0	2013	1.0675	59.4 ± 3.4	160-170
		T2 (10°C)	0.195	-26.7	2013	1.0787	70.5 ± 3.5	140
		T3 (5°C)	0.112	-25.7	2017	1.0662	57.7 ± 2.2	170
	11-33	T1 (5°C)	0.278	-28.2	2013	0.6787	-326.4 ± 2.5	4160
		T2 (10°C)	0.362	-28.5	2013	0.6563	-348.7 ± 1.9	4580
		T3 (5°C)	0.241	-28.1	2017	0.6549	-350.3 ± 1.2	4620
FC4-center	0-6	T1 (5°C)	0.267	-27.7	2013	1.0451	37.2 ± 5.4	220
		T2 (10°C)	0.287	-28.0	2013	1.0424	34.4 ± 3.0	230
		T3 (5°C)	0.176	-27.4	2017	1.0333	25.0 ± 1.9	260
	6-20	T1 (5°C)	0.113	-26.8	2013	0.8244	-181.9 ± 2.5	2000
		T2 (10°C)	0.132	-28.4	2013	0.7883	-217.7 ± 2.3	2460
		T3 (5°C)	0.0913	-27.9	2017	0.7871	-219.1 ± 1.7	2480
	20-34	T1 (5°C)	0.168	-24.4	2013	0.7181	-287.4 ± 2.4	3490
		T2 (10°C)	0.192	-26.9	2013	0.7301	-275.4 ± 2.5	3300
		T3 (5°C)	0.13	-27.9	2017	0.7415	-264.3 ± 1.3	3130
FC4-rim	0-5	T1 (5°C)	0.178	-27.3	2013	1.0948	86.5 ± 3.5	110-120
		T2 (10°C)	0.200	-25.0	2013	1.1056	97.2 ± 3.8	100
		T3 (5°C)	0.135	-26.8	2017	1.1051	96.3 ± 2.0	100
	5-14	T1 (5°C)	0.0555	-25.0	2013	0.8620	-144.5 ± 4.4	1570
		T2 (10°C)	0.0730	-28.3	2013	0.8339	-172.4 ± 2.9	1890
		T3 (5°C)	0.0423	--	--	--	--	--
	14-21	T1 (5°C)	0.130	-25.0	2013	0.7989	-207.1 ± 3.6	2320
		T2 (10°C)	0.137	-28.4	2013	0.7870	-219.0 ± 2.8	2480
		T3 (5°C)	0.0891	-27.8	2017	0.7917	-214.6 ± 1.7	2420
LC1-center	0-14	T1 (5°C)	0.403	-28.7	2013	1.0263	18.6 ± 3.0	290
		T2 (10°C)	0.467	-29.2	2013	1.0188	11.0 ± 3.4	320
		T3 (5°C)	0.294	-28.9	2017	1.0096	1.6 ± 1.8	360
	14-30	T1 (5°C)	0.144	-27.9	2013	0.8468	-141.8 ± 2.8	1540
		T2 (10°C)	0.162	-28.5	2013	0.8552	-151.3 ± 2.5	1650
		T3 (5°C)	0.117	-28.4	2017	0.8460	-160.7 ± 1.5	1750
LC1-rim	0-14	T1 (5°C)	0.404	-27.7	2013	0.9589	-48.3 ± 3.7	680
		T2 (10°C)	0.429	-27.7	2013	0.9490	-58.2 ± 2.7	750
		T3 (5°C)	0.255	-27.1	2017	0.9516	-56.0 ± 1.7	740
	14-35	T1 (5°C)	0.375	-27.5	2013	0.7147	-290.7 ± 2.3	3540
		T2 (10°C)	0.382	-27.8	2013	0.6882	-317.0 ± 2.5	3990
		T3 (5°C)	0.237	-27.4	2017	0.6835	-321.9 ± 1.2	4080

*Average CO_2 production rate for each incubation period
**Calculated with an approximate $\delta^{13}C$ value of -25 ‰

(b) Water, organic carbon, and nitrogen content of bulk soil samples

Profile	Depth (cm)	GWC (g_{water} $g_{drysoil}^{-1}$)	%C	%N	Carbon content (g C)	Carbon content (g C cm^{-2})
HC1-rim	0-14	0.744	15.1	0.83	3.67	0.724
	14-31	2.00	25.3	1.48	3.48	0.687
					Total = 7.15	Total = 1.41
HC1-trough	0-7	3.3	44.4	2.54	1.80	0.356
	7-27	0.240	4.40	0.26	3.03	0.598
	27-37	0.34	8.13	0.46	2.14	0.423
					Total = 6.97	Total = 1.38
HC3-center	0-13	0.978	25.9	1.30	3.33	0.656
	13-27	1.26	24.0	1.30	2.59	0.512
					Total = 5.92	Total = 1.17
FC2-center	0-8	0.314	40.5	2.32	20.6	4.06
	8-26	0.186	3.51	0.18	2.66	0.524
	26-39	0.27	5.71	0.32	2.08	0.410
					Total = 25.3	Total = 4.99
FC2-rim	0-6	2.3	40.4	2.32	1.67	0.329
	6-11	0.44	12.6	0.58	1.47	0.289
	11-33	0.955	18.2	1.03	7.29	1.44
					Total = 10.4	Total = 2.06
FC4-center	0-6	2.7	42.2	2.45	1.83	0.361
	6-20	0.385	9.35	0.50	3.61	0.712
	20-34	0.802	15.0	0.86	3.28	0.646
					Total = 8.71	Total = 1.72
FC4-rim	0-5	2.6	41.0	2.03	1.03	0.204
	5-14	0.327	8.37	0.42	2.92	0.577
	14-21	0.801	19.9	1.15	3.02	0.595
					Total = 6.98	Total = 1.38
LC1-center	0-14	0.299	29.5	1.63	15.5	3.05
	14-30	1.8	26.8	1.43	2.15	0.425
					Total = 17.6	Total = 3.48
LC1-rim	0-14	0.783	19.2	0.88	5.38	1.06
	14-35	1.35	28.5	1.49	6.29	1.24
					Total = 11.7	Total = 2.30

Table 2
Properties of bulk soil and emitted CO_2 in the anaerobic incubation

(a) Effects of depth and oxygen availability on the flux rate, isotopic composition, and turnover time of emitted CO_2

Profile	Depth (cm)	Headspace	CO_2 flux* (μg C d^{-1})	$\delta^{13}C_{CO2}$ (‰)	Analysis year	$F^{14}C$	$\Delta^{14}C_{CO2}$ (‰)	TT_{CO2} (y)
HC1-center	0-11.25	Aerobic	82.3	-26.3	2016	1.0991	90.4 ± 3.5	110
	11.25-22.5	Aerobic	10.2	-22.9	2016	0.6797	-325.7 ± 2.0	4150
	11.25-22.5	Anaerobic	9.10	-25.6	2016	0.6990	-306.6 ± 2.0	3810
HC2-center	0-11	Aerobic	83.4	-27.7	2016	1.0012	-6.8 ± 3.8	400-410
	11-22	Aerobic	12.6	-26.9	2016	0.7741	-232.1 ± 2.2	2660
	11-22	Anaerobic	6.64	-26.3	2016	0.6993	-306.3 ± 2	3810
HC3-center	0-11.23	Aerobic	113	-26.3	2016	1.0370	28.8 ± 3.0	250
	11.25-23.5	Aerobic	10.0	-27.6	2016	0.6808	-324.6 ± 2.0	4130
	11.25-23.5	Anaerobic	7.16	-23.2	2016	0.6583	-346.9 ± 1.9	4550
FC1-center	0-11.5	Aerobic	192	-28.5	2016	1.0365	28.3 ± 3.3	250
	11.5-23	Aerobic	9.29	-26.3	2016	0.8691	-137.8 ± 3.6	1500
	11.5-23	Anaerobic	4.77	-25.3	2016	0.8495	-157.2 ± 2.6	1710
FC3-center	0-8	Aerobic	100	-27.4	2016	1.0320	23.8 ± 3.4	160-170
	8-16	Aerobic	13.6	-27.2	2016	0.8395	-167.1 ± 2.4	1830
	8-16	Anaerobic	8.47	-25.8	2016	0.862	-144.9 ± 2.5	1580
FC4-center	0-15.5	Aerobic	214	-27.7	2016	1.0758	67.2 ± 3.8	140-150
	15.5-31	Aerobic	16.2	-24.4	2016	0.7793	-226.9 ± 2.8	2760
	15.5-31	Anaerobic	8.16	-27.2	2016	0.7666	-239.5 ± 2.8	2580
LC2-center	0-10 (water)	Aerobic	8.80	-32.2	2016	1.0112	3.2 ± 2.9	350
	10-44 (sediment)	Aerobic	87.4	-31.2	2016	1.0298	21.6 ± 3.9	270
	10-44 (sediment)	Anaerobic	47.9	--	--	--	--	--
LC3-center	0-9.5 (water)	Aerobic	4.86	-28.2	2016	0.9294	-78.0 ± 2.7	920
	9.5-41 (sediment)	Aerobic	127	-29.07	2016	1.0771	68.5 ± 3.4	140-150
	9.5-41 (sediment)	Anaerobic	38.2	-16.63	2016	1.0472	38.9 ± 3.0	210-220
LC4-center	0-15 (water)	Aerobic	9.09	--	--	--	--	--
	15-41 (sediment)	Aerobic	118	-19.0	2016	1.0362	28.0 ± 3.0	250
	15-41 (sediment)	Anaerobic	28.9	-31.5	2016	1.0359	27.6 ± 3.0	250

*Average CO_2 flux from the first 189 days of the incubation, prior to notable flux rate decreases

(b) Water, organic carbon, and nitrogen content, isotopic composition, and turnover time of bulk soil samples

Profile	Depth (cm)	Headspace	GWC (g_{water} $g_{drysoil}^{-1}$)	%C	%N	Carbon content (g C)	Carbon content* (g C cm^{-2})	$\delta^{13}C_{SOM}$ (‰)	Analysis year	$F^{14}C$	$\Delta^{14}C_{SOM}$ (‰)	TT_{SOM} (y)
HC1-center	0-11.25	Aerobic	0.431	7.25	0.33	1.09	0.221	-26.1	2017	0.8294	-177.3 ± 1.3	1950
	11.25-22.5	Aerobic	0.434	7.25	0.43	0.427	0.182	-27.1	2017	0.4257	-577.8 ± 0.7	11520
	11.25-22.5	Anaerobic	0.425	7.44	0.44	0.504	0.187	-27.2	2017	0.4210	-582.4 ± 0.7	11740
						Total = 2.05	Total = 0.406					
HC2-center	0-11	Aerobic	2.15	41.0	1.87	1.74	0.348	-26.5	2017	0.9362	-71.4 ± 1.3	860
	11-22	Aerobic	1.16	29.0	1.40	0.660	0.279	-28.1	2017	0.6450	-360.2 ± 1.0	4810
	11-22	Anaerobic	1.11	25.8	1.28	0.664	0.248	-28.0	2017	0.5730	-431.2 ± 0.9	6430
						Total = 3.09	Total = 0.610					
HC3-center	0-11.23	Aerobic	1.58	31.0	1.89	1.67	0.337	-26.8	2017	0.8525	-154.3 ± 1.4	1680
	11.25-23.5	Aerobic	1.07	25.6	1.20	0.621	0.277	-27.1	2017	0.5712	-433.4 ± 0.9	6490
	11.25-23.5	Anaerobic	1.09	25.8	1.19	0.783	0.279	-27.4	2017	0.5859	-418.8 ± 0.8	6120
						Total = 3.12	Total = 0.615					
FC1-center	0-11.5	Aerobic	0.8130	12.6	0.73	2.32	0.469	-27.8	2017	0.9479	-59.7 ± 1.3	760-770
	11.5-23	Aerobic	0.042	1.06	0.06	0.200	0.0789	-27.0	2017	0.5835	-421.2 ± 0.9	6180
	11.5-23	Anaerobic	0.124	1.20	0.07	0.222	0.0891	-27.1	2017	0.6000	-404.9 ± 0.9	5790
						Total = 2.80	Total = 0.553					
FC3-center	0-8	Aerobic	0.769	12.4	0.67	1.87	0.375	-27.8	2017	0.9105	-96.9 ± 1.3	1090
	8-16	Aerobic	0.180	3.45	0.18	0.534	0.213	-29.0	2017	0.6279	-377.1 ± 1.1	5170
	8-16	Anaerobic	0.201	3.55	0.18	0.555	0.219	-27.4	2017	0.6348	-370.4 ± 0.9	5020
						Total = 2.99	Total = 0.591					

(table continues)

Profile	Depth (cm)	Headspace	GWC (g_{water} $g_{drysoil}^{-1}$)	%C	%N	Carbon content (g C)	Carbon content* (g C cm^{-2})	$\delta^{13}C_{SOM}$ (‰)	Analysis year	$F^{14}C$	$\Delta^{14}C_{SOM}$ (‰)	TT_{SOM} (y)
FC4-center	0-15.5	Aerobic	1.39	24.0	1.17	1.98	0.408	-25.9	2017	0.9531	-54.6 ± 1.4	720
	15.5-31	Aerobic	0.16	8.43	0.48	0.467	0.209	-27.1	2017	0.6249	-380.2 ± 0.9	4630
	15.5-31	Anaerobic	0.363	8.18	0.45	0.567	0.202	-26.8	2017	0.6542	-351.1 ± 0.9	5230
						Total = 3.11	Total = 0.613					
LC2-center	0-10 (water)	Aerobic	1900	35.5	2.91	0.00776	0.00205	-31.8	2017	1.0736	65.0 ± 1.4	150
	10-44 (sediment)	Aerobic	4.22	37.0	2.04	0.672	0.242	-28.6	2017	0.9159	-91.5 ± 1.2	1040
	10-44 (sediment)	Anaerobic	5.48	42.3	1.98	0.582	0.273	-29.2	2017	1.0545	46.0 ± 1.4	190-200
						Total = 1.305	Total = 0.258					
LC3-center	0-9.5 (water)	Aerobic	10200	37.0	1.83	0.00116	0.000485	--	--	--	--	--
	9.5-41 (sediment)	Aerobic	5.57	44.7	2.18	0.592	0.295	-27.7	2017	1.0629	54.3 ± 1.4	170-180
	9.5-41 (sediment)	Anaerobic	5.44	45.3	2.33	0.807	0.282	-28.0	2017	0.9762	-31.6 ± 1.5	560
						Total = 1.460	Total = 0.288					
LC4-center	0-15 (water)	Aerobic	1122	39.3	2.32	0.0133	0.00308	-30.0	2017	1.0064	-1.7 ± 1.5	380
	15-41 (sediment)	Aerobic	2.97	41.5	2.39	0.765	0.292	-28.0	2017	0.9734	-34.5 ± 1.3	630
	15-41 (sediment)	Anaerobic	2.86	41.9	2.36	0.661	0.286	-28.1	2017	0.9655	-42.3 ± 1.3	580
						Total = 1.482	Total = 0.293					

*Carbon contents of aerobic and anaerobic subsamples are scaled to the total core increment volume. Totals represent the total profile carbon content, calculated from unscaled aerobic and anaerobic subsamples.

Table 3
Results of statistical models from the anaerobic incubation

Model	DF	*F* value	Pr > *F*	Contrasted levels	*t* value for contrasts	Pr > |*t*|
Shallow $\Delta^{14}C_{CO2}$ ~ Polygon type	2	2.339	0.192	--	--	--
Deep $\Delta^{14}C_{CO2}$ ~ Polygon type	2	94.34	< 0.001 ***	High-centered – Flat-centered	-5.720	0.00313 **
				Low-centered – Flat-centered	7.955	< 0.001 ***
				Low-centered – High-centered	13.676	< 0.001 ***
Aerobic CO_2 evolution ~ Polygon type	2	3.28	0.109	--	--	--
Deep $\Delta^{14}C_{CO2}$ ~ Aerobic/Anaerobic	1	0.195	0.665	--	--	--

Significance codes: 0 *** 0.001 ** 0.01 * 0.05 . 1
Note: Aerobic CO_2 evolution was calculated as the sum of CO_2 produced by the shallow increment and CO_2 produced from the deep aerobic replicate, scaled to the total mass of the deep core increment.

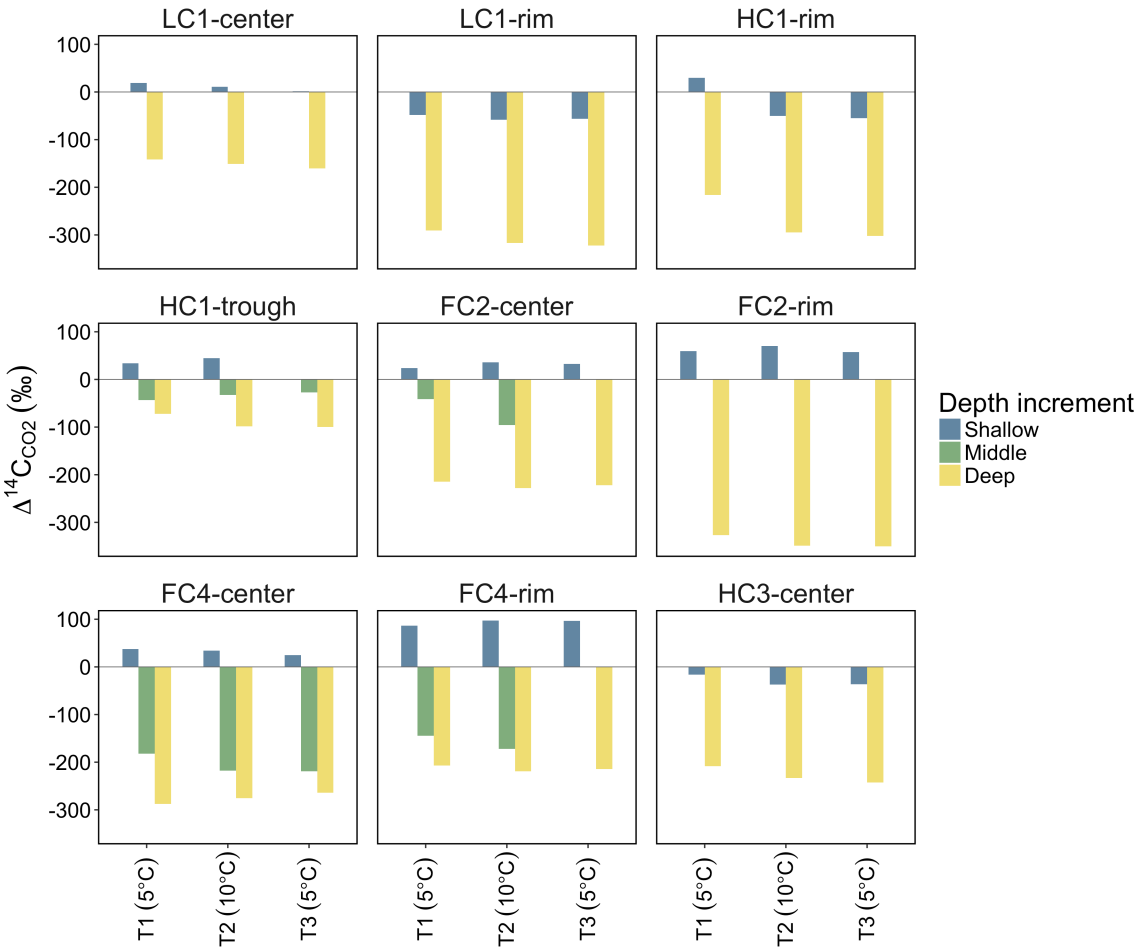

Figure 1. Effects of temperature and incubation duration on $\Delta^{14}C$ of CO_2. Intact core increments were incubated in 3 sequential periods (T1, T2, and T3) for 13, 16, and 21 days. $\Delta^{14}C_{CO2}$ values reflect radiocarbon contents of total CO_2 produced per incubation period.

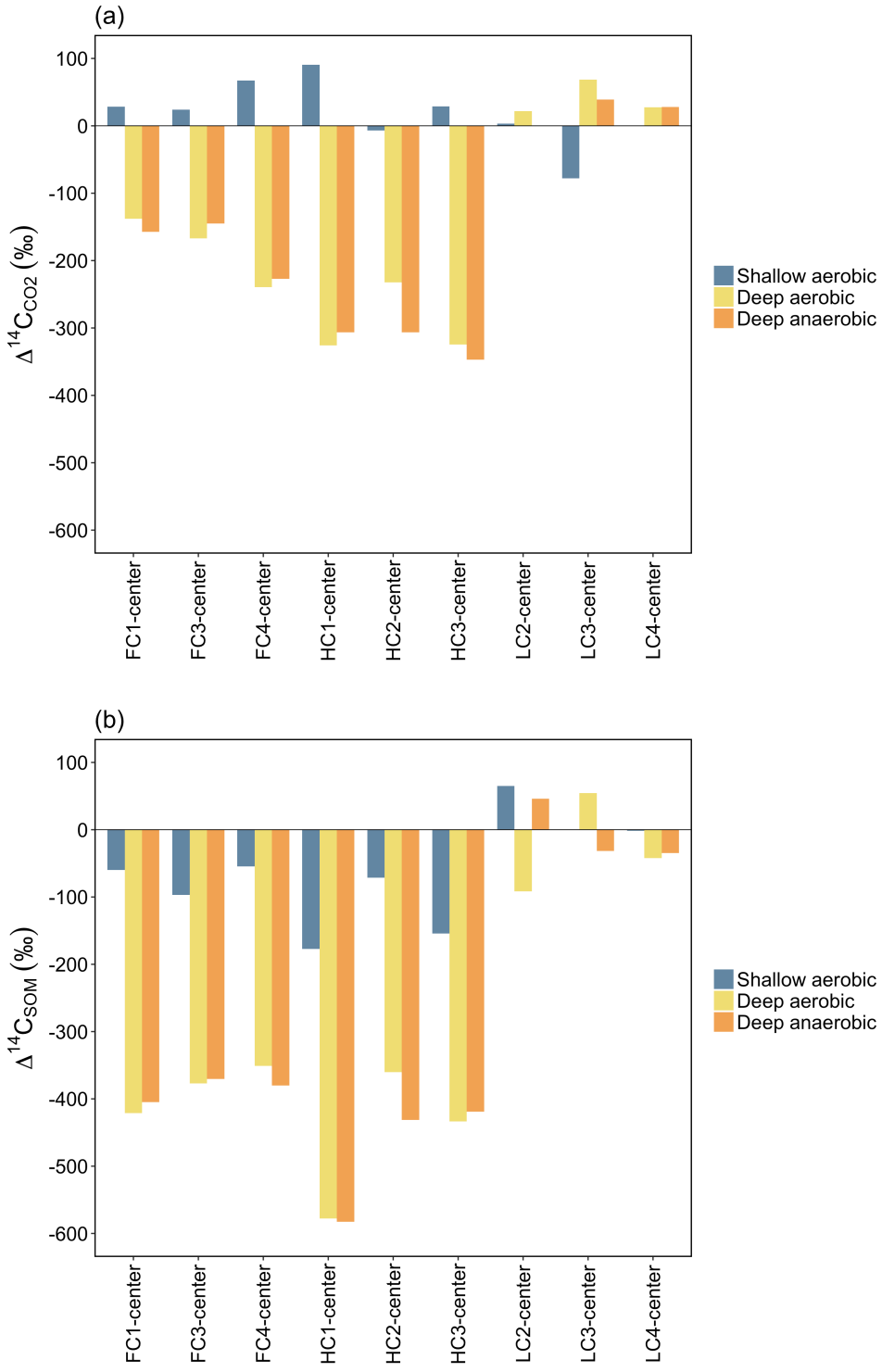

Figure 2. $\Delta^{14}C$ of (a) CO_2 and (b) bulk soil organic matter from soils incubated at 3°C for 379 days. $\Delta^{14}C_{CO2}$ represents cumulative CO_2 production throughout the incubation, and $\Delta^{14}C_{SOM}$ reflects radiocarbon contents of the remaining bulk soil.

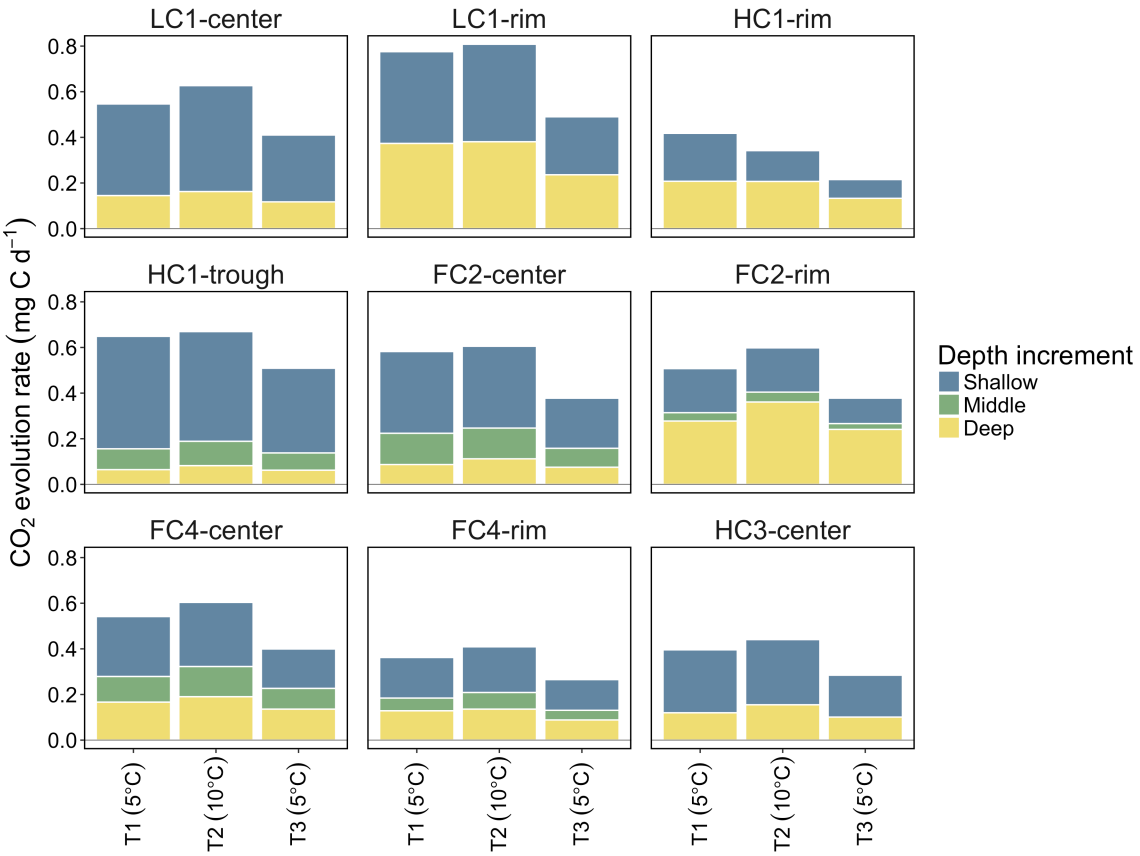

Figure 3. CO_2 production potential from cores incubated sequentially for 13 days at 5°C, 16 days at 10°C, and 21 days at 5°C. CO_2 evolution rates reflect mean CO_2 production per 1" diameter soil core. (Length and dry weight of cores vary.)

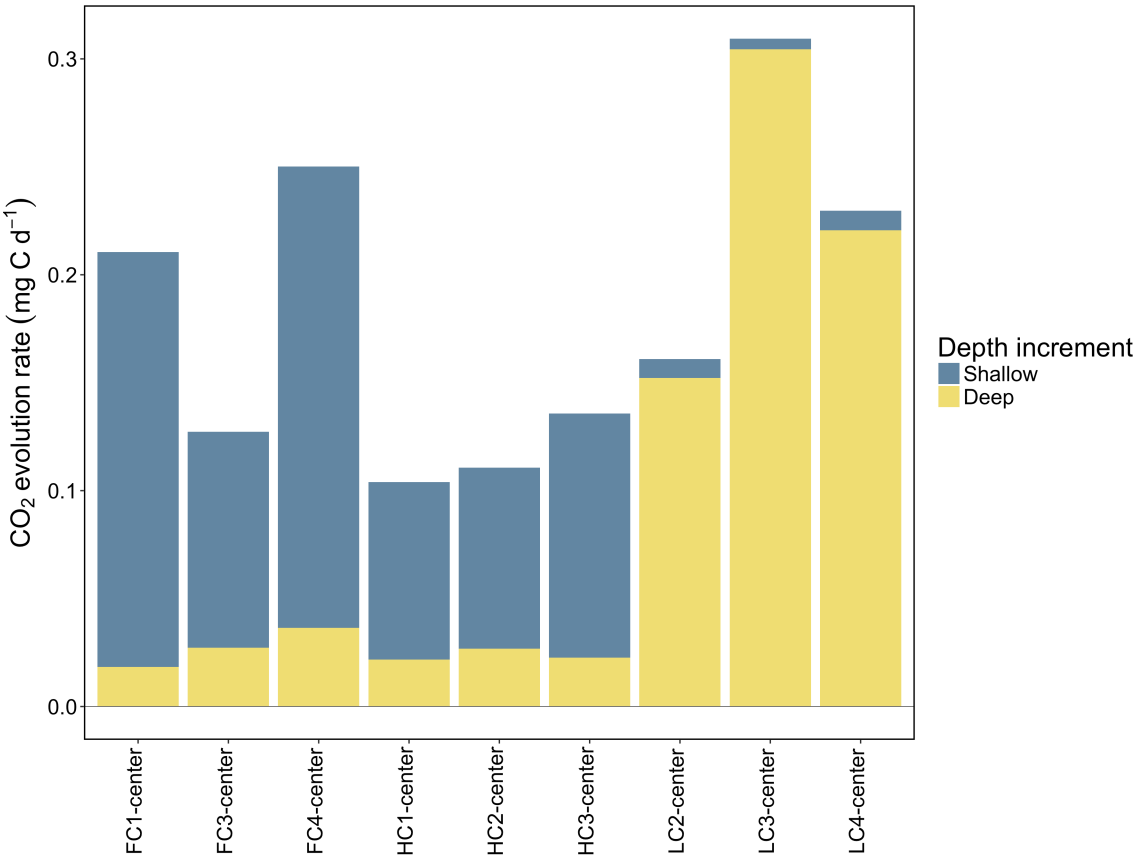

Figure 4. Aerobic CO_2 production potential from soil cores incubated at 3°C. CO_2 evolution rates reflect mean CO_2 production over 189 days per 1" diameter soil core. (Length and dry weight of cores vary.) Deep-soil CO_2 evolution rates are scaled from aerobic replicates to the total carbon content of each 1" diameter soil core increment.

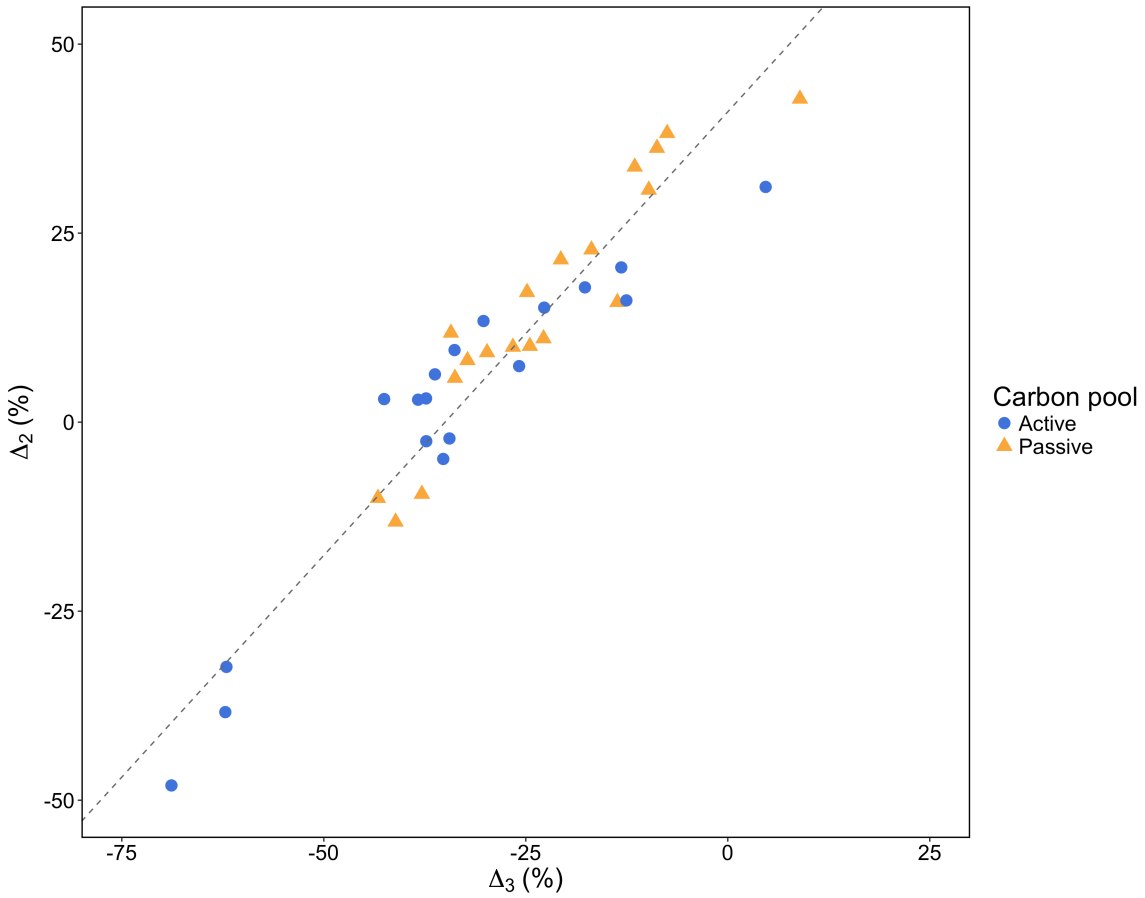

Figure 5. Temperature sensitivity and time effect during the temperature incubation. For each passive-pool (TT=5000 y) or active-pool (TT=50 y) component of CO_2 production, Δ_2 = the difference in CO_2 production between incubation periods 1 (5°C) and 2 (10°C). Δ_3 = the difference in CO_2 production between incubation periods 1 and 3 (both 5°C). The regression line represents the best linear fit from a linear mixed effects model including all incubated core increments. The y-intercept (41.2 ± 2.1) estimates the change in CO_2 production due to a 5°C temperature increase in the absence of any temperature-independent change in the carbon mineralization rate, i.e., when the time effect = 0.

APPENDIX A: VEGETATION COMMUNITY AND CANOPY HEIGHT ON THE BARROW ENVIRONMENTAL OBSERVATORY

Polygon type	Polygon position	*Carex aquatilis* (% cover)	*Eriophorum* species (% cover)	*Dupontia fisheri* (% cover)	Canopy height (cm)
High-centered	Center	0.3 ± 0.3 (n=4)	1.6 ± 2.4 (n=4)	0.7 ± 0.9 (n=4)	1.9 ± 2.5 (n=36)
	Rim	4.4 ± 3.2 (n=4)	2.1 ± 4.1 (n=4)	0.1 ± 0.1 (n=4)	5.6 ± 3.4 (n=36)
	Trough	14.1 ± 5.3 (n=4)	5.8 ± 4.8 (n=4)	4.3 ± 4.2 (n=4)	10.8 ± 5.7 (n=35)
Flat-centered	Center	8.1 ± 8.1 (n=4)	22.8 ± 21.1 (n=4)	6.1 ± 7.4 (n=4)	7.0 ± 3.7 (n=36)
	Rim	3.2 ± 2.7 (n=4)	1.1 ± 1.0 (n=4)	0.3 ± 0.3 (n=4)	4.1 ± 3.5 (n=36)
	Trough	12.4 ± 8.1 (n=4)	2.6 ± 1.5 (n=4)	6.1 ± 3.6 (n=4)	11.3 ± 4.5 (n=36)
Low-centered	Center	24.7 ± 13.3 (n=8)	3.5 ± 4.1 (n=8)	1.3 ± 1.9 (n=8)	13.8 ± 5.6 (n=72)
	Rim	13.9 ± 5.8 (n=8)	12.7 ± 15.4 (n=8)	1.2 ± 1.4 (n=8)	7.9 ± 3.5 (n=72)
	Trough	28.8 ± 10.8 (n-8)	2.4 ± 2.5 (n=8)	4.5 ± 4.8 (n=8)	15.5 ± 5.4 (n=72)

Note: Measurements were made in July 2012. Aerial percent cover and canopy height were estimated from 48 1 × 1 m plots. Canopy heights were measured from the top of the moss layer. Uncertainty ranges indicate standard deviations.

Reference: Sloan, V.L., J.D. Brooks, S.J. Wood, J.A. Liebig, J. Siegrist, C.M. Iversen, R.J. Norby. 2014. Plant community composition and vegetation height, Barrow, Alaska, Ver. 1. Next Generation Ecosystem Experiments Arctic Data Collection, Carbon Dioxide Information Analysis Center, Oak Ridge National Laboratory, Oak Ridge, Tennessee, USA. Data set accessed at http://dx.doi.org/10.5440/1129476

APPENDIX B: LOCAL CH_4 EMISSIONS DECREASE DUE TO A 25% SHIFT IN AREA FROM LOW-CENTERED TO FLAT/HIGH-CENTERED POLYGONS

In the Barrow Environmental Observatory, the percent land surface cover of polygon types is 35.12 % LC polygons and 64.88 % FHC polygons. Given average CH_4 flux rates of 64.3 nmol m^{-2} s^{-1} for LC polygons and 6.75 nmol m^{-2} s^{-1} for FHC polygons, we calculated the percentage change over the BEO in CH_4 due to a 25% shift from LC polygon area to FHC polygon area according to the following:

$$\% \text{ change} = \frac{\Delta \text{Flux}}{\text{Flux}_0} \times 100 = \frac{0.25(0.3512 \times 6.75) - 0.25(0.3512 \times 64.3)}{0.3512 \times 64.3 + 0.6488 \times 6.75} \times 100 = -19\ \%$$

APPENDIX C: COMPARISON BETWEEN GLUCOSE ADDITION AND PRODUCTIVITY INCREASE

Based on observations, the glucose needed to double CO_2 efflux = 5-10 times current rate of 6.125 g glucose per mesocosm, or 30-60 g glucose per mesocosm. This is equivalent to 1-2 moles C per mesocosm, or 20-40 moles C m^{-2}. If we assume root exudation equals 10 % of total net C fixation (Loya *et al.*, 2002; Farrar *et al.*, 2003), our glucose addition of 6.125 g per mesocosm is equivalent to an increase in net C fixation of 200-400 moles C m^{-2}. Assuming NPP/GPP = 0.5 (Turner *et al.*, 2006; Zhang *et al.*, 2009), this corresponds to a gross C fixation increase of 400-800 moles C m^{-2}. With an average growing season (June-September) GPP of ~0.8 μmol m^{-2} s^{-1} (Olivas *et al.*, 2010) or 8.3 moles C m^{-2} y^{-1}, a glucose addition of 30-60 g per mesocosm is equivalent to ~50-100 years of C fixation at current production rates.

References

Farrar J, Hawes M, Jones D, Lindow S (2003) How Roots Control the Flux of Carbon to the Rhizosphere. *Ecology*, **84**, 827–837.

Loya WM, Johnson LC, Kling GW, King JY, Reeburgh WS, Nadelhoffer KJ (2002) Pulse-labeling studies of carbon cycling in arctic tundra ecosystems: Contribution of photosynthates to soil organic matter. *Global Biogeochemical Cycles*, **16**, 1101.

Olivas PC, Oberbauer SF, Tweedie CE, Oechel WC, Kuchy A (2010) Responses of CO2 flux components of Alaskan Coastal Plain tundra to shifts in water table. *Journal of Geophysical Research: Biogeosciences*, **115**, G00I05.

Turner DP, Ritts WD, Cohen WB et al. (2006) Evaluation of MODIS NPP and GPP products across multiple biomes. *Remote Sensing of Environment*, **102**, 282–292.

Zhang Y, Xu M, Chen H, Adams J (2009) Global pattern of NPP to GPP ratio derived from MODIS data: effects of ecosystem type, geographical location and climate. *Global Ecology and Biogeography*, **18**, 280–290.

APPENDIX D: ATMOSPHERIC RADIOCARBON IN BARROW, ALASKA, 1750-2014

To model carbon turnover times from radiocarbon measurements, we constructed an annually resolved time series of atmospheric $\Delta^{14}C$ for Barrow, Alaska.

Datasets used

1. The IntCal13 dataset provides pre-bomb radiocarbon values at 5-year resolution until 1950 (Reimer *et al.*, 2013).
2. Radiocarbon measurements made in Fruholmen, Norway cover the period from December 1962 through June 1993 (Nydal & Lövseth, 1996). Limited measurements from Point Barrow between 1985 and 1991 confirm that this dataset provides a close approximation for Barrow, Alaska values (Meijer *et al.*, 2008).
3. Radiocarbon measurements made in Point Barrow between June 1999 through December 2007 were published in Graven *et al.*, (2012).
4. On August 12, 2012, July 13, 2013, September 2, 2014 and September 7, 2014, we collected air samples from the Barrow Environmental Observatory in 3 L evacuated stainless steel canisters. CO_2 was extracted from air samples and analyzed for radiocarbon according to the methods described in chapter 4.

Data selection and Gap-filling

Due to seasonal cycles of ecosystem carbon exchange, atmospheric radiocarbon values vary seasonally by ~10 ‰ in Barrow, peaking in late winter. Because CO_2 fixation occurs primarily in summer, summertime radiocarbon values best represent atmospheric inputs for turnover time modeling. For each year with available radiocarbon data, we calculated an annual summertime average using measurements from July and August, the months of maximum CO_2 uptake in Barrow (cite Zona et al 2014 Dennis et al). Because July/August data were unavailable for 2014, we used the average of the measurements made on September 2 and 7. From the IntCal13 dataset, annually resolved data were interpolated using a smoothing spline with 1 degree of freedom (R version 3.3.3 "Another Canoe," 2017-03-06).

With these annualized datasets, no data were available for the following years: 1951-1962, 1992-2000, and 2008-2011. For each of the latter two gaps, we predicted missing data from an exponential model using up to 10 years of annualized data preceding or following the gap. The first model ($R^2 = 0.9976$) included data from 1983-2010, and the second model ($R^2 = 0.9658$) covered the years 1999-2014. The gap between 1951 and 1962 spanned the period of rapid atmospheric radiocarbon increase from nuclear weapons testing. For this period, we used a constant $\Delta^{14}C$ value of -24.5 ‰ through 1957 and interpolated a linear increase until 1963.

References

Graven HD, Guilderson TP, Keeling RF (2012) Observations of radiocarbon in CO2 at seven global sampling sites in the Scripps flask network: Analysis of spatial gradients and seasonal cycles. *Journal of Geophysical Research: Atmospheres*, **117**.

Meijer HJ, Pertuisot MH, Plicht J van der (2008) High-accuracy 14C measurements for atmospheric CO2 samples by AMS. *Radiocarbon*, **48**, 355–372.

Nydal R, Lövseth K (1996) *Carbon-14 measurements in atmospheric CO2 from northern and southern hemisphere sites, 1962-1993*. Oak Ridge National Lab., TN (United States); Oak Ridge Inst. for Science and Education, TN (United States).

Reimer PJ, Bard E, Bayliss A et al. (2013) IntCal13 and Marine13 Radiocarbon Age Calibration Curves 0–50,000 Years cal BP. *Radiocarbon*, **55**, 1869–1887.

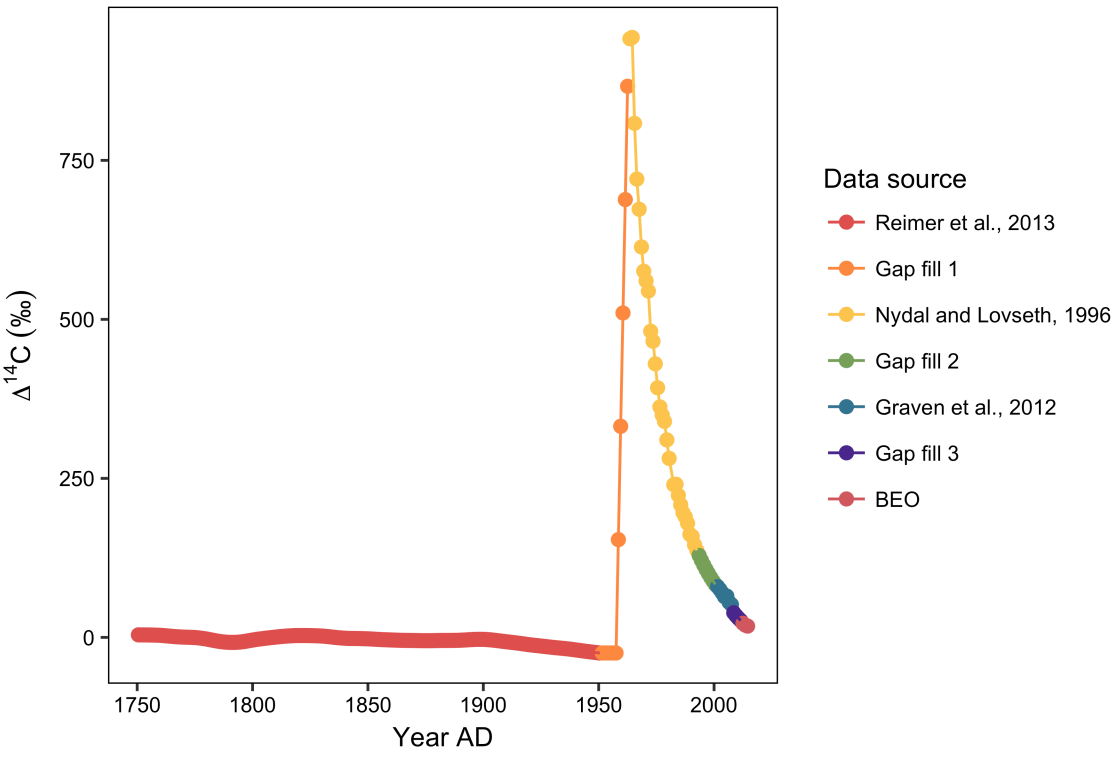

Figure D1. Compiled time series of atmospheric $\Delta^{14}C$ in Barrow, Alaska. Points represent summertime averages based on recent measurements (BEO), published values, and interpolated estimates.

Table D1
Compiled time series of atmospheric $\Delta^{14}C$ in Barrow, Alaska

Data source	Year	$\Delta^{14}C$ (‰)
Reimer *et al.*, 2013	1750	4.0
Reimer *et al.*, 2013	1751	3.9
Reimer *et al.*, 2013	1752	3.9
Reimer *et al.*, 2013	1753	3.9
Reimer *et al.*, 2013	1754	3.8
Reimer *et al.*, 2013	1755	3.8
Reimer *et al.*, 2013	1756	3.7
Reimer *et al.*, 2013	1757	3.6
Reimer *et al.*, 2013	1758	3.5
Reimer *et al.*, 2013	1759	3.3
Reimer *et al.*, 2013	1760	3.1
Reimer *et al.*, 2013	1761	2.8
Reimer *et al.*, 2013	1762	2.5
Reimer *et al.*, 2013	1763	2.1
Reimer *et al.*, 2013	1764	1.8
Reimer *et al.*, 2013	1765	1.5
Reimer *et al.*, 2013	1766	1.2
Reimer *et al.*, 2013	1767	0.9
Reimer *et al.*, 2013	1768	0.7
Reimer *et al.*, 2013	1769	0.5
Reimer *et al.*, 2013	1770	0.4
Reimer *et al.*, 2013	1771	0.3
Reimer *et al.*, 2013	1772	0.2
Reimer *et al.*, 2013	1773	0.0
Reimer *et al.*, 2013	1774	-0.2
Reimer *et al.*, 2013	1775	-0.4
Reimer *et al.*, 2013	1776	-0.7
Reimer *et al.*, 2013	1777	-1.2
Reimer *et al.*, 2013	1778	-1.7
Reimer *et al.*, 2013	1779	-2.3
Reimer *et al.*, 2013	1780	-2.9
Reimer *et al.*, 2013	1781	-3.6
Reimer *et al.*, 2013	1782	-4.3
Reimer *et al.*, 2013	1783	-5.0
Reimer *et al.*, 2013	1784	-5.7
Reimer *et al.*, 2013	1785	-6.3
Reimer *et al.*, 2013	1786	-6.8

(table continues)

Data source	Year	$\Delta^{14}C$ (‰)
Reimer *et al.*, 2013	1787	-7.2
Reimer *et al.*, 2013	1788	-7.5
Reimer *et al.*, 2013	1789	-7.8
Reimer *et al.*, 2013	1790	-7.9
Reimer *et al.*, 2013	1791	-7.9
Reimer *et al.*, 2013	1792	-7.8
Reimer *et al.*, 2013	1793	-7.6
Reimer *et al.*, 2013	1794	-7.3
Reimer *et al.*, 2013	1795	-6.9
Reimer *et al.*, 2013	1796	-6.4
Reimer *et al.*, 2013	1797	-5.8
Reimer *et al.*, 2013	1798	-5.1
Reimer *et al.*, 2013	1799	-4.5
Reimer *et al.*, 2013	1800	-3.9
Reimer *et al.*, 2013	1801	-3.3
Reimer *et al.*, 2013	1802	-2.8
Reimer *et al.*, 2013	1803	-2.3
Reimer *et al.*, 2013	1804	-1.8
Reimer *et al.*, 2013	1805	-1.4
Reimer *et al.*, 2013	1806	-1.0
Reimer *et al.*, 2013	1807	-0.5
Reimer *et al.*, 2013	1808	-0.1
Reimer *et al.*, 2013	1809	0.3
Reimer *et al.*, 2013	1810	0.7
Reimer *et al.*, 2013	1811	1.0
Reimer *et al.*, 2013	1812	1.4
Reimer *et al.*, 2013	1813	1.7
Reimer *et al.*, 2013	1814	2.0
Reimer *et al.*, 2013	1815	2.3
Reimer *et al.*, 2013	1816	2.5
Reimer *et al.*, 2013	1817	2.7
Reimer *et al.*, 2013	1818	2.8
Reimer *et al.*, 2013	1819	2.9
Reimer *et al.*, 2013	1820	2.9
Reimer *et al.*, 2013	1821	2.9
Reimer *et al.*, 2013	1822	2.9
Reimer *et al.*, 2013	1823	2.9
Reimer *et al.*, 2013	1824	2.8
Reimer *et al.*, 2013	1825	2.7
Reimer *et al.*, 2013	1826	2.6

(table continues)

Data source	Year	$\Delta^{14}C$ (‰)
Reimer *et al.*, 2013	1827	2.5
Reimer *et al.*, 2013	1828	2.4
Reimer *et al.*, 2013	1829	2.2
Reimer *et al.*, 2013	1830	2.0
Reimer *et al.*, 2013	1831	1.7
Reimer *et al.*, 2013	1832	1.3
Reimer *et al.*, 2013	1833	0.9
Reimer *et al.*, 2013	1834	0.5
Reimer *et al.*, 2013	1835	0.1
Reimer *et al.*, 2013	1836	-0.3
Reimer *et al.*, 2013	1837	-0.7
Reimer *et al.*, 2013	1838	-1.0
Reimer *et al.*, 2013	1839	-1.2
Reimer *et al.*, 2013	1840	-1.4
Reimer *et al.*, 2013	1841	-1.6
Reimer *et al.*, 2013	1842	-1.6
Reimer *et al.*, 2013	1843	-1.7
Reimer *et al.*, 2013	1844	-1.7
Reimer *et al.*, 2013	1845	-1.8
Reimer *et al.*, 2013	1846	-1.9
Reimer *et al.*, 2013	1847	-1.9
Reimer *et al.*, 2013	1848	-2.1
Reimer *et al.*, 2013	1849	-2.2
Reimer *et al.*, 2013	1850	-2.4
Reimer *et al.*, 2013	1851	-2.5
Reimer *et al.*, 2013	1852	-2.8
Reimer *et al.*, 2013	1853	-3.0
Reimer *et al.*, 2013	1854	-3.2
Reimer *et al.*, 2013	1855	-3.4
Reimer *et al.*, 2013	1856	-3.6
Reimer *et al.*, 2013	1857	-3.7
Reimer *et al.*, 2013	1858	-3.9
Reimer *et al.*, 2013	1859	-4.0
Reimer *et al.*, 2013	1860	-4.1
Reimer *et al.*, 2013	1861	-4.3
Reimer *et al.*, 2013	1862	-4.4
Reimer *et al.*, 2013	1863	-4.5
Reimer *et al.*, 2013	1864	-4.6
Reimer *et al.*, 2013	1865	-4.7
Reimer *et al.*, 2013	1866	-4.8

(table continues)

Data source	Year	$\Delta^{14}C$ (‰)
Reimer *et al.*, 2013	1867	-4.8
Reimer *et al.*, 2013	1868	-4.8
Reimer *et al.*, 2013	1869	-4.9
Reimer *et al.*, 2013	1870	-4.9
Reimer *et al.*, 2013	1871	-5.0
Reimer *et al.*, 2013	1872	-5.1
Reimer *et al.*, 2013	1873	-5.1
Reimer *et al.*, 2013	1874	-5.2
Reimer *et al.*, 2013	1875	-5.2
Reimer *et al.*, 2013	1876	-5.2
Reimer *et al.*, 2013	1877	-5.1
Reimer *et al.*, 2013	1878	-5.0
Reimer *et al.*, 2013	1879	-5.0
Reimer *et al.*, 2013	1880	-4.9
Reimer *et al.*, 2013	1881	-4.9
Reimer *et al.*, 2013	1882	-4.8
Reimer *et al.*, 2013	1883	-4.8
Reimer *et al.*, 2013	1884	-4.8
Reimer *et al.*, 2013	1885	-4.8
Reimer *et al.*, 2013	1886	-4.8
Reimer *et al.*, 2013	1887	-4.7
Reimer *et al.*, 2013	1888	-4.6
Reimer *et al.*, 2013	1889	-4.5
Reimer *et al.*, 2013	1890	-4.4
Reimer *et al.*, 2013	1891	-4.2
Reimer *et al.*, 2013	1892	-4.0
Reimer *et al.*, 2013	1893	-3.7
Reimer *et al.*, 2013	1894	-3.5
Reimer *et al.*, 2013	1895	-3.3
Reimer *et al.*, 2013	1896	-3.2
Reimer *et al.*, 2013	1897	-3.1
Reimer *et al.*, 2013	1898	-3.1
Reimer *et al.*, 2013	1899	-3.1
Reimer *et al.*, 2013	1900	-3.2
Reimer *et al.*, 2013	1901	-3.4
Reimer *et al.*, 2013	1902	-3.7
Reimer *et al.*, 2013	1903	-4.0
Reimer *et al.*, 2013	1904	-4.4
Reimer *et al.*, 2013	1905	-4.8
Reimer *et al.*, 2013	1906	-5.3

(table continues)

Data source	Year	$\Delta^{14}C$ (‰)
Reimer *et al.*, 2013	1907	-5.7
Reimer *et al.*, 2013	1908	-6.2
Reimer *et al.*, 2013	1909	-6.6
Reimer *et al.*, 2013	1910	-7.1
Reimer *et al.*, 2013	1911	-7.5
Reimer *et al.*, 2013	1912	-7.9
Reimer *et al.*, 2013	1913	-8.4
Reimer *et al.*, 2013	1914	-8.8
Reimer *et al.*, 2013	1915	-9.3
Reimer *et al.*, 2013	1916	-9.8
Reimer *et al.*, 2013	1917	-10.3
Reimer *et al.*, 2013	1918	-10.8
Reimer *et al.*, 2013	1919	-11.3
Reimer *et al.*, 2013	1920	-11.8
Reimer *et al.*, 2013	1921	-12.2
Reimer *et al.*, 2013	1922	-12.6
Reimer *et al.*, 2013	1923	-13.0
Reimer *et al.*, 2013	1924	-13.4
Reimer *et al.*, 2013	1925	-13.8
Reimer *et al.*, 2013	1926	-14.2
Reimer *et al.*, 2013	1927	-14.6
Reimer *et al.*, 2013	1928	-15.1
Reimer *et al.*, 2013	1929	-15.5
Reimer *et al.*, 2013	1930	-15.9
Reimer *et al.*, 2013	1931	-16.2
Reimer *et al.*, 2013	1932	-16.6
Reimer *et al.*, 2013	1933	-16.9
Reimer *et al.*, 2013	1934	-17.3
Reimer *et al.*, 2013	1935	-17.6
Reimer *et al.*, 2013	1936	-18.0
Reimer *et al.*, 2013	1937	-18.5
Reimer *et al.*, 2013	1938	-19.0
Reimer *et al.*, 2013	1939	-19.4
Reimer *et al.*, 2013	1940	-19.9
Reimer *et al.*, 2013	1941	-20.4
Reimer *et al.*, 2013	1942	-20.9
Reimer *et al.*, 2013	1943	-21.4
Reimer *et al.*, 2013	1944	-21.9
Reimer *et al.*, 2013	1945	-22.4
Reimer *et al.*, 2013	1946	-22.8

(table continues)

Data source	Year	$\Delta^{14}C$ (‰)
Reimer *et al.*, 2013	1947	-23.3
Reimer *et al.*, 2013	1948	-23.7
Reimer *et al.*, 2013	1949	-24.1
Reimer *et al.*, 2013	1950	-24.6
Gap fill 1	1951	-24.5
Gap fill 1	1952	-24.5
Gap fill 1	1953	-24.5
Gap fill 1	1954	-24.5
Gap fill 1	1955	-24.5
Gap fill 1	1956	-24.5
Gap fill 1	1957	-24.5
Gap fill 1	1958	153.7
Gap fill 1	1959	331.9
Gap fill 1	1960	510.1
Gap fill 1	1961	688.3
Gap fill 1	1962	866.5
Nydal & Lövseth, 1996	1963	941.2
Nydal & Lövseth, 1996	1964	943.3
Nydal & Lövseth, 1996	1965	808.2
Nydal & Lövseth, 1996	1966	720.6
Nydal & Lövseth, 1996	1967	673.2
Nydal & Lövseth, 1996	1968	613.8
Nydal & Lövseth, 1996	1969	575.7
Nydal & Lövseth, 1996	1970	560.6
Nydal & Lövseth, 1996	1971	544.5
Nydal & Lövseth, 1996	1972	481.3
Nydal & Lövseth, 1996	1973	465.7
Nydal & Lövseth, 1996	1974	430.1
Nydal & Lövseth, 1996	1975	392.5
Nydal & Lövseth, 1996	1976	362.4
Nydal & Lövseth, 1996	1977	349.7
Nydal & Lövseth, 1996	1978	339.6
Nydal & Lövseth, 1996	1979	310.5
Nydal & Lövseth, 1996	1980	281.4
Nydal & Lövseth, 1996	1982	240.0
Nydal & Lövseth, 1996	1983	240.8
Nydal & Lövseth, 1996	1984	223.4
Nydal & Lövseth, 1996	1985	208.5
Nydal & Lövseth, 1996	1986	196.1
Nydal & Lövseth, 1996	1987	189.5

(table continues)

Data source	Year	$\Delta^{14}C$ (‰)
Nydal & Lövseth, 1996	1988	179.4
Nydal & Lövseth, 1996	1989	162.0
Nydal & Lövseth, 1996	1990	158.8
Nydal & Lövseth, 1996	1991	145.6
Nydal & Lövseth, 1996	1992	137.0
Gap fill 2	1993	128.9
Gap fill 2	1994	121.1
Gap fill 2	1995	113.8
Gap fill 2	1996	106.9
Gap fill 2	1997	100.5
Gap fill 2	1998	94.4
Gap fill 2	1999	88.7
Gap fill 2	2000	83.4
Graven *et al.*, 2012	2001	79.8
Graven *et al.*, 2012	2002	75.3
Graven *et al.*, 2012	2003	70.0
Graven *et al.*, 2012	2004	64.0
Graven *et al.*, 2012	2005	64.9
Graven *et al.*, 2012	2006	55.2
Graven *et al.*, 2012	2007	51.5
Gap fill 3	2008	38.7
Gap fill 3	2009	34.2
Gap fill 3	2010	30.2
Gap fill 3	2011	26.6
Barrow Environmental Observatory	2012	22.2
Barrow Environmental Observatory	2013	19.3
Barrow Environmental Observatory	2014	17.8

Note: $\Delta^{14}C$ values represent mean summertime atmospheric radiocarbon in Barrow, Alaska, based on recent measurements (Barrow Environmental Observatory), published values, and interpolated estimates.

APPENDIX E: RADIOCARBON MEASUREMENTS OF ECOSYSTEM RESPIRATION AND SOIL PORE SPACE CO_2

Methods

Sample collection and field measurements

In August and October 2012, July and September 2013, and September 2014, we measured ecosystem respiration and collected CO_2 from soil pore space and soil surface emissions for radiocarbon analysis. Samples were collected from a range of polygon types (LC, FC, and HC) and positions within polygons (centers, rims, and troughs) representing a broad range of surface vegetation, microtopography, hydrology, and subsurface ice properties. Surface CO_2 fluxes were measured in 2013 and 2014 using opaque static chambers (25 cm diameter, 15-20 cm height) seated on PVC bases extending ~15 cm below the soil surface. Chambers were vented according to Xu *et al.*, (2006) to minimize pressure changes due to the Venturi effect, and bases were installed at least two days before each measurement to limit the influence of disturbance on flux rates and radiocarbon values. For each ecosystem respiration measurement, we seated the chamber in a 3 cm-deep water-filled trench in the base's top rim to create an airtight seal. Over a period of 4-8 minutes, we measured CO_2 concentrations within the chamber using a Los Gatos Research, Inc. Portable Greenhouse Gas Analyzer, and calculated the CO_2 flux rate (equivalent to ecosystem respiration) as the slope of the linear portion of the concentration vs. time curve.

In August and October 2012, July and September 2013, and September 2014, we collected CO_2 from non-vented soil chambers for radiocarbon analysis. In 2013 and 2014, samples were collected within 2 days of each ecosystem respiration measurement. After circulating chamber gas through soda lime for 20 minutes to remove CO_2, we allowed CO_2 to accumulate over 2 to 48 hours, depending on the CO_2 flux rate. Prior to sampling, we measured the CO_2 concentration in the chamber by passing 30 mL of gas through a LI-820 CO_2 gas analyzer (LI-COR). Samples were collected in one or more 500-1000 mL evacuated stainless steel canisters connected to chamber sampling ports via capillary tubing. High-concentration samples were collected with a syringe and needle through a septum in the sampling port and immediately injected into evacuated glass vials sealed with 14 mm-thick chlorobutyl septa (Bellco Glass, Inc.). To correct chamber gas samples for atmospheric contamination, we collected local air samples in 3000 mL stainless steel canisters on August 12, 2012, July 13, 2013, and September 2 and 7, 2014.

In August 2012 and July 2013, we collected soil pore gas through 1/4" stainless steel probes capped with gastight septa. Probes were inserted at 45° into the soil profile to depths of 10, 20, and 30 cm, or to 2 cm above the frost table if thaw depth was less than 30 cm. Before collecting each sample, we purged 10 mL of gas from the probe and measured the CO_2 concentration from an additional 30 mL sample. Radiocarbon samples were collected in evacuated 500-1000 mL stainless steel canisters to probes via flow restricting tubing (Upchurch scientific, 0.01" ID × 10 cm length) to fill the canisters slowly over 4 hours with minimal disturbance to the soil CO_2 concentration gradient (Gaudinski *et al.*, 2000). As with surface emissions samples, high concentration samples were collected with syringes and immediately injected into evacuated glass vials.

Laboratory analyses

CO_2 from gas samples was cryogenically purified under vacuum, divided for ^{14}C and ^{13}C analysis, and sealed in 9 mm quartz tubes. For radiocarbon analysis, we sent samples to Lawrence Livermore National Laboratory's Center for Accelerator Mass Spectrometry (CAMS) or the Carbon, Water, and Soils Research Lab at the USDA-FS Northern Research Station, where CO_2 was reduced to graphite on iron powder under H_2. ^{14}C abundance was then measured at CAMS using a HVEC FN Tandem Van de Graaff accelerator mass spectrometer or at UC Irvine's Keck Carbon Cycle AMS facility. $^{13}C/^{12}C$ in CO_2 splits was analyzed on the UC Davis Stable Isotope Laboratory GVI Optima Stable Isotope Ratio Mass Spectrometer.

Following the conventions of Stuiver and Polach (1977), radiocarbon results are presented as fractions of the modern NBS Oxalic Acid I (OX1) standard ($F^{14}C$), and deviations in parts per thousand (‰) from the absolute (decay-corrected) OX1 standard ($\Delta^{14}C$). All results have been corrected for mass-dependent isotopic fractionation using ^{13}C measurements.

Data processing and analysis

We corrected surface chamber radiocarbon measurements for atmospheric contamination using the method described in Schuur & Trumbore (2006). Briefly, we determined fractional contributions of background atmosphere and ecosystem respiration to total chamber gas using ^{13}C values in a two-pool mixing model:

$$^{13}C_S = f_{Reco} \times {}^{13}C_{Reco} + f_{atm} \times {}^{13}C_{atm}$$

$$f_{Reco} + f_{atm} = 1$$

where, f_{Reco} and f_{atm} are the fractional contributions of ecosystem respiration and background atmosphere, $^{13}C_S$ and $^{13}C_{atm}$ are the measured ^{13}C abundances in the sample and background atmosphere, and $^{13}C_{Reco}$ is the ^{13}C abundance in ecosystem respiration, approximated separately for each polygon type as the mean ^{13}C of chamber CO_2 samples with $[CO_2] > 4000$ ppm. For quality control, we omitted samples with $f_{Reco} < 0.5$. With each remaining sample, we calculated $\Delta^{14}C$ of ecosystem respiration ($\Delta^{14}C_{Reco}$):

$$\Delta^{14}C_S = f_{Reco} \times \Delta^{14}C_{Reco} + f_{atm} \times \Delta^{14}C_{atm}$$

where $\Delta^{14}C_S$ and $\Delta^{14}C_{atm}$ are the measured $\Delta^{14}C$ values of the sample and background atmosphere and f_{Reco} and f_{atm} were calculated above.

With soil pore space radiocarbon data, we omitted measurements with CO_2 concentrations less than 400 ppm due to possible leakage and atmospheric contamination during sampling, with the exception of one sample from 31 cm depth with highly negative $\Delta^{14}C$. Because ^{13}C values at depth vary greatly due to methanogenic processes, samples could not be corrected for atmospheric contamination. Radiocarbon values thus

represent the total CO_2 present in the soil pore space, sourced from both ecosystem respiration and downward atmospheric diffusion.

With surface chamber and soil pore space radiocarbon measurements, we modeled turnover times according to the method described in chapter 4.

We used a linear mixed effects model to evaluate spatial and temporal predictors of atmosphere-corrected surface chamber $\Delta^{14}C$, using all available data from 2012-2014. Possible predictor variables included thaw depth, polygon type (LC, FC, or HC), position (center, rim, or trough), day of year, and all two- and three-way interactions, with profile as a random effect to account for repeated measurements. From the set of all possible models, we performed variable selection using Akaike information criterion (AIC) values and a significance cutoff of $p < 0.05$ for fixed effects, based on incremental *F*-tests with Satterthwaite's approximation for denominator degrees of freedom. We tested for pairwise differences within categorical variables with Tukey's Honest Significant Difference test, using Satterthwaite's degrees of freedom. Statistical analyses were conducted in R version 3.3.3 "Another Canoe" (2017-03-06), using the packages lme4 (Bates *et al.*, 2014) and lmerTest (Kuznetsova *et al.*, 2014) for fitting and significance testing.

Results

Radiocarbon in ecosystem respiration

Radiocarbon content of soil surface CO_2 emissions, equivalent to ecosystem respiration ($\Delta^{14}C_{Reco}$), ranged from +60.5 to -160 ‰ (Table E1), corresponding to calculated turnover times (TT_{Reco}) of 160 to 1,700 y. TT_{Reco} followed an approximately lognormal distribution ($\mu = 5.73$ and $\sigma = 0.486$), centered at 245 y with only 4 measurements greater than 500 y. These 4 long TT_{Reco} values, from samples collected in August (HC1-center), September (HC1-center and HC2-center), and October (LC1-center), reflect inputs of very old carbon and/or low rates of autotrophic respiration.

To evaluate how carbon turnover varied with spatial and temporal variables, we used a linear mixed effects model to test thaw depth, polygon type, position within polygon, and day of year (DOY) as possible predictors of $\Delta^{14}C_{Reco}$. We found that position within polygon (center, rim, or trough) and the polygon type × DOY interaction were significant predictors of $\Delta^{14}C_{Reco}$ (Table E3). From Tukey's HSD test, CO_2 from polygon centers was significantly depleted in ^{14}C relative to rims and only marginally depleted relative to troughs, with no significant differences between rims and troughs. Underlying the type × DOY interaction, we observed a peak in $\Delta^{14}C_{Reco}$ in July, decreasing to the lowest measured values in September (Fig. E2). This trend, which appeared across all samples and across repeated measurements from individual profiles (Table E1), was stronger in HC than FC or LC polygons. We note that our sample set was balanced and random only in September 2014, as many sampled profiles in 2012 and 2013 had too little ecosystem-derived CO_2 relative to background atmosphere to produce a high-quality sample. In October 2012 in particular, we were able to obtain samples only from soils that were partially thawed at the surface. Due to this sampling constraint, our dataset reflects only the soil profiles contributing most substantially to total ecosystem respiration.

In July and September 2013 and September 2014, surface CO_2 flux varied between 0.32 and 2.5 μmol m^{-2} s^{-1} (Table E1). We found no significant correlation between

ecosystem respiration and TT_{Reco} (Fig. E4), indicating concurrent changes in respiration rates from both fast- and slow-cycling carbon pools (e.g., autotrophic respiration and deep heterotrophic respiration). We did find, however, that no samples had both high ecosystem respiration had long TT_{Reco}. Rather, particularly in September, long calculated turnover times coincided with low rates of ecosystem respiration (Fig. E4, Table E1). This observation reflects seasonal changes in the fraction of ecosystem respiration derived from autotrophic respiration. In July, autotrophic respiration rates were high and thaw depths were relatively shallow, so ecosystem respiration was largely derived from a homogeneous, fast-cycling carbon pool. Later in the season, when vegetation activity decreased, variable contributions from slower cycling soil carbon pools led to widely ranging measurements of TT_{Reco}.

Radiocarbon in soil pore space CO_2

From a subset of locations and sampling dates, we measured the radiocarbon content of CO_2 in soil pore gas ($\Delta^{14}C_{CO2p}$). This CO_2 was derived from in situ carbon mineralization and autotrophic respiration, as well as diffusion of background atmosphere and CO_2 produced elsewhere in the profile. $\Delta^{14}C_{CO2p}$ varied widely among profiles and sampling dates, with the general trend of increasingly negative $\Delta^{14}C_{CO2p}$ with depth in the soil (Fig. E3). In contrast with $\Delta^{14}C_{Reco}$ values, many of which were >0 ‰, these soil profile measurements ranged from -7.1 to -280 ‰, indicating that rapidly cycling carbon contributed minimally to heterotrophic respiration. Calculated turnover times of pore space CO_2 (TT_{CO2p}) ranged from 410 y in one 10 cm sample to 3,350 y at only 20 cm depth, indicating that slow-cycling carbon contributes substantially to soil carbon turnover, even in relatively shallow soils (Table E2). As with surface emissions measurements, we observed that HC polygon centers produced pore space CO_2 with particularly long turnover times, with values >3000 y from HC3-center in July 2013 and HC1-center in August 2012 and September 2013. Due to sampling limitations, however, we note that soil profile ^{14}C data are unavailable from certain polygon types and positions, particularly where soils were saturated.

In three cases (HC3-trough, HC3-center, and FC2-center), soil pore space CO_2 became less depleted in radiocarbon with depth, indicating more rapid carbon turnover deeper in the profile. In all three of these profiles, CO_2 concentrations in recovered samples increased with depth to levels 6 to 25 times higher than background atmosphere, so we infer that the higher $\Delta^{14}C_{CO2p}$ values at depth were not caused by downward diffusion of atmospheric CO_2. Instead, these inverted profiles suggest that either short-term processes such as rhizodeposition and leaching or the longer-term process of cryoturbation contributed rapidly cycling carbon to deeper soils.

References

Bates D, Maechler M, Bolker BM, Walker S (2014) *lme4: Linear mixed-effects models using Eigen and S4. R package version 1.1-7*.

Gaudinski JB, Trumbore SE, Davidson EA, Zheng S (2000) Soil carbon cycling in a temperate forest: radiocarbon-based estimates of residence times, sequestration rates and partitioning of fluxes. *Biogeochemistry*, **51**, 33–69.

Kuznetsova A, Brockhoff PB, Christensen RHB (2014) *lmerTest: Tests for random and fixed effects for linear mixed effect models (lmer objects of lme4 package).. R package version 2.0-11*.

Schuur E a. G, Trumbore SE (2006) Partitioning sources of soil respiration in boreal black spruce forest using radiocarbon. *Global Change Biology*, **12**.

Stuiver M, Polach HA (1977) Discussion reporting of 14C data. *Radiocarbon*, **19**, 355–363.

Xu L, Furtaw MD, Madsen RA, Garcia RL, Anderson DJ, McDermitt DK (2006) On maintaining pressure equilibrium between a soil CO_2 flux chamber and the ambient air. *Journal of Geophysical Research*, **111**.

Tables and Figures

Table E1
Flux rate and radiocarbon abundance of soil surface CO_2 emissions

Profile	Date	Thaw depth (cm)	CO_2 flux (μmol m^{-2} d^{-1})	Analysis year	$F^{14}C$	$\Delta^{14}C_{CO2}$ (‰)*	TT_{CO2} (y)
HC1-center	8/9/12	31	--	2013	1.0298	-58.4 ± 6.1	750
	9/2/14	32	0.547 ± 0.0047	2016	0.8916	-115.5 ± 10.2	1270
HC1-rim	10/6/12	--	--	2013	1.0298	22.0 ± 4.1	270
HC1-trough	8/8/12	32	--	2017	1.0420	33.6 ± 3.5	230
	8/11/12	32	--	2017	1.0501	41.6 ± 4.1	210
	10/6/12	--	--	2013	0.9936	-14.0 ± 3.2	450
	9/6/13	36	1.53 ± 0.016	2013	1.0271	19.3 ± 3.6	280
HC2-center	9/7/14	23	0.425 ± 0.0038	2016	0.9775	-31.3 ± 5.0	550
HC3-center	8/13/12	29	--	2013	1.0408	32.9 ± 5.2	230-240
	9/7/14	31	0.408 ± 0.0043	2017	0.9991	-9.0 ± 1.9	420
HC3-trough	7/12/13	--	1.65 ± 0.0070	2013	1.0520	44.0 ± 6.0	200
	9/6/13	32	0.489 ± 0.0033	2013	1.0211	13.3 ± 3.7	310
FC1-center	9/2/14	37	0.572 ± 0.0066	2016	1.0044	-3.6 ± 2.9	390
FC2-rim	8/12/12	--	--	2017	1.0343	25.9 ± 2.5	260
	10/6/12	--	--	2013	1.0375	29.7 ± 3.3	240-250
FC2-trough	8/11/12	27	--	2017	1.0428	34.3 ± 3.4	230
	7/14/13	25	2.47 ± 0.011	2013	1.0372	29.3 ± 3.7	250
	9/6/13	30	1.50 ± 0.0076	2013	1.0171	9.4 ± 3.6	320-330
FC3-center	9/2/14	44	0.464 ± 0.0043	2016	1.0173	9.2 ± 3.6	320-330
FC4-center	9/7/14	34	0.312 ± 0.0032	2016	1.0418	33.5 ± 4.1	230
FC4-trough	9/5/13	36	0.471 ± 0.0029	2013	1.0163	8.6 ± 3.9	330
LC1-center	8/10/12	31	--	2017	1.0317	23.3 ± 2.5	270
	10/6/12	--	--	2013	0.8470	-159.5 ± 13.1	1740
	9/7/13	34	0.825 ± 0.0092	2013	1.0026	-5.0 ± 4.4	390-400
LC1-rim	10/6/12	--	--	2013	1.0663	58.2 ± 7.3	160-170
LC1-trough	8/10/12	33	--	2017	1.0464	40.0 ± 3.7	220
	10/6/12	--	--	2013	1.0339	26.1 ± 6.5	260
	9/7/13	41	0.320 ± 0.0033	2013	1.0389	31.0 ± 4.6	240
LC2-center	9/2/14	29	0.372 ± 0.0032	2016	1.0221	14.0 ± 3.8	300-310

(table continues)

Profile	Date	Thaw depth (cm)	CO_2 flux (μmol m^{-2} d^{-1})	Analysis year	$F^{14}C$	$\Delta^{14}C_{CO2}$ (‰)*	TT_{CO2} (y)
LC3-center	10/6/12	--	--	2013	1.0304	22.5 ± 3.4	270
	7/12/13	23	0.607 ± 0.0032	2013	1.0336	25.8 ± 3.6	260
	9/7/13	33	1.12 ± 0.019	2013	1.0386	30.7 ± 4.2	240
	9/2/14	27	0.521 ± 0.0023	2016	1.0167	8.6 ± 3.7	330
LC3-trough	10/6/12	--	--	2013	1.0686	60.5 ± 9.8	160
	7/12/13	31	0.674 ± 0.0021	2013	1.0445	36.5 ± 4.1	220
	9/7/13	37	1.31 ± 0.0046	2013	1.0686	27.3 ± 4.1	250
LC4-center	9/7/14	28	0.463 ± 0.0029	2016	1.0031	-4.9 ± 3.8	390-400

*Values have been corrected to exclude atmospheric CO_2 using a 2-pool mixing model.

Table E2
Isotopic composition of soil profile CO_2

Profile	Month	Depth (cm)	$\delta^{13}C_{CO2}$ (‰)	Analysis year	$F^{14}C$	$\Delta^{14}C_{CO2}$ (‰)	TT_{CO2} (y)
HC1-center	8/2012	31	--	2013	0.7464	-259.2 ± 7.5	3050
	9/2013	20	-23.7	2013	0.7270	-278.6 ± 2.6	3350
HC3-center	8/2012	10	-20.1	2013	0.9473	-59.9 ± 3.0	770
	8/2012	20	--	2013	0.8864	-120.3 ± 3.2	1320
	8/2012	29	-21.7	2013	0.8944	-112.4 ± 2.7	1240
	7/2013	10	--	2013	0.9037	-101.3 ± 4.4	1150
	7/2013	20	--	2013	0.7382	-267.4 ± 2.6	3170
HC3-trough	7/2013	10	--	2013	0.7898	-216.2 ± 3.3	2440
	7/2013	20	-23.7	2013	0.8447	-161.7 ± 2.4	1760
FC2-center	8/2012	10	-24.8	2013	0.9509	-56.3 ± 2.8	740
	8/2012	20	-24.9	2013	0.9729	-34.5 ± 2.9	580
FC4-center	7/2013	20	-24.8	2013	0.8034	-202.7 ± 2.1	2260
LC3-trough	7/2013	10	-24.7	2013	1.0005	-7.1 ± 3.9	410
	7/2013	20	--	2013	0.8755	-131.2 ± 3.7	1430

Table E3
Significant predictors of $\Delta^{14}C$ in soil surface emissions

Fixed effect	DF	*F* value	Pr > *F*	Contrasted levels	*t* value for contrasts	Pr > |*t*|
Position	20.175	6.3542	0.007241 **	Rim – Center	3.221	0.0111 *
				Trough – Center	2.397	0.0641 .
				Trough – Rim	-1.355	0.3777
Type × DOY	19.895	7.0110	0.004959 **	--	--	--

Significance codes: 0 *** 0.001 ** 0.01 * 0.05 . 1

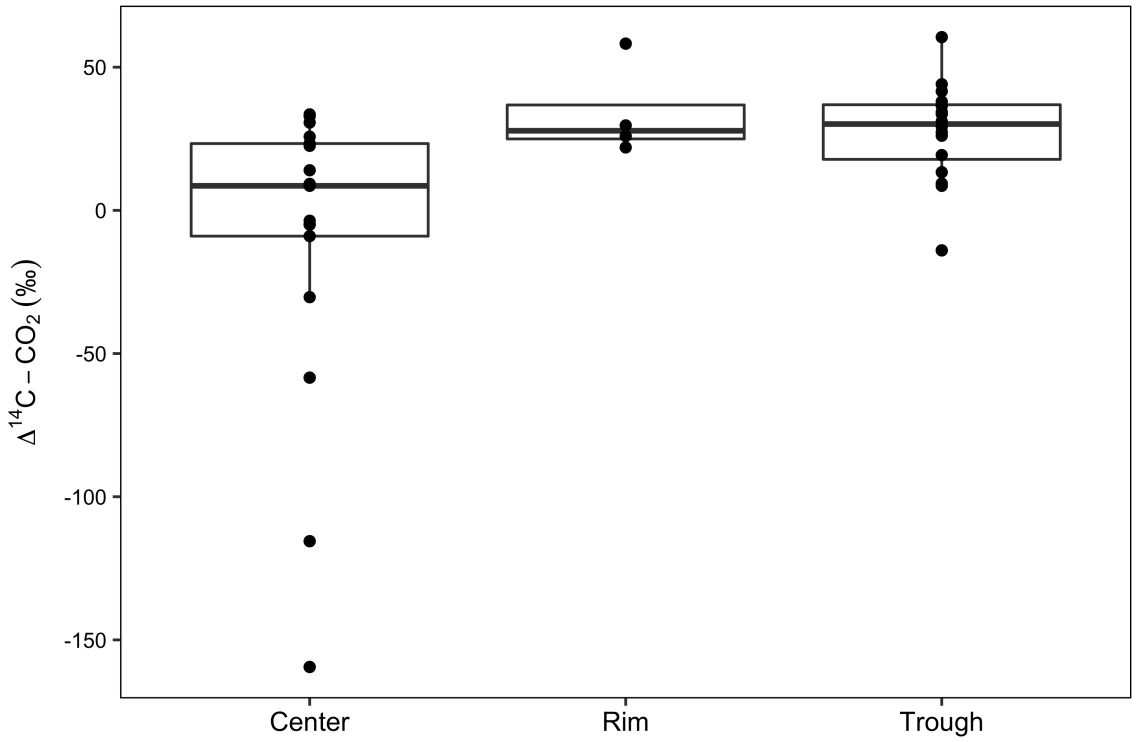

Figure E1. Radiocarbon content of ecosystem respiration from all profiles and sampling dates, separated by position within polygon. Boxes represent the first and third quartiles, and whiskers extend to the farthest values within 1.5 times this range.

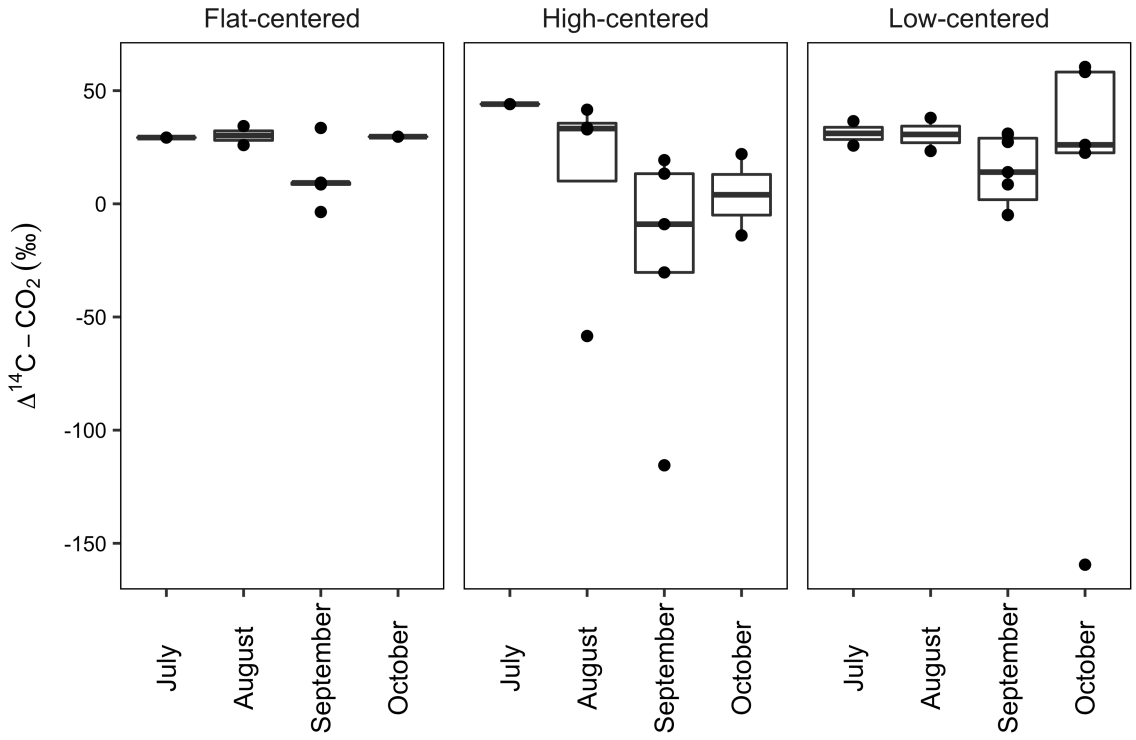

Figure E2. Radiocarbon content of ecosystem respiration, separated by polygon type and sampling month. Boxes represent the first and third quartiles, and whiskers extend to the farthest values within 1.5 times this range.

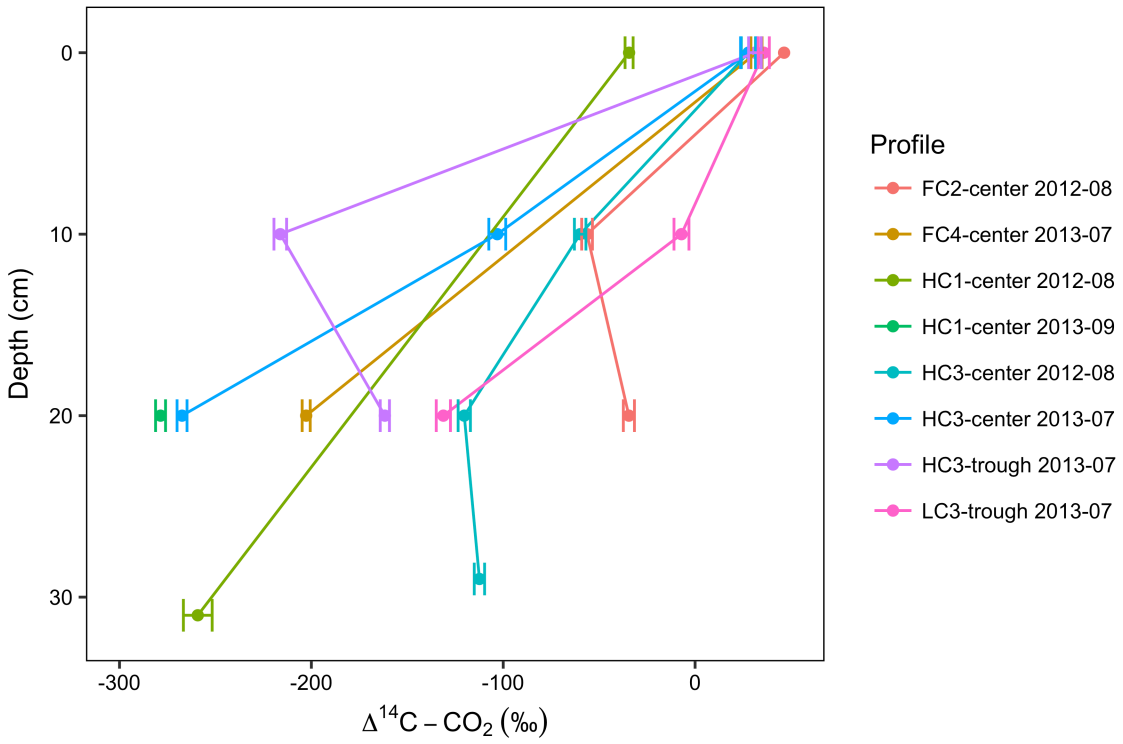

Figure E3. Depth profiles of $\Delta^{14}C$ in soil pore space. Lines connect samples collected in the same vertical profile and month. Surface samples (depth = 0 cm) were collected from soil chambers, and all other samples were collected from soil wells. Data presented here have not been corrected for background atmosphere.

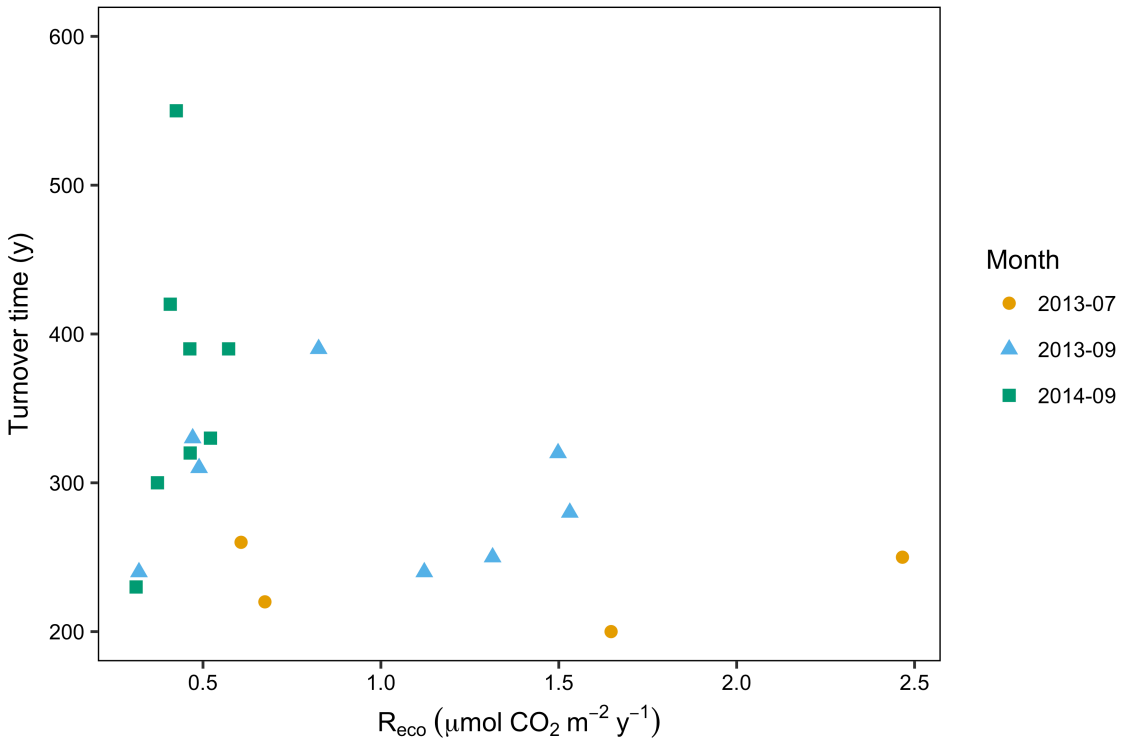

Figure E4. Turnover time and ecosystem respiration from surface chambers in July and September 2013 and September 2014.